The NUP107-160 complex members NUP96/MOS3 and NUP160 are required for defence gene expression in *Arabidopsis*

Dissertation

for the award of the degree

“Doctor rerum naturalium”

of the University of Goettingen

within the doctoral program

International Research Training Group 2172 - PRoTECT

of the Georg-August University School of Science (GAUSS)

submitted by

Denise Hartken

from Mettingen, Germany

Göttingen 2020

Für meine Eltern

Thesis Committee

PD Dr. Marcel Wiermer
Molecular Biology of Plant-Microbe Interactions Research Group, Albrecht-von-Haller Institute for Plant Sciences, University of Goettingen

Prof. Dr. Volker Lipka
Department of Plant Cell Biology, Albrecht-von-Haller Institute for Plant Sciences, University of Goettingen

Prof. Dr. Xin Li
Department of Botany, Michael Smith Laboratories, University of British Columbia

Members of the Examination Board

Referee: **PD Dr. Marcel Wiermer**
Molecular Biology of Plant-Microbe Interactions Research Group, Albrecht-von-Haller Institute for Plant Sciences, University of Goettingen

2nd Referee: **Prof. Dr. Volker Lipka**
Department of Plant Cell Biology, Albrecht-von-Haller Institute for Plant Sciences, University of Goettingen

Further members of the Examination Board

Prof. Dr. Xin Li
Department of Botany, Michael Smith Laboratories, University of British Columbia

Prof. Dr. Ivo Feussner
Department of Plant Biochemistry, Albrecht-von-Haller Institute for Plant Sciences, University of Goettingen

Prof. Dr. Gerhard Braus
Department of Molecular Microbiology and Genetics, Institute of Microbiology and Genetics, University of Goettingen

Prof. Dr. Kai Heimel
Department of Molecular Microbiology and Genetics, Institute of Microbiology and Genetics, University of Goettingen

Date of oral examination: 07th October 2020

Abstract

Nuclear pore complexes (NPCs) are composed of nucleoporin proteins (NUPs) and are embedded in the double membrane of the nuclear envelope (NE). *Arabidopsis* NUP96/MOS3 and NUP160 are members of the evolutionary conserved NUP107-160 nuclear pore sub-complex and required for basal resistance and TIR-type NLR protein mediated immunity. Previous data indicated that both NUPs are also involved in the regulation of gene expression. A genome-wide transcriptome analysis was conducted on unchallenged *mos3* and *nup160* mutant plants using an RNAseq approach to identify new components of *MOS3/NUP96*- and *NUP160*-dependent defence responses. This transcriptome analysis revealed mild but significant transcriptional changes of 471 genes that are differentially expressed in both nucleoporin mutants, including the key defence regulator *ENHANCED DISEASE SUSCEPTIBILITY1 (EDS1)* and its signalling partner *PHYTOALEXIN DEFICIENT4 (PAD4)* as well as the pattern recognition receptor *EF-Tu RECEPTOR* (*EFR*). Notably, only the expression of a certain set of defence-related genes was affected in *mos3* and *nup160* plants, suggesting that MOS3 and NUP160 are involved in regulating the expression of specific target genes. The phenotypical consequences of reduced *EFR* transcript abundance in *mos3* and *nup160* were investigated in more detail and revealed that both mutants display elevated *Agrobacterium*-mediated transient transformation efficiency, which is consistent with the function of EFR in restricting plant transformation by *Agrobacterium*. Reduced *EFR* gene expression, which is also reflected in reduced EFR protein abundance and impaired EFR-dependent elf18-triggered reactive oxygen species (ROS) production is likely to cause the enhanced transformation events in both mutants. The two genes whose expression was most strongly decreased in the transcriptomes of both *mos3* and *nup160* mutants are the predicted pumilio family (PUF) RNA binding protein *PUM9* (AT1G35730) and the predicted methyl esterase *MES18* (AT5G58310), whose functions have not been previously addressed in plant immunity. Using a reverse genetic approach, this study shows that *MES18* but not *PUM9* is required for basal resistance to the hemi-biotrophic pathogen *Pseudomonas syringae* pv. *tomato* (*Pst*) DC3000. Heterologous expression of MES18 and its subsequent purification and functional characterization showed that MES18 possesses esterase activity towards the methylated, biologically inactive transport forms of the plant hormones indole-3-acetic acid (MeIAA) and jasmonic acid (MeJA). The MES18-mediated hydrolysis of MeIAA to IAA and/or MeJA to JA may therefore be involved in regulating basal resistance to *Pst* DC3000.

List of abbreviations

::	fused to (in the context of gene fusion constructs)
α	alpha/anti
°C	degree Celsius
µ	micro
m	milli
n	nano
AA	amino acid
ABA	abscisic acid
A. thaliana	*Arabidopsis thaliana*
ARM	armadillo
AUX	auxin
avr	avirulence
AXR1	AUXIN RESISTANT1
BR	brassinosteroids
BSA	bovine serum albumin
Ca^{2+}	calcium
CBC	cap-binding complex
CC	coiled-coil
CDPK	calcium-dependent protein kinases
cDNA	complementary DNA
CERK1	CHITIN ELICITOR RECEPTOR KINASE1
cfu	colony forming unit
Col-0	Columbia-0
COI1	CORONATINE INSENSITIVE1
CPR5	CONSTITUTIVE EXPRESSION OF PR GENES5
CK	cytokinin
CTD	carboxy-terminal domain
CUL1	CULLIN1
CW	cell wall
DEG	differential expressed genes
ddH_2O	double-distilled water
DNA	deoxyribonucleic acid
DNase	deoxyribonuclease
dNTP	desoxyribonucleotidetriphosphate

DMSO	dimethylsulfoxide
DTT	dithiothreitol
E	glutamate
E. coli	*Escherichia coli*
e.g.	exempli gratia
EDS1	ENHANCED DISEASE SUSCEPTIBILITY1
EDTA	ethylenediaminetetraacetic acid
EFR	elongation factor thermo unstable receptor
EF-Tu	elongation factor thermo unstable
et al.	*et alii*; and others
ET	ethylene
ETI	effector triggered immunity
EtOH	ethanol
ETS	effector triggered susceptibility
FDR	false discovery rate
FG-NUP	phenylalanine-glycine-rich nucleoporin
flg22	flagellin (22 amino acid peptide)
FLS2	FLAGELLIN SENSING2
g	gramm
GA	gibberellic acid
GDP	guanosindiphosphate
GH3	GRETCHEN HAGEN3
GO	gene ontology
GTP	guanosintriphosphate
GUS	β-glucuronidase
h	hour(s)
HCl	hydrochloric acid
HR	hypersensitive response
HOS1	HIGH EXPRESSION OF OSMOTICALLY RESPONSIVE GENES1
HRP	horseradish peroxidase
Hz	hertz (cycles per second)
IAA	Indole-3-acetic acid
i.e.	*id est*
ITC	Isothermal Titration Calorimetry
JA	jasmonic acid
JA-Ile	jasmonic acid-isoleucine

JAR1	JASMONATE RESISTANT1
K	lysine
Kaps	karyopherins
kDa	kilo Dalton
L	liter
L-012	(8-amino-5-chloro-7-phenyl-pyrido[3,4-d]pyridazine-1,4(2H,3H)dione); luminol-based chemiluminescent probe)
log_2FC	log_2 fold change
LOS4	LOW EXPRESSION OF OSMOTICALLY RESPONSIVE GENES4
LRR	leucine-rich repeat
M	molar (mol/l)
mA	milli Ampere
MAMP	microbe associated molecular pattern
MAPK	mitogen activated protein kinase
Me	methyl
MES	methyl esterase
min	minute(s)
ml	milliliter
mM	millimolar
MOS	MODIFIER OF SNC1
MPK	MITOGEN-ACTIVATED PROTEIN KINASE
m-RNA	messenger ribonucleic acid
mi-RNA	micro ribonucleic acid
MS	Murashige-Skoog
MT	methyl transferase
MTI	MAMP triggered immunity
NADPH	nicotinamide adenine dinucleotide phosphate hydrogen
NASC	Nottingham Arabidopsis Stock Centre
NE	nuclear envelope
NB	nucleotide-binding
NDR1	NON-RACE SPECIFIC DISEASE RESISTANCE1
NES	nuclear export signals
NLS	nuclear localization signals
NMD	nonsense-mediated decay
NPC	nuclear pore complex
NPR1	NONEXPRESSER OF PR GENES1

NSD	nonstop decay
NTF2B	NUCLEAR TRANSPORT FACTOR2B
NTR	nuclear transport receptor
NUP	nucleoporin
OD_{600}	optical density at a wavelength of 600 nm
PAD4	PHYTOALEXIN DEFICIENT4
PAMP	pathogen associated molecular pattern
PCA	principal component analysis
PCR	polymerase chain reaction
pH	negative decimal logarithm of the H^+ concentration
PIC	protease inhibitor cocktail
PM	plasma membrane
PPT	DL-Phosphinothricin
PR1	PATHOGENESIS-RELATED GENE1
PRE	pumilio response elements
PRR	pattern recognition receptor
P. syringae	*Pseudomonas syringae*
Pst DC3000	*Pseudomonas syringae* pv. *tomato* (*Pst*) DC3000
PTI	PAMP triggered immunity
PUF	Pumilio RNA-binding protein family
PUM	pumilio
PUM-HD	pumilio homology domain
qRT-PCR	quantitative real-time polymerase chain reaction
RAE1	RNA EXPORT FACTOR1
RAN1	RAS-RELATED NUCLEAR PROTEIN1
RAN2	RAS-RELATED NUCLEAR PROTEIN2
RBP	ribonucleic acid-binding protein
RPKM	reads per kilobase per million
rpm	rounds per minute
RLK	receptor-like kinase
RLP	receptor-like protein
RLU	relative luminescence units
r-RNA	ribosomal ribonucleic acid
RNA	ribonucleic acid
RNAPII	ribonucleic acid polymerase II
RNAseq	ribonucleic acid sequencing
RNP	ribonucleoprotein particles

ROS	reactive oxygen species
RPKM	reads per kilo million
RT	room temperature
RUB1	RELATED TO UBIQUITIN1
s	second(s)
SA	salicylic acid
SAG	salicylate 2-O-β-D-glucoside
SABP2	SALICYLIC ACID BINDING PROTEIN2
SAR	systemic acquired resistance
SA-Asp	salicyloyl-L-aspartate
SEC13B	SECRETORY13
SEH1	SEC13 HOMOLOGUE1
SEM	standard error of the mean
SD	standard deviation
SDS	sodium dodecyl sulfate
SDS PAGE	sodium dodecyl sulfate polyacrylamide gel electrophoresis
SNC1	SUPPRESSOR OF NPR1-1
T3SS	type III secretion system
T4SS	type IV secretion system
Taq	*Thermus aquaticus*
TAE	tris-acetic acid ethylenediaminetetraacetic acid
TBS-T	tris buffered saline – Tween-20
T-DNA	transfer deoxyribonucleic acid
THO/ TREX	TRanscription-EXport complex
TIR	Toll/ interleukin-1 receptor
TRP	tryptophan
t-RNA	transfer ribonucleic acid
TEMED	tetramethylethylenediamine
TMV	tobacco mosaic virus
U	unit
UPLC-nanoESI-MS/MS	Ultra Performance Liquid Chromatography coupled with nanoelectrospray ionization and Tandem Mass Spectrometry
UTR	untranslated region
V	volt
XPO1B	EXPORTIN1B

Table of contents

1 Introduction

1.1 The plant immune system

Unlike animals, plants do not have an adaptive immune system that relies on the transport of highly specialised systemic cells via a circulatory system to counteract pathogen attacks (Litman *et al.*, 2010; Yuan *et al.*, 2014). Since plants are sessile and therefore constantly exposed to abiotic and biotic stresses that they cannot escape from, they have the need to distinguish between harmless and potentially harmful stimuli (Doughari, 2015). Although plants have to cope with a large number of threats such as bacteria, fungi, oomycetes or insects, infected plants are rather an exception than the rule. This is due to the fact that plants have evolved an efficient cellular innate immune system. Each single plant cell can react to a pathogen attack and trigger immunity responses (Jones and Dangl, 2006). Since immune responses require energy and are not needed to be active continuously the balance between plant growth and plant immunity is precisely regulated and defence responses are only induced after pathogen attack (Glazebrook, 2005; Huot *et al.*, 2014). The cell wall and the cuticle protect plant cells from the invasion of pathogens. These are the first preformed physical barriers that microbial pathogens need to overcome (Nawrath, 2002; Houston *et al.*, 2016). However, some adapted microbes can pass these physical barriers of the plant either by entering plant tissues via natural openings such as stomata or wounds, or by active penetration using mechanical pressure and/or the secretion of cell wall degrading enzymes (Melotto *et al.*, 2008; Bellincampi *et al.*, 2014). After successful invasion, microbial pathogens are confronted with the plant plasma membrane and the efficient plant innate immune system that is composed of two evolutionarily linked layers.

The first layer of defence is referred to as microbe/pathogen associated molecular pattern (MAMP/PAMP) triggered immunity (MTI/PTI) and confers resistance against non-adapted pathogens (Chisholm *et al.*, 2006; Jones and Dangl, 2006; Zipfel, 2009). MTI/PTI is triggered when plasma membrane-localized pattern recognition receptors (PRRs) recognise conserved microbial structures known as MAMPs/PAMPs (Boller and He, 2009) as non-self molecules. MAMPs/PAMPs are unique microbe-derived structures that are essential for the microbial lifestyle, but absent from the host organism (Nürnberger *et al.*, 2004).

Microbial pathogens are categorised into biotrophs, hemi-biotrophs or necrotrophs, based on their particular lifestyle. Biotrophic microbes obtain nutrients from living tissue of the host plant. In contrast, necrotropic pathogens induce cell necrosis during the course of infection and depend on dead cells and tissue of their host. Hemi-biotrophic pathogens are characterised by a switch from a biotrophic phase at early stages of an infection to a necrotic phase later in the infection process (McDowell, 2013; Wang *et al.*, 2014; Spanu and Panstruga, 2017).

Well-characterized MAMPs/PAMPs are the conserved 22 amino acid epitope (flg22) of bacterial flagellin, the N-acetylated 18 amino acid peptide (elf18) of the N-terminus of the bacterial elongation factor Tu (EF-Tu) as well as the fungal cell wall component chitin, which are sensed by the PRRs FLAGELLIN SENSITIVE2 (FLS2), EF-Tu RECEPTOR (EFR) and the CHITIN ELICITOR RECEPTOR KINASE1 (CERK1), respectively (Gómez-Gómez and Boller, 2002; Kunze *et al.*, 2004; Zipfel *et al.*, 2006; Zipfel, 2008; Petutschnig *et al.*, 2010; Monaghan and Zipfel, 2012). Interestingly, flagellin of the hemi-biotrophic bacterial pathogen *Pseudomonas syringae* acts as a PAMP in *Arabidopsis*, while its EF-Tu shows only weak elicitor activity (Kunze *et al.*, 2004; Zipfel *et al.*, 2006). In contrast, the soil-born biotrophic pathogen *Agrobacterium tumefaciens* is not recognized by the PRR FLS2, but instead by EFR (Felix *et al.*, 1999). *A. tumefaciens* causes crown gall disease and relies for the infection process on the transfer and integration of the bacterial transfer DNA (T-DNA) into the plant host genome (Escobar and Dandekar, 2003). Consequently, *Arabidopsis efr* mutant plants exhibit higher levels of *Agrobacterium*-mediated plant transformation events (Zipfel *et al.*, 2006).

The perception of a MAMP/PAMP molecule by the respective PRR leads to early and late plant defence responses that are activated within minutes or in hours to days, respectively (Boller and Felix, 2009). Early responses, that are activated after the perception of a MAMPs/PAMPs are the NADPH oxidase mediated generation of reactive oxygen species (ROS; Torres *et al.*, 2006; Kadota *et al.*, 2015), the influx of calcium ions into the cytosol and further downstream signalling events, including the activation of mitogen-activated protein kinase (MAPK) cascades (Meng and Zhang, 2013), activation of calcium-dependent protein kinases (CDPKs; Gao *et al.*, 2014) and the transcriptional reprogramming of defence genes inside the host cell nucleus (Dangl *et al.*, 2013; Figure 1 (1)). Later responses include for example the deposition of callose at attempted pathogen penetration sites to restrict plant infection by non-adapted pathogens (Boller and Felix, 2009).

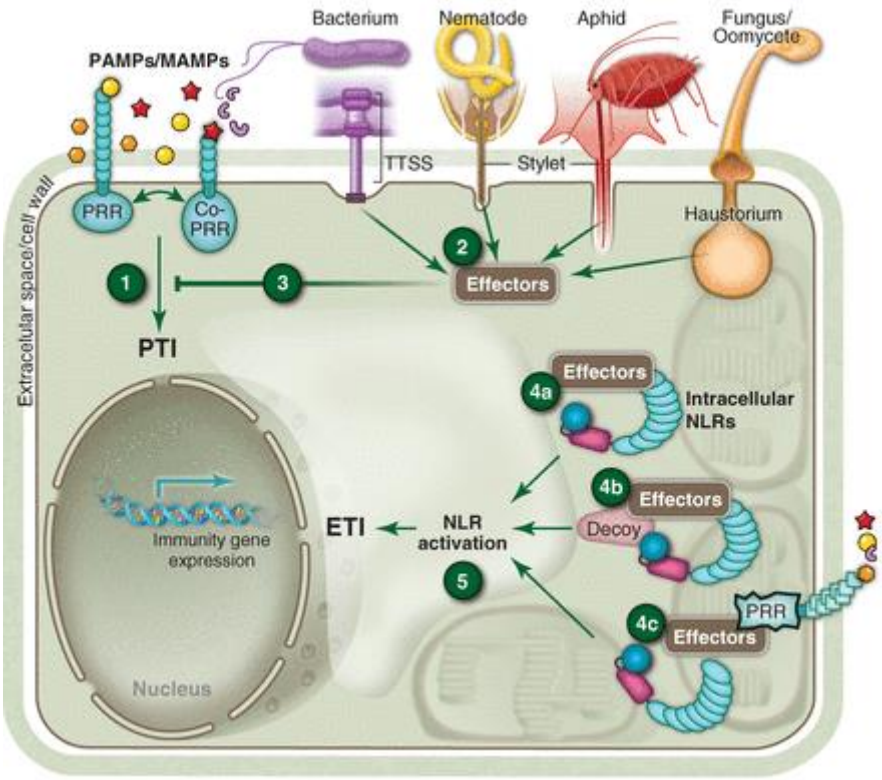

Figure 1: Schematic overview of the two-layered immune system in plants. Cell surface pattern recognition receptors (PRRs) perceive pathogen- or microbe associated molecular patterns (PAMPs/MAMPs) which lead to the activation of PAMP-triggered immunity (PTI) (**1**). Host-adapted pathogens evolved virulence effector molecules, which are secreted into the plant cell apoplast (not shown) or into the plant cell interior (**2**) to suppress PTI and facilitate virulence (**3**). The successful suppression of PTI results in effector triggered susceptibility (ETS). Plants, in turn, evolved intracellular NLR receptors, containing a nucleotide-binding domain and a leucine rich repeat domain (NLRs) which can sense effector molecules either directly (**4a**), or indirectly by recognizing the effector activity on its host target (**4c**) or on a non-functional decoy that mimics such effector target (**4b**). NLR activation (**5**) elicits NLR-dependent effector triggered immunity (ETI). The figure is taken from Dangl *et al.* (2013).

Host-adapted plant pathogens secrete effector molecules into the apoplast or the cytosol to interfere with PTI responses of the host plant in order to promote disease symptoms (Chaudhari *et al.*, 2014). This mechanism is called effector triggered susceptibility (ETS; Dangl *et al.*, 2013; Ma *et al.*, 2018; Figure 1 (2) and (3)). Whereas fungal and oomycete derived effectors are delivered into the apoplast or host cell via haustoria or intracellular hyphae, bacterial pathogens secrete effector molecules directly into the host cell using syringe-like secretion systems, such as the type III secretion system (T3SS) that is described for *Pseudomonas syringae* or the T4SS that is used by *Agrobacterium tumefaciens* (Ghosh, 2004; Aguilar *et al.*, 2011; Chatterjee *et al.*, 2013; Chaudhari *et al.*, 2014; Selin *et al.*, 2016).

Plants, however, possess a second layer of innate immunity which is referred to as effector-triggered immunity (ETI) that is capable to counteract ETS by either direct or indirect

recognition of specific effector molecules. Effectors are recognized via intracellular nucleotide-binding/leucine-rich repeat receptors (NLRs), also referred to as resistance (R) proteins (Chisholm *et al.*, 2006; Bonardi and Dangl, 2012). Generally, NLRs consists of a central nucleotide-binding (NB) domain and a C-terminal leucine-rich repeat (LRR) domain, but differ in their N-terminus. The two major classes of NLRs can be distinguished by their N-terminal Toll/interleukin-1 receptor (TIR) and coiled-coil (CC) domains, respectively (Jacob *et al.*, 2013).

The recognition of effectors by intracellular NLRs can occur in three basic ways. NLRs either recognize effectors directly via physical association (Figure 1 (4a)), or they indirectly recognize the activity of pathogen effectors on their host target(s). This host target of effector action can either be the operational effector target which is guarded by the NLR protein (Figure 1 (4c)), or be a non-functional decoy protein that mimics such effector target (Figure 1 (4b); Caplan *et al.*, 2008; Dangl *et al.*, 2013). In *Arabidopsis*, two major *R* gene-mediated downstream signaling pathways exists (Aarts *et al.*, 1998). TIR-type NLRs usually rely on ENHANCED DISEASE SUSCEPTIBILITY1 (EDS1) as downstream component. In contrast, the membrane localized protein NON-RACE SPECIFIC DISEASE RESISTANCE1 (NDR1) is needed for CC-type NLR signalling (Knepper *et al.*, 2011).

The perception of effectors leads to strong defence responses (Figure 1 (5)) including the accumulation of the plant hormone salicylic acid (SA), the rapid activation of defence genes in the nucleus and a hypersensitive cell death response (HR) to restrict pathogenic growth of biotrophic host-adapted microbes. ETI is also referred to as R protein-mediated resistance and ETI responses are thought to be an accelerated and amplified PTI/MTI response (Jones and Dangl, 2006; Boller and He, 2009; Tsuda and Katagiri, 2010; Dangl *et al*., 2013).

Interestingly, SA does not only play a key role in local defence responses by inducing defence gene expression (e.g. *PATHOGENESIS-RELATED GENE1*, *PR1*) and host cell death, but also the accumulation of SA is important for the establishment of systemic acquired resistance (SAR; Vlot *et al.*, 2009). SAR is an inducible form of resistance that confers a long-lasting protection against a broad-spectrum of pathogens including bacteria, fungi and oomycetes in distantly located uninfected plant tissue (Vlot *et al.*, 2008b; Fu and Dong, 2013). This data illustrate the importance of the phytohormone SA in plant immunity responses. In addition to SA, jasmonic acid and ethylene are described as canonical plant defence hormones (Glazebrook, 2005). The last decades of research have demonstrated the huge impact of the tightly regulated plant hormone signalling network for plant immunity.

1.2 Phytohormones and their functions in plant immunity

Plant hormones, also known as phytohormones, are small organic molecules that are important for plant development processes, and also crucial signalling molecules in plant

immune responses. Canonical defence-related phytohormones are salicylic acid (SA), jasmonic acid (JA) and ethylene (ET; Glazebrook, 2005; Shigenaga and Argueso, 2016). SA is a phenolic compound that is derived from chorismate and positively regulates plant immunity against biotrophic and hemibiotrophic plant pathogens and is required for the activation of SAR (Vlot *et al.*, 2009; Ding and Ding, 2020). In contrast, the lipid-derived signalling molecules JA and the gaseous plant hormone ET are associated with defence responses against herbivores and necrotrophic pathogens (Pieterse *et al.*, 2012; Campos *et al.*, 2014; Pandey *et al.*, 2016). All three plant hormones play an important role in PTI and ETI responses (Tsuda *et al.*, 2009).

Classical plant growth hormones include abscisic acid (ABA), gibberellic acid (GA), cytokinin (CK), auxin (AUX) and brassinosteroids (BR). These hormones are typically associated with plant development and/or responses to the abiotic environment, but have more recently also been described to play a role in plant resistance (Denancé *et al.*, 2013; De Bruyne *et al.*, 2014; Huot *et al.*, 2014; Lozano-Durán and Zipfel, 2015).

A widely acknowledged concept proposes that SA and JA/ET signalling pathways work antagonistically to each other accordingly to the different lifestyle of the attacking pathogen (Spoel and Dong, 2008; Van der Does *et al.*, 2013). In general, the infection with a biotrophic or hemi-biotrophic pathogen leads to the accumulation of SA while the attack of a pathogen with a necrotrophic lifestyle triggers JA and ET accumulation in the plant host cell (Pieterse *et al.*, 2012). However, to date the concept of a strict antagonistic interaction of SA and JA/ET is questioned and instead a concept of a highly interconnected hormone signalling network is proposed where also classical growth hormones such as auxin contribute to plant defence responses (Fu and Wang, 2011; Naseem *et al.*, 2015; Kunkel and Harper, 2018; Figure 2). In plants, the most abundant naturally occurring auxin is indole-3-acetic acid (IAA) which derives from the amino acid tryptophan (Trp; Dai *et al.*, 2013; Korasick *et al.*, 2013; Zhao, 2014).

In general, plant immune responses are not controlled by single hormones, but rather through antagonistic or synergistic interactions of different plant hormones that work interdependently which results in a tightly regulated hormone signalling network (Shigenaga and Argueso, 2016). In return, pathogens have evolved different strategies to interfere with the fine-tuned plant hormone signalling in such a way that the hormone balance is shifted to their benefit and that the chance of successful reproduction is greatly enhanced. The manipulation of the hormone balance in the plants cell generally leads to a suppression of host defence or interferes with physiological processes such as stomata closure or stimulates plant cell death and the activation of necrosis (Kunkel and Harper, 2018). For instance, Type III-secreted effector molecules manipulate hormone homeostasis and/or signalling in the host plant. The *P. syringae* HopXI is just one example for an effector

molecule that effects JA signalling (Gimenez-Ibanez *et al.*, 2014) leading to stomata reopening to facilitate a successful invasion of the bacterium into the host cell. Several other effectors are described such as the *Pseudomonas* AvrPtoB or the *Xanthomonas* XopD which influence ABA signalling or inhibiting ethylene production, respectively (De Torres-Zabala *et al.*, 2007; Kim *et al.*, 2013).

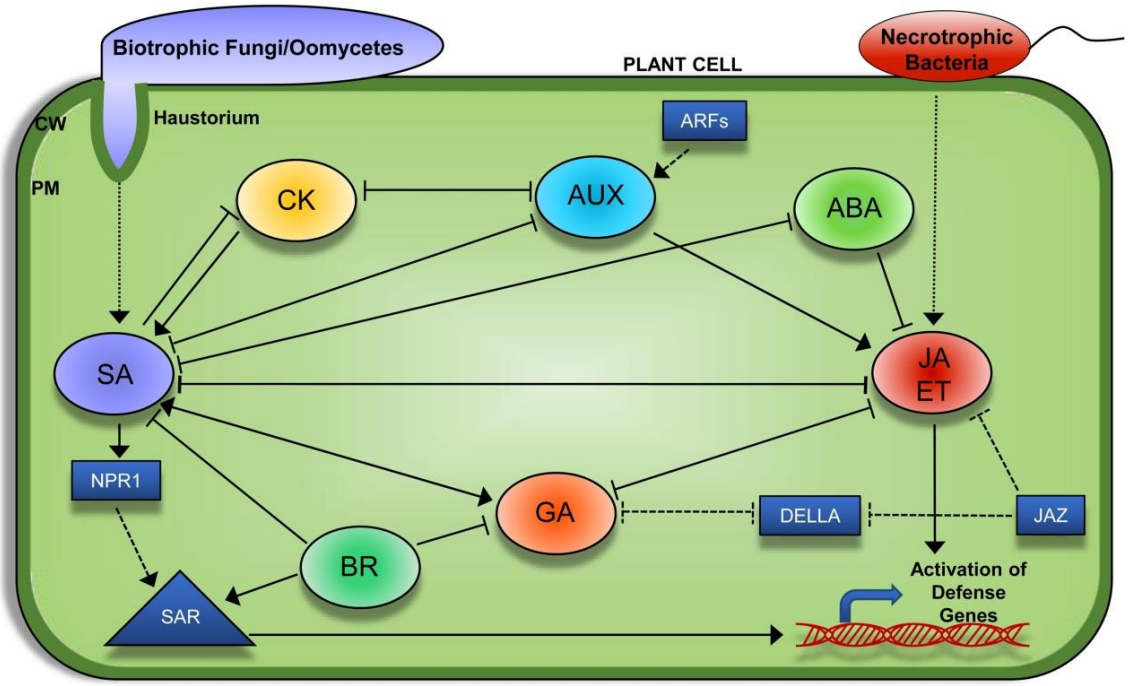

Figure 2: A schematic model of the phytohormone signalling network in plant immunity. Typically, SA levels increase in the plant host cell upon attack of biotrophic pathogens. In contrast, the interaction with necrotrophic pathogens induces JA and ET production. Further hormones such as ABA, CK, AUX, GA, and BR are involved in fine-tuning host immune responses via up- or down-regulation of either the SA or JA/ET signalling pathways. The phytohormones are encircled and marked in different colours. Transcription factors and processes activated in the nucleus are marked in blue shapes. Dotted arrow lines represent recognition of the pathogens by the plant cell. Solid lines with arrow denote up-regulation and solid lines with blunt-ends denote inhibition of hormone signalling. Dashed lines symbolize effects of particular transcription factors or processes that are involved in the hormone signalling network. CW, cell wall; PM, plasma membrane; SA, salicylic acid; JA, jasmonic acid; ET, ethylene; CK, cytokinin; AUX, auxin; GA, gibberellic acid; BR, brassinosteroids. Figure taken from Shigenaga and Argueso (2016).

As described above, the highly regulated plant hormone network facilitates plant defence responses. Accordingly, it is crucial for the plant to tightly regulate the activity of certain hormones. Chemical modifications are a suitable way to modulate hormone activity and allow fine-tuning of hormone function, accumulation and/or mobility. Phytohormones undergo a number of biologically relevant chemical modifications including amino acid (AA) conjugation or methylation (Dempsey *et al.*, 2011; Korasick *et al.*, 2013; Wasternack and Song, 2017). Since the plant hormones SA, JA and IAA are of particular relevance for

enzymatic analyses conducted in this study, the research findings that are described below focus mainly on these particular hormones.

A prominent example for an important conjugate is JA-Ile which is the most common biologically active form of JA and binds to the F-box protein CORONATINE INSENSITIVE1 (COI1) mediating JA signalling. In *Arabidopsis*, the isoleucine-conjugated form of JA (JA-Ile) is formed by the GH3 acyl adenylase protein JAR1 (Staswick *et al.*, 2002; Staswick and Tiryaki, 2004; Fonseca *et al.*, 2009; Sheard *et al.*, 2010). Interestingly, the conjugation of amino acids such as aspartate or glutamate to IAA leads to the inactivation or degradation of this hormone (Östin *et al.*, 1998; Ljung *et al.*, 2002; Ludwig-Müller, 2011). In contrast to JA and IAA conjugates, very little is known about AA conjugates of SA and their potential functions. The most stable SA-AA conjugate that has been detected in *Arabidopsis* is salicyloyl-L-aspartate (SA-Asp; Steffan *et al.*, 1988; Bourne *et al.*, 1991). It has been shown that the endogenous SA-AA conjugates act as mobile signals and induce *PR* gene expression and enhance disease resistance to *P. syringae* (Chen *et al.*, 2013). This data illustrate that AA conjugations can also play a rather direct role in plant immune responses.

Methylations of phytohormons lead to an increase in membrane permeability and volatility, allowing a more effective long distance transport. In the genomes of a variety of flowering plants carboxyl methyl transferases (MTs) have been identified, which are collectively grouped into the SABATH protein family (D'Auria *et al.*, 2003). In *Arabidopsis*, 24 genes belong to this family, which encode for proteins that catalyse substrate-specific methylation processes of phytohormones such as SA, JA or IAA within the plant cell (Ross *et al.*, 1999; Seo *et al.*, 2001; Zubieta *et al.*, 2003; Qin *et al.*, 2005; Zhao *et al.*, 2008). In contrast, de-methylation processes are catalysed by methyl esterases (MESs). In *Arabidopsis*, 20 MESs have been identified referred to as MES1 to MES20 (Yang *et al.*, 2006; Vlot *et al.*, 2008a; Yang *et al.*, 2008). Notably, MeSA has a negative effect on parasitoid host-finding behaviour (Snoeren *et al.*, 2010), and is involved in plant immunity. Early studies in 1997 showed that defence responses in tobacco can be induced by vaporized MeSA that was emitted from neighbouring plants (Shulaev *et al.*, 1997). Interestingly, transgenic *Arabidopsis* plants, which accumulate high levels of MeSA and do not longer accumulate SA/SAG, became more susceptible to bacterial infection with *P. syringae* in comparison to wild-type plants. It was further shown that emitted MeSA induced *PR1* gene expression in neighbouring plants (Koo *et al.*, 2007). However, tabacco plants silenced for the MeSA esterase SALICYLIC ACID BINDING PROTEIN2 (SABP2) failed to induce gene expression of *PR1* and showed only little SAR responses after tobacco mosaic virus (TMV) infection (Kumar and Klessig, 2003; Forouhar *et al.*, 2005), indicating that MeSA is biologically inactive and needs to be converted into its active form SA to induce defence gene expression. It seems more likely that MeSA serves as airborne signal for

plant-to-plant communication (Koo *et al.*, 2007; Ueda *et al.*, 2012). Furthermore, MeSA is controversially discussed as long-distance signalling molecule implicated in SAR (Park *et al.*, 2007; Vlot *et al.*, 2008b; Attaran *et al.*, 2009; Shah, 2009; Liu *et al.*, 2010; Liu *et al*., 2011a; Liu *et al.*, 2011b; Shah and Zeier, 2013).

Similar to MeSA, methyl JA (MeJA) also plays a role as airborne signalling molecule in plant communication. Due to the strong volatility of MeJA, it can easily penetrate the cell membrane without carrier assistance and spread from locally wounded leaves to distant leave tissue and adjacent plants (Farmer and Ryan, 1990; Thorpe *et al.*, 2007; Heil and Ton, 2008). However, MeJA itself is not biologically active, but needs to be converted back into jasmonates (JAs, e.g. JA or JA-Ile). This conversion presumably affects the jasmonate metabolic network, which works as positive feedback regulation of the JA biosynthesis pathway (Wu *et al.*, 2008; Stitz *et al.*, 2011; Cao *et al.*, 2016). In *Arabidopsis*, exogenously applied MeJA induces the expression of genes involved in various processes such as JAs biosynthesis, defence as well as signal transduction (Devoto *et al.*, 2005).

The methylation of IAA leads to the formation of non-polar IAA methyl ester (MeIAA) that presumably can move transporter-independently from cell to cell and through the whole plant (Li *et al.*, 2008; Yang *et al.*, 2008) as it has also been described for MeSA and MeJA. Equally, MeIAA is reported to be a biologically inactive signalling molecule that needs to be converted back into free and active IAA for induction of auxin dependent processes in the plant (Li *et al.*, 2008; Yang *et al.*, 2008). Since 1982, MeIAA was postulated as storage form of auxin that might influence auxin sensitivity or auxin transport (Cohen and Bandurski, 1982). It is likely, that the rapid conversion of inactive IAA storage forms including IAA conjugates and MeIAA contributes to the regulation of auxin homeostasis (Korasick *et al.*, 2013). However, so far, only a few studies have analysed the molecular function of MeIAA. The low abundance and its fast turnover makes it difficult to address its *in vivo* function in plants. Recently, it was reported that the methylation of IAA is particularly important in gravity-sensing cells to restrict polar auxin transport and to regulate the auxin distribution across the hypocotyl in *Arabidopsis* (Abbas *et al.*, 2018). The findings for the phytohormones SA, JA and auxin introduced above illustrate exemplarily how important chemical modification are for the activation and function of hormones in the plant cell. Accordingly, enzymes including the SABATH methyl transferases or methyl esterases have a huge impact on controlling the dose of the bioactive forms of the particular phytohormones, thus contributing to a hormone signalling network that is implicated in cellular processes such plant immunity responses.

Notably, nucleoporins that are part of the nuclear pore complex (NPC) are involved in auxin signaling (Parry *et al.*, 2006; Jacob *et al.*, 2007; Ferrández-Ayela *et al.*, 2013; Boeglin *et al.*, 2016). Furthermore, two nuclear import receptors of the β-family karyopherins are

described as negative regulators of ABA responses (Verslues *et al.*, 2006; Luo *et al.*, 2013). This data indicate that ABA and auxin signaling is particularly sensitive to dysfunctional nucleocytoplasmic transport and illustrate the role of the NPC in hormone signaling.

1.3 The structure and function of the nuclear pore complex (NPC)

In all eukaryotic cells, including plant cells, transcriptional processes occur in the nucleus while protein translation happens in the cytoplasm. The transport of proteins and RNAs between the cytoplasm and the nucleus is mediated by the nuclear core complex (NPC) which represents one of the largest multi-protein complexes in eukaryotic cells. The NPC is embedded in the nuclear envelope (NE) which acts as a physical barrier and separates gene transcription and protein translation (Meier, 2007; Xu and Meier, 2008; Strambio-de-castillia *et al.*, 2010; Evans *et al.*, 2011; Raices and D'Angelo, 2012; Tamura and Hara-Nishimura, 2013; Parry, 2015; Beck and Hurt, 2017).

NPCs are composed of multiple copies of approximately 30 different proteins known as nucleoporins (NUPs; Strambio-de-castillia *et al.*, 2010; Raices and D'Angelo, 2012). The 3D-ultrastructure of the NPCs is highly conserved among evolutionarily distant eukaryotes. Although eukaryotic NPCs share functional similarities, differences in the composition exist (Fiserova *et al.*, 2009; DeGrasse *et al.*, 2009; Neumann *et al.*, 2010; Tamura and Hara-Nishimura, 2011; Raices and D'Angelo, 2012; Tamura and Hara-Nishimura, 2013). To date, three plant-specific nucleoporins have been identified, namely NUP136/NUP1, HIGH EXPRESSION OF OSMOTICALLY RESPONSIVE GENES1 (HOS1) and CONSTITUTIVE EXPRESSION OF PR GENES5 (CPR5; Tamura *et al.*, 2010; Gu *et al.*, 2016). Furthermore, a proteomic approach has revealed that the composition of plant NPCs is more similar to mammalian NPCs than yeast NPCs (Tamura *et al.*, 2010). The NPCs show an eight-fold rational symmetry and consist of a nuclear (inner) ring with an extended peripheral structure named the nuclear basket, an inner pore (core) ring which builds the central transport channel and a cytoplasmic (outer) ring with eight cytoplasmic filaments (Alber *et al.*, 2007; Wente and Rout, 2010; Tamura *et al.*, 2010; Tamura and Hara-Nishimura, 2011; Grossman *et al.*, 2012; Tamura and Hara-Nishimura, 2013; Beck and Hurt, 2017; Meier *et al.*, 2017). The central channel of the NPC is filled by intrinsically disordered phenylalanine-glycine-rich nucleoporins (FG-NUPs). This results in the formation of a meshwork that is critical for the highly selective control of nucleocytoplasmic trafficking through the nuclear pore (Terry and Wente, 2009; Tetenbaum-Novatt and Rout, 2010; Tamura and Hara-Nishimura, 2013).

In contrast to ions and small molecules (< 40 kDa) which can passively diffuse through the pore, macromolecules larger than 40-60 kDa in size are actively chaperoned from the cytosol into the nucleus or *vice versa*. This transport is mediated by nuclear transport

receptors (NTRs) that interact with the FG-Nups in the central channel of the NPC (Li *et al.*, 2016; Schmidt and Görlich, 2016; Aramburu and Lemke, 2017). Important NTRs are karyopherins (Kaps), which includes nuclear import receptors (importins) and export receptors (exportins), that recognize specific amino acid sequences referred to as nuclear localization signals (NLSs) or nuclear export signals (NESs) of their specific cargos. Binding of the transport receptors to these signals determines a nuclear or cytoplasmic destination of the cargo protein, respectively (Xu *et al.*, 2010; Merkle, 2011; Tamura and Hara-Nishimura, 2014). The directionality of Kap-mediated nucleocytoplasmic transport is established by a concentration gradient of the small GTPase RAS-RELATED NUCLEAR PROTEIN (RAN) across the NE in its GTP-bound (nuclear) or GDP-bound (cytoplasmic) form (Izaurralde *et al.*, 1997; Tetenbaum-Novatt and Rout, 2010). Cargos bind their NTRs either directly or via adapter proteins. Importin β are major transport receptors mediating the nuclear transport of proteins and certain classes of RNAs (Lott and Cingolani, 2011; Merkle, 2011; Kimura and Imamoto, 2014). A well-known adapter protein is importin α (Görlich *et al.*, 1994). Importin α proteins typically possess ten armadillo (ARM) repeats that bind NLSs on their specific cargos in the cytoplasm. For nuclear import, Importin α forms a trimeric complex with the cargo protein and the import receptor Importin β, which interacts with FG-NUPs in the central channel of the NPC. For nuclear export, exportins bind to the NESs of their cargo proteins. This export complex is shuttled through the NPC to the cytoplasm (Goldfarb *et al.*, 2004; Wiermer *et al.*, 2007; Tetenbaum-Novatt and Rout, 2010; Merkle, 2011; Raices and D'Angelo, 2012).

Both the protein transport and the nuclear export of RNAs through the NPC are tightly regulated. Small RNAs such as transfer (t) RNAs or micro (mi) RNAs as well as ribosomal (r) RNAs are exported from the nucleus into the cytoplasm by exportins of the karyopherin family. Similar to protein transport, this exportin-dependent transport is also regulated via the RAN-GTP gradient. In contrast, the export of messenger (m) RNAs is regulated differently and relies on a karyopherin-independent transport receptor that does not directly depend on the RAN-GTP gradient (Köhler and Hurt, 2007; Stewart, 2007; Williams *et al.*, 2018). In yeast and vertebrates, essential evolutionarily conserved heterodimeric mRNA export receptors are the mRNA export factor 67–mRNA transport regulator 2 (Mex67–Mtr2) in *Saccharomyces cerevisiae* and the Tap–p15 (also called NXF1–NXT1) in humans that are capable to directly interact with FG-NUPs in the nuclear pore (Segref *et al.*, 1997; Katahira *et al.*, 1999; Guzik *et al.*, 2001).

Mature mRNA molecules are synthesized by RNA polymerase II (RNAPII) as precursor mRNAs (pre-mRNAs) and are processed in the nucleus of eukaryotic cells before being transported into the cytosol for translation. mRNA processing includes capping at the

5' ends, splicing and cleavage/polyadenylation at the 3' ends and adds an additional layer of regulation to the whole process of gene expression (Hocine *et al.*, 2010). During mRNA processing, a multitude of RNA-binding proteins (RBPs; e.g. the mammalian or *A. thaliana* genome encodes for over 600 and over 200 different RBPs, respectively) are co-transcriptionally coupled with the nascent mRNA transcripts to form mature export-competent ribonucleoprotein particles (RNPs). RBPs possess several conserved motifs and domains that enable the proteins to interact with RNA (Lorković, 2009; Müller-Mcnicoll and Neugebauer, 2013; Mitchell and Parker, 2014). The RNP assembly is orchestrated by the carboxy-terminal domain (CTD) of RNAPII and associated factors (Tutucci and Stutz, 2011; Bentley, 2014). The THO/TREX (TRanscription-EXport) is a conserved protein complex found in various species including *Arabidopsis* and an important component that couples transcription with RNA processing and mRNA export. The plant mRNA export machinery is illustrated in Figure 3.

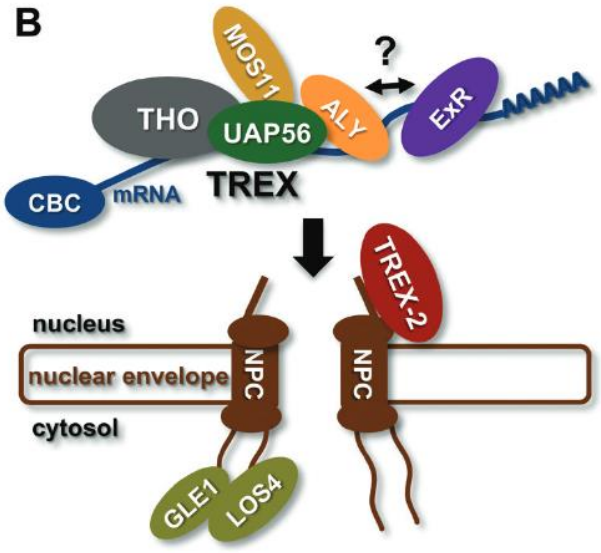

Figure 3: Schematic representation of the plant mRNA export machinery. Inside the nucleus, the mRNA is processed before being exported into the cytosol. A processed mRNA is spliced and possesses a cap-binding complex (CBC) at the 5'-end as well as a poly(A) tail at the 3'-end. Export factors including the THO/TREX complex are recruited to the nascent mRNPs by the splicing machinery. The RNA helicase UAP56 facilitates the interaction of MOS11 and export adaptors, such as ALYs. These export adaptors are proposed to be required for the recruitment of a yet unknown plant export receptor (ExR). The export-competent RNPs are translocated through the nuclear pore complex (NPC). The function of the plant TREX-2 complex in this process is not fully understood. On the cytoplasmic site of the NPC, the ATP-dependent RNA helicases LOS4 and GLE1 triggers the dissociation of export factors from the mRNPs and preventing thereby a return back into the nucleus. CBC, cap-binding complex; MOS11, MODIFIER OF SNC1, 11. ExR, unknown export receptor; TREX-2, mRNA export complex; NPC, nuclear pore complex; GLE1, RNA helicase; LOS4, LOW EXPRESSION OF OSMOTICALLY RESPONSIVE GENES4. The figure was taken from Ehrnsberger *et al.*, 2019.

In *Arabidopsis*, the DEAD-box RNA Helicase UAP56 interacts with the nucleoporin MODIFIER OF SNC1, 11 (MOS11) and further mRNA export factors such as ALY2 to form

the plant TREX complex (Kammel *et al.*, 2013; Sørensen *et al.*, 2017). In yeast, the complex travels together with the RNAPII along the transcribed gene and facilitates mRNP assembly while in metazoans the TREX complex is recruited to the nascent mRNPs by the splicing machinery (Katahira *et al.*, 1999; Yelina *et al.*, 2010; Katahira, 2012; Heath *et al.*, 2016). There are several lines of evidence indicating that components of the THO/TREX complex in plants are also essential for proper mRNA export (Xu *et al.*, 2015; Sørensen *et al.*, 2017). In yeast and vertebrates, mRNPs are directly guided through the NPC via interaction of mRNA export receptors that bind to the mRNPs and interact with FG-repeat containing NUPs localized inside the NPC and the mRNA export complex TREX-2. This complex which is localized on the nuclear side of the NPC is conserved among yeast and metazoan. The TREX-2 complex provides a docking platform for mRNA export receptors (Katahira, 2012; Heath *et al.*, 2016) and is proposed to be involved in gene regulation (Cheng *et al.*, 2018; Stewart, 2019). In 2010, the *Arabidopsis* TREX-2 complex was described, but still neither the composition nor its function in mRNA export is fully clear (Lu *et al.*, 2010; Sørensen *et al.*, 2017; Pfab *et al.*, 2018). On the cytoplasmic site of the NPC, an mRNP remodeling machinery dissociates the export factors from the mRNP, thus preventing a return back into the nucleus and conferring directionality to the mRNA export (Katahira, 2012; Björk and Wieslander, 2014; Katahira, 2015). In yeast, the DEAD-box ATP-dependent RNA helicase Dbp5, localized to the cytoplasmic side of the NPC, triggers the release of mRNP associated proteins such as Mex67 for translation in the cytoplasm, thereby ensuring transport directionality. In *Arabidopsis*, the DEAD-box RNA helicase LOW EXPRESSION OF OSMOTICALLY RESPONSIVE GENES4 (LOS4) was identified as homologue of Dbp5 (Gong *et al.*, 2005; Lund and Guthrie, 2005). It was shown that LOS4 is activated by the mRNA export factor GLE1 (Lee *et al.*, 2015). The energy for mRNA export is provided by ATP while protein transport depends on the RAN-GTP gradient.

mRNAs that are aberrantly formed during nuclear processing are degraded. Several pathways of eukaryotic mRNA decay have been described, that can be either deadenylation-dependent or independent. In the case of deadenylation-dependent mRNA decay, various mRNA deadenylases catalyse the deadenylation of the 3′ end of the poly(A) tail. It was proposed that the constitution of the RNP substrate influences which deadenylases is involved. However, this mechanism is not well understood (Schoenberg and Maquat, 2012). Deadenylated mRNAs are further processed by either removal of the 5‘ cap structure to allow 5′→3′ digestion by a exonuclease or are degraded in a 3′→5′ direction by the cytoplasmic exosome (Parker and Song, 2004; Garneau *et al.*, 2007; Schoenberg and Maquat, 2012; Łabno *et al.*, 2016). In yeast and vertebrates, the exonuclease XRN1 was described to mediate the 5′→3′ decay. In *Arabidopsis* XRN4 was proposed as functional homolog of XRN1, however the exact function of *At*XRN4 in mRNA decay is not completely

understood (Jinek *et al.*, 2011; Rymarquis *et al.*, 2011; Jones *et al.*, 2012; Nagarajan *et al.*, 2013). Decapping enzymes harbor the two catalytic subunits DCP1 and DCP2 that facilitate the process of 5‘ cap removal (Li and Kiledjian, 2010). Alternatively, endonuclease cleavage can initiate the degradation of specific mRNAs, which is a deadenylation-independent way of mRNA decay, followed by 5′→3′ or 3′→5′ degradation (Dodson and Shapiro, 2002; Schoenberg, 2011). Further pathways are the nonsense-mediated decay (NMD) or the nonstop decay (NSD) where either RNAs containing a premature translational stop codon (“nonsense transcripts“) or mRNAs lacking codons for translational termination are recognized and degraded (Parker and Song, 2004; Garneau *et al.*, 2007; Schoenberg and Maquat, 2012). The mRNA decay mechanisms play a key role in gene expression by regulating mRNA turnover. In addition, many other processes of the RNA metabolism including RNA splicing, polyadenylation, capping, transport or stability have an important role for gene regulation. RNA metabolism is mediated by diverse RNA-binding proteins (RBPs), which can influence the stability, translation, and location of the RNA (Keene, 2007; Glisovic *et al.*, 2008; Ray *et al.*, 2013).

Members of the Pumilio RNA-binding protein family (PUF family) are RBPs that are predominately involved in post-transcriptional processes including RNA decay (Wang *et al.*, 2018a). The PUF family is a conserved family of proteins that can be found in various eukaryotic organisms including yeast, humans and plants (Wickens *et al.*, 2002; Spassov and Jurecic, 2003; Tam *et al.*, 2010). The amount of genes that encode for PUF proteins varies among species. In *Arabidopsis*, 26 PUF proteins are described that are referred to as Pumilio Protein 1 to Pumilio Protein 26 (PUM1 to PUM26; Wickens *et al.*, 2002; Francischini and Quaggio, 2009; Tam *et al.*, 2010; Wang *et al.*, 2018a). In general, PUF proteins possess a conserved PUF/Pumilio homology domain (PUM-HD) that is composed of eight tandem repeats. PUM proteins bind specific regulatory *cis*-elements in the 3’ untranslated region (3’UTR) of their target mRNAs which are defined as PUM Response Elements (PREs). The binding to these regulatory elements governs decay and translational repression of their mRNA targets. Furthermore, it can lead to the recruitment of microRNAs and indirectly facilitates stability of long noncoding RNAs (Wickens *et al.*, 2002; Tam *et al.*, 2010; Friend *et al.*, 2012; Miles *et al.*, 2012; Lee *et al.*, 2016). The functional role of PUF proteins was mostly studied in *Saccharomyces cerevisiae*, *Caenorhabditis elegans* and *Drosophila melanogaster*, whereas much less is known in plants including *Arabidopsis* (Wang *et al.*, 2018a). For certain yeast, nematode, fly and human PUMs it has been shown that they preferentially interact with a certain subset of mRNA targets (Gerber *et al.*, 2004; Bernstein *et al.*, 2005; Gerber *et al.*, 2006; Uyhazi *et al.*, 2019) which indicates that individual PUF proteins might be involved in coordinating certain cellular processes. Interestingly, recent studies on the human pumilio proteins, PUM1 and PUM2 revealed that both PUMs do

not only repress translation as expected and described previously for this class of proteins, but also enhance translation (Uyhazi *et al.*, 2019). In fact, effected mRNA targets of human PUM1 and PUM2 are involved in cancer, neurological disorders and cardiovascular disease (Bohn *et al.*, 2018).

The data described above illustrate that the NPC associated proteins and RBPs, which are involved for example in the translocation of macromolecules such as proteins and RNAs between the nucleus and the cytoplasm, are indispensable for cellular signaling processes and gene regulation in eukaryotic cells. Accordingly, the NPCs and the nuclear transport machinery are of crucial importance for hormone signalling as described in the previous session (1.2) and for immune responses in eukaryotes including plants.

1.4 The role of nucleocytoplasmic transport in plant immunity

In *Arabidopsis*, several components that are associated with plant immunity and contribute to nucleocytoplasmic trafficking have been identified in a genetic mutant screen that aimed to identify suppressors of the auto-immune phenotype of *suppressor of npr1-1, constitutive1* (*snc1)* plants. SNC1 is a TIR-type NLR protein. A gain of function mutation in the *SNC1* gene leads to an amino acid exchange from glutamate (E) to lysine (K) in the linker region between the NB and LRR domain of SNC1. This $E_{552}K$ mutation results in constitutive defence gene expression, accumulation of SA without pathogen interaction, as well as enhanced resistance towards pathogens including the hemi-biotrophic bacterium *P. syringae* and the biotrophic oomycete *Hyaloperonospora arabidopsidis*. Furthermore, *snc1* mutant plants show a stunted morphology in comparison to wild-type plants (Li *et al.*, 2001; Zhang *et al.*, 2003). This stunted morphology is caused by constantly activated immunity responses that compromise growth fitness. From the *snc1* suppressor screen, several mutants have been identified that either partially or fully abolish the constitute immune responses of *snc1* mutant plants and were referred to as *MODIFIER OF SNC1* (*MOS*). The MOS proteins that have been characterized so far are involved in several cellular functions and processes including nucleocytoplasmic transport, control of epigenetic gene expression, RNA processing, protein modification as well as plant immunity (Zhang and Li, 2005; Goritschnig *et al.*, 2007; Palma *et al.*, 2007; Cheng *et al.*, 2009; Li *et al.*, 2011; Xu *et al.*, 2011; Xu *et al.*, 2012; Copeland *et al.*, 2013).

MOS6 (*MODIFIER OF SNC1, 6*) encodes for IMPORTIN-α3, which is one of the nine importin-α isoforms in *Arabidopsis,* and contributes to basal disease resistance (Palma *et al.*, 2005; Wirthmueller *et al.*, 2015). IMPORTIN-α3/MOS6 acts as nuclear transport adapter for the NLR proteins TN13 and SNC1, indicating that IMPORTIN-α3/MOS6 contributes to R-mediated resistance. Accordingly, MOS6 is selectively required for autoimmunity of *snc1*

among the nine α-importins in *Arabidopsis* (Palma *et al.*, 2005; Roth *et al.*, 2017; Lüdke *et al.*, 2018; Lüdke *et al.*, 2020). MOS7 is the *Arabidopsis* homologue of the vertebrate nucleoporin 88 (NUP88), that is required for basal and R protein-mediated resistance as well as for constitutive resistance mediated by *snc1*. *Arabidopsis mos7-1* single mutants show elevated nuclear export rates of important immune regulators such as EDS1, NPR1, MPK3 and SNC1, illustrating the important role of MOS7 in the nuclear retention of certain immune regulators (Cheng *et al.*, 2009; Genenncher *et al.*, 2016). Whereas MOS7 is involved in regulating nuclear protein export, MOS11, which is homologous to the human RNA binding protein CIP29, has a critical role in mRNA export in *Arabidopsis*. MOS11 interacts directly with the DEAD-box RNA Helicase UAP56 and together with mRNA export factors (e.g. ALY2) it forms the plant TREX complex (Kammel *et al.*, 2013; Sørensen *et al.*, 2017). The complex contributes to the shuttling of mature mRNA from the nucleus to the cytoplasm (Figure 3). Accordingly, *Arabidopsis mos11* single mutants exhibit nuclear accumulation of polyadenylated mRNA (Germain *et al.*, 2010; Kammel *et al.*, 2013; Sørensen *et al.*, 2017). Another component of the MOS11-dependent nuclear mRNA export pathway in *Arabidopsis* is MOS3, the homologue of vertebrate NUP96 and yeast C-NUP145p (Zhang and Li, 2005). In vertebrates, NUP96 is involved in immune responses. *NUP96* defective mice show export defects for a specific subset of mRNAs that encode for interferon-regulated genes which are part of the regulatory network of innate and acquired immunity in mice (Faria *et al.*, 2006). Consistently, *Arabidopsis* MOS3/NUP96 is required for basal plant defence, TIR-type NLR-mediated immunity as well as *snc1*-mediated auto-immunity (Zhang and Li, 2005; Wiermer *et al.*, 2012).

MOS3/NUP96 was also identified in another genetic screen for suppressors of the *auxin-resistant1* (*axr1*) mutant that display reduced auxin responses and auxin-regulated growth and developmental defects and is referred to as SUPPRESSOR OF AUXIN RESISTANCE 3 (Del Pozo *et al.*, 1998; Del Pozo *et al.*, 2002; Parry *et al.*, 2006). The heterodimer AXR1-ECR1 activates the RELATED TO UBIQUITIN1 (RUB1) protein. The RUB1 conjugation and deconjgation of canonical cullin protein CUL1 which is part of the SCF^{TIR1} complex regulates its activity. The SCF^{TIR1} complex facilitates the degradation of auxin-response pathway repressors via the proteasome. This process regulates normal auxin responses in the plant (Gray and Estelle, 2000; Dharmasiri and Estelle, 2002; Moon *et al.*, 2004). In addition, *mos3/nup96/sar3* mutant plants exhibit mild pleiotropic growth defects including an early flowering phenotype (Parry *et al.*, 2006; Wiermer *et al*., 2012). Similar to vertebrates and yeast, and consistent with its predicted localization to the NPC, GFP-tagged *Arabidopsis* NUP96/MOS3/SAR3 is localized to the NPC (Zhang and Li, 2005; Parry *et al.*, 2006; Germain *et al.*, 2010). As it has been shown for vertebrate *nup96*, *mos3/sar3* mutants also accumulate polyadenylated RNA within the nucleus, suggesting that NUP96/MOS3/SAR3 is

involved in nuclear mRNA export (Faria *et al.*, 2006; Parry *et al.*, 2006; Wiermer *et al.*, 2012). MOS3 appears to function downstream of MOS11 in the same mRNA export pathway and to have a partially overlapping role with MOS11 (Germain *et al.*, 2010; Dong *et al.*, 2011). Moreover, NUP96/MOS3/SAR3 has been identified as constituent member of the NUP107-160 complex.

1.5 The composition and function of the plant NUP107-160 complex

The evolutionary conserved NUP107-160 complex (called the NUP84 complex in yeast) is also referred to as the Y-complex and is the largest subunit of the NPC (Von Appen *et al.*, 2015; Stuwe *et al.*, 2015). The NUP107-160/NUP84 complex is symmetrically distributed to the cytoplasmic and nucleoplasmic side of the NPC, builds the structural scaffold in the NPC and can be found in all eukaryotes (Figure 4; Harel *et al.*, 2003; Walther *et al.*, 2003; Tran and Wente, 2006; Alber *et al.*, 2007).

The plant NUP107-160 complex is constituted of eight nucleoporins: NUP96/MOS3/SAR3, NUP160/SAR1, NUP133, NUP107, NUP75/NUP85, NUP43, SECRETORY13 (SEC13) and SEC13 HOMOLOGUE1 (SEH1) (Xu and Meier, 2008; Tamura *et al.*, 2010; Wiermer *et al.*, 2012; Tamura and Hara-Nishimura, 2013; Meier *et al.*, 2017). In *Arabidopsis*, two genes encode for SEC13, named *At*SEC13A and *At*SEC13B (Hino *et al.*, 2011).

Previous research in vertebrates provides evidence that SEH1 might be not permanently associated with the NUP107-160 complex (Loïodice *et al.*, 2004; Zuccolo *et al.*, 2007). In *Arabidopsis*, SEH1 exhibits a nuclear-cytoplasmic subcellular localization in addition to its localization to the nuclear rim, indicating that part of the cellular pool of SEH1 might also not be permanently associated with the plant NUP107-160 complex (Roth and Wiermer, 2012; Wiermer *et al.*, 2012). Besides being a member of the NUP107-160/NUP84 complex, SEC13 also mediates protein trafficking from the ER to the Golgi apparatus in eukaryotes including plants (Leksa and Schwartz, 2010; Hino *et al.*, 2011). This might also indicate that the whole cellular pool of SEC13 is not permanently associated with the NUP107-160 complex.

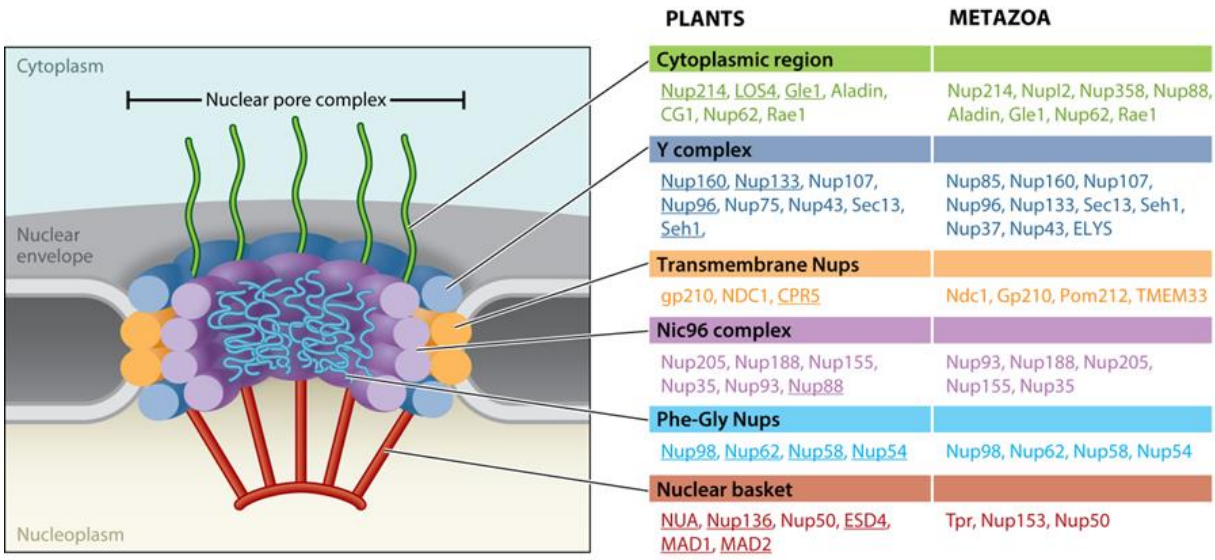

Figure 4: Constituent member of the plant nuclear pore complex (NPC) and nuclear pore-associated proteins. A schematic view of the NPC composed of several sub-complexes (colour-coded, see below) is depicted on the left. List of the constituent nucleoporin members in the plant and metazoan NPC is shown on the right. Metazoan nucleoporins (NUPs) are grouped accordingly to Knockenhauer and Schwartz (2016). Plant NUPs and nuclear pore-associated proteins are assigned to particular sub-complexes based on yeast and metazoan NPCs. Sub-complexes are colour-coded in the following way: cytoplasmic region (green), NUP107-160 complex (plants) / Y complex (metazoan) (dark blue), transmembrane NUPs (orange), Nic96 complex (purple), Phe-Gly NUPs (light blue), and nuclear basket (auburn). Proteins that have been functionally analysed in plants are underlined. Figure adapted from Meier *et al.* (2017).

Previous studies in yeast and vertebrates illustrates that the NUP107-160/NUP84 complex is essential for NPC assembly, kinetochore assembly and function as well as for DNA damage repair (Walther *et al.*, 2003; Loïodice *et al.*, 2004; Zuccolo *et al.*, 2007; Nagai *et al.*, 2008; Platani *et al.*, 2009). In plants, members of the NUP107-160 complex are involved in various cellular processes including plant immune responses, microbial symbiosis, hormone signalling, abiotic stress responses and flowering (Zhang and Li, 2005; Dong *et al.*, 2006; Parry *et al.*, 2006; Jacob *et al.*, 2007; Saito *et al.*, 2007; Groth *et al.*, 2010; Robles *et al.*, 2012; Wiermer *et al.*, 2012; Ohtsu *et al.*, 2014; Zhu *et al.*, 2017).

Several *nucleoporin* mutants display an early flowering phenotype which also includes *nup96/mos3* and *nup160/sar1* mutant plants (Dong *et al.*, 2006; Parry *et al.*, 2006; Wiermer *et al.*, 2012). Recent studies showed that MOS3/NUP96 and NUP160/SAR1, together with the E3 ubiquitin ligase HOS1, are involved in the regulation of flowering time in *Arabidopsis* (Cheng *et al.*, 2020; Li *et al.*, 2020).

Notably, three of the eight *Arabidopsis* NUP107-160 complex members show defence-related functions including NUP160/SAR1, SEH1 and NUP96/MOS3/SAR3 (Zhang and Li, 2005; Wiermer *et al.*, 2012). Furthermore, another member, NUP75/NUP85 is implicated in disease resistance in tobacco (Ohtsu *et al.*, 2014). Similar to NUP96/MOS3/SAR3, NUP160/SAR1 and SEH1 are also required for basal disease resistance and are implicated

in TIR-type NLR mediated resistance as well as for autoimmunity of *snc1* in *Arabidopsis*. However, it was shown that NUP160, in comparison to SEH1, plays a more important role in TIR-type NLR mediated resistance and autoimmunity *of snc1* (Roth and Wiermer, 2012; Wiermer *et al.*, 2012). As it has been reported for *nup96/mos3/sar3*, *nup160/sar1* and *seh1* mutant plants also accumulate polyadenylated mRNA inside the nucleus, indicating that NUP160/SAR1 and SEH1, like NUP96/MOS3/SAR3, have a function in nuclear mRNA export (Parry *et al.*, 2006; Roth and Wiermer, 2012; Wiermer *et al.*, 2012). Interestingly, *nup160* mutant plants exhibit reduced transcript abundance of the defence regulator *EDS1*, suggesting that NUP160 is required for the full gene expression of *EDS1* (Wiermer *et al.*, 2012).

The findings summarised above illustrate how important the nucleocytoplasmic transport machinery is for cellular processes, including plant defence responses and that NUPs are involved in the regulation of gene expression.

1.6 Aim of the study

Arabidopsis MOS3/NUP96 and NUP160 are constituent members of the evolutionally conserved NUP107-160 complex, which is the largest sub-complex of the NPC. Both, MOS3/NUP96 and NUP160 are required for basal defence to *Pseudomonas syringae* and *Hyaloperonospora arabidopsidis*, auto-immunity of *snc1* and resistance conditioned by TIR-type NLR immune receptors (Zhang and Li, 2005; Wiermer *et al.*, 2012). Furthermore, *mos3/nup96* and *nup160* mutant plants display defects in mRNA export (Dong *et al.*, 2006; Parry *et al.*, 2006; Muthuswamy and Meier, 2011; Wiermer *et al.*, 2012). In addition, *nup160* mutants show reduced transcript abundance of the key defence regulator *EDS1,* indicating that *NUP160* is essential for full *EDS1* gene expression (Zhang and Li, 2005; Parry *et al.*, 2006; Roth and Wiermer, 2012; Wiermer *et al.*, 2012).

Previous published and unpublished data indicate that *mos3* and *nup160* are impaired in the expression of certain defence genes including *EDS1* that may contribute to the immunity defects of *mos3* and *nup160* mutant plants*.* The major aim of this study was to conduct an RNAseq-based transcriptome analysis of *mos3/nup96* and *nup160* mutant plants to investigate changes in gene expression on a genome-wide level. Promising candidate genes that show reduced expression in *mos3* and *nup160* mutant plants as compared to Col-0 wild-type should be characterized with regard to their potential function in plant immunity.

Since previous preliminary data suggests that the PPR gene *EFR* shows reduced expression in *mos3* and *nup160* mutant plants, another aim of this study was to investigate phenotypic consequences of decreased *EFR* transcript abundance in both nucleoporin mutants.

2 Material and Methods

The Material and Methods part is subdivided into two sections. The Material part (2.1) provides information about plant material, bacteria, fungi, vectors, oligonucleotides, enzymes, antibiotics, antibodies, chemicals, media, buffer and solutions that were used in this study. In the Methods part (2.2) detailed information about the conduced methods used in this study are listed.

2.1 Material

2.1.1 Plant material

2.1.1.1 *Arabidopsis thaliana*

A. thaliana accession Columbia-0 (Col-0) was used as wild type accession (Table 1). T-DNA insertion lines from the SALK collection (Alonso *et al.*, 2003), SAIL collection (Sessions *et al.*, 2002) and the GABI-KAT collection (Kleinboelting *et al.*, 2012) were ordered from the Nottingham Arabidopsis Stock Centre (NASC; Scholl *et al.*, 2000) and are listed in Table 2. Information about *A. thaliana* crosses and transgenic lines are listed in Table 3 and Table 4.

Table 1: *A. thaliana* wild-type accession used in this study.

Accession	Abbr.	Reference / Source
Columbia	Col-0	J. Dangl[1]

[1]University of North Carolina, Chapel Hill, NC, USA

Table 2: *A. thaliana* single mutant lines used in this study.

Gene name	AGI locus	Accession	Mutagen / T-DNA	Reference/Source
mos3-1	AT1G80680	Col-0	fast neutron mutagenesis, point mutation	Zhang and Li, 2005
mos3-2	AT1G80680	Col-0	SALK_109959, T-DNA insertion	Zhang and Li, 2005
nup160-3	AT1G33410	Col-0	SAIL_877_B01, T-DNA insertion	Wiermer *et al.*, 2012
nup160-4	AT1G33410	Col-0	SALK_126801,	Wiermer *et al.*,

			T-DNA insertio	2012
sec13b-1	AT3G01340	Col-0	SALK_045825, T-DNA insertion	Wiermer *et al.*, 2012
efr-1	AT5G20480	Col-0	Salk_044334, T-DNA insertion	G. Felix[2]
Col *fls2*	AT5G46330	Col-0	SAIL_691_C4, T-DNA insertion	Zipfel *et al.*, 2004
cerk1-2	AT3G21630	Col-0	GABI_096F09; T-DNA insertion	Miya *et al.*, 2007
mes18-1	AT5G58310	Col-0	SALKseq_067028	NASC_ N924207
pum9-1	AT1G35730	Col-0	GK-152E12.04	Nyikó *et al.*, 2019 NASC_ N397865
pum9-2	AT1G35730	Col-0	SALK_135897	Nyikó *et al.*, 2019 NASC_ N677658
Col *eds1*-2	AT3G48090	Col-0	fast neutron mutagenesis	Bartsch *et al.*, 2006
ndr1-1	AT3G20600	Col-0	fast neutron mutagenesis	Century *et al.*, 1997

[2] University of Tübingen, Tübingen, Germany
[3] Nottingham *Arabidopsis* Stock Centre, Nottingham, UK

Table 3: *A. thaliana* crosses used in this study.

Abbreviation	Reference
promEFR::EFR-eGFP-HA x *mos3-2*	double mutant was generated in this study by crossing
promEFR::EFR-eGFP-HA x *nup160-3*	double mutant was generated in this study by crossing

prom: endogenous promoter

Table 4: Transgenic *A. thaliana* lines used in this study.

Background	Construct	Reference
efr-1	promEFR::EFR-eGFP-HA	Nekrasov *et al.*, 2009

prom: endogenous promoter; g: genomic

2.1.1.2 *Nicotiana benthamiana*

N. benthamiana wild-type seeds were originally obtained from T. Romeis (Max-Planck-Institute for Plant Breeding Research, Cologne, Germany) and used for transient *Agrobacterium tumefaciens*-mediated leaf transformation.

2.1.2 Pathogens

2.1.2.1 *Pseudomonas syringae* pv. *tomato* (*Pst*)

The *Pseudomonas syringae* pv. *tomato* (*Pst*) strain DC3000 harbouring empty pVSP61 vector (Innes *et al*., 1993) or expressing the avirulence determinants *avrRps4* (Hinsch and Staskawicz, 1996) or *avrRpm1* (Grant *et al.*, 1995) was used in this study to infect *Arabidopsis* leaves. The *Pst* isolates were originally obtained from R. Innes (Indiana University, Bloomington Indiana, USA).

2.1.3 Bacterial strains (used for cloning approaches, transient expression and generation of stabile transgenic *Arabidopsis* plants)

2.1.3.1 *Escherichia coli*

For plasmid amplification the chemically competent *Escherichia coli* (*E. coli*) strain TOP10 was used in this study (Invitrogen™, Karlsruhe, Germany). The strain harbours the following genotype: F^- *mcr*A Δ(*mrr-hsd*RMS-*mcr*BC) Φ80*lac*ZΔM15 Δ*lac*X74 deoR *rec*A1 *ara*D139 Δ(*ara-leu*)7697 *gal*U *gal*K *rps*L (Str^R) *end*A1 *nup*G. For heterologous protein expression, the *E. coli* Rosetta 2 (DE3) pLysS strain (Invitrogen™, Karlsruhe, Germany) was used.

2.1.3.2 *Agrobacterium tumefaciens*

For generation of stabile transgenic *Arabidopsis* plants, the electro competent *Agrobacterium tumefaciens* (*A. tumefaciens*) strain GV3101 (Koncz and Schell, 1986) was used. Depending on the construct that are transformed into the *A. tumefaciens* strain, two different strains were used that either harbours the helper plasmid pMP90RK, which confers resistance to kanamycin (Koncz and Schell, 1986) or pSoup, which confers resistance to tetracyclin (Hellens *et al.*, 2000). The *A. tumefaciens* GV3101 pMP90RK strain was used for transient expression of constructs in *N. benthamiana*.

2.1.4 Vectors

Table 5: Vectors used in this study.

Construct name	Use and Description
pET28a (+) MES18	Heterologous expression of AT5G58310 (MES18) in *E. coli*
pXCSG GUS-intron::3xHA-StrepII	Binary Gateway® destination vector with a β-glucuronidase (GUS)-intron reporter gene with a C-terminal 3xHA-StrepII-tag is expressed under the control of a *35SS* promoter for plant-specific expression.

2.1.5 Oligonucleotides

The Oligonucleotides used in this study were designed with the Geneious™ software version 8.1.8 (Biomatters Ltd., Kearse *et al*., 2012) and ordered from Invitrogen™ (Karlsruhe, Germany). The lyophilized primers were diluted with ultrapure water to a stock-concentration of 100 µM (100 pmol/µl). For standard usage, 10 µM (10 pmol/µl) dilutions were prepared. For quantitative real time PCR, the stock solutions (100 pmol/µl) were diluted to 4 µM (4 pmol/µl) working solutions. The oligonucleotides were stored at -20°C. Table 6 shows all primers used in this study.

Table 6: Oligonucleotides used in this study.

Abbreviation.	Sequence [5'→3']	Use
Primers for cloning		
DH131 (forward)	CGGAATTCAGTGAGCATCATTTTGTGTTTG	Amplification of g AT5G58310 (*MES18*) with *Eco*RI and *Not*I restriction site from Col-0 cDNA for cloning into pET28a (+) vector
DH132 (reverse)	CGCGGCCGCTCAGGGAGAAAGAGATGAG GC	
DH149 (forward)	ATATATGGTCTCTGATTGGAATGTGATGTA CGAGAAGGTTTTAGAGCTAGAAATAGCAAG	Generation of CRISPR/Cas9 k.o. in AT5G58310 (*MES18*) target site 1
DH150 (reverse)	ATTATTGGTCTCTAAACCAGGGCCAACATT	

	ACCTCTTCAATCTCTTAGTCGACTCTACC	
DH151 (forward)	ATATATGGTCTCTGATTGTTTGTGTTTGTGC ATGGTGCGTTTTAGAGCTAGAAATAGCAAG	Generation of CRISPR/Cas9 k.o. in AT5G58310 (*MES18*) target site 2
DH152 (reverse)	ATTATTGGTCTCTAAACGACAGTGACCACT CTGCTTTCAATCTCTTAGTCGACTCTACC	
Primers for sequencing		
DH119 (forward)	CTGCCAATGTGTAAGCGACTAG	Sequencing of gAT5G58310 (*MES18*)
DH120 (forward)	CGAGAAGAGGATTAAAGATGAGTG	
MW6 (forward)	GTAAAACGACGGCCAG	M13 fwd. and rev. primer for sequencing and Colony-PCR
MW7 (reverse)	CAGGAAACAGCTATGAC	
Primers for expression analysis		
DH47 (forward)	AGGACCTGTTCGTGCTAAATTGG	AT1G35730 (*PUM9*) mRNA for qRT-PCR
DH48 (reverse)	TCTTGCAGTAAGGGCTCGAGTG	
DH124 (forward)	ACCAAACCCGAAGAACAGTTCC	
DH126 (reverse)	CAATCATCTTCTGCACAACCC	AT1G35730 (*PUM9*) mRNA for semi-quantitative RT-PCR
DH127 (forward)	TGCTATTCATCGACACGGATGC	
DH130 (reverse)	GCTCGAGTGTAGTTTCCCGTAC	
DH51 (forward)	AAACCTGAGTATGTTCGGGACAAG	AT5G58310 (*MES18*) mRNA

DH52 (reverse)	GTGGTTGCCAGTGTGTAATCCTC	for qRT-PCR
DH108 (forward)	CTATGCCTTCCTCTCCCAACTTC	*MES18* mRNA (AT5G58310) for semi-quantitative RT-PCR
DH109 (reverse)	CGGACGCAGAAGTGTGGTTG	
DH121 (forward)	GTGTTTGTGCATGGTGCAGG	
MW12 (forward)	ACGTATCGATGTCTATTTCAACG	AT5G44340 (*TUBULIN*4) mRNA for semi-quantitative RT-PCR
MW13 (reverse)	ATATCGTAGAGAGCCTCATTGTCC	
MW185 (forward)	GACGCTTCATCTCGTCC	AT3G62250 (*UBIQUITIN5*) mRNA for qRT-PCR
MW186 (reverse)	GTAAACGTAGGTGAGTCCA	
MW191 (forward)	TTCCGGTGTATTCACCACCCTGTC	AT1G79530 *(GAPCp-1)* mRNA for qRT-PCR
MW192 (reverse)	TAACTTTCTTGGCACCGCCCTTC	
MW306 (forward)	CGGATGAAGCAGTACGAGAA	AT5G20480 (*EFR*) mRNA for qRT-PCR
MW307 (reverse)	CCATTCCTGAGGAGAACTTTG	
MW183 (forward)	GCTCAATGACCTTGGAGTGAGC	AT3G48090 (*EDS1A*) mRNA for qRT-PCR
MW184 (reverse)	TCTTCCTCTAATGCAGCTTGAACG	
MW344 (forward)	TCGGATTCTAGGTTTCCGCGAAG	AT5G46330 (*FLS2*) mRNA for qRT-PCR
MW345 (reverse)	ACCCTCGAAGGCTGATGTTGAAG	

MS122 (forward)		TCGAAACAGTTCTTGGCGGAAC	AT3G21630 (*CERK1*) mRNA for qRT-PCR
MS123 (reverse)		CAATATCCAATCAGGCGAACC	
Primers for genotyping			
MW10		ATTTTGCCGATTTCGGAAC	T-DNA primer SALK-LBb1.3 for PCR
MW11		CGTCCGCAATGTGTTATTAAG	T-DNA primer SAIL.1F for PCR
DH65		ATAATAACGCTGCGGACATCTACATTTT	T-DNA primer GABI-KAT for PCR
DH66	LP	CAAAAACAACAGTCTCAGCACATT	Genotyping of GABI_15E12/T-DNA
DH67	RP	AAGATACAGTACTAATCGGT	k.o. in AT1G35730 (*pum9)*
DH74	LP	TAAACAGGACAAGGGTTGTGC	Genotyping of SALK_135897/T-DNA
DH75	RP	GAGCATTGGCCTAAAACACAG	k.o. in AT1G35730 (*pum9)*
DH72	LP	GCTGCTTGAAGGAGGAATTG	Genotyping of SALKseq_067028/T-DNA k.o. in AT5G58310 (*mes18)*
DH73	RP	ATGTGTTTGGGCCTTCAAAG	
DH102 (forward)		GTGAGCAAGGGCGAGGAGC	genotyping for GFP in *efr-1* line transgenic for pEFR-eGFP-HA
DH103 (reverse)		GATGTTGTGGCGGATCTTGAAG	

prom: endogenous promoter; g: genomic

2.1.6 Enzymes

2.1.6.1 Restriction endonucleases

Restriction endonucleases were obtained from Thermo Fisher Scientific (Waltham, USA) or New England BioLabs (NEB, Franktfurt (Main), Germany), respectively. Enzymes were used with the supplied 10x reaction buffers according to the manufacturer's instructions.

2.1.6.2 Polymerases and nucleic acid modifying enzymes

Homemade *Taq* DNA polymerase was used for standard polymerase chain reactions (PCR, 2.2.3.3.1). PCR products for cloning were amplified with the proofreading iProof™ High-Fidelity DNA polymerase (Bio-Rad, Munich, Germany). To perform LR recombination reaction between entry and destination vectors compatible for the Gateway system, the Gateway LR Clonase™ enzyme mix (Invitrogen™, Karlsruhe, Germany) was used. DNase I treatment (Thermo Fisher Scientific, Waltham, USA) was performed to avoid genomic DNA contaminations after RNA extraction (2.2.3.12). cDNA was synthesized from total RNA using the RevertAid™ H Minus Reverse Transcriptase (Thermo Fisher Scientific, Waltham, USA; 2.2.3.13). Enzymes were used with their respective buffer and accordingly to manufacturer's instructions.

2.1.7 Antibiotics

Ampicillin (Amp)	100 mg/mL dissolved in ddH_2O
Carbenicillin (Carb)	50 mg/mL dissolved in ddH_2O
Gentamycin (Gent)	15 mg/mL dissolved in ddH_2O
Kanamycin (Kan)	50 mg/mL dissolved in ddH_2O
Rifampicin (Rif)	100 mg/mL dissolved in DMSO
Chloramphenicol	34 mg/mL in ddH_2O

Aqueous solutions were sterile filtrated. The indicated stock solutions (1000x) were stored at -20°C.

2.1.8 Antibodies

Primary and secondary antibodies used for immunoblot detection are listed below (Table 7). The antibodies were aliquoted and kept at -80 °C for long term storage. Aliquots in use were kept at 4°C.

Table 7: Antibodies used in this study.

	Source	Dilution	Milk	Supplier
Primary antibody				
α-GFP	mouse monoclonal	1:5000	0 %	Roche (Mannheim, Germany)
Secondary antibody				
α-mouse IgG-HRP	goat polyclonal	1:5000	5 %	Thermo Scientific (Waltham, MA, USA)
α-mouse IgG-poly HRP	goat polyclonal	1:5000	5 %	Thermo Scientific (Waltham, MA, USA)

HRP: Horseradish peroxidase

2.1.9 Chemicals

Standard laboratory grade chemicals and reagents used in this study were purchased from
AppliChem GmbH (Darmstad, Germany),
Bio-Rad (Munich, Germany),
BD (Dickinson and Company, Sparks, USA),
Difco (Heidelberg, Germany),
Duchefa (Haarlem, Netherlands),
Fermentas (St. Leon-Rot, Germany),
GE Healthcare (Munich, Germany),
Invitrogen (Karlsruhe, Germany),
Macherey Nagel (Düren, Germany),
Merck (Darmstadt, Germany),
New England BioLabs (NEB) (Frankfurt/Main, Germany),
Roche (Mannheim, Germany),
Roth (Karlsruhe, Germany),
Thermo Fisher Scientific (Waltham, USA),
VWR™ (Darmstadt, Germany; Radnor, USA),

unless otherwise indicated.

2.1.10 Media

The media were prepared accordingly to the recipes below (Table 8) using ultrapure water and autoclaved at 121°C for 20 min. Liquid and solid media were stored at RT. Heat labile compounds such as antibiotics were filter sterilized and added to pre-cooled medium (55°C).

Table 8: Media used in this study.

Medium	Composition	
***E. coli* growth medium**		
Luria-Bertani broth (LB)	Peptone	10.0 g/L
	Yeast extract	5.0 g/L
	NaCl	10.0 g/L
	pH	7.0
	for LB agar plates 1.5 % (w/v) agar (bacterial grade) was added.	
***P. syringae* growth medium**		
NYG broth	Peptone	5.0 g/L
	Yeast extract	3.0 g/L
	Glycerol	20.0 mL/L
	pH	7.0
	for NYG agar plates 1.5 % (w/v) agar (bacterial grade) was added.	
***A. tumefaciens* growth medium**		
Double yeast, tryptone (DYT) medium	Yeast extract	10.0 g/L
	Tryptone	16.0 g/L
	NaCl	10.0 g/L
	pH	7.0
	for DYT agar plates 1.5 % (w/v) agar (bacterial grade) was added.	

***A. thaliana* growth medium**

	½ MS (Murashige and Skoog) + Gamborg vitamins B5	2.2 g/L
	Sucrose	10.0 g/L
	pH	5.8
	for solid ½ MS agar plates 0.75 % (w/v) and for semi- solid ½ MS agar plates 0.2 % (w/v) plant agar (plant grade) was added.	

Transgenic *Arabidopsis* plants harbouring the *phosphinothricin acetyltransferase* (*PAT*) gene that confers Basta® (glufosinate-ammonium) resistance were selected on solid ½ MS agar plates supplied with DL-Phosphinothricin (PPT, 1:1000 from 10 mg/mL stock).

2.1.11 Buffer and Solutions

Table 9: List of buffers and solutions.

Agarose gel electrophoresis and PCR		
Agarose solution	Agarose	1 – 2 % (w/v)
	TAE-Buffer	1x
DNA loading dye (6x)	Xylene xyanole	0.01 % (w/v)
	Orange-G	0.01 % (w/v)
	Bromophenol blue	0.01 %(w/v)
	Glycerol	30 % (w/v)
FTA buffer for punch-PCR (50x)	TRIS	10 mM
	EDTA	2 mM
	Tween 20	0.1 % (w/v)
	pH	7.5 (HCl)
PCR reaction buffer for *Taq* (10x)	TRIS base	100 mM
	KCl	500 mM
	MgCl2	15 mM
	Triton X-100	1 % (w/v)
	pH	9.0 (KOH)

TAE (50x)	TRIS base	2 M
	Glacial acetic acid	57.1 mL/L
	EDTA (0.5 M, pH 8.0)	50 mM
TE buffer for primer/plasmids (1x)	TRIS	10 mM
	EDTA	1 mM
	pH	8.0 (HCl)
TE-1 buffer for punch-PCR	TRIS	10 mM
	EDTA	0.1 mM
Bacterial infiltration		
Agrobacterium infiltration medium	$MgCl_2$	10 mM
	Acetosyringone	150 µM
SDS PAGE and Immunoblot analysis		
Laemmli sample buffer (2x)	TRIS	0.125 M
	SDS	4 % (w/v)
	Glycerol	20 % (w/v)
	Bromophenol blue	0.02 % (w/v)
	DTT	0.2 M
	pH	6.8 (HCl)
Ponceau S solution	Ponceau S	0.2 % (w/v)
	Acetic acid	5 %
Resolving gel buffer (4x)	TRIS	1.5 M
	pH	8.8 HCl
Resolving gel (7.5 %)	H_2O	4.82 mL
	Resolving gel buffer (4x)	2.5 mL
	10 % SDS (pure grade)	0.1 mL
	30 % Acrylamide/Bis solution, 29:1	2.5 mL
	TEMED	5.0 µL

	10 % APS	75 µL
Resolving gel (10 %)	H_2O	4.1 mL
	Resolving gel buffer (4x)	2.5 mL
	10 % SDS (pure grade)	0.1 mL
	30 % Acrylamide/Bis solution 29:1	3.3 mL
	TEMED	5.0 µL
	10 % APS	75 µL
Stacking gel buffer (4x)	TRIS	0.5 M
	pH	6.8 HCl
Stacking gel (4 %)	H_20	6.1 mL
	Resolving gel buffer	2.5 mL
	10 % SDS	0.1 mL
	30 % Acrylamide/ Bis solution, 29:1	1.3 mL
	TEMED	10 µL
	10 % APS	100 µL
Transfer buffer	TRIS	250 mM
	Glycine	40 mM
	SDS	0.0125 % (w/v)
	pH	9.2 (HCl)
	Before use 20 % (v/v) methanol was added.	
Protein extraction buffer	Sucrose	250 mM
	HEPES (pH 7.5)	100 mM
	Glycerol	5 %
	Sodium molybdate	1 mM
	Sodium fluoride	25 mM
	EDTA (0.5 M)	10 mM
	DTT	2 mM
	Triton X-100	0.5 %
	pH	8.3 HCl

	Protease Inhibitor Cocktail (PIC) was added freshly before use	
TBS-T buffer	NaCl	87.6 g/L
	TRIS	12.1 g/L
	Tween® 20	0.5 %
RNA extraction		
High salt precipitation buffer	NaCl	1.2 M
	Tri-sodium citrate dehydrate	0.8 M
TRIzol buffer	Guanidinium thiocyanate	0.8 M
	Ammonium thiocyanate	0.4 M
	Glycerol	5 % (v/v)
	Sodium acetate (3 M, pH 5.0)	33.4 mL/L
	Phenol with 0.1 M saturated citrate solution (pH 4.3)	380 mL/L
Heterologous Expression		
Buffer A	TRIS	50 mM
	NaCl	500 mM
	DTT	1 mM
Buffer B	TRIS	50 mM
	NaCl	50 mM
	Imidazole	500 mM
	DTT	1 mM
Puffer C	TRIS	50 mM
	NaCl	10 mM
ROS Burst		
L-012	Horseradish Peroxidase	10 µg/mL
	L-012	100 µM
		in ddH_20

GUS reporter assay		
GUS staining solution	0.1 M Sodium phosphate (pH 7.2)	12.5 mL
	0.5 M EDTA (pH 8.0)	500 µL
	50 mM $K_3Fe(CN)_6$	250 µL
	50 mM $K_4Fe(CN)_6$	250 µL
	Triton® X-100 (10 %)	500 µL
	X-GlcA (5-Bromo-4-chloro-3-indolyl-β-D-glucuronide cyclohexylammonium salt) in DMSO	25 mg in 500 µL
	dH_20	to 25 mL

Competent *E. coli* cells		
TFB1	KAc	30 mM
	MnCl2	50 mM
	RbCl	100 mM
	CaCl2	10 mM
	glycerol	15 %
	pH	5.8
TFB2	MOPS	10 mM
	CaCl2	75 mM
	RbCl	10 mM
	glycerol	15 %
	pH	7.0

2.2 Methods

2.2.1 Methods for the work with plants

2.2.1.1 Surface sterilization of seeds

After seed harvest, seeds were stored for two days at -20°C to eliminate potential contaminations. This procedure was followed by different methods of surface sterilization depending on the purpose of the seeds.

2.2.1.1.1 Surface sterilization using ethanol

For seeds grown on soil, seeds were surface sterilized with EtOH before use. Seeds were placed in 1.5 mL reaction tube and incubated with 1 mL 70 % EtOH for 5 minutes. Subsequently, two washing steps with 1 mL autoclaved dH_20 were performed. Sterilized seeds were placed in 0.1 % agarose and stored for two days in the fridge to break seed dormancy before being sown on damped soil.

2.2.1.1.2 Surface sterilization using chlorine gas

Transgenic seeds for glufosinate selection were sterilized using chlorine gas before being sown on damped soil. Therefore, seed packages were placed in a desiccator. A glass beaker in the desiccator was filled with 15 mL NaClO. After 5 mL HCl (37 %) was pipetted into the beaker the reaction started and the lid of the desiccator was closed immediately. The seed packages were incubated overnight in the emerging gas. As the gas is harmful, the whole procedure was conducted in a fume hood.

2.2.1.1.3 Surface sterilization for *in vitro* assays

Seeds that were used for *in vitro* assays were washed in several EtOH steps. Therefore, seeds were placed in 1.5 mL reaction tube and incubated with 1 mL 70 % EtOH + 0.05 % Tween 3x for 2 minutes. Subsequently, the seeds were incubated with 1 mL 100 % EtOH 2x for 1 minute. During the washing steps, reaction tubes were rotated and the EtOH was replaced for each new washing step. Next, seeds were placed in 1 mL fresh EtOH (100 %) and put on sterile filter paper until all remaining EtOH was evaporated. Dry seeds were placed on semi solid ½ MS plates.

2.2.1.2 Maintenance and cultivation of plant material on soil

The soil (Frühstorfer Erde, Type T, Archut) that was used in all experiments was steamed prior to use (90°C for 30 min) to avoid soil-born pests and other contaminations. Soil grown plants were cultivated in growth chambers (JC-ESC 300 chamber system, Johnson Controls, Milwaukee, WI, USA).

For *Arabidopsis* plant cultivation, sterilized seeds (2.2.1.1) were sown on steamed soil and grown under short-day conditions (8 h light at 22°C / 16 h darkness at 20°C,

65 % rel. humidity). To promote seed germination, pots were covered with transparent lids for two to three days. For seed production, plants were grown under long-day conditions (16 h light at 22°C / 8 h darkness at 20 °C, 65 % rel. humidity).

Surface sterilized *Nicotiana benthamiana* seeds (2.2.1.1) were sown on steamed soil and grown under long-day conditions (16 h light at 25 °C / 8 h darkness at 20°C, 65 % rel. humidity) for rapid plant growth. For transient expression studies four to six week old plants were used.

2.2.1.3 Plant growth conditions for *in vitro* culture

For *in vitro* selection of *Arabidopsis* transformants (2.2.1.6.2), seeds were sterilized as described in 2.2.1.1.3 and sown on solid ½ MS agar plates containing phosphinothricin (PPT) and grown for approx. ten days in a growth cabinet (CLF Plant Climatics, Wertingen, Germany) under short-day conditions (12 h light, 12 h darkness).

2.2.1.4 Generation of *Arabidopsis* F1 and F2 progeny

Plants were crossed by hand using fine tweezers and magnifying glasses. For crossing only closed flower buds were selected. Three to four inflorescences of the maternal line were chosen. The carpel of the maternal flower was exposed by removal of sepals, petals and stamina. Afterwards, fresh pollen from the chosen parental line was applied onto the dissectematernal stigma. Treated stigmas were labelled and protected in small plastic bags for three to five days. Finally, the seeds of mature siliques were collected and plants of the F1 generation were grown as described earlier (2.2.1.2). Plants were tested for heterozygosity using PCR-based genotyping (2.2.3.3.1) and self-pollination was allowed if success of the crosses was determined.

2.2.1.5 Generation of transgenic *Arabidopsis* plants using the floral dip method

In order to generate stabile transgenic *Arabidopsis* lines the previously described *floral dip* method (Clough and Bent, 1998) was used. Plants were grown under long-day conditions (2.2.1.2) to allow flowering. *Agrobacterium* strains were grown in 5 mL selective DYT medium overnight at 28°C and 180 rpm. Overnight culture was used to inoculate a main culture of 250 mL selective DYT medium. The main culture was grown at the same conditions as the overnight culture. On the next day, cells were harvested in a 500 mL centrifuge cup at 1200 *g* for 20 minutes at RT. The pellet was re-suspended in 5 % sucrose solution. Subsequently, 25 µL Silwet L-77 (final concentration of 0.01 %) was added to the solution. *Arabidopsis* flowers were gently dipped into the *Agrobacterium* solution. Afterwards, *Arabidopsis* plants were bagged and kept in a black plastic bag overnight. On the next day, the plastic bag was removed and plants were grown under long-day conditions (2.2.1.2) to allow seed production.

2.2.1.6 Selection of stably transformed *Arabidopsis* plants

2.2.1.6.1 Glufosinate selection of *Arabidopsis* transformants on soil

First generation transformants were surface sterilized with chlorine gas (2.2.1.1.2) and afterwards sown densely on soil. Seeds were allowed to germinate as described in 2.2.1.2. Approximately five day old seedlings were evenly sprayed with diluted (0.1 %) herbicide Basta® (200 g/L glufosinate ammonium solution, Bayer, Leverkusen, Germany). This procedure was repeated three to four times in two day intervals. Seedlings that were successfully transformed with constructs that harboured a Basta resistance cassette survived the herbicide treatment whereas non-transformed seedlings died. About 24 seedlings per construct were transplanted to single-plant-pots and cultivated for further analyses (2.2.1.2).

2.2.1.6.2 *In vitro* selection of *Arabidopsis* transformants

Segregation pattern of T2 and T3 transgenic *Arabidopsis* plants were analyzed in an *in vitro* selection assay. Seeds were sterilized as described in 2.2.1.1.3 and afterwards c. 100 seeds were placed on ½ MS agar plates containing phosphinothricin (PPT; final concentration of 10 µg/mL). Seedlings were grown for approx. ten days under short-day conditions as described in 2.2.1.3 until positively transformed seedlings could be clearly differentiated form non-resistant seedlings. Transformed single insertion seedlings were transferred onto soil for further propagation (2.2.1.2). T3 seeds were sterilized and grown as described above. Survival of all seedlings on ½ MS agar plates containing PPT indicates homozygosity of the transferred T-DNA.

2.2.2 Methods for the work with bacteria

2.2.2.1 Maintenance and cultivation of *Escherichia coli*

E. coli strains (2.1.3.1) were cultivated either on solid LB agar plates or in liquid LB medium (2.1.10) containing appropriate antibiotics as selection marker. Plate-grown *E. coli* cells were incubated at 37°C overnight and stored afterwards at 4°C. If necessary, bacteria were re-streaked on fresh selective LB plates. Liquid cultures of *E. coli* cells were grown at 37°C and 200 rpm. For heterologous protein expression (2.2.6.5) liquid cultures of *E. coli* cells were grown in a temperature range of 37°C to 16°C while shaking at 200 rpm.

2.2.2.2 Maintenance and cultivation of *Pseudomonas syringae* pv. *tomato* (*Pst*) cultures

The different *Pst* strains (2.1.2.1) were grown on selective NYG agar plates. Every two to three weeks the bacteria were re-streaked on fresh selective NYG plates and incubated at 28°C for two days and stored afterwards in the fridge at 4°C. If necessary bacteria were streaked out freshly from glycerol stocks on new NYG agar plates. Liquid culture of *P. syringae* cells were grown at 28°C and 180 rpm overnight.

2.2.2.3 Maintenance and cultivation of *Agrobacterium tumefaciens* strains

The different *A. tumefaciens* strains (2.1.3.2) were grown on selective DYT agar plates. Every two to three weeks the bacteria were re-streaked on fresh selective DYT plates and incubated at 28°C for three days and stored afterwards in the fridge at 4°C. If necessary bacteria were streaked out freshly from glycerol stocks on new DYT plates. Liquid culture of *A. tumefaciens* cells were grown at 28°C and 180 rpm overnight.

2.2.2.4 Preparation of chemically competent *E. coli* cells

First, *E. coli* TOP10 (2.1.3.1) cells were grown in 5 mL LB-medium at 37°C and 200 rpm overnight. The next day, the overnight culture was used to inoculate 500 mL LB-medium. The main culture was incubated at 37°C and 200 rpm for approx. three hours until the cells reached an OD_{600} of 0.5. Next, the culture was transferred to 50 mL falcon tubes under sterile conditions and put on ice for approx. 15 – 30 minutes. All following steps were performed at 4 C. The cells were centrifuged for 15 minutes at 1200 *g*. The supernatant was discarded and the pellet was carefully resuspended in 80 mL ice cold TFB1 buffer (Table 9) under the sterile bench. The cells were incubated for 15 minutes on ice before the next centrifugation step followed (15 minutes, 1200 *g*). The pellet was re-suspended in 8 mL ice cold TFB2 buffer (Table 9) by carful pipetting under sterile conditions. As a last step, the resuspended pellet was aliquoted (50 µL) and aliquots were frozen in liquid nitrogen before being stored at -80°C.

2.2.2.5 Transformation of chemically competent *E. coli* cells

In order to transform chemically competent *E. coli* TOP10 cells (2.1.3.1 and 2.2.2.4) with the desired plasmids the heat shock method was used (Inoue *et al.*, 1990). Cells were thawed on ice, before up to 1 µg plasmid DNA was added to the cells. After a 10 minute incubation step on ice was performed, a 45 seconds heat shock of 42°C was carried out. Afterwards the cells were put on ice immediately and incubated for 2 minutes. Next, 800 µL LB medium was added and the competent cells were incubated for approx. 60 minutes at 37°C while shaking (200 rpm). After incubation the cells were centrifuged gently for 5 minutes at 3,500 *g* in a table top centrifuge. Nearly all of the supernatant was discarded and the cells were re-suspended gently in circa 50 µL LB medium that was still in the reaction tube. The re-suspended pellet was plated onto selective LB agar plates that were incubated at 37°C overnight.

2.2.2.6 Preparation of electro-competent *A. tumefaciens* cells

A. tumefaciens GV3101 pMP90RK cells (2.1.3.2) were grown as overnight culture in 5 mL DYT medium containing appropriate antibiotics at 28°C and 180 rpm. The whole overnight culture was used to inoculate a main culture of 200 mL liquid DYT medium without any

antibiotics. The main culture was incubated for approx. three hours at 28 C and 180 rpm until bacterial growth reached an OD_{600} of 0.6. All following steps were performed at 4°C and pipetting steps were carried out under sterile conditions in a sterile bench. The main culture was transferred to four sterile 50 mL falcon tubes and subsequently put on ice for approx. 15 – 30 minutes. Next, cells were centrifuged for 15 minutes at 6000 *g*. The supernatant was discarded and the cell pellets were re-suspended in 200 mL ice cold sterile dH_2O. Several centrifugation steps were performed to reduce the volume of the cells. All centrifugation steps were carried out for 15 minutes at 6000 *g*. First, the volume was reduced by half, from 200 mL steril dH_20 to 100 mL sterile dH_20. Next, cells were re-suspended in 5 mL ice cold sterile 10 % glycerol (1/40 volume of the starting culture). Finally, the cell pellet was re-suspended in 3 mL ice cold sterile 10 % glycerol (1/66 volume of the starting culture). As a last step, aliquots of 60 µL were prepared in pre-cooled 1.5 mL reaction tubes and immediately frozen in liquid nitrogen before being stored at -80°C. Electro-competent *A. tumefaciens* cells were used for transformation (2.2.2.7).

2.2.2.7 Transformation of electro-competent *A. tumefaciens* cells

Electro-competent *A. tumefaciens* GV3101 pMP90RK cells (2.1.3.2 and 2.2.2.6) were transformed by electroporation as described by Koncz and Schell (1986). First, a 60 µL aliquot of competent cells was thawed on ice before 50 ng of plasmid DNA was added. Subsequently, cells were incubated for 10 minutes on ice. Next, cells were transferred to a pre-cooled electroporation cuvette with 0.1 cm electrode distance. Transformation was carried out using a Micro Pulser™ (BioRad, Munich, Germany) electroporation apparatus with *Agr* program (settings: 25 µF, 2.5 kV and 400 Ω). Each transformation was pulsed once and placed immediately back on ice. 800 µl pre-cooled liquid DYT were added to electro shocked cells and transferred to a 1.5 mL reaction tube. The sample was incubated at 28°C and 180 rpm for two to three hours. As a last step, 50 µl of the transformation was plated on selective DYT agar plate and incubated at 28°C for two to three days.

2.2.2.8 Storage of bacterial cultures

For short-term storage, bacteria were kept on selective agar plates at 4°C for up to three weeks. For long-term storage, glycerol stocks of respective bacterial cells were made by mixing 500 µL of fresh overnight culture with 500 µL sterile 50 % glycerol. Subsequently, cells were frozen in liquid nitrogen and stored at -80°C.

2.2.2.9 *Pseudomonas syringae* pv. *tomato* growth assay

Five week old *Arabidopsis* plants, grown under short-day conditions (2.2.1.2), were used for *Pst* growth assays. Plate-grown cells of the *Pseudomonas* strain of interest (2.1.2.1 and 2.2.2.2) were used to inoculate 25 mL selective NYG liquid culture. The liquid culture was

incubated at 28°C and 200 rpm overnight. 2.5 mL of the pre-culture were added to 25 mL liquid NYG medium with appropriate antibiotics and the culture was shaken at 200 rpm and 28°C for approx. three to four hours until a OD_{600} of 0.2 was reached. Subsequently, cells were harvested by centrifugation at 1200 *g* and RT for 20 minutes. Afterwards, the cell pellet was resuspended in 25 mL 10 mM $MgCl_2$ solution. Finally, the optical density of the cell culture was measured and diluted to a concentration of $1x10^5$ colony-forming units (cfu) ml^{-1} (OD_{600} of 0.2 equals 10^8 cfu mL^{-1}). Two hours before infiltration, *Arabidopsis* plants were taken out of the growth chamber and placed well-watered on the bench. Petioles of chosen leaves for infiltration were marked with a black marker before being syringe-infiltrated with bacterial solution. For day zero (d0) samples, two leaf discs from independent plants per genotype were harvested with a cork borer (∅ = 0.55 cm) in a microcentrifuge tube (in duplicates), approx. 1 hour after infiltration. Subsequently, 50 µL of 10 mM $MgCl_2$ were added to the leaf material and crushed with a plastic pistil until a solution without any debris remained. Next, a 1:1 dilution was prepared and 50 µL of the diluted leaf material was plated on selective NYG agar plates and incubated at 28°C for two days before colonies were counted. Infiltrated plants were transferred to a growth cabinet (CLF Plant Climatics, Wertingen, Germany) and grown under short-day conditions (2.2.1.2) for three days. For day three (d3) samples, four leaf discs from four independent plants per genotype were harvested with a cork borer (Ø 0.55 cm) and put into microcentrifuge tubes (in quadruplicates). In each microcentrifuge tube 100 µL of 10mM $MgCl_2$ solution was added. Next, a dilution series (10^{-1} to 10^{-7}) was prepared in a 96 well plate and 5 µL of each dilution was pipetted on selective NYG agar plates. The plates were incubated at 28°C for two days and the numbers of colonies was counted.

2.2.2.10 *Agrobacterium tumefaciens* growth assay

Five week old *Arabidopsis* plants, grown under short-day conditions (2.2.1.2), were used for the *Agrobacterium* growth assays. First, plate-grown *Agrobacterium* cells (2.1.3.2 and 2.2.2.3) were used to inoculate a 25 mL selective DYT liquid culture. The liquid culture was incubated at 28°C and 200 rpm overnight. 4 mL of the pre-culture were added to 25 mL liquid DYT medium with appropriate antibiotics and incubated at 200 rpm and 28°C for approx. three hours until a final OD_{600} of 0.9 was reached. Subsequently, cells were harvested by centrifugation at 1200 *g* and RT for 20 minutes. Afterwards, the cell pellet was re-suspended in 25 mL 10 mM $MgCl_2$ solution. Finally, the optical density of the cell culture was measured and diluted to a concentration of $1x10^5$ colony-forming units (cfu) mL^{-1} (OD_{600} of 0.9 equals 10^9 cfu mL^{-1}). Two hours before infiltration, *Arabidopsis* plants were taken out of the growth chamber and placed well-watered on the bench. Petioles of chosen leaves for infiltration were marked with a black marker before being syringe-infiltrated with

bacterial solution. For day zero (d0) samples, two leaf discs from independent plants per genotype were harvested with a cork borer (Ø 0.55 cm) in a microcentrifuge tube (in duplicates), approx. one hour after infiltration. Subsequently, 50 µL of 10 mM $MgCl_2$ were added to the leaf material and crushed with a plastic pistil until a solution without any debris remained. Next, a 1:1 dilution was prepared and 50 µL of the diluted leaf material was plated on selective NYG agar plates and incubated at 28°C for two days before colonies were counted. Infiltrated plants were transferred to a growth cabinet (CLF Plant Climatics, Wertingen, Germany) and grown under short-day conditions (2.2.1.2) for three days. For day three (d3) samples, four leaf discs from four independent plants per genotype were harvested with a cork borer (∅ = 0.55 cm) and put into microcentrifuge tubes (in quadruplicates). In each microcentrifuge tube 100 µL of 10 mM $MgCl_2$ solution was added. Next, a dilution series (10^{-1} to 10^{-7}) was prepared in a 96 well plate and 5 µL of each dilution was pipetted onto selective DYT agar plates. The plates were incubated at 28°C for three to four days and the numbers of colonies was counted.

2.2.2.11 β-glucuronidase (GUS) reporter assay for *Agrobacterium*-mediated transient transformation of *Arabidopsis* plants

A β-glucuronidase (GUS) reporter assay was conducted to investigate *Agrobacterium*-mediated transient transformation of *Arabidopsis* plants. Four week old *Arabidopsis* plants, grown under short-day conditions (2.2.1.2), were used for this assay. First, plate-grown cells of *A tumefaciens* strain GV3101 pMP90RK harbouring the pXCSG GUS-intron::3xHA-StrepII construct (Table 5) were used to inoculate 25 mL liquid DYT culture that was cultured at 28°C and 180 rpm overnight. Cells were harvested for 20 minutes at 1200 *g*. Subsequently, cells were resuspended in 25 mL 10 mM $MgCl_2$ solution. Finally, the optical density of the cell culture was mesured at a wave length of 600 and diluted to OD_{600} of 0.3. Three hours before infiltration, *Arabidopsis* plants were taken out of the growth chamber and placed well-watered on the bench for two hours. Petioles of chosen leaves for infiltration were marked with a black marker. At least three plants per genotype and four leaves per plant were syringe-infiltrated with the bacterial solution per experiment. Infiltrated plants were transferred to a growth cabinet (CLF Plant Climatics, Wertingen, Germany) and grown under short-day conditions (2.2.1.2) for three days. After three days, infiltrated leaves were harvested and placed into 15 mL tubes with rounded bottom and were immediately submerged in GUS-staining-solution (Table 9). Subsequently, reaction tubes were placed into a desiccator and *Arabidopsis* leaves were vacuum infiltrated for 105 seconds and left in the desiccator for additional 15 seconds without further vacuum supply before the vacuum was gently released. Infiltrated leaves were incubated for approx. 16 hours at 37°C, before the staining-solution was removed and leaves were rinsed with water. Chlorophyll of the

leaves was removed by destaining with 70 % ethanol for several days under continuous shaking until only the GUS-staining remained visible in the leaves. Finally, ethanol was removed and stained leaves were stored in 75 % glycerol.

2.2.3 Molecular biological methods

2.2.3.1 Preparation of genomic DNA from *Arabidopsis* leaves with FTA paper for Punch PCR

This method can be used to prepare genomic DNA from plant tissues and is very quick. The method was adapted from Tsukaya *et al.* (2005) and Ndunguru *et al.* (2005). Briefly, plants were labelled and a small leaf was cut from each plant. Subsequently, leaf prints were made onto the surface of a FTA® classic card (Whatman™) using Parafilm and the round end of a glass tube. The leaf prints were dried for at least one hour at RT before being further processed. To extract genomic DNA for a PCR reaction, one leaf punch was taken using a Micro-punch™ (∅ = 1mm; Sigma-Aldrich, Munich, Germany) and put into a PCR reaction tube. Afterwards, 50 µL FTA buffer (Table 9) was added to the leaf punch and incubated for 5 minutes at RT. Next, the liquid was replaced by 140 µL TE-1 buffer (2.1.11) and incubated as described above. After 5 minutes the TE-1 buffer was replaced by a PCR reaction mix and subsequently a PCR reaction was performed as described in 2.2.3.3.1.

2.2.3.2 Preparation of genomic DNA from *Arabidopsis* leaves with DNA extraction buffer

Genomic DNA was extracted for cloning approaches or PCR-based genotyping. One leaf of a four week old *Arabidopsis* plant was placed in a 2 mL Eppendorf® Safe-Lock tube containing 2 stainless steel beads (∅ = 3 mm) and immediately frozen in liquid nitrogen. The leaf material was homogenized twice for 60 seconds using a bead mill with 50 Hz (TissueLyser LT, Qiagen, Hilden, Germany). Next, the lid of the reaction tube was carefully opened and 300 µL DNA extraction buffer was added to the sample. Subsequently, the sample was shaken vigorously for 5 minutes, followed by a 1 minute incubation step at RT. Afterwards the sample was centrifuged for 5 minutes at 17,000 *g*. Next, the supernatant was transferred to a new 1.5 mL reaction tube and mixed with 300 µL ice cold isopropanol. After a 5 minute incubation step at RT, the sample was centrifuged for 5 minutes at 17,000 *g*. The supernatant was removed and the pellet was dried in a heat block at 55°C for 30 minutes. As a last step, the dry pellet was resuspended in 50 µL TE-RNase mix (1 µL/mL RNase; Table 9) and incubated for additional 10 minutes in the heat block at 55°C. Genomic DNA was stored at 4°C and used for PCR reaction (2.2.3.3).

2.2.3.3 Polymerase chain reaction (PCR)

2.2.3.3.1 PCR-based genotyping and colony-PCR

This standard PCR protocol was used for genotyping approaches and colony-PCR. All PCR reactions were carried out in MyCycler™ Thermal Cycler System (BioRad, Munich, Germany) and performed with homemade *Taq* polymerase (2.1.6.2) and appropriate *Taq* buffer mix (Table 9). In order to genotype *Arabidopsis* plants, genomic DNA (2.2.3.1 or 2.2.3.2) was used as a template in the PCR mix listed in Table 10 and PCR reactions were conducted under PCR conditions shown in Table 11. Colony-PCR was used to confirm the presence of the desired plasmid. Therefore, plate-grown bacterial colonies were picked with a toothpick and used as PCR template, without further cultivation steps or plasmid purification, in the PCR mix (Table 10). PCR was conducted under PCR conditions shown in Table 11. Primers used in this study are listed in Table 6 and PCR fragments are visualized by agarose gel electrophoresis and HDGreen™ staining (2.2.3.4).

Table 10: PCR reaction mix used for PCR-based genotyping and colony PCR.

Reagent	Volume [µL]
10x *Taq* buffer	2.0
dNTP's (10 mM)	0.5
Forward primer (10 µM)	1.0
Reverse primer (10 µM)	1.0
Template	0 - 2.0
Taq-polymerase	0.5
dH_2O	add to 20.0

Table 11: Temperature profile of PCR reaction performed with *Taq* polymerase.

Reaction step	Temperature [°C]	Time [minutes]	Cycles
Initial denaturation	94	03:00	1
Denaturation	94	00:30	35
Annealing	$T_m - 5$	00:30	
Elongation	72	01:00 / kb	
Final elongation	72	05:00	1
Final hold	4	15:00	1

T_m: calculated melting temperature of used primer pair

2.2.3.3.2 PCR for cloning approaches

Since accurate dsDNA synthesis is a crucial step for the amplification of PCR products used for cloning approaches, the proofreading iProof™ High-Fidelity DNA polymerase PCR kit (Bio-Rad, Munich, Germany) was used according to manufacturer's instructions.

2.2.3.4 Agarose gel electrophoresis of DNA

Agarose gel electrophoresis was used to separate and visualize DNA fragments resulting from PCR (2.2.3.3) or plasmid digestion (2.2.3.7). Depending on the DNA fragment size, agarose gels consisted of 0.8 to 2.0 % (w/v) agarose that was dissolved in 1x TAE buffer (Table 9) by heating in the microwave. Before the gel was poured into a gel casting device, the agarose solution was cooled down to approx. 60°C and HDGreen™ DNA-Dye (INTAS Göttingen, Germany) was added (5 µL/100 mL) to the agarose mix. Depending on the sample size, a comb with the desired number of pockets was placed into the casting device and solidification of the gel was allowed at RT. The solid gel was transferred into a Sub-Cell GT tank (Bio-Rad, Munich, Germany) filled with 1x TAE buffer (2.1.11). The comb was removed and DNA-samples mixed with 6x DNA loading dye (2.1.11) were loaded into the pockets. GeneRuler™ 1 kB and 100 bp DNA ladder (Thermo Fisher Scientific, Waltham, USA) was used as size standards. Electrophoretic separation was carried out at 90 to 120 V for 30 to 90 minutes depending on the size of DNA fragments. Gels were analyzed with a G:Box Genoplex Transilluminator gel documentation and analysis system (VWR, Radnor, USA).

2.2.3.5 Purification of DNA fragments

PCR products and DNA fragments for cloning approaches and sequencing were either isolated directly after PCR reaction (2.2.3.3) or after agarose gel electrophoresis (2.2.3.4). For latter, DNA fragments were visualized under UV-light (365 nm), cut from the gel using a clean scalpel and placed in a 1.5 mL reaction tube. For the purification of DNA fragments from both, PCR reactions and after gel electrophoresis, the NucleoSpin® Gel and PCR Clean-up kit (Macherey-Nagel, Düren, Germany) was used according to the manufacturer's instructions.

2.2.3.6 DNA sequencing and sequence analysis

Single sequencing reactions of purified plasmids or PCR products (2.2.3.5) were conducted by SeqLab (Göttingen, Germany) using the Barcode Economy Run Service. The resulting sequences were analyzed with Geneious™ software version 8.1.8 (Biomatters Ltd.; Kearse *et al.*, 2012). If analyzed sequences were correct, PCR fragments or plasmids were used for further experiments.

2.2.3.7 Restriction endonuclease digestion of DNA

The restriction enzymes used in this study were standard or FastDigest® enzymes from Thermo Fisher Scientific (Waltham, USA) and were used according to the manufacturer's instructions. 10 µL restriction digestion reactions were incubated at 37°C for 45 minutes (FastDigest®) or up to four hours (standard enzymes). Restriction digestion was used for genotyping (CAPS analyses), cloning and analysis of plasmids.

2.2.3.8 Ligation of DNA fragments

For the construction of desired plasmids, the vector backbone and inserts were cut with suitable endonucleases (2.2.3.7), cleaned (2.2.3.5) and the DNA concentrations were determined (2.2.3.10). For the ligation reaction mix, a vector to insert molar ratio of 1 to 3 was used. Required volumes of the backbone and inserts were calculated with an *in-silico* LIGATION CALCULATOR (www.insilico.uni-duesseldorf.de) based on vector size, vector amount and insert size. Ligation was performed with T4 DNA ligase (Thermo Fisher Scientific, Waltham, USA) and the supplied reaction buffer. Reaction mix of 10 µL were prepared and ligation was performed at 16°C overnight. 5 to 10 µL ligation mix were transformation into *E. coli* TOP10 cells (2.1.3.1).

2.2.3.9 Plasmid DNA isolation from *Escherichia coli*

E. coli TOP10 cells (2.1.3.1) were used to amplify plasmid DNA. NucleoSpin® Plasmid Mini kit (Macherey-Nagel, Düren, Germany) was used to isolate plasmid DNA according to the manufacturer's instructions. Plasmids were isolated from 4 mL overnight culture of *E. coli* cells, cultivated in selective LB medium at 37°C and 180 rpm.

2.2.3.10 Photometric measurement of DNA and RNA concentration

For determination of DNA and RNA concentrations and for analyzing the purity of nucleic acids, the NanoDrop™ One Microvolume UV-Vis Spectrophotometer (Thermo Fisher Scientific, Waltham, USA) was used. 1 to 2 µL of the sample was used to measure the absorption of the sample at 260 nm and 280 nm. The ratio of absorbance at 260 nm and 280 nm is used to determine the purity of the sample. A ratio (260/280) of ~ 1.8 indicates "pure" DNA and a ratio (260/280) of ~ 2.0 indicates "pure" RNA.

2.2.3.11 Isolation of total RNA from *Arabidopsis* leaves

To isolate RNA form *Arabidopsis* leave material, plant material was ground either with stainless steel beads (∅ = 3 mm) in a bead mill at 50 Hz (TissueLyser LT, Qiagen, Hilden, Germany) or with pestle and mortar and frozen immediately in liquid nitrogen. 100 mg frozen leaf powder was mixed with 1.3 mL home-made TRIzol buffer (Table 9) in a 2 mL reaction tube and vortexed vigorously for 5 minutes for cell lysis. 250 µL ice cold chloroform was added and incubated for 2-3 minutes at RT before the reaction tube was shaken vigorously

for 3 minutes. Subsequently, the sample was centrifuged at 17,000 *g* and 4°C for 45 minutes. In the meantime, 320 µL of ice cold isopropanol and 320 µL of ice cold high salt precipitation buffer were filled into a new 1.5 mL reaction tube. After the centrifugation step, 600 µl of the upper, aqueous phase was taken and mixed with the cold isopropanol-high salt precipitation buffer mix. Subsequently, the 1.5 mL tube was inverted gently several times. To allow precipitation of the RNA, the samples were kept at RT for 10 minutes. This was followed by a 30 minutes centrifugation step at 17,000 *g* at 4°C. Afterwards, the supernatant was removed by pipetting and the RNA pellet was washed with 800 µL of ice cold EtOH (75 %) and inverted several times. Finally, the sample was centrifuged at 17,000 *g* and 4°C for 15 minutes before the EtOH was discarded. The pellet was allowed to dry for 10-15 minutes at RT before being dissolved in 50 µL nuclease-free water. RNA samples were stored at -80°C.

2.2.3.12 DNase I digest of total RNA from *Arabidopsis*

Before the reverse transcription polymerase chain reaction (2.2.3.13) was performed, RNA samples were digested with DNase I (Thermo Fisher Scientific, Waltham, USA) to avoid gDNA contamination in the cDNA later. The digest reaction was carried out according to the manufacturer's instructions. 17 µL of total RNA were mixed with 2 µL of supplied 10x DNase I buffer and 1 µL DNase I (1 U/µL Thermo Fisher Scientific, Waltham, USA; 2.1.6.2). The reaction mix was incubated for 30 minutes at 37°C. Next, 1 µL EDTA (50 mM, Thermo Fisher Scientific, Waltham, USA; 2.1.6.2) was added to the mix and incubated for 10 minutes at 65°C. Afterwards, RNA concentration of DNase I treated samples were measured using NanoDrop™ One Microvolume UV-Vis Spectrophotometer (Thermo Fisher Scientific, Waltham, USA; 2.2.3.10). Afterwards, RNA samples were adjusted with nuclease-free water to a final concentration of 250 ng/µL. Samples were either used directly for reverse transcription polymerase chain reaction (2.2.3.13) or stored at -80°C.

2.2.3.13 Reverse transcription-polymerase chain reaction (RT-PCR)

The reverse transcription-polymerase chain reaction was carried out in PCR tubes using Reverd Aid H Minus RT polymerase (Thermo Fisher Scientific, Waltham, USA) according to the manufacturer's instructions. 1500 ng of total RNA in a volume of 6 µL was mixed with 1 µL oligo $d(T)_{18}$ primer (100 µM) and 6 µL nuclease-free water. The mix was incubated for 5 minutes at 65°C. Afterwards the samples were chilled on ice for 2 minutes before a reaction mix containing 4 µL of supplied 5x RT buffer, 2 µL dNTPs and 1 µL Reverd Aid H Minus RT polymerase (200 U/µL, Thermo Fisher Scientific, Waltham, USA; 2.1.6.2) was added to each sample. The samples were incubated for 70 minutes at 42°C, followed by 5 minute at 75°C. Undiluted cDNA samples were stored at -20°C.

2.2.3.14 Semi-quantitative RT-PCR

For semi-quantitative RT-PCR, cDNA (2.2.3.13) was diluted 1:5 and used as template in the PCR reaction mix listed in Table 12. The PCR was performed under the conditions shown in Table 13. Primers used for target genes and reference genes are listed in Table 6. The cycle number was adjusted for each target gene and PCR products were visualized (2.2.3.4).

Table 12: PCR reaction mix used for semi-quantitative RT-PCR.

Reagent	Volume [µL]
10x *Taq* buffer	2.0
dNTP's (10 mM)	0.5
Forward primer (10 µM)	1.0
Reverse primer (10 µM)	1.0
DMSO	0.5
Template	2.0
Taq-polymerase	0.5
dH_2O	add to 20.0

Table 13: Temperature profile of PCR reaction using *Taq* polymerase.

Reaction step	Temperature [°C]	Time [minutes]	Cycles
Initial denaturation	94	01:00	1
Denaturation	94	00:30	28- 35
Annealing	$T_m - 5$	00:30	
Elongation	72	01:00 / kb	
Final elongation	72	05:00	1
Final hold	4	15:00	1

2.2.3.15 Quantitative real time PCR (qRT-PCR)

For quantitative real time PCR, cDNA (2.2.3.13) was diluted 1:7.5 and used as template in the PCR mix containing SsoFast EvaGreen Supermix (Bio-Rad, Munich, Germany) as listed in Table 12. qRT-PCRs were performed with a CFX96™ Real-Time PCR System (Bio-Rad, Munich, Germany) equipped with the CFX Manager™ Software Version 3.1 (Bio-Rad, Hercules, USA) in qRT-PCR-96-well plates (Bio-Rad, Munich, Germany) under the

conditions shown in Table 15. Primers used for target genes and reference gens are listed in Table 6.

Table 14: PCR reaction mix used for quantitative real time PCR.

Reagent	Volume [µL]
ddH_20	7.0
SsoFast EvaGreen Supermix (2x)	10.0
Primer fwd + rev (4 µM)	2.0
cDNA	1.0

Table 15: Temperature profile of quantitative real time PCR.

Reaction step	Temperature [°C]	Time [minutes]	Cycles
Initial denaturation	95	00:30	1
Denaturation	95	00:05	45
Annealing/Elongation	58	00:10	

The Melting curves were recorded from 60°C to 95°C in 0.5°C temperature steps that occurred every 5 seconds. As quality check, resulting melting curves were analyzed.

2.2.4 Transcriptome analysis

Transcriptome analysis was conducted of four week old *Arabidopsis* plants, grown under short-day conditions (2.2.1.2). For each sample, the whole rosettes of 15 *Arabidopsis* plants per genotype were collected and pooled to one biological replicate. Samples were stored at -80 C. The experiment was repeated four times with batches of independently grown plants. RNA was extracted by the TRIzol method (2.2.3.11). The isolated total RNA was quantified in a NanoDrop™ spectrophotometer and its sufficient quality was verified by a fragment analyser (Agilent, Santa Clara, USA). Library preparation and RNA sequencing was conducted for each biological replicate by the NGS-Integrative Genomics Core Unit (NIG; Dept. of Human Genetics, University Medical Centre Göttingen). 50 bp single end reads and 30 million reads per sample were generated by the Illumina HiSeq 2000 platform. Sequence images were transformed with the Illumina software BaseCaller to bcl files, which were demultiplexed to fastq files with the bcl2fastq v2.17.1.14. Quality check was done using FastQC (*S. Andrews:http://www.bioinformatics.babraham.ac.uk/projects/fastqc/*; version 0.11.5, Babraham Bioinformatics). Next, sequences were aligned to *A. thaliana* reference

genome (version TAIR 10) using the STAR aligner software (Dobin *et al.*, 2013) version 2.5, allowing for 2 mismatches within 50 bases. Subsequently, read counting was performed using featureCounts (Liao *et al.*, 2013). Read counts were analysed in the R/Bioconductor environment (version 3.4.2, www.bioconductor.org) using the DESeq2 package (Love *et al.*, 2014) version 1.14.1. Reads per kilobase per million (RPKM) values were generated from raw counts using the method described and published by Mortazavi *et al.* (2008). Candidate genes were filtered using threshold log_2FC >0.5 or <-0.5 and FDR-corrected p-value < 0.05. Gene annotation was performed using *A. thaliana* entry from Ensembl Plants (www.ensembl.org) database using the biomaRt (Durinck *et al*., 2009) package version 2.32.1. To perform Gene Ontology (GO) enrichment analysis, the Singular Enrichment Analysis (SEA) function of the web-based analysis tool kit agriGO v2.0 (Tian *et al.*, 2017) was used.

2.2.5 Measurement of reactive oxygen species (ROS)

To access the production of reactive oxygen species (ROS) upon elicitor treatment of *A. thaliana* leaf discs*,* a chemiluminescence-based assay was conducted in a 96-well plate. Seven week old *Arabidopsis* plants, grown under short-day conditions (2.2.1.2) were used in this assay. Therefore, eight leaves from independent plants per genotype were harvested. Subsequently, leave discs with a diameter of 4 mm were isolated using a Biopsy Puncher and placed in individual wells that were already filled with 100 µl tap water. The 96-well plate was covered with a lid and incubated overnight at RT. The next day L-012 solution (2.1.11) was prepared freshly. The tap water was removed carefully form each well and replaced immediately prior the start of the measurement with either 100 µl L-012 solution (water control), L-012 solution with elf18 (100 nM), L-012 solution with flg22 (100 nM) or L-012 solution with chitin (100 µg/mL). The chemiluminescence was detected every minute with a TECAN infinite® M200 plate reader (Tecan Group Ltd, Männedorf, Switzerland) over a time period of one hour. The obtained data were analysed with Excel.

2.2.6 Biochemical methods

2.2.6.1 Total protein isolation of *Arabidopsis* leaves for immunoblot analysis

For protein isolation 90 mg fresh leaf material was used. Samples were collected in 1.5 mL Eppendorf® Safe-Lock tubes and immediately frozen in liquid nitrogen. Following steps are performed on ice. To each sample 200 µL protein extraction buffer (Table 9) containing protease inhibitor cocktail (PIC), and one small spatula of quartz sand were added. The plant material was ground with a rotating glass pestle (1000 rounds/min) for 30 to 60 seconds using an IKA® RW 20 digital drill (IKA- Werke, Staufen, Germany). Afterwards, 200 µL protein extraction buffer containing PIC was used to wash remaining leaf material on the

glass pestle into the reaction tube. Next, additional 800 µL of the extraction buffer containing PIC was added to the samples to obtain a total volume of 1200 µL extract. This was followed by a 10-minute centrifugation step at 17,000 *g* at 4°C. The supernatant was transferred into a fresh 1.5 mL reaction tube and subsequently the protein concentration was determined via Bradford assay (2.2.6.2).

2.2.6.2 Determination of protein concentration using Bradford assay

The protein concentration of total protein extracts was determined using a Bradford assay. The protocol was based on the method described by Bradford (1976). The assay was carried out in cuvettes and protein extracts are measured in duplicates. First, Bradford reagent (Roti®-Quant, Roth, Karlsruhe, Germany) was mixed with ddH_20 (1:5) to obtain the working solution. Next, the standards for the calibration curve were prepared using a 1 mg/mL bovine serum albumin (BSA) solution (0, 3, 5, 7, 10 and 15 µL). Three microliter protein extract was transferred into a cuvette (in duplicates). Each cuvette was filled with 1 mL Bradford working solution and mixed gently with the protein extract. After a 5-10 minute incubation step at RT, the absorption at 595 nm was measured using a Biowave II photometer (Biochrom AG, Berlin, Germany). The absorption of the BSA standard solutions was plotted against the protein amount. Next, the total protein amount was calculated, and all samples were adjusted to the same protein concentration. Samples were stored at -20°C.

2.2.6.3 Denaturing SDS polyacrylamide gel electrophoresis (SDS PAGE)

2.2.6.3.1 Preparation of SDS polyacrylamide gels

The Mini-PROTEAN® Tetra Cell system (BioRad, Munich, Germany) was used to cast polyacrylamide gels according to the manufacturer's instructions. In this study, resolving gels of different percentages were used according to the molecular weight of investigated proteins. Briefly, the resolving gel (2.1.11) was poured between two glass plates that were spaced either 1.5 mm or 0.75 mm, overlaid with isopropanol and left at RT to polymerize. After complete polymerization, the isopropanol was removed, and the stacking gel (2.1.11) was poured on top of the resolving gel. A comb with either 10 or 15 pockets was inserted in the stacking gel and left at RT for polymerization. Gels were either used directly for SDS PAGE (2.2.6.3.2) or stored at 4°C. For storage in the fridge, the gels were wrapped in wet paper towels.

2.2.6.3.2 Sepation of denatured protein samples on SDS polyacrylamide gels

Prepared polyacrylamide gels were placed in the Mini-PROTEAN® Tetra Cell electrophoresis tank (BioRad, Munich, Germany) and filled with 1x SDS running buffer (Table 9). Next, combs were removed and denatured protein samples were loaded onto the gel together with

either a pre-stained molecular weight marker (PageRuler™ Plus Prestained Protein Ladder, Thermo Fisher Scientific, Waltham, USA) or unstained molecular weight marker (PageRuler™ Plus Unstained Protein Ladder Thermo Fisher Scientific, Waltham, USA). Gels were run at 90 V for approx. 2.5 hours. Resolving of the marker bands was used as indicator for sufficient separation.

2.2.6.4 Immunoblot analysis

For immunoblot analysis, the Mini Trans-Blot® system (BioRad, Munich, Germany) was used and assembled according to the manufacturer's instruction. Proteins separated by SDS PAGE (2.2.6.3) were blotted for 1.5 hours to Amersham™ Protran® nitrocellulose membrane (pore size of 0.45 µm, GE Healthcare Life Sciences, Munich, Germany). Briefly, after SDS PAGE, blotting apparatus was disassembled, and the stacking gel was removed. Subsequently, sponges, Whatman paper and nitrocellulose membrane were equilibrated in 1x transfer buffer (Table 9). Next, the gel and membrane were assembled in the blotting apparatus according to the manufacturers instructions.

The transfer was carried out for 1.5 h at 100 V. After the transfer, the blotting cassette was disassembled. The SDS gels were discarded, and the membranes were incubated with Ponceau S (PonS) staining solution for approx. 5 minutes. The PonS solution was used to monitor equal loading and efficient transfer of the proteins to the nitrocellulose membrane. The membranes were washed with ddH_20 and scanned afterwards. Subsequently, membranes were blocked with 1x TBS-T containing 5 % milk powder (2.1.11) for circa one hour with agitation at RT. After blocking, the membranes were incubated with the primary antibody solution with agitation overnight at 4°C. Used antibodies are listed in Table 7. Next day, the antibody solution was decanted, and the blot was rinsed twice with 1x TBS-T containing 5 % milk powder before being washed six times for 8 minutes in 1x TBS-T containing 5 % milk powder at RT with agitation. Next, membranes were incubated with secondary antibodies for at least 2.5 hours at RT and agitation. The secondary antibodies are listed in Table 7. After incubation with the secondary antibody solution the membranes were washed as described above in 1xTBS-T (Table 9). Afterwards, membranes were incubated with a 3:1 to 1:1 mix of SuperSignal® West Pico solution and SuperSignal® West Femto Maximum Sensitivity solution (Thermo Fisher Scientific, Waltham, USA) according to the manufacturer instructions. Resulting chemiluminescence was detected using a detection device (ChemiDoc Touch; Bio-Rad, Munich, Germany).

2.2.6.5 Expression of 6xHis-fusion MES18 in *E. coli* and cell harvest

For heterologous expression of N-terminal 6x His-tagged *MES18* protein, the coding sequence of *MES18* (AT5G58310) was cloned into pET28a (+) vector (Invitrogen™, Karlsruhe, Germany; Table 5) using *EcoR*I and *Not*I restriction sites. The respective

oligonucleotides are listed in Table 6. The correct construct was transformed into *E. coli* strain TOP10 (2.1.3.1). The *E. coli* Rosetta 2 (DE3) pLysS strain (2.1.3.1) was used for heterologous expression after chemically competent cells were transformed with the pET28a (+) MES18 construct (Table 5). DE3 cells carry a chromosomal copy of the T7 RNA polymerase gene under control of the lacUV5 promoter and are suitable for protein production of target genes in pET vectors by induction with IPTG. For expression, 800 mL of liquid LB medium containing kanamycin and chloramphenicol (2.1.7) was inoculated with *E. coli* cells harbouring the pET28a (+) *MES18* construct and grown in a biofermenter (B. Braun Biotech Melsungen, Germany) at 37°C overnight in chicane flasks at 180 rpm. The overnight culture was used to inoculate 10 L liquid LB culture containg kanamycin and chloramphenicol to a OD_{600} of 0.1. The culture was divided into 20 x 0.5 L cultures in 2 L-chicane flasks. The cell culture was grown at 37°C and the optical density was monitored over time. After the cultures reached an OD_{600} of 0.6, a 1 mL sample from one of the 20 flasks was saved as a non-induced control (for analysis by SDS PAGE, see below), before the production of MES18 was induced by 0.4 mM IPTG and 5 mL EtOH (100 %) that was added to the cells. The cell culture was incubated for additional three hours at 37°C, before the cells were grown at 16°C overnight. The next day, an additional 1 mL aliquot of cell culture was saved for later analysis by SDS PAGE before the liquid cultures were harvested. The samples for the SDS PAGE (2.2.6.3) were spined down (17,000 *g*, 5 minutes). The cell pellet was mixed with laemmli sample buffer (Table 9). To harvest the cells, cultures were placed into 1 L-centrigugation cups and centrifuged at 1200 *g* and 4°C for 20 minutes. The cell pellets were re-suspended in 5-10 mL buffer A (Table 9) on ice and transferred into 50 mL falcon tubes and centrifuged at 1200 *g* and 4°C for 20 minutes. Afterwards, the supernatant was discarded and the cell pellets were weighted and stoted at -70°C.

2.2.6.6 *E. coli* cell disruption

First, cold buffer A (Table 9) containing 100 µM of the protease inhibitor phenylmethylsulfonyl fluoride (PMSF), a spatula tip of lysozyme, 5 µg/mL DNase I (2.1.6.2) and 1 mM $MgCl_2$ was added to the frozen cell pellets (4 mL/g cells). The buffer cell mix was gently stirred on a magnetic stirrer at 4°C for a minimum of 30 minutes or until the whole cell pellet was re-suspended. Next, a fluidizer (Microfluidizer®) was used to further facilitate the cell lysis. In the fludizer the cell membrane of the *E. coli* cells can be efficiently broken by mechanical disruption. The cell solution was filled into the Microfluidizer® and six pump cycles with a pressure of 15000 psi were carried out. After the cell disruption, the suspension was placed into reaction tubes and ultra-centrifuged at 75.000 *g* and 4°C for 30 minutes to separate cell debris from the soluble fraction**.** For later analysis by SDS PAGE (2.2.6.3), 1 mL of the supernatant was saved. The 1 mL cell suspension was spined down (17,000 *g*,

5 minutes) and the remaining pellet was mixed with laemmli sample buffer (Table 9). The remaining cell free extract was stored on ice and subsequently used for affinity chromatography (2.2.6.7).

2.2.6.7 Protein Purification

For the purification of heterologously expressed MES18 proteins a two-step purification strategy was used. First, affinity chromatography was performed at 4°C using a HISTrap® FF (5 mL) column (GE Healthcare Life Sciences, Munich, Germany) that was operated by an ÄKTAprime® system (GE Healthcare Life Sciences, Munich, Germany). Heterologously expressed proteins with a His-tag are attracted by the positively charged nickel ions in the HISTrap® column and can be eluted by imidazole. The amount of protein in the elution fractions was monitored during the whole elution process by UV-Vis spectroscopy at 280 nm and the purity of the fraction was later analyzed by SDS PAGE (2.2.6.3). As a first step, the HISTrap® FF (5 mL) column was equilibrated with buffer A (Table 9) with a flow rate of 3 mL/min. Next, the cooled protein extract was loaded onto the column with a flow rate of 2 mL/min using a superloop (GE Healthcare Life Sciences, Munich, Germany). After loading, the column was washed (flow rate of 3 mL/min) with buffer A (Table 9) to remove contaminations. These fractions (flow-through) were saved for later analysis on the SDS PAGE (2.2.6.3). To elute His-tagged proteins from the column, 30 % of buffer B (Table 9) was used (final concentration of 150 nM imidazole concentration). In a final step, the amount of buffer B (Table 9) was set to 100 % (500 mM imidazole) to remove remaining components from the column. Eluted fractions that contained His_6-MES18 were pooled and stored at 4°C. Finally, Size Exclusion Chromatography was performed. Protein fractions were desalted using HiPrep™ 26/10 column (53 mL; GE Healthcare Life Sciences, Munich, Germany). Therefore, the column was equilibrated with buffer C (Table 9) and afterwards loaded with the eluted fractions containing His_6-MES18 with a flow rate of 4 mL/min using a superloop (50 mL; GE Healthcare Life Sciences, Munich, Germany). Fractions of 5 mL volume were collected and eluted fractions with high absorbance at 280 nm were analyzed on SDS PAGE (2.2.6.3). Fractions containing desalted His_6-MES18 protein were pooled and the concentration of the protein was determined (2.2.6.8). The samples for the SDS PAGE (2.2.6.3) were spined down (17,000 *g*, 5 minutes). The cell pellet was mixed with laemmli sample buffer (Table 9).

2.2.6.8 Determination of protein concentration using NanoDrop™ One Microvolume UV-Vis Spectrophotometer

The concentration of His_6-MES18 (2.2.6.7) was determined spectroscopically using the NanoDrop™ One Microvolume UV-Vis Spectrophotometer (Thermo Fisher Scientific, Waltham, USA). 2 µL of the protein sample was used to measure the absorption at 280 nm.

Using the following formula:

$$\text{mg/mL} = \frac{E * V\varepsilon}{\varepsilon} * MW$$

E = measured value
V = dilution factor
ε = Ext. Coefficient (M^{-1} cm^{-1})
MW = Molecular Weight (Da)

the concentration of the protein was determined. Molar extinction coefficient for MES18 was calculated with ProtParam (https://web.expasy.org/protparam/).

2.2.6.9 Photometric esterase activity assay

General esterase activity of MES18 was tested by with a photometric esterase assay using the artificial esterase substrate *p*-nitrophenyl acetate (*p*-NPA). The method was adapted from Yang *et al.* (2008). Purified recombinant His_6-MES18 protein was incubated in 10 mM NaCl and 50 mM TRIS-HCl buffer (pH 8.0) with 1 mM *p*-NPA substrate at RT. The assay was conducted in a 96-well plate and a reaction volume of 200 µL was used. The absorbance of the hydrolysis product (*p*-nitrophenol) was measured photometrically at 405 nm every 30 seconds over a time period of 30 minutes in a TECAN infinite® M200 plate reader (Tecan Group Ltd, Männedorf, Switzerland). The obtained data were analysed with Excel.

2.2.6.10 Ultra Performance Liquid Chromatography Mass Spectrometry (UPLC-nano ESI-MS/MS)

The three methylated plant hormones (MeSA, MeIAA and MeJA) were tested as potential substrates of MES18. The substrates were dissolved in EtOH. His_6-MES18 which was dissolved in 10 mM NaCl, 50 mM TRIS-HCl, pH 8.0 was inbubated with the substrates (see Table 16) in a 200 µL reaction volume in a 1.5 mL reaction tube at 24°C for 30 minutes. Reactions were stopped by addition of 100 µL pure (100 %) acetonitrile either immediately (t0) or after 30 minutes incubation time (t30). Subsequently, samples were centrifuged for 5 minutes at 17,000 *g*. Samples were measured by Dr. Cornelia Herrfurth (University of Goettingen, Germany). Analysis of the esterase substrates and products was performed using an ACQUITY UPLC® system (Waters Corp., Milford, MA, USA) and analysed by nanoelectrospray ionization (nanoESI) (TriVersa Nanomate®; Advion BioSciences, Ithaca, NY, USA) coupled with an AB Sciex 4000 QTRAP® tandem mass spectrometer (AB Sciex, Framingham, MA, USA) employed in scheduled multiple reaction monitoring mode (Herrfurth and Feussner, 2020). Mass transitions were as follows: in negative ionization mode, 137/93 [declustering potential (DP) -25 V, entrance potential (EP) -6 V, collision energy (CE) -20 V] for SA, 209/59 (DP -30 V, EP -4.5 V, CE -24 V) for JA and in positive ionization mode, 176/130 (DP 31 V, EP 4 V, CE 17 V) for IAA, 153/120 (DP 90 V, EP 10 V, CE 20 V) for

MeSA, 190/130 (DP 90 V, EP 10 V, CE 20 V) for MeIAA and 225/151 (DP 90 V, EP 10 V, CE 20 V) for MeJA.

Table 16: Substrates used in this study.

Name	Chemical formula	Molar mass	Supplier
Methyl salicylate	$C_8H_8O_3$	152.15 g/mol	Sigma-Aldrich, Munich, Germany
Methyl jasmonate	$C_{13}H_{20}O_3$	224.30 g/mol	Sigma-Aldrich, Munich, Germany
Methyl indole-3-acetate	$C_{11}H_{11}NO_2$	189.21 g/mol	Sigma-Aldrich, Munich, Germany

2.2.7 Biophysical methods

2.2.7.1 Isothermal Titration Calorimetry (ITC)

In order to determine the enzyme activity of MES18 with different substrates (MeSA, MeJA and MeIAA) and to investigate the influence of product inhibition of IAA to the reaction of MeIAA to IAA, kinetic Isothermal Titration Calormetry (ITC, PEAQ-ITC Malvern Panalytical) was used. The sample cell was loaded with the substrate. The substrates were dissolved in DMSO and buffer (10 mM NaCl, 50 mM TRIS-HCl, pH 8.0). His_6-MES18 was dissolved in the same buffer as the substrates and also containg DMSO. The syringe was loaded with the enzyme buffer mix and a volume of 10 µL was injected into the sample cell per injection. All measurements were performed at a temperature of 20°C, a reference power of 10 µcal/s, 750 rpm sirring speed, a initial delay of 60 seconds and a spacing time of 4000 seconds. At the end of the reaction a second injection was executed in order to confirm that the substrate was completely consumed. The substrates/product that was used in the ITC measurments are listed in Table 16 and Table 17.

Table 17: Product used for product inhibition assay using ITC.

Name	Chemical formula	Molar mass	Supplier
Indole-3-acetic acid (IAA)	$C_{10}H_9NO_2$	175.2 g/mol	Duchefa

The samples were measured with the help of Lisa-Marie Funk (University of Goettigen, Germany).

2.2.7.2 ITC data analysis

The kinetic ITC analysis was applied according to Kupski (2016). During the ITC measurement the substrate is converted into the product which is catalyzed by a enzyme. Product formation generates heat which is measured by the ITC device in µcal/s during the reaction. For each data point the sum of the heat (cp_{total}) is calculated and used to approximate the thermal energy that is realed during the reaction. The molar reaction enthalpy (Δ*H*) was calculated by dividing cp_{total} with the amount of substrate $n(substrate)$, [1].

$$\Delta H = \frac{\sum_{t=0}^{t_i} c\ p}{n\ (substrate)} \quad [1]$$

The conversion rate $CR(mol/s)$ express the amount of substrate that is turned over into the product per time unit. *CR* is approximately described by dividing cp_{total} with the molar reaction enthalpy Δ*H* [2].

$$CR(t) = \frac{c\ p\ (t)}{\Delta H} \quad [2]$$

To obtain the the total product formation (CR_{total}) the sum of the conversion rate *CR* for each data point was calculated [3].

$$CR_{total}(t) = \sum_{t=0}^{t} CR(t) \quad [3]$$

The total amount of substrate $\left(n_{t,total}(S)\right)$ at each time point (t) was determined by subtracting the total product formation (CR_{total}) from the initial amount of substrate $n_0(S)$ [4].

$$n_{t,total}(S) = n_0(s) - CR_{total}(t) n_0\ (S) \quad [4]$$

To obtain the substrate concentration at each time point $c_t(s)$ the total substrate amount $n_{t,total}(S)$ was divided by the volume *V* of the sample cell of the ITC device [5].

$$c_t(s) = \frac{n_{t,total}\ (S)}{V} \quad [5)]$$

The observed rate constant k_{obs} which correspond to the reaction velocity was calculated by dividing the conversion rate $CR(t)$ by the amount of the enzyme $n\ (QC)$ in the syringe [6].

$$k_{obs} = \frac{CR(t)}{n(QC)} \quad [6]$$

The determined variables k_{obs} and $c_t(S)$ were plotted and fitted according to the Michaelis-Menten Equation (Formula 7) using SigmaPlot from Systat Software Inc.

$$v = \frac{k_{cat}*[S]}{K_M*[S]} \quad [7]$$

2.2.8 Statistical analysis

Statistical significances were determined with unpaired, two-tailed Student t-tests performed in Excel. One-way Anova and tukey's post hoc test were performed using RStudio (v 1.2.5033).

3 Results

In *Arabidopsis*, the nucleoporins MOS3/NUP96 and NUP160 belong to the evolutionary conserved NUP107-160 sub-complex of the NPC. *Arabidopsis* mutants of both genes are impaired in basal and TIR-NB-LRR (TNL)-triggered immune responses towards bacterial and oomycete pathogens and show defects in mRNA export (Zhang and Li, 2005; Parry *et al.*, 2006; Wiermer *et al.*, 2012). In addition, transcripts of the defence regulator *EDS1* are depleted in *nup160* mutant plants, suggesting that NUP160 is required for full gene expression in EDS1-mediated and potentially other resistance pathways in *Arabidopsis* (Wiermer *et al.*, 2012).

The result chapter is divided into three sections. The first section (3.1) describes a transcriptome analysis that was conducted to identify new candidates involved in plant disease resistance. An RNAseq experiment was performed on wild-type, *mos3*, *nup160* and *sec13b* mutant plants and revealed mild but significant transcriptional changes in *mos3* and *nup160* mutants. Several differentially expressed genes (DEGs) potentially implicated in plant immunity were identified, including the known defence genes *EDS1, PAD4* and *EFR*.

The characterization of defence phenotypic consequences of reduced *EFR* transcript abundance in *mos3* and *nup160* mutants is the second aim of this study. The results of this analysis are displayed in the second section (3.2).

The third section (3.3) describes the functional characterization of the predicted methyl esterase *MES18* and the RNA-binding protein *PUM9* with regard to their potential roles in plant immunity. *MES18* and *PUM9* are the two genes showing the most strongly decreased expression in unchallenged *mos3* and *nup160* mutant plants as revealed by the RNAseq experiment in section 3.1. Since *mos3* and *nup160* mutant plants show immunity defects (Roth and Wiermer, 2012; Wiermer *et al.*, 2012), these two genes are promising candidates to investigate their role in plant immunity.

3.1 Transcriptome analysis using RNAseq revealed global transcriptional changes in *mos3* and *nup160* mutant plants

The immunity defects of *mos3* and *nup160* mutants and the alterations in *EDS1* mRNA levels in *nup160* mutant plants suggest that *MOS3* and *NUP160* are involved in the transcriptional regulation of certain defence-related genes, including *EDS1*. Differential expression of defence-associated genes in *mos3* and *nup160* as compared to wild-type plants could at least partially explain the observed immunity defects. The identification of additional deregulated defence genes will be helpful to dissect the underlying molecular mechanism on how MOS3 and NUP160 regulate plant immune responses. To investigate

potential transcriptional changes in both nucleoporin mutants on a genome-wide level, a transcriptome analysis using RNAseq was performed (Figure 5).

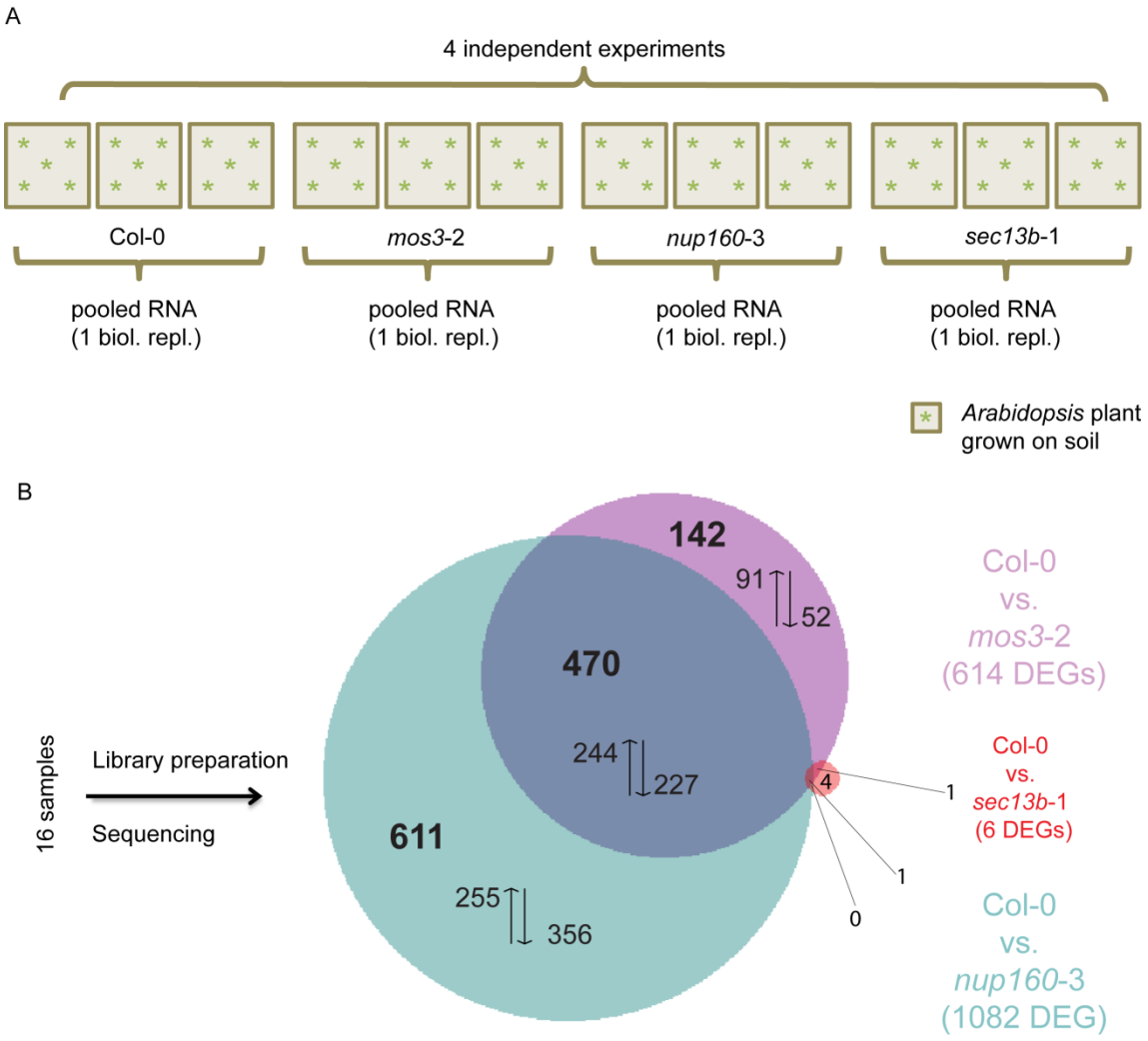

Figure 5: Transcriptome analysis of of Col-0 wild-type, *mos3*-2, *nup160*-3 and *sec13b*-1 control plants using RNAseq. (**A**) The transcriptome analysis was conducted on four week old unchallenged *Arabidopsis* plants of the indicated genotypes. All plants (green asterisks) were grown under short day conditions on soil. Total RNA for RNA sequencing was extracted from pools of 15 individual rosettes per genotype. The experiment was repeated four times with independently grown plants (i.e. four biological replicates, 16 samples in total). The 16 RNA samples were used for RNAseq analysis. (**B**) Venn diagram illustrating differentially expressed genes (DEGs; $log_2FC > 0.5$ or < -0.5, False Discovery Rate (FDR) < 0.05) in *mos3*-2, *nup160*-3 and control *sec13b*-1 compared to Col-0 wild-type plants. Library preparation and RNA sequencing was conducted on four biological replicates per genotype (total of 16 samples) by the NGS-Integrative Genomics Core Unit (NIG; Dept. of Human Genetics, University Medical Center Göttingen). Bold numbers in the diagram indicate total amount of DEGs, which include higher expressed (↑) and lower expressed (↓) genes in the respective mutant as compared to Col-0 wild-type. The Venn diagram was generated using BioVenn© (Hulsen *et al.*, 2008).

The RNAseq analysis was conducted on four week old unchallenged Col-0 wild-type, *mos3*-2 (SALK_109959), *nup160*-3 (SAIL_877_B01) and *sec13b*-1 (SALK_045825) *Arabidopsis* plants. For each genotype whole rosettes of 15 individual plants were

harvested. SEC13B is a member of the NUP107-160 complex. *Sec13b* mutant plants are not affected in basal resistance to *Pseudomonas syringae* pv. *tomato* (*Pst*) DC3000 (Wiermer *et al.*, 2012) and served as control. The rosette material of each genotype was ground in liquid nitrogen and total RNA was extracted. The isolated total RNA was quantified in a NanoDrop™ spectrophotometer and its sufficient quality was verified by a fragment analyzer (Agilent, Santa Clara, USA). RNA sequencing was conducted on total RNA of four biological replicates for each plant genotype (total of 16 samples) by the NGS-Integrative Genomics Core Unit (NIG; Dept. of Human Genetics, University Medical Center Göttingen; Figure 5 A).

A principal component analysis (PCA) was performed to obtain initial insight into the variance between the transcriptome profiles of Col-0 with *mos3*-2, *nup160*-3 or *sec13b*-1. The results of the PCA analysis are depicted in Supplementary Figure 1 A-C. The PCA revealed a clear separation between the transcriptome profile of Col-0 and *mos3*-2 (Supplementary Figure 1 A). The analysis also showed that the transcriptome profiles of Col-0 and *nup160*-3 are different under the chosen conditions (Supplementary Figure 1 B). In contrast, *sec13b*-1 and Col-0 profiles are more similar to each other (Supplementary Figure 1 C). However, the PCA data also illustrate that the expression pattern of the biological replicates of Col-0 wild-type, *mos3*-2, *nup160*-3 and *sec13b*-1 differ among identical genotypes (Supplementary Figure 1 A-C), indicating biological variances between the biological replicates. The results demonstrate differences between the Col-0 wild-type and the *mos3* or *nup160* datasets, whereas the transcriptome profiles of Col-0 and *sec13b* are more similar.

614 differentially expressed genes (DEGs) were identified in *mos3*-2 mutant plants and 1082 DEGs in *nup160*-3 mutant plants in comparison to Col-0 wild-type ($log_2FC > 0.5$ or < -0.5, False Discovery Rate (FDR) < 0.05; Figure 5 B). In contrast, only 6 genes were differentially expressed in the *sec13b*-1 mutant as compared to Col-0 wild-type. This suggests a highly similar gene expression profile in Col-0 and *sec13b* under the chosen conditions (Figure 5 B, C). Among the total amount of identified DEGs, 471 genes were differentially expressed (i.e. 244 genes were expressed higher and 227 genes were expressed lower) in both *mos3* and *nup160* as compared to Col-0 wild-type and *sec13b*-1 (Figure 5 B). The dataset of these 471 genes was analysed in more detail. Among the 471 genes, the expression of 332 genes was more drastically affected in *nup160*-3 in comparison to *mos3*-2 (Figure 6; Supplementary Table 1). In contrast, the transcript abundance of 135 genes was more drastically changed in *mos3*-2 as compared to *nup160*-3. These findings indicate a more severely affected gene expression in *nup160*-3 mutant plants as compared to *mos3*-2.

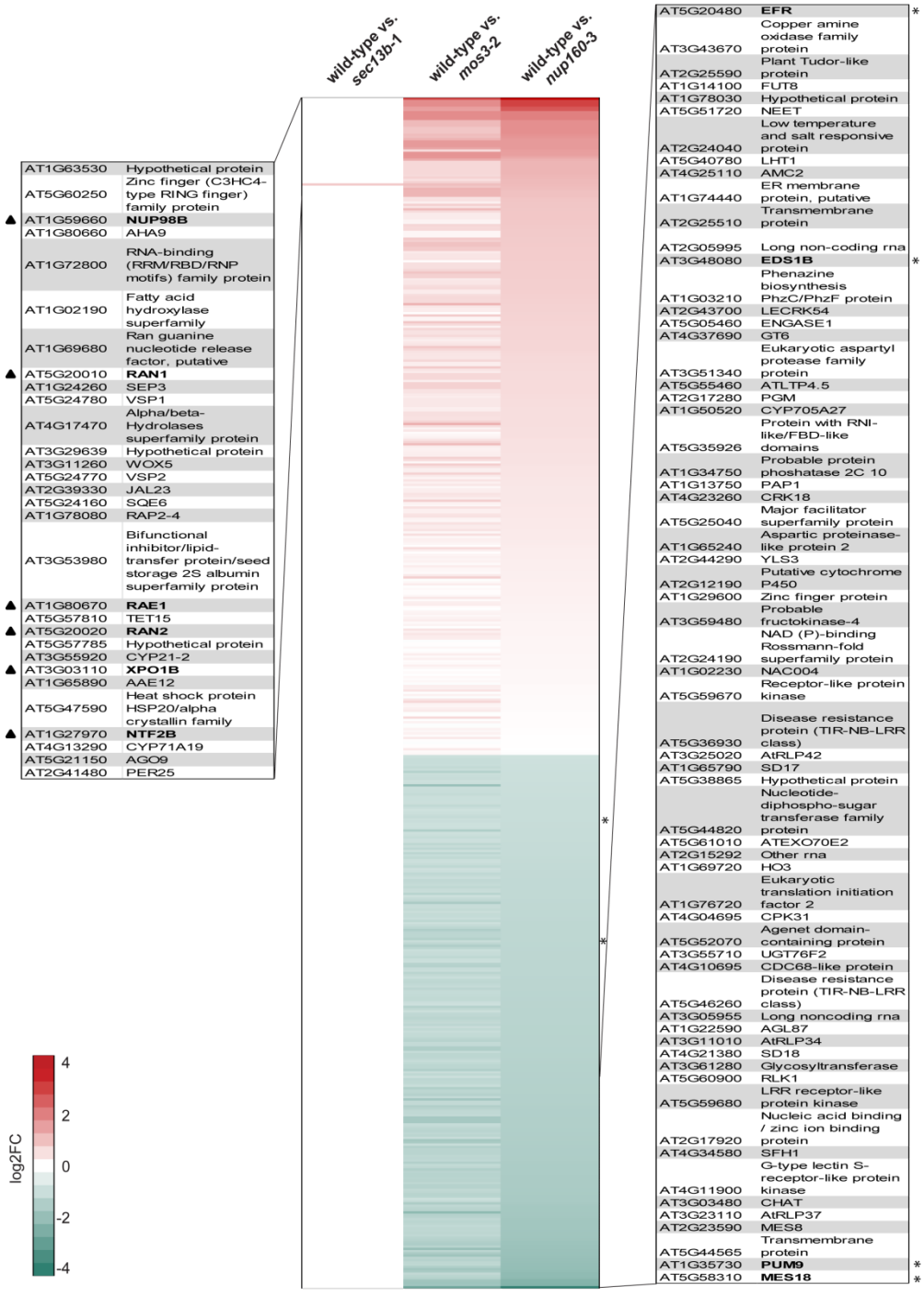

Figure 6: 471 genes are differentially expressed in *mos3*-2 and *nup160*-3 as compared to Col-0 wild-type and *sec13b*-1 control plants. Genome-wide gene expression was analyzed in four week old unchallenged *Arabidopsis* Col-0 wild-type, *mos3*-2, *nup160*-3 and *sec13b*-1 plants as described in Figure 5. Differential gene expression between mutant and wild-type is depicted as fold change after $\log_2$ transformation ($\log_2$FC) and visualized by color changes from red (high expression) to green (low expression; see colour bar). Genes are sorted according to their $\log_2$FC values and based on comparison between *nup160*-3 and Col-0 wild-type. Left table shows the top 30 differentially expressed genes (DEGs) with the highest increase in expression in comparison to Col-0. Black triangles indicate the nuclear transport-related genes *NUP98B*, *RAN1*, *RAE1*, *RAN2*, *XPO1B* and *NTF2B*. Right table illustrates the top 65 DEGs with the strongest decrease in expression as compared to Col-0. Asterisks indicate the two most strongly affected genes *MES18* and *PUM9*, as well as the known immunity genes *EDS1B*, *EFR* (listed in table), *PAD4* (position 114) and *EDS1A* (position 166, not listed in table). Tables illustrate AGI code and corresponding gene name/description.

3.1.1 The gene ontology terms defence and innate immune response are significantly overrepresented among the 471 DEGs identified in *mos3*-2 and *nup160*-3

A gene ontology (GO) enrichment analysis was conducted to obtain insights into the biological processes associated with the 471 genes that are differentially expressed in both *mos3*-2 and *nup160*-3 as compared to the Col-0 wild-type reference transcriptome Figure 5 B). The analysis was performed using the web-based analysis toolkit agriGO v2.0 (Tian *et al.*, 2017). The investigation revealed that among the 471 DEGs 13 GO terms were significantly overrepresented (Fisher Test, $P < 0.001$ and FDR < 0.05). The results of the GO enrichment analysis are depicted in Figure 7. The percentage of genes that were assigned to the respective GO term in the *Arabidopsis thaliana* Col-0 reference genome (TAIR 10, 28397 annotated genes) as well as the percentage of genes that were assigned from the 471 DEGs in both *mos3* and *nup160* is displayed.

GO terms that represent processes causing cellular or organismal changes in response to a stimulus (GO:0050896), including chemical (GO:0042221) and biotic (GO:0009607) stimuli, as well as responses to organic substances (GO:0010033) were overrepresented among the DEGs. Additional GO terms that describe chemical reactions and pathways involving aromatic compounds (GO:0006725) and amino acids (GO:0006575) were overrepresented as well. GO terms describing secondary metabolic processes (GO:0019748) and metabolic processes that result in a change of the redox status (GO:0055114) were also identified. Responses to other organisms such as bacteria, fungi, insects, nematodes and others are summarized in the GO term “response to multi-organism process” (GO:0051704), which was also overrepresented among the 471 DEGs in *mos3*-2 and *nup160*-3 (Figure 7).

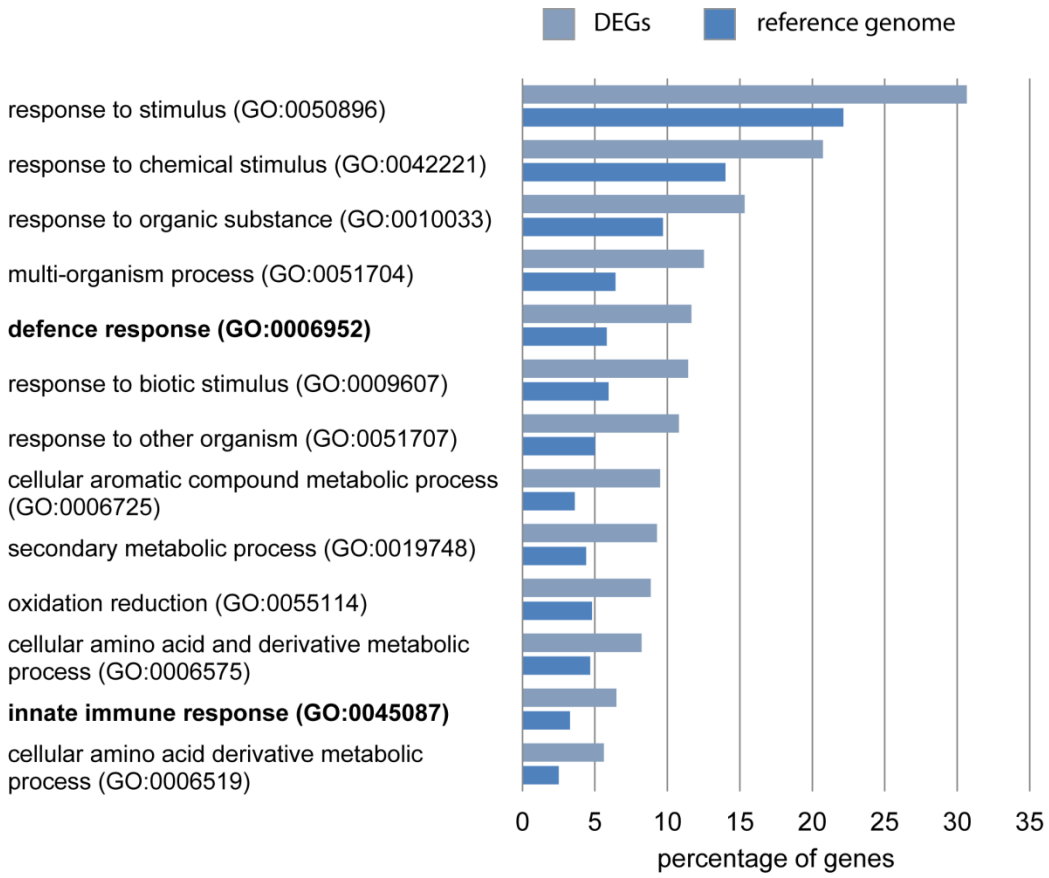

Figure 7: Gene ontology enrichment analysis of the 471 genes that are differentially expressed in *mos3*-2 and *nup160*-3 mutants in comparison to Col-0 wild-type. The graph shows the distribution of significantly enriched gene ontology (GO) terms found among the 471 differentially expressed genes (DEGs) common in *mos3*-2 and *nup160*-3 compared to Col-0 wild-type. Percentage of genes that are assigned to the respective GO terms from the set of 471 DEGs (light blue) and the reference genome (dark blue; TAIR 10, 28397 annotated genes) are displayed. 11.6 % and 6.5 % of the DEGs are assigned to the GO terms “defence response” and “innate immune response”, respectively. Only GO terms with more than 23.5 assigned genes from the DEGs set are displayed (> 5 %). For GO enrichment analysis, the web-based analysis toolkit agriGO v2.0 was used (Fisher Test, $P < 0.001$ and FDR < 0.05; (Tian *et al.*, 2017).

Notably, the GO terms “defence response” (GO:0006952) and “innate immune response” (GO:0045087) were significantly enriched. Here, 11.7 % (54 genes) of the 471 DEGs were assigned to the GO term of “defence response” compared to 6 % (1653 genes) that were generally assigned to this GO term in the *A. thaliana* genome. Similarly, 6.5 % (30 genes) of DEGs belong to the GO term “immune response” compared to 3.2 % (930 genes) of the reference genome (Figure 7).

In summary, the GO analysis revealed that the set of 471 DEGs in *mos3*-2 and *nup160*-3 contains genes involved in a variety of different biological processes. However, the overrepresentation of the two GO terms “defence response” and “innate immune response” demonstrates that defence-associated genes are represented among the 471 DEGs. These findings are consistent with the functional involvement of both *MOS3*/*NUP96* and *NUP160* in plant immunity (Roth and Wiermer, 2012; Wiermer *et al.*, 2012). Furthermore, the GO

analysis support the idea that, beside the central defence regulator *EDS1* (Wiermer *et al.*, 2012), additional defence-associated genes are differentially expressed in loss-of-function mutants of the *Arabidopsis* nucleoporins *MOS3/NUP96* and *NUP160.*

3.1.2 Nuclear transport-related genes show higher expression in *mos3* and *nup160* mutant plants as compared to Col-0 wild-type

A closer inspection of the 244 DEGs showing elevated expression in *mos3*-2 and *nup160*-3 compared to Col-0 (Figure 5 B) revealed multiple genes that are involved in nuclear transport mechanisms. Among the 30 DEGs showing the highest increase in expression, six genes were identified, namely the nucleoporin *NUP98B*, the nuclear export factor *RAE1*, the nuclear transport regulators *RAN1* and *RAN2*, the exportin *XPO1B* and the nuclear transport factor *NTF2B*, that play important roles in nuclear transport processes (Haasen *et al.*, 1999; Zhao *et al.*, 2006; Ma *et al.*, 2007; Blanvillain *et al.*, 2008; Tamura *et al.*, 2010; Figure 6, left side; Supplementary Table 1). Among these six nuclear transport-related genes, *NUP98B* showed the highest increase in differential gene expression in *nup160*-3 (log_2FC of 2.82) and *mos3*-2 (log_2FC of 1.85) in comparison to Col-0 wild-type. In contrast, *NTF2* showed the lowest increase in differential gene expression in *nup160*-3 and *mos3*-2 (log_2FC of 1.35 and 0.9; Figure 8) as compared to Col-0. Altered transcript levels of the six identified nuclear transport-related genes were also identified in a gene expression analysis conducted by Parry (2014) with specific emphasis to transcriptional changes in 7-day-old *nup160* seedlings.

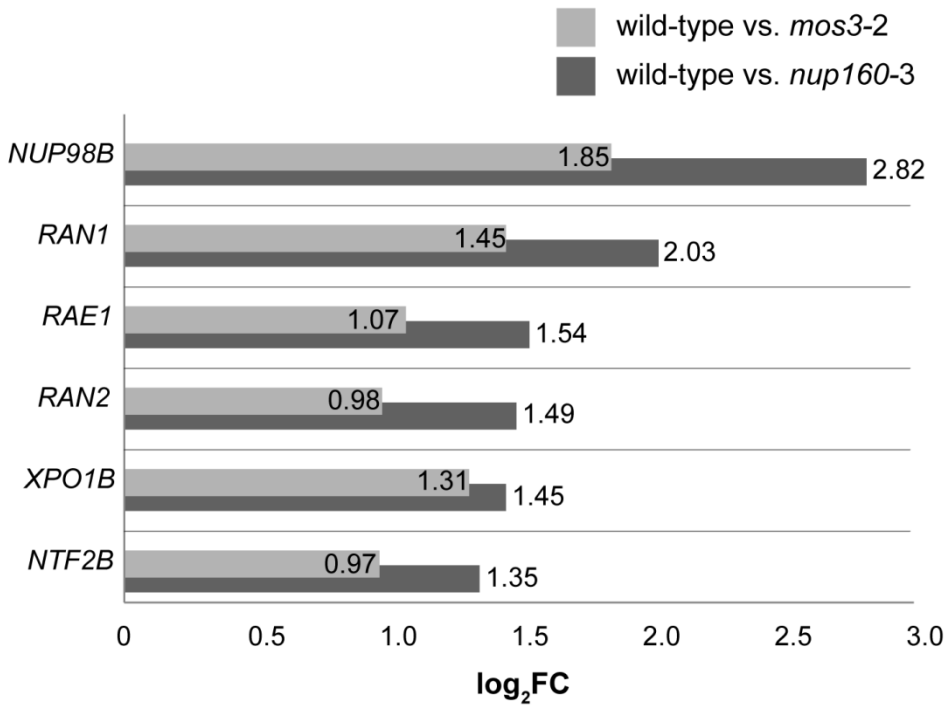

Figure 8: Nuclear transport-related genes are higher expressed in *mos3*-2 and *nup160*-3 as compared to Col-0 wild-type. Genome-wide gene expression was analyzed in four week old unchallenged *Arabidopsis* Col-0 wild-type, *mos3*-2 and *nup160*-3 as described in Figure 5. The differential gene expression between wild-type and mutant is depicted as fold change after $\log_2$ transformation ($\log_2$FC). Bars represent $\log_2$FC values of the six nuclear transport associated genes that were identified among the 244 DEGs showing elevated expression in *mos3*-2 and *nup160*-3 as compared to Col-0 wild-type. Light grey, wild-type versus *mos3*-2; dark grey, wild-type versus *nup160*-3.

The obtained data suggest that the lack of certain nucleoporins such as MOS3 and NUP160 alters the transcript abundance of nuclear transport-related genes. Such compensatory upregulation in the expression of genes involved in nuclear transport may provide plants with a regulatory mechanism to counteract defects in the nuclear transport machinery.

3.1.3 Transcript levels of immunity-related genes are reduced in *mos3*-2 and *nup160*-3 mutant plants as compared to Col-0 wild-type

A previous study in mice indicated that a defect in NUP96, the homologue of MOS3 in vertebrates, decreases the expression of interferon-regulated genes that are part of the regulatory network of innate and acquired immunity in the mouse model (Faria *et al.*, 2006). In order to examine the influences caused by the loss of MOS3 and NUP160 function in *Arabidopsis*, in particular on the down-regulation of gene expression, a closer look was taken at the 227 genes that showed lower expression in *mos3*-2 and *nup160*-3 as compared to Col-0. It has been previously reported, that the transcript abundance of the immune regulator *EDS1A* (*AT3G48090*) is mildly reduced in unchallenged *nup160* mutant plants

(Wiermer *et al.*, 2012). Importantly, *EDS1A* (*AT3G48090*) and its tandem copy *EDS1B* (*AT3G48080*) were found among the 227 DEGs (Figure 6, right side; Supplementary Table 1) and showed slightly but significantly reduced expression in both *mos3*-2 (log_2FC of -0.63, *EDS1A*; -0.95, *EDS1B*) and *nup160*-3 (log_2FC of -0.79, *EDS1A*; -1.27, *EDS1B*) mutant plants (Figure 9). This confirms the previous qRT-PCR data (Wiermer *et al.*, 2012) and proves the validity of the experimental RNAseq approach (Figure 5) to identify immune-regulatory genes with slightly reduced expression levels in *mos3*-2 and *nup160*-3. Beside the altered gene expression of *EDS1*, transcript levels of its signalling partner *PHYTOALEXIN DEFICIENT4 (PAD4*; AT3G52430) were also reduced in *mos3*-2 (log_2FC of -0.82) and *nup160*-3 (log_2FC of -0.97; Figure 9). These findings can at least partially explain the observed immunity defects of *mos3* and *nup160* mutants against virulent *Pseudomonas syringae* pv. *tomato* (*Pst*) DC3000 and avirulent *Pst* DC3000 expressing the effector *avrRps4* (Roth and Wiermer, 2012; Wiermer *et al.*, 2012).

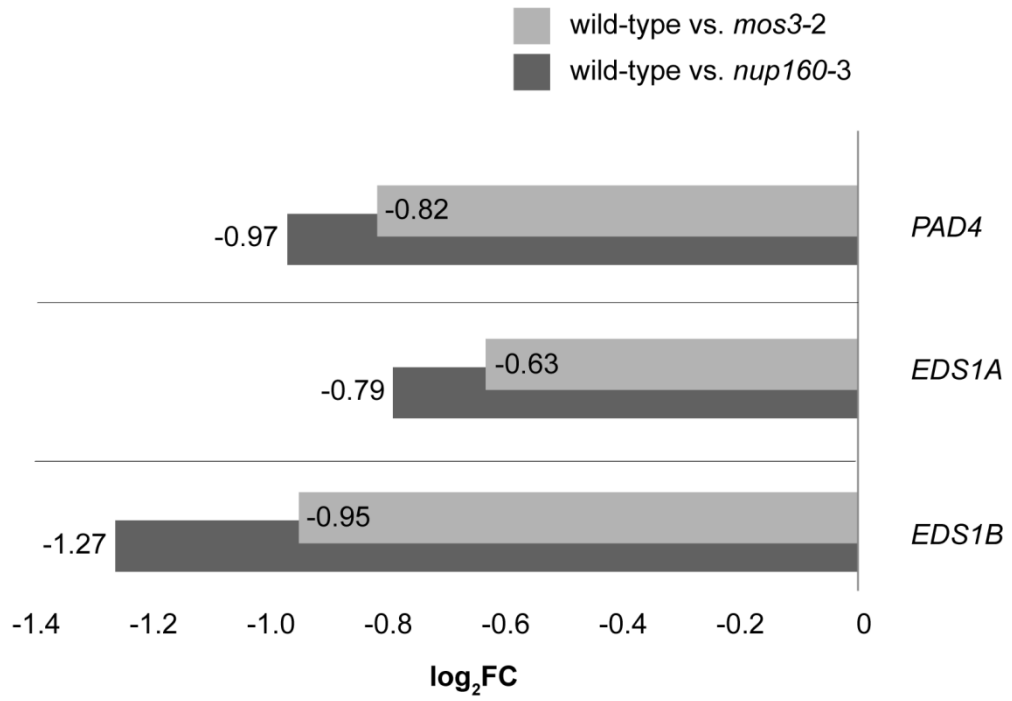

Figure 9: The defence-related genes *EDS1A, EDS1B* and *PAD4* show reduced expression in *mos3*-2 and *nup160*-3 plants as compared to wild-type. Genome-wide gene expression was analyzed in four week old unchallenged *Arabidopsis* Col-0 wild-type, *mos3*-2 and *nup160*-3 plants as described in Figure 5. The differential gene expression between wild-type and mutant is depicted as fold change after log_2 transformation (log_2FC). Bars represent log_2FC values of the defence-related genes *PAD4* (AT3G52430), *EDS1A* (AT3G48090) and *EDS1B* (AT3G48080). Light grey, wild-type versus *mos3*-2; dark grey, wild-type versus *nup160*-3.

Beside the altered gene expression of *EDS1* and *PAD4*, additional genes with known functions or potential implications in innate immunity were identified among the 227 lower expressed genes in *mos3*-2 and *nup160*-3 in comparison to Col-0 (Figure 6, right side;

Supplementary Table 1). This includes genes encoding for the TIR-NB-LRR class disease resistance proteins with described function in plant immunity, *BAR1* (AT5G18360; Laflamme *et al.*, 2020) and *SOC3* (AT1G17600; Zhang *et al.*, 2017), as well as three additional predicted TIR-type resistance proteins of yet unknown function (AT1G72840, AT5G36930, AT5G46260; Supplementary Table 1).

In addition, several predicted receptor-like proteins (RLPs) and receptor-like kinases (RLKs) were identified in the dataset. Previous research indicates that RLPs and RLKs can be implicated in developmental processes or play a role in plant resistance. Two RLPs (AT3G23110, AT3G11010) and seven RLKs (AT5G59680, AT4G21380, AT1G65790, AT5G59670, AT5G60900, AT1G65800, AT5G39030) were identified among the 227 DEGs with reduced expression. Furthermore, the calcium-dependent kinase (CPK) 31 (AT4G04695) and the two cysteine-rich receptor-like kinases (CRKs) 18 and 34 (AT4G23260, AT4G11530) were found in the dataset. Moreover, the three lectin-domain containing receptor kinases (LECRK) 12, 53, 54 (AT3G45390, AT2G43690, AT2G43700) and four LRR receptor-like kinases were revealed (AT1G51790, AT4G20140, AT5G20480, AT1G56120; Supplementary Table 1).

Importantly, the well characterized LRR receptor-like kinase *EFR* was found among the 277 DEGs (Figure 6, right side; Supplementary Table 1). Reduced expression of *EFR* as identified in this RNAseq experiment (Figure 5) are consistent with previous findings in the Wiermer group (Stepanets, M.Sc. Thesis, 2013; Lüdke, B.Sc. Thesis, 2014), showing reduced *EFR* transcript abundance in *nup160* and *mos3* mutant plants by qRT-PCR.

Whereas *EFR* was identified among the 227 DEGs, two other well-characterized PRRs, *FLS2* and *CERK1*, were not found among the 277 DEGs that show altered gene expression in *mos3*-2 and *nup160*-3 in comparison to Col-0. The expression pattern of *EFR*, *FLS2* and *CERK1* were evaluated by calculating the mapped reads per kilobase per million (RPKM) from the RNAseq experiment. Among the three investigated PRR genes only *EFR* showed significantly reduced transcript levels in both nucleoporin mutants (Figure 10).

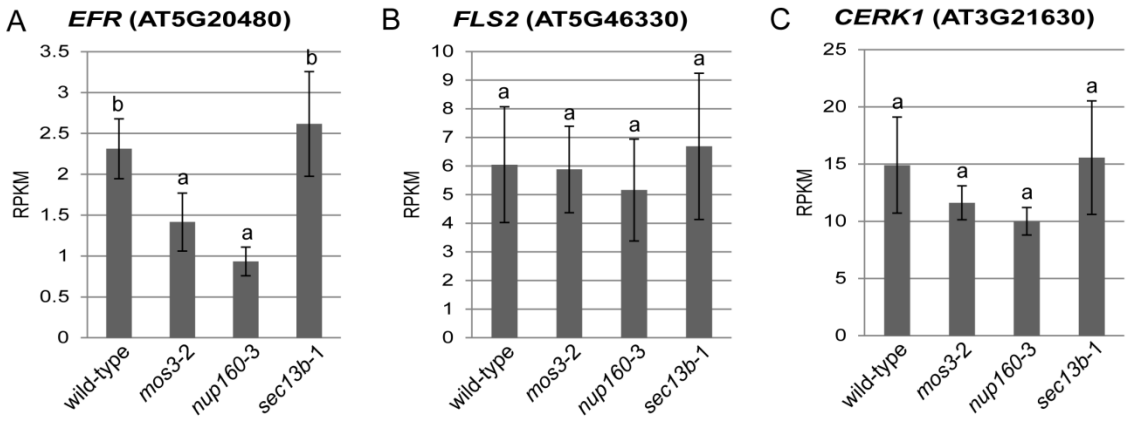

Figure 10: Expression profiles of the *PRR* genes *EFR*, *FLS2* and *CERK1* as revealed by the RNAseq analysis described in Figure 5. The expression profiles of (**A**) *EFR*, (**B**) *FLS2* and (**C**) *CERK1* are derived from the transcriptome analysis of four week old unchallenged *Arabidopsis* Col-0 wild-type, *mos3*-2, *nup160*-3 and *sec13b*-1 plants as described in Figure 5. Bars represent the average of mapped reads per kilobase per million (RPKM) ± SD of four biological replicates of each genotype. For each biological replicate the RNA was extracted from pools of 15 individual rosettes per genotype. Different letters indicate statistical significant differences between the genotypes (one-way Anova and tukey-post hoc test, $P < 0.05$).

Together, the reproducibly lower expression levels of both *EDS1A* and *EFR* in *mos3* and *nup160* are in line with previously published (Wiermer *et al.*, 2012) and unpublished data (Stepanets, M.Sc. Thesis, 2013; Lüdke, B.Sc. Thesis, 2014) and demonstrate the validity of the conducted RNAseq experiment. The abundance of transcripts encoding for *EFR* are reduced, but mRNA level of other known PRRs such as *FLS2* and *CERK1* are not altered in *mos3* and *nup160* in comparison to Col-0. These findings indicate that the defects of *mos3* and *nup160* plants selectively affect the expression of certain immune response genes.

3.1.4 Expression levels of the predicted methyl esterase *MES18* and the RNA-binding protein *PUM9* are most strongly decreased in unchallenged *mos3* and *nup160* mutant plants

Consistent with previous qRT-PCR data (Wiermer *et al.*, 2012; Stepanets, M.Sc. Thesis, 2013; Lüdke, B.Sc. Thesis, 2014), the RNAseq analysis (Figure 5) revealed changes in expression of the immune response genes *EDS1* and *EFR* in *mos3* and *nup160* plants. However, a major aim of this RNAseq approach was to identify unknown components of plant immunity. Since *mos3* and *nup160* are impaired in immunity (Wiermer *et al.*, 2012), the genes showing lower expression levels in *mos3*-2 and *nup160*-3 were promising candidates to investigate their role in plant immunity.

Among the 227 genes showing reduced expression in *mos3*-2 and *nup160*-3, the two genes whose expression is most strongly decreased as compared to the expression in wild-type plants are the predicted methyl esterase *MES18* (AT5G58310) and the predicted

pumilio family (PUF) RNA binding protein *PUM9* (AT1G35730; Figure 6, right side; Supplementary Table 1). *MES18* was differentially expressed with log_2FC values of -2.59 (*mos3*-2) and -3.96 (*nup160*-3), whereas PUM9 was differentially expressed in *mos3*-2 and *nup160*-3 with log_2FC values of -1.5 and -2.17, respectively (Figure 11).

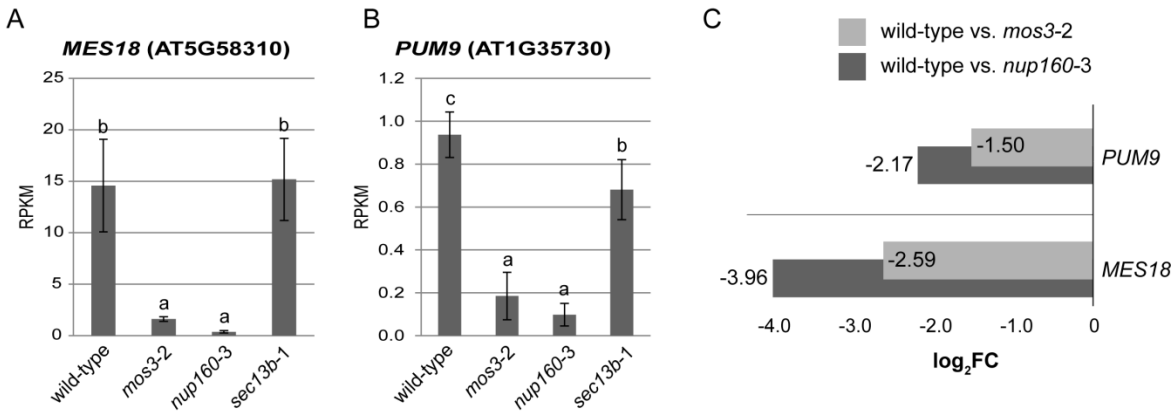

Figure 11: The predicted methyl esterase *MES18* and the pumilio family (PUF) RNA binding protein *PUM9* show reduced expression in *mos3*-2 and *nup160*-3 as compared to Col-0 wild-type. The expression profiles of (**A**) *MES18* and (**B**) *PUM9* are derived from the transcriptome analysis of four week old unchallenged *Arabidopsis* Col-0 wild-type, *mos3*-2, *nup160*-3 and *sec13b*-1 plants as described in Figure 5. Bars represent the average of mapped reads per kilobase per million (RPKM) ± SD of four biological replicates of each genotype. For each biological replicate the RNA was extracted from pools of 15 individual rosettes per genotype. Different letters indicate statistical significant differences between the genotypes (one-way Anova and tukey-post hoc test, $P < 0.05$). (**C**) The differential gene expression between wild-type and mutant is depicted as fold change after log_2 transformation (log_2FC). Bars represent log_2FC values of the genes *MES18* and *PUM9*. Light grey, wild-type versus *mos3*-2; dark grey, wild-type versus *nup160*-3.

The reduced expression of *MES18* and *PUM9* in both nucleoporin mutants and their predicted functions made these genes promising candidates to investigate their contributions to plant immunity. A previous phylogenetic analysis indicates that MES18 is related to the SALICYLIC ACID BINDING PROTEIN2 (SABP2) from *Nicotiana tabacum* (Vlot *et al.*, 2008a; Yang, *et al.*, 2008). It has been reported that *Nt*SABP2 has esterase activity on methyl salicylate (MeSA) and is implicated in plant innate immunity (Forouhar *et al.*, 2005). The predicted RNA binding protein PUM9 belongs to the highly conserved family of PUF RNA-binding proteins that contribute to post-transcriptional gene regulations such as mRNA localization, mRNA stability control and mRNA decay as well as translation (Francischini and Quaggio, 2009; Tam *et al.*, 2010). Since *mos3* and *nup160* mutant plants accumulate poly(A)-mRNA inside the nucleus (Wiermer *et al.*, 2012), the reduced expression of *PUM9* might contribute to the nuclear mRNA export defects in *mos3* and *nup160*.

In summary, unchallenged *mos3* and *nup160* mutant plants show mild but significant transcriptional changes. In total, 471 genes were differentially expressed in both nucleoporin mutants in comparison to Col-0 wild-type (log_2FC > 0.5 or < -0.5, FDR < 0.05; Figure 5 B).

Among the 471 genes, the expression of 332 genes is more drastically affected (i.e. 157 genes that are higher expressed and 173 genes that are lower expressed) in *nup160*-3 in comparison to *mos3*-2 (Figure 6; Supplementary Table 1). The GO terms “defence response” and “innate immunity response” were significantly overrepresented among the 471 DEGs (Figure 7), indicating that several genes with potential implications in plant immune responses are present among the identified DEGs. Out of these 471 genes, 244 genes showed higher and 227 genes showed lower expression in the mutants (Figure 5 B). Among the higher expressed genes, six nuclear-transport related genes have been identified (Figure 6, left side; Figure 8; Supplementary Table 1). Since MOS3 and NUP160 are two components of the NPC, the higher expression of nuclear-transport related genes in *mos3* and *nup160* mutant plants as compared to Col-0 indicates a regulatory mechanism to compensate for the loss of MOS3 and NUP160 function. In the set of the 227 genes showing reduced expression (Figure 5 B), several DEGs potentially implicated in plant immunity were identified (Figure 6, right side; Supplementary Table 1). This includes the known defence genes *EDS1* and *EFR* (Figure 6, 9 and 10; Supplementary Table 1) confirming previous published and unpublished results (Wiermer *et al.*, 2012; Stepanets, M.Sc. Thesis, 2013; Lüdke, B.Sc. Thesis, 2014). Whereas the transcript levels of *EFR* are reduced, mRNA amounts of the other well-characterized PRRs *FLS2* and *CERK1* are not significantly changed in the nucleoporins mutants (Figure 10), suggesting selective contributions of MOS3 and NUP160 to the regulation of *PRR* gene expression. The predicted methyl esterase *MES18* and the predicted RNA binding protein *PUM9* were identified as the two genes with the most strongly affected expression in *mos3*-2 and *nup160*-3 as compared to Col-0 wild-type (Figure 6, right side; Figure 11; Supplementary Table 1).

The defence phenotypic consequences of reduced *EFR* transcript abundance in *mos3* and *nup160* mutants are characterized in the second section (3.2). The functional characterization of *MES18* and *PUM9* and their potential roles in plant immunity is described in the third section (3.3) of the results chapter.

3.2 Defence phenotypic consequences of reduced *EFR* transcript accumulation in *mos3* and *nup160*

The RNAseq approach depicted in Figure 5 revealed reduced transcript levels of the well characterized PRR gene *EFR* in *mos3* and *nup160* mutant plants as compared to Col-0 (Figure 6 and 10). The phenotypic consequences of the reduced *EFR* transcript accumulation are described in the following section.

3.2.1 Independent validation of reduced *EFR* transcript abundance in *mos3* and *nup160* mutants by qRT-PCR

The well characterized PRR gene *EFR* showed reduced transcript levels in *mos3*-2 and *nup160*-3 mutant plant as compared to Col-0 wild-type (Figure 6 and 10). In contrast, transcript levels of the PRR genes *FLS2* and *CERK1* were unaffected (Figure 10). This suggests a selective involvement of the two nucleoporins *MOS3* and *NUP160* in the regulation of *EFR* expression (Figure 10). In order to independently validate the data revealed by RNAseq, the *EFR* transcript abundance was analysed in Col-0 wild-type, two independent mutant alleles of *mos3* and *nup160*, as well as *sec13b*-1 mutant plants, using qRT-PCR. In contrast to Col-0 wild-type and the *sec13b*-1 (SALK_04582) control, the *EFR* transcript abundance was significantly reduced in *mos3*-1 (Zhang and Li, 2005), *mos3*-2 (SALK_109959), *nup160*-3 (SAIL_877_B01) and *nup160*-4 (SALK_126801) mutant plants (Figure 12).

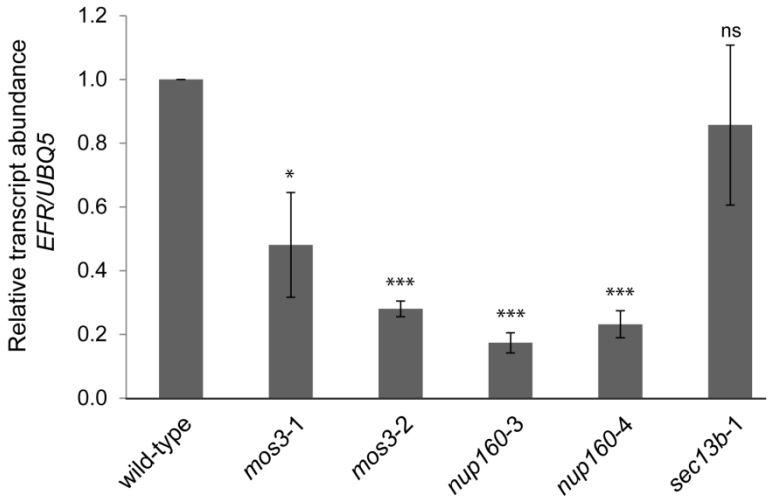

Figure 12: *EFR* gene expression is reduced in *mos3* and *nup160* mutant plants. Expression of *EFR* was analysed by qRT-PCR of four week old unchallenged *Arabidopsis* plants of the indicated genotypes. All plants were grown under short day conditions on soil. Total RNA for gene expression analysis was extracted from pools of 5 individual plants per genotype. The experiment was repeated three times with independently grown plants to obtain three biological replicates. *UBIQUITIN5* (*UBQ5*; AT3G62250) served as reference gene for normalizing the expression of *EFR.* Bars represent mean values of three biological replicates and error bars represent SEM. Relative transcript abundance of *EFR* in the mutant plants was normalized to Col-0 wild-type which is set to 1.0. Statistical analysis was performed using Student's t-test for comparison of Col-0 wild-type and mutants; not significant (ns), *P < 0.05, ** P < 0.01, *** P < 0.001.

The qRT-PCR analysis shown in Figure 12 independently validates the reduced *EFR* gene expression in unchallenged *mos3* and *nup160* plants that was uncovered in the RNAseq experiment and reported previously by D. Stepanets (2013) and D. Lüdke (2014; Figure 5 and 6). The results of the RNAseq experiment also indicate that the differential gene expression of *EFR* is more severely affected in the *nup160*-3 mutant in comparison to

mos3-2. These findings were confirmed in the qRT-PCR analysis. By contrast, the transcript levels of the PRR genes *FLS2* and *CERK1* were not significantly altered in *mos3*-2 and *nup160*-3 in the RNAseq analysis and this was also confirmed by qRT-PCR analysis (Supplementary Figure 2).

The differential gene expression of *EDS1A* was less severely affected in the two nucleoporins mutants as compared to the tandem copy *EDS1B* (Figure 9). The reduced expression of *EDS1A* that was revealed by the RNAseq experiment was also validated using qRT-PCR analysis (Supplementary Figure 3). The mildly reduced expression of *EDS1A* in the *nup160* mutant plants confirmed previous data (Wiermer *et al.*, 2012). Since the requirement of *MOS3* and *NUP160* in EDS1-dependent basal and TIR-type NB-LRR mediated resistance pathways has previously been reported (Wiermer *et al.*, 2012), the involvement of both nucleoporins in *EFR*-dependent plant defence responses was investigated in more detail, using the two independent mutant alleles of both *mos3* and *nup160* for the functional investigations.

3.2.2 *Mos3* and *nup160* mutants are more susceptible to *Agrobacterium tumefaciens* mediated transient transformation

The PRR EFR recognizes the N-terminal 18 amino acid peptide elf18 of the *Agrobacterium tumefaciens* translation elongation factor thermo unstable (EF-Tu) that acts as a PAMP in *Arabidopsis thaliana* and other *Brassicaceae* (Kunze *et al.*, 2004; Zipfel *et al.*, 2006). Interestingly, preliminary investigations of the Wiermer group showed that leaves of *mos3* and *nup160* mutant plants display chlorotic disease symptoms after the contact with an agrobacterial solution, whereas no disease symptoms were visible on Col-0 wild-type leaves (Stepanets, M.Sc. Thesis, 2013; Lüdke, B.Sc. Thesis, 2014). These initial data raised the questing whether the loss of *MOS3* and *NUP160* results in a higher susceptibility towards the biotrophic plant pathogen *A. tumefaciens*. For the infection process, *A. tumefaciens* relies on the transfer and integration of the bacterial transfer DNA (T-DNA) into the genome of plant hosts (Escobar and Dandekar, 2003), and the T-DNA transfer to plant cells can serve as a readout for the success of *Agrobacterium* to infect its host (Zipfel *et al.*, 2006). Accordingly, *efr* mutant plants show enhanced transformation rates by *A. tumefaciens* (Zipfel *et al.*, 2006), and initial investigations by D. Stepanets (2013) and D. Lüdke (2014) suggested that *mos3* and *nup160* are more susceptible to transformation. To corroborate the previous preliminary findings and investigate in detail whether *MOS3* and *NUP160* play a role in restricting *Agrobacterium*-mediated plant transformation, a β-glucuronidase (GUS) reporter assay was conducted as described previously (Zipfel *et al.*, 2006). Col-0 wild-type, *mos3*-1, *mos3*-2, *nup160*-3, *nup160*-4, *sec13b*-1 and *efr*-1 rosette leaves of four week old soil-grown plants were pressure infiltrated with a bacterial suspension of the non-tumorigenic

A. tumefaciens strain GV3101 pMP90K containing a binary plasmid with a *GUS + intron* reporter gene construct under control of the constitutive *35S* promoter. This construct allows for plant-specific expression of the GUS reporter after transformation of plant cells, but not for bacterial expression. Three days after pressure-infiltration of bacteria with a needleless syringe, only few GUS stained spots were visible on wild-type and *sec13b*-1 control leaves, indicating weak GUS activity and thus low transformation rates (Figure 13). In contrast, *efr*-1 leaves showed strong GUS staining, confirming previous results of Zipfel *et al.*, (2006) showing elevated transformation rates of *efr*-1 (Figure 13). Notably, both mutant lines of *mos3* and *nup160* exhibited stronger GUS activity compared to Col-0 wild-type and *sec13b*-1 control plants. However, in several independent experiments, leaves of the *mos3*-1 mutant allele showed a tendency towards less efficient transient transformation levels as compared to the *mos3*-2 and both *nup160* mutant alleles, which showed a higher and more uniform level of GUS activity staining similar to the *efr*-1 mutant (Figure 13). Several independent experimental repetitions also revealed that different Col-0 wild-type leaves show a variable amount of blue spots and considerable leaf-to-leaf variation that was already described previously for Col-0 plants (Zipfel *et al.*, 2006).

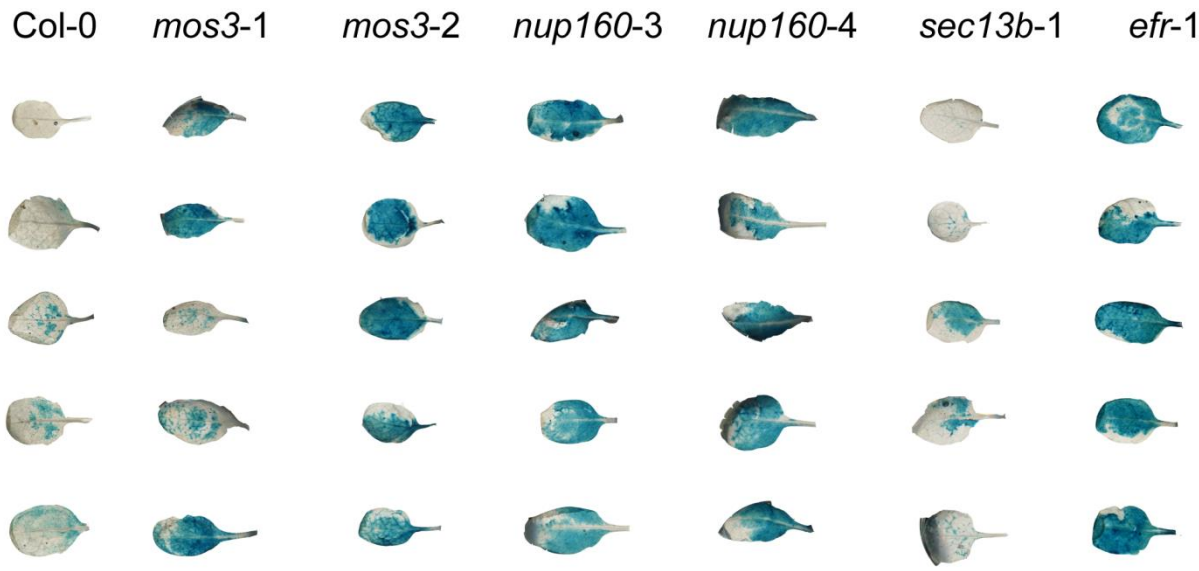

Figure 13: *Mos3* and *nup160* mutant plants are more susceptible to *Agrobacterium tumefaciens* mediated transient plant transformation. Rosette leaves of four week old soil-grown plants of the indicated genotypes were syringe-infiltrated with a bacterial suspension (OD_{600} = 0.3) of *A. tumefaciens* GV3101 pMP90RK harbouring a *35S::GUS+intron::3xHA-StrepII* construct. For each genotype, four leaves of three individual plants were inoculated and stained for GUS activity three days post inoculation (3 dpi). Representative images of five rosette leaves for each genotype are depicted. The experiment was repeated twice with independently grown plants showing similar results.

In summary, the GUS reporter assays revealed higher GUS activity staining in *mos3* and *nup160* mutant plants as compared to Col-0 and *sec13b*-1 control plants, indicating that

these mutants are more susceptible to transient *Agrobacterium*-mediated plant transformation. This effect seems to be less pronounced in *mos3* (in particular in *mos3*-1) as compared to *nup160*. The stronger GUS activity staining in *mos3* and *nup160* mutant plants compared to Col-0 might be a consequence of the reduced *EFR* transcript level in these mutants (Figure 12). Accordingly, a more severe impact on *EFR* gene expression in *nup160* as compared to *mos3* (in particular to *mos3*-1; Figure 6, right side; Supplementary Table 1; Figure 12) might explain the consistently higher transient *Agrobacterium*-mediated transformation rates of *nup160* as compared to *mos3*.

To investigate the possibility whether the enhanced transformation rates of *mos3* and *nup160* are simply caused by increased propagation of Agrobacteria in the leaf tissues, bacterial growth assays were conducted. *Agrobacterium* proliferation was investigated in Col-0 wild-type, *mos3*, *nup160* and *efr,* since these mutant plants showed enhanced transient transformation rates as compared to wild-type. Therefore, Col-0, *mos3*-1*, mos3*-2*, nup160*-3*, nup160*-4, and *efr*-1 plants were syringe-inoculated with the same non-tumorigenic *Agrobacterium* strain that was used for the GUS reporter assay. Three days after inoculation, the amount of viable bacteria in the leaves of the individual mutant plants were determined. All tested mutants showed similar bacterial propagation that was not significantly different from the growth in Col-0 wild-type (Figure 14).

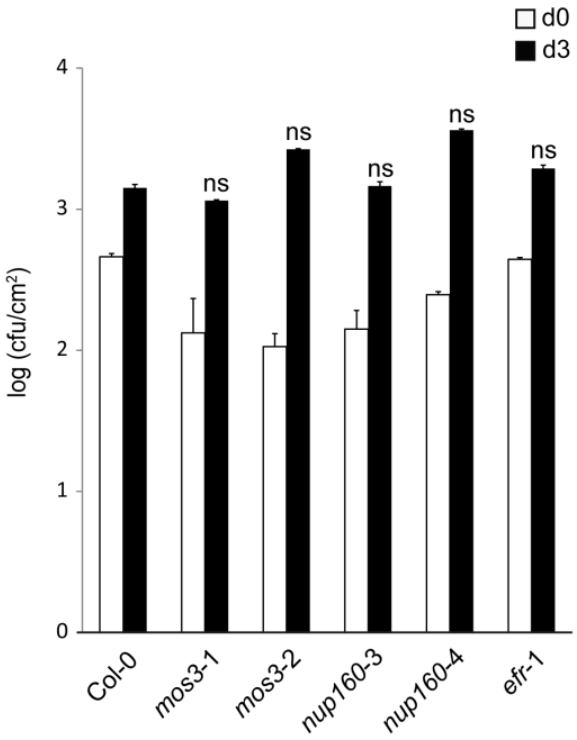

Figure 14: *Mos3*, *nup160* and *efr* mutants show similar *A. tumefaciens* growth compared to wild-type plants three days after pressure infiltration of agrobacterial solution into rosette leaves. Rosette leaves of five week old plants of the indicated genotypes were pressure-infiltrated with a bacterial suspension of $1x10^5$ colony-forming units ml^{-1} of *A. tumefaciens* GV3101 pMP90RK strain carrying a *35S::GUS+intron::3xHA-StrepII* vector construct. Bacterial growth in infiltrated leaves was quantified directly after infiltration (day 0, d0) and three days after infiltration (d3). Bars represent mean values of viable bacteria per cm^2 of leaf tissue ±SD. The experiment was conducted three times with similar results. Statistical analysis was performed using Student's t-test for comparison of Col-0 wild-type vs. mutant. ns, not significant; Cfu = colony-forming units.

The data from bacterial growth assays suggest that the enhanced GUS activity staining in *mos3* and *nup160* (as well as *efr*-1) leaves after pressure-infiltration of *A. tumefaciens* harbouring the *GUS + intron* reporter gene construct (Figure 13) is likely caused by enhanced transformation rates, rather than increased bacterial growth.

3.2.3 *Mos3* and *nup160* mutant plants are impaired in reactive oxygen species (ROS) production upon elf18 treatment

In *Arabidopsis* leaves, perception of the N-terminal 18 amino acid peptide of *A. tumefaciens* EF-Tu, termed elf18, by EFR triggers basal defence responses such as the production of reactive oxygen species (ROS; Zipfel *et al.*, 2006). A potential explanation for the higher transient transformation rates of *mos3* and *nup160* mutant plants by *A. tumefaciens* (Figure 13) is an impaired perception of this plant pathogen by the PRR EFR. To investigate whether the reduced *EFR* gene expression in *nup160* and *mos3* mutant plants (Figure 12) correlates with impaired basal defence responses, the production of ROS was analyzed in response to treatment with the PAMP elf18, using a luminol-based assay. Leave discs of

seven week old Col-0, *mos3*-1, *mos3*-2, *nup160*-3, *nup160*-4 and *efr*-1 control plants were incubated with a luminol-based chemiluminescent probe (L-012) with elf18 or without the PAMP as mock control. Mock-treatment of leaf discs caused no obvious ROS production (Supplementary Figure 4 A). Values measured for the mock-treatment were subtracted from values measured for the elf18 treated samples. Upon elf18 treatment, a clear ROS burst was observed of Col-0 wild-type plants (Figure 15), where ROS production reached its maximum at about 14-16 minutes (Figure 15 A). In the elf18 non-responsive *efr*-1 mutant control, ROS production was abolished as previously reported (Zipfel *et al.*, 2006). The overall ROS production that was measured in a time period of 60 minutes in the *mos3* and *nup160* mutants upon elf18 treatment was significantly reduced when compared to Col-0 wild-type levels (Figure 15 A, B). The ROS production in the *mos3* and *nup160* mutants was intermediate between wild-type levels and the non-responsive *efr* control (Figure 15 A). Similar to wild-type plants, elf18-treated *mos3* and *nup160* mutants also showed the maximum of ROS production at about 14-20 minutes after elf18 treatment (Figure 15 A), indicating that the timing of signal transduction leading to ROS production was not obviously affected in these plants. Due to technical reasons, ROS production in *sec13b*-1 plants was investigated in independently performed experiments including Col-0, *mos3*-2, *nup160*-3 and *sec13b*-1 plants. The overall ROS production in *sec13b*-1 mutant plants upon elf18 treatment was similar to the response observed in Col-0 wild-type (Supplementary Figure 4 and 5 B), suggesting a wild-type like perception of elf18 in these plants. The observed data are consistent with data from the GUS reporter assay, which revealed that *sec13b*-1 plants do not show enhanced transformation rates compared to Col-0 wild-type (Figure 13). Furthermore, *sec13b*-1 mutant plants show a wild-type like expression of *EFR* as revealed in the RNAseq experiment (Figure 10) and qRT-PCR analysis (Figure 12). Together, these data suggest that the reduced *EFR* expression in *mos3* and *nup160* in comparison to Col-0 and *sec13b* (Figure 6, 10 and 12) contributes, at least in part, to the reduced EFR-dependent ROS production of *mos3* and *nup160* upon elf18 treatment (Figure 15, Supplementary Figure 4 and 5).

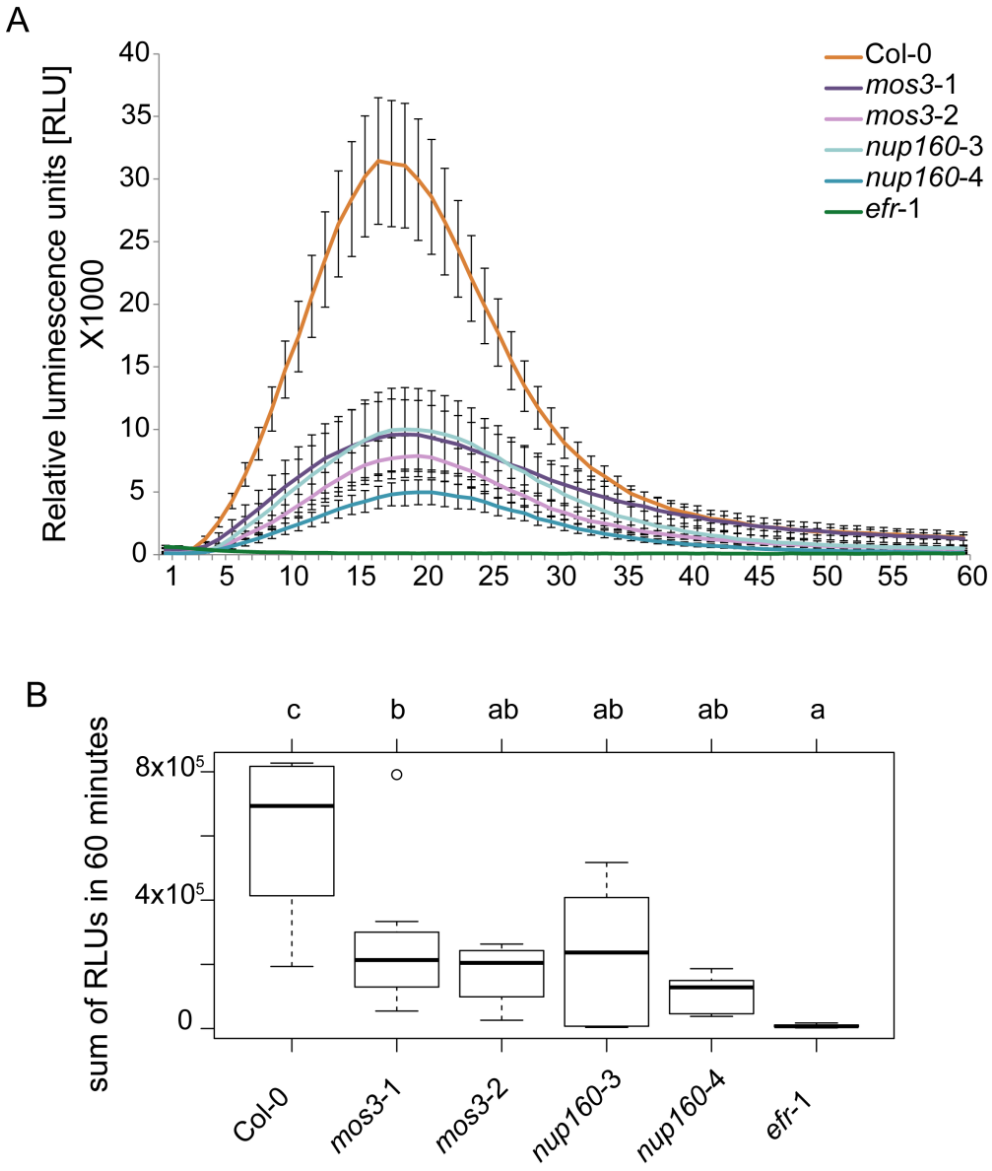

Figure 15: *Mos3* and *nup160* mutant plants are impaired in elf18-triggered ROS production. (**A**) Leaf discs of seven week old soil-grown *Arabidopsis* plants were treated with 100 nM elf18/L-012 solution (L-012, luminol-based chemiluminescent probe) or L-012 solution without elf18 peptide (mock control; see Supplementary Figure 4 A). Relative luminescence units (RLU) were recorded for the indicated genotypes after elf18 or mock treatment in 1 minute intervals for a period of 60 minutes. Data show mean values of eight leaf disc per genotype after subtraction of respective mock control. Error bars denote (SEM). The experiment was performed three times with similar results. (**B**) Box plots representing data from (**A**) of eight technical replicates per genotype. Each technical replicate is the sum of all measured RLUs for a time window of 60 minutes. Lower and upper whiskers indicate the 25th and 75th percentile, respectively, and median is depicted by the black line. Open circles represents outliers. Different letters indicate statistical significant differences between the genotypes (one-way Anova and tukey-post hoc test, $P < 0.05$).

3.2.4 Reduced *EFR* transcript abundance correlates with reduced EFR protein levels in the *mos3-2* mutant background

The data presented above suggest that the reduced *EFR* gene expression in *mos3* and *nup160* mutants contributes to the reduced elf18-induced ROS production and enhanced

transient transformation rates by *A. tumefaciens* (Figure 12, 13 and 15). To test whether the reduced *EFR* expression is also reflected at the EFR protein level, *EFR* promoter-driven EFR-eGFP-HA transgenic *efr*-1 plants have been obtained from the lab of Prof. C. Zipfel (University of Zurich; Nekrasov *et al.*, 2009) and the transgene was introgressed into the *mos3*-2 (SALK_019959) and *nup160*-3 (SAIL_877_B01) mutant backgrounds by crossing. This approach was used as there is no antibody available for detection of the endogenous EFR protein by immunoblot analysis. The *EFR* gene expression is less severely affected in *mos3*-2 as compared to *nup160*-3 mutant plants (Figure 10 and 12). These findings suggest that EFR protein levels are probably less strongly affected in the *mos3*-2 mutant plants.

Plants of the F1 generation (♀ EFR-eGFP-HA in *efr*-1 x ♂ *mos3*-2) were analyzed for the presence of the T-DNA in the *MOS3* gene to confirm the success of the crossing event of the *pEFR::EFR-eGFP-HA* transgenic *efr*-1 plants and *mos3*-2 mutant plants. F2 plants were analysed for homozygosity of the *mos3*-2 mutation by PCR-based genotyping. Since the chromosomal integration locus of the *pEFR::EFR-eGFP-HA* transgene is not known (personal communication with the Zipfel lab) and an approach to map the transgene was not successful (data not shown), PCR-based genotyping could not be used to investigate the homozygosity of the transgene in the F2 generation. However, the presence of the *pEFR::EFR-eGFP-HA* transgene in *mos3*-2 homozygous plants was confirmed by PCR-based amplification of the *GFP* marker gene in the F2 generation. Consequently, F3 progeny were analysed to identify plants homozygous for both the *mos3*-2 mutation and the transgene. Since *pEFR::EFR-eGFP-HA* transgenic *efr*-1 plants carry a Basta® (glufosinate) herbicide resistance cassette, this resistance marker was used to evaluate *mos3*-2 homozygous F3 plants for homozygosity of the transgene. However, no plant homozygous for both the *mos3*-2 mutation and the transgene was identified when growing F3 plants on phosphinotrycin (PPT)-containing agar plates. Therefore, plants of the F2 generation that are segregating for the *mos3*-2 mutation were reanalysed and plants contain the *pEFR::EFR-eGFP-HA* transgene were selected via PCR-based amplification of the *GFP* marker gene. Basta® (glufosinate) herbicide selection of F3 progeny was used to identify plants homozygous for the transgene. One plant line was identified that shows homozygosity of the transgene and was subsequently also verified for homozygousity of the *mos3*-2 mutation.

F3 plants homozygous for the transgene and the *mos3*-2 mutation were grown and total protein extracts were isolated from three individual plants. Isolated total protein extracts were used for immunoblot analysis. In addition, plants that are homozygous for the transgene but wild-type for the *MOS3* gene were selected during the genotyping process and total protein extracts of these plants were used as internal control. The immunoblot analysis revealed that similar amounts of EFR protein accumulates in the control plants (that are wild-type for

MOS3) and the parental EFR-eGFP-HA transgenic line obtained from the Zipfel lab (Figure 16). In contrast, plants homozygous for both the transgene and the *mos3*-2 mutation showed reduced EFR protein levels in comparison to the parental line and the internal control plants (Figure 16).

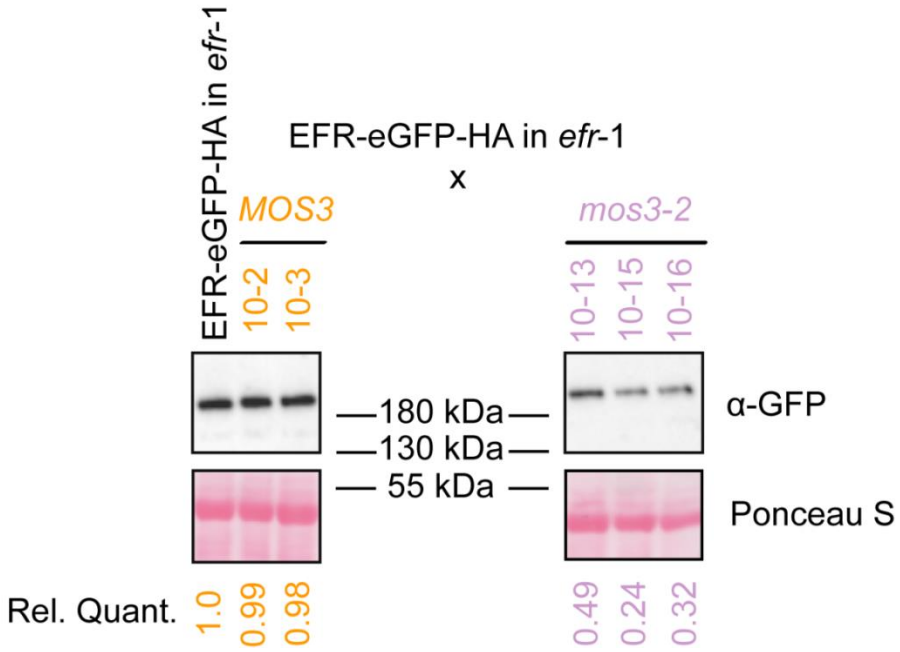

Figure 16: EFR protein accumulation is reduced in *mos3-2* mutant plants. The Effect of the *mos3-2* mutation on EFR protein levels are depicted in this figure. Total protein extracts were prepared from individual plants (indicated by different numbers) and the concentration of total protein extracts was measured using Bradford assay. The parental *efr*-1 line transgenic for *pEFR::EFR-eGFP-HA* was used as control. For each sample 30 µg of total protein was loaded per lane. All samples were run on one SDS gel and the same exposure time was used for all samples. The EFR-GFP-HA protein was detected via Western Blotting using α-GFP antibody. Individual F3 plants homozygous for the *EFRp::EFR-eGFP-HA* transgene and either wild-type for the *MOS3* gene (indicated in orange) or homozygous for the *mos3*-2 mutation (indicated in light purple) were used to determine EFR protein levels. Lower panels show Ponceau S staining of the membrane as loading control. Relative quantification (Rel. Quant.) of EFR-eGFP-HA abundance was calculated using BIO RAD Image Lab™ software and is indicated as numbers below the immunoblot relative to the amount in the *efr*-1 line transgenic for *pEFR::EFR-eGFP-HA*.

The EFR-GFP-HA protein levels were assessed by quantifying the α-GFP immunoblot signal intensity between the parental line and plants that derived from the cross using the BIO RAD Image Lab™ software. In the wild-type situation for *MOS3,* the α-GFP immunoblot signal varies between 1.0 and 0.98, whereas the α-GFP signal was reduced in plants that are homozygous for the *mos3*-2 mutation. Relative quantification values varied from 0.49 to 0.24, suggesting that the EFR-eGFP-HA protein amount is reduced in these plants. However, quantification of the GFP signal also revealed some variation between the investigated siblings.

Since the *EFR* gene expression is more drastically affected in the *nup160*-3 mutant plants as compared to *mos3*-2 (Figure 10 and 12), the decrease in total EFR protein levels is likely even more pronounced in the *nup160* mutant background. To test this, the pEFR::EFR-eGFP-HA transgenic *efr*-1 plants were also crossed with the *nup160*-3 (SAIL_877_B01) mutant for subsequent analysis of the EFR-eGFP-HA abundance.

After conformation of a successful crossing event in the F1 generation, F2 plants were analysed for homozygosity of the *nup160*-3 mutation by PCR-based genotyping. The herbicide selection approach that was used for the *mos3*-2 mutant background and that is described above was not feasible to identify lines that are homozygous for the *pEFR::EFR-eGFP-HA* transgene in the *nup160*-3 mutant background. The *nup160*-3 (SAIL_877_B01) mutant plants as well as the transgenic line both carry a Basta® (glufosinate) herbicide resistance cassette. F2 plants homozygous for the T-DNA insertion in the *NUP160* gene and verified for the presence of the *pEFR::EFR-eGFP-HA* transgene using PCR were selected. The F3 progeny will be analysed for the segregation pattern of the transgene by PCR-based detection of the *GFP* marker gene. To date this genotyping approach is still ongoing and so far no plants could be isolated that are homozygous for both, the transgene and the *nup160*-3 mutation. However, based on the more severely reduced *EFR* transcript abundance in n*up160*-3 as compared to *mos3*-2, it can be hypothesised that the EFR protein level in the *nup160*-3 background are similarly or probably even more drastically reduced as observed for the *mos3*-2 mutant background.

To summarize, *mos3* and *nup160* mutant plants show reduced amounts of *EFR* transcripts as revealed by the RNAseq experiment and independently verified by qRT-PCR analysis. The differential *EFR* gene expression appears to be more severely affected in *nup160* mutant plants as compared to *mos3* (Figure 10 and 12). GUS reporter assays revealed that *mos3* and *nup160* mutant plants show higher transient transformation rates by the plant pathogen *A. tumefaciens* when compared to wild-type and *sec13b* plants. This enhanced susceptibility to *Agrobacterium*-mediated transformation appears to be more pronounced for the *nup160* mutants (Figure 13 and 14). The reduced elf18-triggered ROS production in *mos3* and *nup160* mutants suggests that the perception of this *A. tumefaciens* derived PAMP is impaired (Figure 15). This defect may partially be caused by the reduced *EFR* gene expression in *mos3* and *nup160* mutants (Figure 10 and 12), which compromises EFR protein accumulation as shown for the *mos3*-2 mutant and which is expected to be even more pronounced in the *nup160*-3 mutant (Figure 16). I further conclude, that the *mos3*-2 mutant which is less strongly impaired in *EFR* gene expression compared to *nup160*-3 mutant, serves as a useful tool to assess altered EFR protein levels.

3.3 Functional characterization of the predicted methyl esterase *MES18* and the RNA-binding protein *PUM9*

The RNAseq approach depicted in Figure 5 identified *MES18* (AT5G58319) and *PUM9* (AT1G35730) as the two DEGs whose expression is most strongly affected in *mos3* and *nup160* (Figure 6, right side; Supplementary Table 1). Since *mos3* and *nup160* mutant plants show immunity defects (Roth and Wiermer, 2012; Wiermer *et al.*, 2012), *MES18* and *PUM9* are interesting candidates to analyze for their potential roles in plant immunity. The results of the functional characterization are described in the following section.

3.3.1 Independent validation of reduced *MES18* and *PUM9* transcript abundance in *mos3* and *nup160* mutants by qRT-PCR

The RNAseq approach depicted in Figure 5 revealed that the predicted methyl esterase *MES18* and the RNA-binding protein *PUM9* show lower expression in *mos3* and *nup160* mutant plants (Figure 11). These findings were independently validated by qRT-PCR analysis. *MES18 and PUM9* transcript abundance were analysed in Col-0, two independent mutant alleles of *mos3* and *nup160* as well as *sec13b*-1 mutant plants. In contrast to Col-0 wild-type and *sec13b*-1 control plants, the amount of *MES18* transcripts (Figure 17 A) and *PUM9* transcripts (Figure 17 B) were significantly reduced in *mos3*-1, *mos3*-2, *nup160*-3 and *nup160*-4 mutant plants.

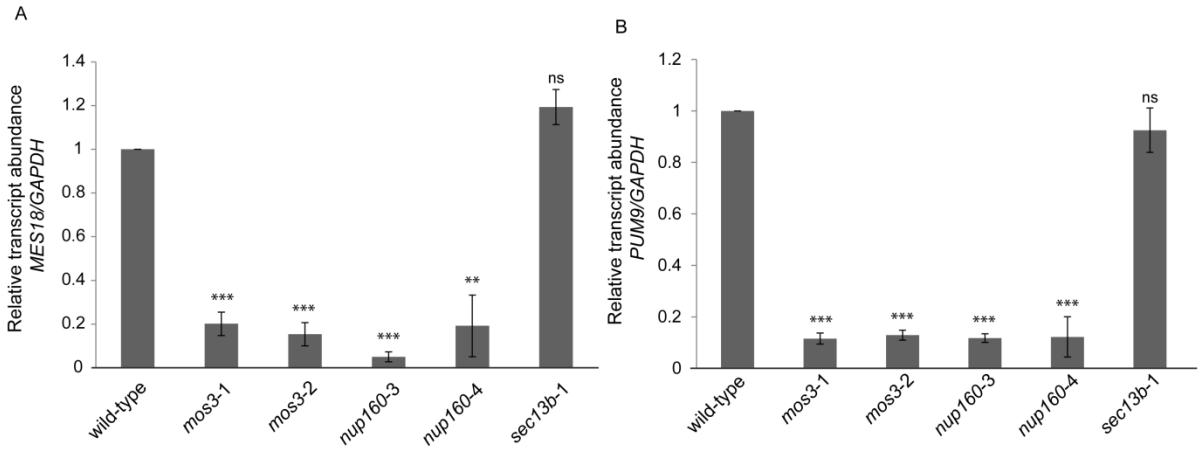

Figure 17: *MES18 and PUM9* transcript abundance are reduced in *mos3* and *nup160* mutants as quantified by qRT-PCR analysis. Expression of (**A**) *MES18* and (**B**) *PUM9* was analysed by qRT-PCR of four week old unchallenged *Arabidopsis* plants of the indicated genotypes. All plants were grown under short day conditions on soil. Total RNA for gene expression analysis was extracted from pools of five individual plants per genotype. The experiment was repeated three times with independently grown plants to obtain three biological replicates. *GAPDH* (*GAPCp-1;* At1g79530) served as reference gene for normalizing the expression of *MES18* and *PUM9.* Bars represent mean values of three biological replicates and error bars represent SEM. qRT-PCRs were performed by Jonas Appel. Relative transcript abundance of (**A**) *MES18 and* (**B**) *PUM9* in the mutant plants was normalized to Col-0 wild-type which is set to 1.0. Statistical analysis was performed using Student's t-test for comparison of Col-0 wild-type and mutants; not significant (ns), *P < 0.05, ** P < 0.01, *** P < 0.001.

The qRT-PCR analysis shown in Figure 17 independently validates the reduced *MES18* and *PUM9* gene expression in unchallenged *mos3* and *nup160* plants in comparison to Col-0 wild-type and the *sec13b*-1 control.

3.3.2 Isolation of *mes18* and *pum9* T-DNA insertion lines

MES18 is related to SABP2 from tobacco (Vlot *et al.*, 2008a; Yang, *et al.*, 2008), which is implicated in plant innate immunity (Forouhar *et al.*, 2005). The predicted pumilio family (Puf) RNA-binding protein PUM9 is described to reduce seed dormancy (Xiang *et al.*, 2014) and plays a role in mRNA destabilization and in the regulation of plant development (Nyikó *et al.*, 2019).

To further investigate the contribution of *MES18* and *PUM9* to plant immunity, T-DNA insertion lines in the Col-0 background were obtained for both genes from the European Arabidopsis Stock Centre (NASC, Scholl *et al.*, 2000). For *MES18* the two lines *mes18*-1 (SALKseq_067028) and *mes18*-2 (SAIL_609_A08) were characterized. For *PUM9* two previously described lines were used (GK_152E12 and SALK_135897; Nyikó *et al.*, 2019). In this study, the lines were named *pum9*-1 (GK_152E12) and *pum9*-2 (SALK_135897). PCR-based genotyping was used to identify homozygous mutant plants for each line. The position of the respective T-DNAs was determined by PCR and sequencing. *MES18* consist of three exons and the T-DNAs were either located in the first exon (*mes18*-1) or in the promoter region (*mes18*-2). *PUM9* consist of five exons and T-DNAs were either located in the fourth (*pum9*-1) or in the first exon (*pum9*-2) (Figure 18 A). In order to test for the absence of functional transcripts, semi-quantitative RT-PCR was performed with cDNA-specific primers flanking either the T-DNA insertion site or located downstream of it (Figure 18 A and B). These analyses revealed that the *mes18*-2 mutant still contains a transcript 3' of the T-DNA insertion site in the promoter region. This suggests that full-length functional *MES18* transcripts are likely produced in this line. Hence, this line was not used for further analysis. The *mes18*-1, *pum9*-1 and *pum9*-2 mutant plants did not show full length transcripts (Figure 18 B), and were used for *Pseudomonas* growth assays. Unfortunately, a second *mes18* mutant line was not available during this study, albeit the generation of a second *mes18* mutant allele using CRISPR/Cas9-based genome editing was started. The generation of this mutant as well as a transgenic *mes18*-1 line for complementation analysis of the mutation by the wild-type *MES18* gene is currently still ongoing.

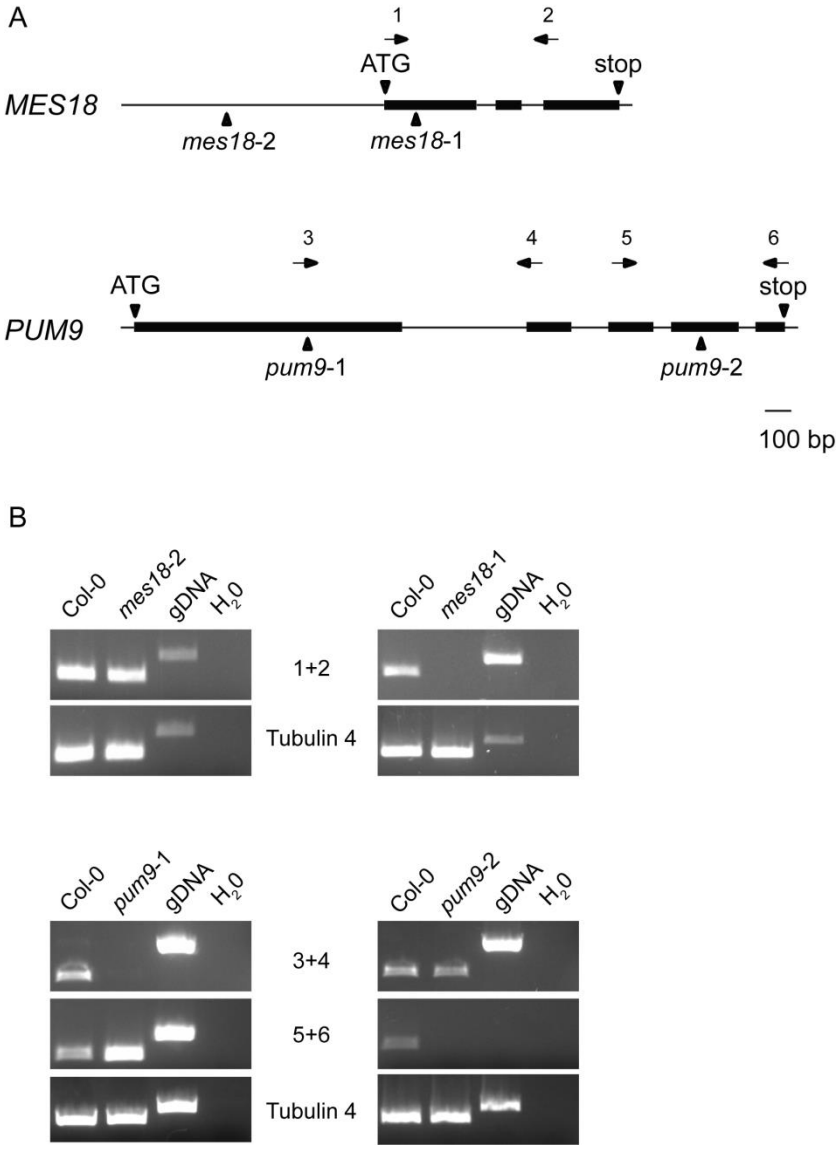

Figure 18: Characterization of *mes18*-1, *mes18*-2, *pum9*-1 and *pum9*-2 T-DNA insertion lines used in this study. (**A**) Schematic gene structures of *MES18* (top) and *PUM9* (bottom). Exons are depicted as black boxes and introns as solid lines. Start and stop codons of the genes are indicated as ATG and stop. Position of T-DNA insertions are indicated with black triangles. The positions of primers used to investigate transcript abundance are indicated with black arrows and numbers. (**B**) Semi-quantitative RT-PCRs were conducted on cDNA of the indicated genotype to investigate the disruption of functional transcripts. Col-0 wild-type cDNA was used as control. gDNA was used to address gDNA contaminations. gDNA control for primer pair 5+6 is only shown on the left-hand side. Primer combinations used for PCR are indicated by numbers and shown in the gene structures in **A**. *Tubuli4* was used as reference gene.

3.3.3 *Mes18* mutant plants are impaired in basal resistance to *Pseudomonas syringae*

To address whether *MES18* and *PUM9* are implicated in plant immunity, *Pseudomonas* growth assays were performed. First, leaves of homozygous *mes18*-1, *pum9*-1 and *pum9*-2 mutant lines were infected with virulent *Pseudomonas syringae* pv. *tomato* (*Pst*) strain DC3000 (Figure 19 A). Basal resistance against *Pst* DC3000 was significantly compromised

in *mes18*-1 mutant plants as indicated by 10-fold increase in bacterial growth three days after inoculation in comparison to Col-0 wild-type. In contrast, the two independent *pum9* mutant alleles did not show enhanced disease susceptibility towards this pathogen (Figure 19 A). The enhanced disease susceptibility of *mes18*-1 towards *Pst* DC3000 was less strong as the complete breakdown of basal resistance observed for the hyper-susceptible Col-0 *eds1*-2 control (Bartsch *et al.*, 2006; Figure 19 A). Although these findings need to be verified with an independent mutant allele of *MES18*, the infection data indicate that a mutation in *MES18* impairs basal defence towards the hemi-biotrophic pathogen *Pst* DC3000. Mutations in *PUM9* did not compromise basal resistance towards *Pseudomonas* (Figure 19 A). This suggests that *PUM9* is either not required for basal resistance towards this bacterial pathogen or may function redundantly with other *PUM* genes in *Arabidopsis* (Francischini and Quaggio, 2009; Tam *et al.*, 2010).

To investigate a potential contribution of *MES18* and *PUM9* in effector-triggered immunity, leaves of homozygous *mes18*-1, *pum9*-1 and *pum9*-2 mutant lines were infected with an avirulent *Pst* DC3000 strain, expressing the effector *avrRps4*, that is recognized by the TNL receptor RPS4 (Hinsch and Staskawicz, 1996; Figure 19 B). Neither mutations in *MES18* nor *PUM9* led to compromised RPS4-mediated resistance as indicated by similar bacterial growth of *Pst* DC3000 (*avrRps4*) in *mes18*-1 and both mutant alleles of *pum9* in comparison to Col-0 wild-type. The hypersusceptible Col-0 *eds1*-2 null mutant showed enhanced bacterial growth as expected (Figure 19 B). Similarly, resistance conferred by the CNL receptor RPM1 to the *Pst* DC3000 strain expressing the effector *avrRpm1* (Mackey *et al.*, 2002) also remained intact in *mes18*-1 and both alleles of *pum9*. The bacterial growth observed in the hyper-susceptible *ndr1*-1 mutant was increased as compared to Col-0 wild-type (Aarts *et al.*, 1998; Figure 19 C).

In summary, bacterial growth assays indicate that a mutation in *MES18* compromises basal resistance, but not RPS4- or RPM1-mediated resistance towards the hemi-biotrophic pathogen *P. syringae*, whereas *pum9* mutant plants are neither impaired in basal nor in RPS4- and RPM1-triggered immunity.

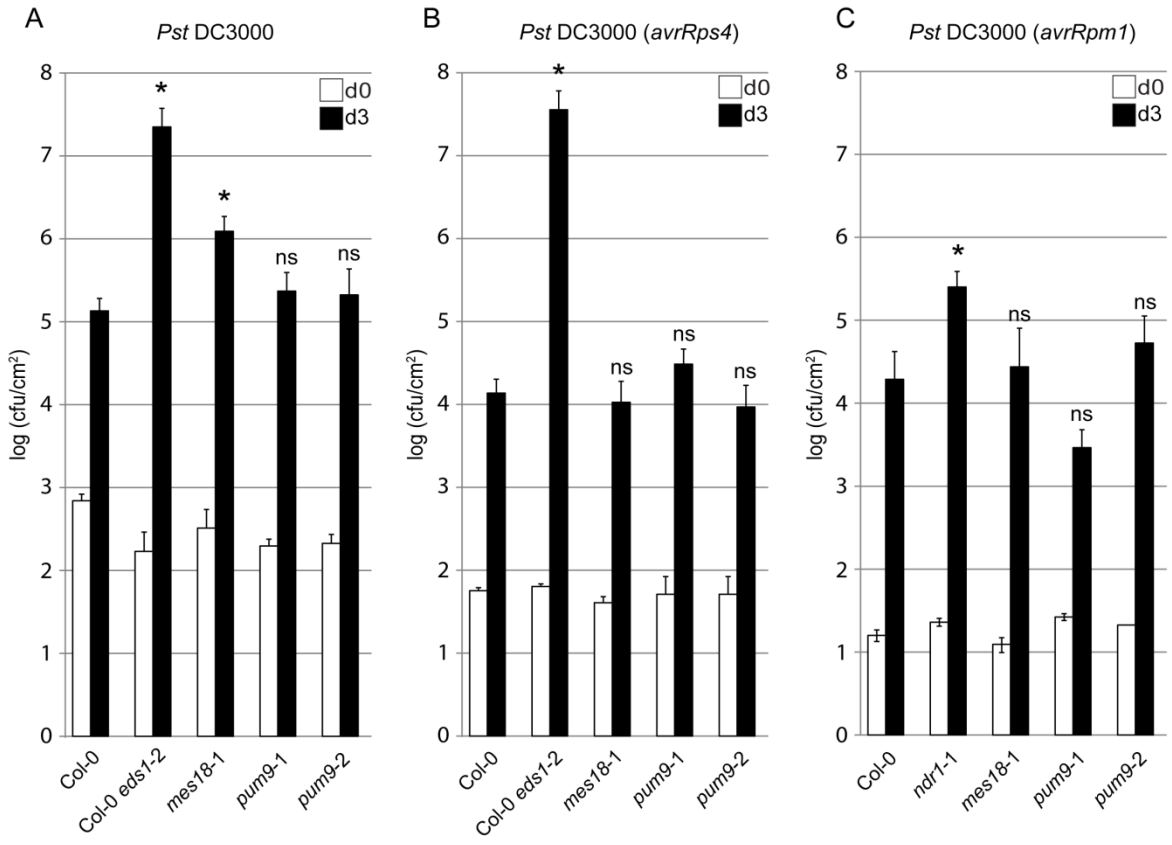

Figure 19: *Mes18* is impaired in basal resistance towards *Pseudomonas syringae.* Leaves of five week old plants of the indicated genotypes were pressure-infiltrated with a bacterial suspension of $1x10^5$ colony-forming units ml^{-1} of (**A**) virulent *Pseudomonas syringae* pv. *tomato* (*Pst*) strain DC3000 or (**B**) *Pst* DC3000 strain expressing *avrRps4* or (**C**) *Pst* DC3000 strain expressing *avrRpm1*. Bacterial growth was quantified on infiltrated leave material one hour (d0) and three days (d3) after infiltration. Bars represent mean values of viable bacteria per cm^2 of leaf tissue ±SD at d0 (white bars) and d3 (black bars). The experiment was conducted for (**A**) three times and (**B, C**) two times with similar results. Statistical analysis was performed using Student's t-test for comparison of Col-0 wild-type and mutants; not significant (ns), *P < 0.05. Col-0 *eds1*-2 and *ndr1*-1 are used as hyper-susceptible controls. Cfu = colony-forming units.

One aim of this study was to identify new components that play a role in plant immunity. Since the methyl esterase *MES18* is involved in basal resistance towards the plant pathogen *P. syringae*, the function of MES18 was analysed in more detail.

3.3.4 The *Arabidopsis* genome encodes for 20 predicted methyl esterases that show sequence homology to *Nt*SABP2 and *Le*MJE

In *Arabidopsis*, 24 genes belong to the *SABATH* family (D'Auria *et al*., 2003) encoding for proteins that catalyse methylation of small molecules such as salicylic acid (SA), jasmonic acid (JA) or indole-3-acetic acid (IAA) within the plant cell (Ross *et al.*, 1999; Seo *et al.*, 2001; Zubieta *et al.*, 2003; Qin *et al.*, 2005; Zhao *et al.*, 2008). In contrast, de-methylation processes are catalysed by methyl esterases (Stuhlfelder *et al.*, 2002; Stuhlfelder *et al.*, 2004; Yang *et al.*, 2006; Vlot *et al.*, 2008; Yang *et al.*, 2008). Figure 20 illustrates methylation

and de-methylation processes that are catalysed by methyl transferases (MTs) of the *SABATH* family or methyl esterases (MESs). One well characterized methyl esterase is the SALICYLIC ACID BINDING PROTEIN2 (SABP2) from *N. tabacum*, which showed methyl salicylate (MeSA) esterase activity (Forouhar *et al.*, 2005). In addition, a methyl jasmonate esterase (MJE) was identified in tomato (Stuhlfelder *et al.*, 2002; Stuhlfelder *et al.*, 2004). In *Arabidopsis*, 20 genes have been identified encoding for proteins that show sequence homology to tobacco SABP2 and tomato MJE (Yang *et al.*, 2006; Yang *et al.*, 2008; Vlot *et al.*, 2008a). These 20 orthologs of *Nt*SABP2 and *Le*MJE belong to the α/β hydrolase superfamily named methylesterase 1 to methylesterase 20 (MES1-20; Yang *et al.*, 2008).

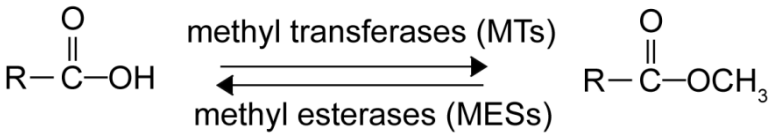

Figure 20: Schematic methylation and de-methylation reactions. Methylation processes catalysed by MTs is carried out on the carboxyl group. De-methylation processes catalysed by esterases convert methyl esters back to free acids (Adapted from Yang *et al.*, 2006). MT, methyl transferases; MES, methyl esterases.

Multiple sequence alignment using the web-based alignment tool ClustalW (Thompson *et al*., 2002), Kyoto University Bioinformatics Center revealed that the catalytic triad that is needed for enzymatic activity and characteristic for the α/β hydrolase family is conserved in 15 methyl esterases in *Arabidopsis* (Supplementary Figure 6). The catalytic triad is represented by the residues serine (S81), histidine (H238) and aspartic acid (D210) in *Nt*SABP2. In the protein sequence of MES11, MES13, and MES15, the conserved serine residue is replaced by an additional aspartic acid residue. MES19 and MES20 are truncated proteins that lack one or more residues of the highly conserved catalytic triad, suggesting that the proteins are non-functional. Therefore, MES19 and MES20 were excluded from further analysis.

3.3.5 MES18 is most closely related to MES16 and MES17

To further investigate the phylogenetic relationship of MES1-18, a bootstrap consensus tree was constructed, using the neighbor-joining method. The analysis involved the full length amino acid sequences of MES1-18, *Nt*SABP2 and *Le*MJE and was conducted with the Molecular Evolutionary Genetics Analysis X tool (MEGA X, Kumar *et al.*, 2018). The phylogenetic tree illustrates that MES18 is most closely related to MES16 and that MES17 is closely related to MES18 and MES16 (Figure 21).

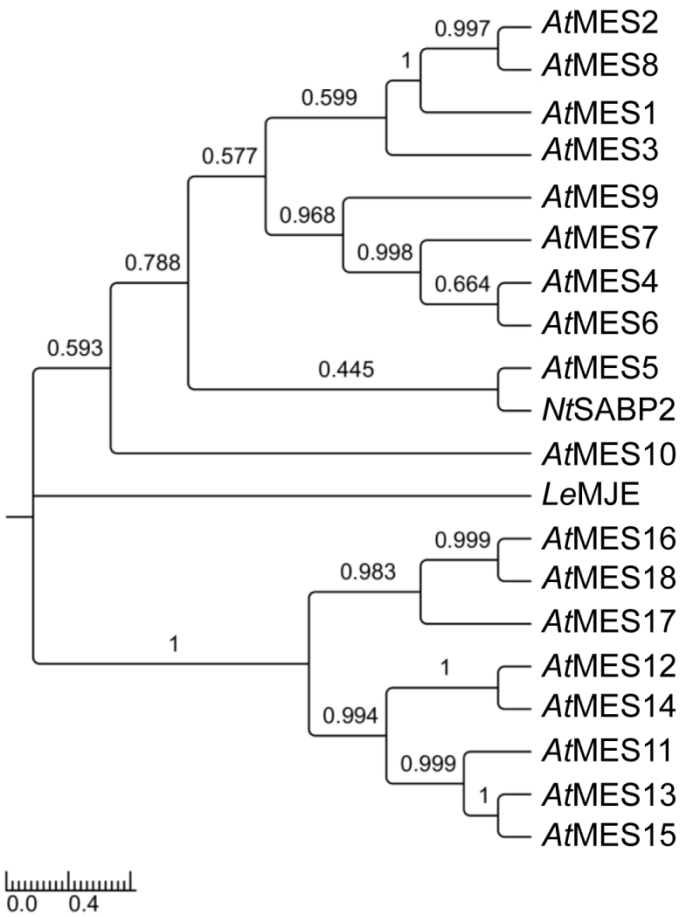

Figure 21: Tree showing the phylogenetic relationship among the methyl esterase family in *Arabidopsis*. The phylogenetic relationship of *At*MES family members was inferred using the neighbor-joining method (Saitou and Nei, 1987). The bootstrap consensus tree was inferred from 1000 replicates (Felsenstein, 1985) and values of replicate trees in which the associated taxa cluster together are indicated next to the branches. The evolutionary distances were calculated using the poisson correction method (Zuckerkandl and Pauling, 1965). Scale bar represents the number of amino acid substitutions per site. The analysis involved protein sequences of 18 *Arabidopsis* MES members (MES1-MES18), tobacco *Nt*SABP2 and tomato *Le*MJE. All ambiguous positions were removed for each sequence pair (pairwise deletion option). Evolutionary analysis was conducted in MEGA X (Kumar *et al.*, 2018) and results were visualized in *TreeGraph 2* (Stöver and Müller, 2010).

3.3.6 MES18 shows esterase activity

Since MES18 belongs to the α/β hydrolase superfamily and is an orthologue of *Nt*SABP2 and *Le*MJE, it was investigated if the *MES18* gene also encodes for a functional esterase. A photometric esterase assay was used to investigate whether a recombinant MES18 protein has esterase activity. The assay was adapted from a method previously described in Yang *et al.* (2008).

E. coli was used as heterologous expression system for MES18. The *MES18* gene was amplified from Col-0 wild-type cDNA and cloned into the pET28a (+) expression vector that allows for expression of MES18 with an N-terminal 6x His tag. After sequencing and confirmation of the expression vector, the vector was transformed into *E. coli* Rosetta 2 cells.

A single *E. coli* colony harbouring the pET28a (+) *His_6-MES18* construct was grown in selective LB medium for large scale expression. The recombinant His_6-MES18 was purified by affinity and size exclusion chromatography (Supplementary Figure 7). The purified His_6-MES18 protein was dissolved in 10mM NaCl and 50 mM TRIS-HCl (pH 8.0) at a concentration of 1.53 mg/mL in a volume of 16 mL and stored at 4°C until further use.

MES18 has a predicted size of 29.1 kDa (The Arabidopsis Information Resource, TAIR) and the purified His_6-MES18 migrated at approximately this size in a SDS PAGE analysis (Supplementary Figure 7). In an analytic gel filtration His_6-MES18 eluted with an estimated molecular mass of 84 kDa, indicating that His_6-MES18 is at least a dimer in solution (Figure 22). The analysis was performed with ~1 mg protein (Figure 22, blue peak) and ~0.5 mg protein (Figure 22, organge peak). Since molecular masses that are determined by analytical gel filtration are only full accurate if the investigated protein is globular, the estimate molecular mass of His_6-MES18 needs to be interpreted with caution. So far no information about the structure of MES18 is known. Importantly, only one single peak was detected by analytic gel filtration, independent of the protein concentration (Figure 22), indicating that only one species of His_6-MES18 exists in solution and no further contaminations are present.

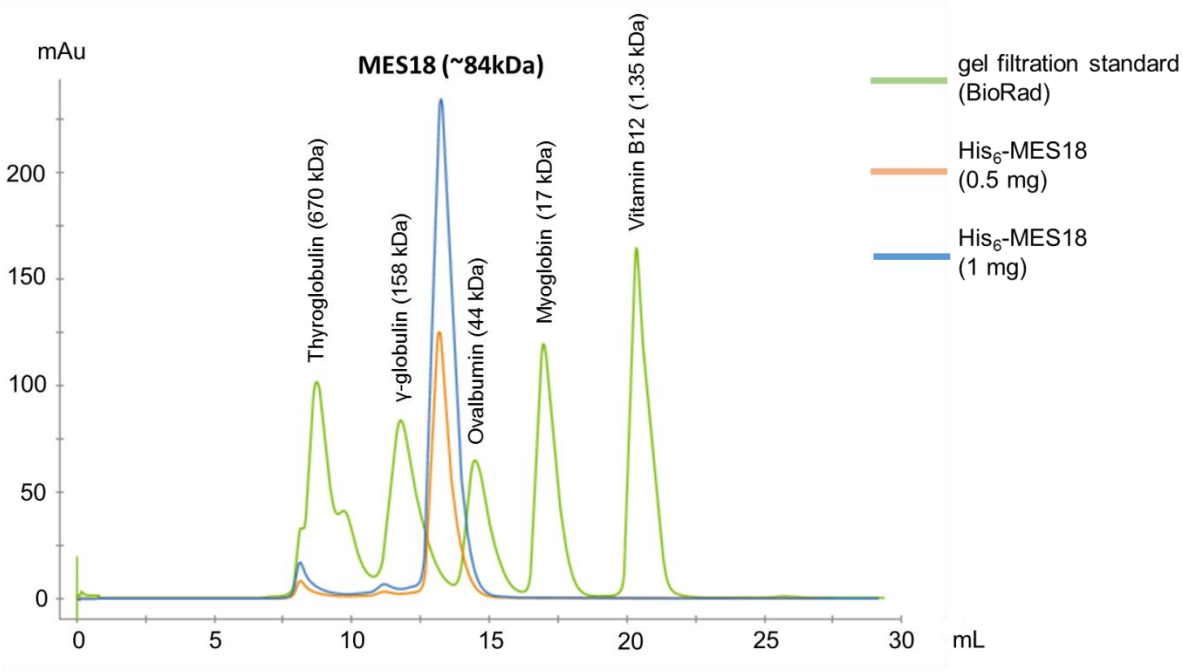

Figure 22: Analytic gel filtration indicates that His_6-MES18 is a dimer in solution. Analytic gel filtration shows that His_6-MES18 (predicted size of 32.6 kDa) elutes with an estimated molecular mass of ~84 kDa, independently of the used His_6-MES18 concentration (1 mg protein, blue peak; 0.5 mg protein, orange peak). The results indicate that MES18 is at least a dimer in solution. Gel filtration standard (BioRad, Munich, Germany) was used to evaluate the molecular mass of MES18 (green peak). mAU; milli absorbance unit.

Esterases are catalysing the hydrolysis of esters in the presence of water. The commonly used esterase substrate *p*-nitrophenyl acetate (*p*-NPA) is hydrolysed to acetate and *p*-nitrophenol which can be measured photometrically (Figure 23 A). In order to investigate whether MES18 possesses esterase activity, ~0.03 mg purified recombinant His_6-MES18 protein was incubated in 10 mM NaCl and 50 mM TRIS-HCl buffer (pH 8.0) with 1 mM *p*-NPA at room temperature. Absorbance of the hydrolysis product *p*-nitrophenol was measured at an absorbance of 405 nm in a plate reader system over a time period of 30 minutes. During this time period, a six-fold increase in absorbance was detectable in the reaction of the active enzyme with *p*-NPA, whereas the absorbance in the reaction mix containing the heat inactivated enzyme and the esterase substrate *p*-NPA did hardly increase over time (Figure 23 B). These findings demonstrate that MES18 is capable to catalyse the hydrolysis of *p*-NPA to acetate and *p*-nitrophenol and strongly suggest that MES18 is an active esterase.

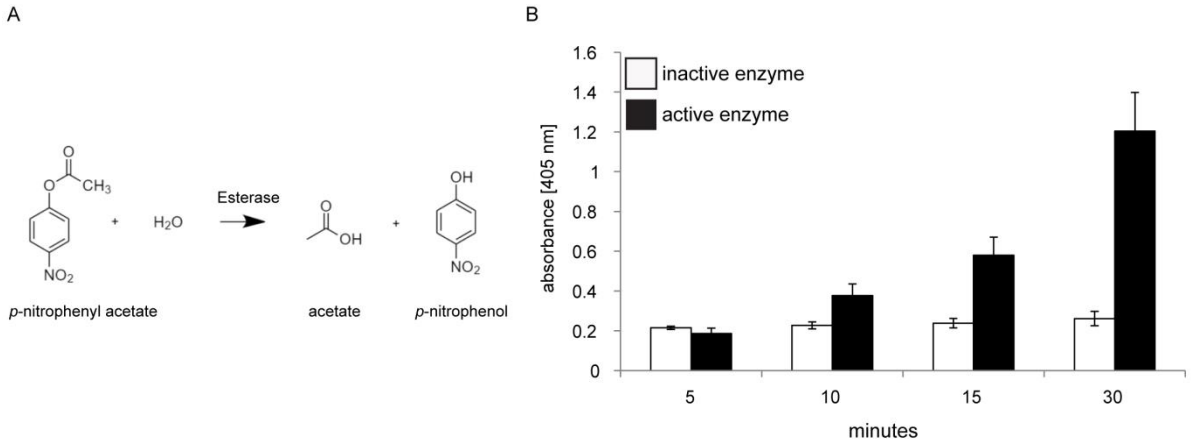

Figure 23: MES18 shows esterase activity. (**A**) Reaction scheme of the hydrolysis of *p*-nitrophenyl acetat (*p*-NPA) to acetate and *p*-nitrophenol. *p*-NPA is commonly used as substrate in esterase and lipase activity assays. The hydrolysis product *p*-nitrophenol is released and the absorbance can be monitored at 405 nm. (**B**) Recombinant MES18 shows esterase activity. Heat-inactivated or active His_6-MES18 protein was dissolved in 10 mM NaCl and 50 mM TRIS-HCl buffer (pH 8.0) mixed with 1 mM *p*-NPA as substrate. The absorbance of the hydrolysis product (*p*-nitrophenol) was measured photometrically at 405 nm every 30 seconds over a time period of 30 minutes (see Supplementary Figure 8 for all time points). Bars represent mean values of three technical replicates of 5, 10, 15 and 30 minute time point, respectively, for reactions with heat-inactivated His_6-MES18 (white bars) and active His_6-MES18 (black bars). Values of reaction without enzyme (buffer control; see Supplementary Figure 8) were substracted from values measured with heat-inactivated and active enzyme. Error bars represent standard deviations of three technical replicates. The experiment was performed five times with independently expressed and purified His_6-MES18 protein, which resulted in similar results. Protein amounts of 0.015 mg to 0.03 mg were used in this experiment.

3.3.7 MES18 catalyses the formation of IAA and JA in the presence of the substrates MeIAA, MeJA and MeSA.

The orthologues of MES18, the esterase SABP2 from tobacco and MJE from tomato catalyze the hydrolysis of methyl salicylic acid (MeSA) and methyl jasmonic acid (MeJA), respectively (Stuhlfelder *et al.*, 2002; Stuhlfelder *et al.*, 2004; Forouhar *et al.*, 2005). Therefore, it was further investigated if MES18 has esterase activity on these methylated plant hormones. Previous data suggest esterase activity of MES18 towards methyl indole-3-acetic acid (MeIAA; Yang *et al.*, 2008). Hence, MeIAA was also included in this analysis.

In order to test if MeSA, MeJA or MeIAA are substrates of MES18, the product formation in samples incubated with the active enzyme and the different substrates were analysed by Ultra Performance Liquid Chromatography (UPLC) coupled with nanoelectrospray ionization (nanoESI) and Tandem Mass Spectrometry (MS/MS). ~0.015 mg recombinant His_6-MES18 was incubated in 10 mM NaCl and 50 mM TRIS-HCl buffer (pH 8.0) containing as substrate either 1 mM MeSA, MeJA or MeIAA, or a mixture of all three compounds, respectively at 24°C for 30 minutes. In addition, the heat inactivated His_6-MES18 enzyme was incubated as control at the same reaction conditions to confirm the hydrolytic specificity by the active enzyme. Samples taken immediately after the start of the reaction (t0 samples) were analysed to determine the rate of the non-enzymatic hydrolysis during the incubation procedure. In addition, the substrates (MeSA, MeJA and MeIAA) were incubated with the buffer without enzyme for 30 minutes to determine unspecific product formation due to spontaneous degradation or instability of the substrates in the chosen buffer system. Due to the insolubility of the three substrates in water, 100 mM stock solutions of the substrates were prepared in ethanol. Therefore, the active and inactive enzyme was additionally incubated in buffer and ethanol (equal volume as used of the substrate stock solutions) for 30 minutes as negative control.

The UPLC-nanoESI-MS/MS analysis provides high sensitivity and selectivity to detect both the substrates as well as the products (SA, JA and IAA) of the enzymatic reaction. The exact mass-to-charge (*m/z*) ratio of the precursor ions and product ions of the compounds of interest were analysed in the multiple reaction monitoring mode at their specific retention time. The samples were measured by Dr. Cornelia Herrfurth (Department of Plant Biochemistry, Albrecht-von-Haller-Institute for Plant Sciences).

Samples incubated with the active His_6-MES18 and MeIAA showed an increase in indole-3-acetic acid (IAA) formation after 30 minutes of incubation (Figure 24 A). In contrast, samples with the heat inactivated His_6-MES18 and MeIAA showed only very low IAA formation resulting presumably from non-enzymatic hydrolysis. Since the peak area of IAA detected in the buffer control was comparable to the peak area of the heat-inactivated

sample (Figure 24 A), this indicates an MES18-specific formation of IAA from the substrate MeIAA.

Similarly, an increase in jasmonic acid (JA) formation was detected in samples with active His_6-MES18 and the substrate MeJA after 30 minutes. Samples with the heat-inactivated His_6-MES18 and MeJA showed again an unspecific low-level product formation similar to the JA levels in the buffer control without any enzyme (Figure 24 A).

Notably, the hydrolysis product salicylic acid (SA) was not detectable at all, neither in samples with active His_6-MES18 and MeSA that were incubated for 30 minutes, nor in t0 samples or samples with heat-inactivated His_6-MES18 (Figure 24 A). These findings indicate that SA is not formed from MeSA in the present of MES18. However, the complete absence of SA in the MeSA-containing samples, especially in the buffer controls, suggests that no enzymatic or non-enzymatic hydrolysis of MeSA to SA is taking place under the chosen reaction conditions.

In samples of the active His_6-MES18 enzyme incubated with a mixture of all three substrates for 30 minutes, IAA and JA, but not SA was detected. In contrast to the samples incubated with active His_6-MES18, t0 samples showed non-specific low-level product formation similar to the buffer control of all three substrates (Figure 24 B). Importantly, negative controls with and without active His_6-MES18 and just EtOH without MeIAA, MeJA or MeSA as potential substrates did not result in any background signal (Figure 24 A).

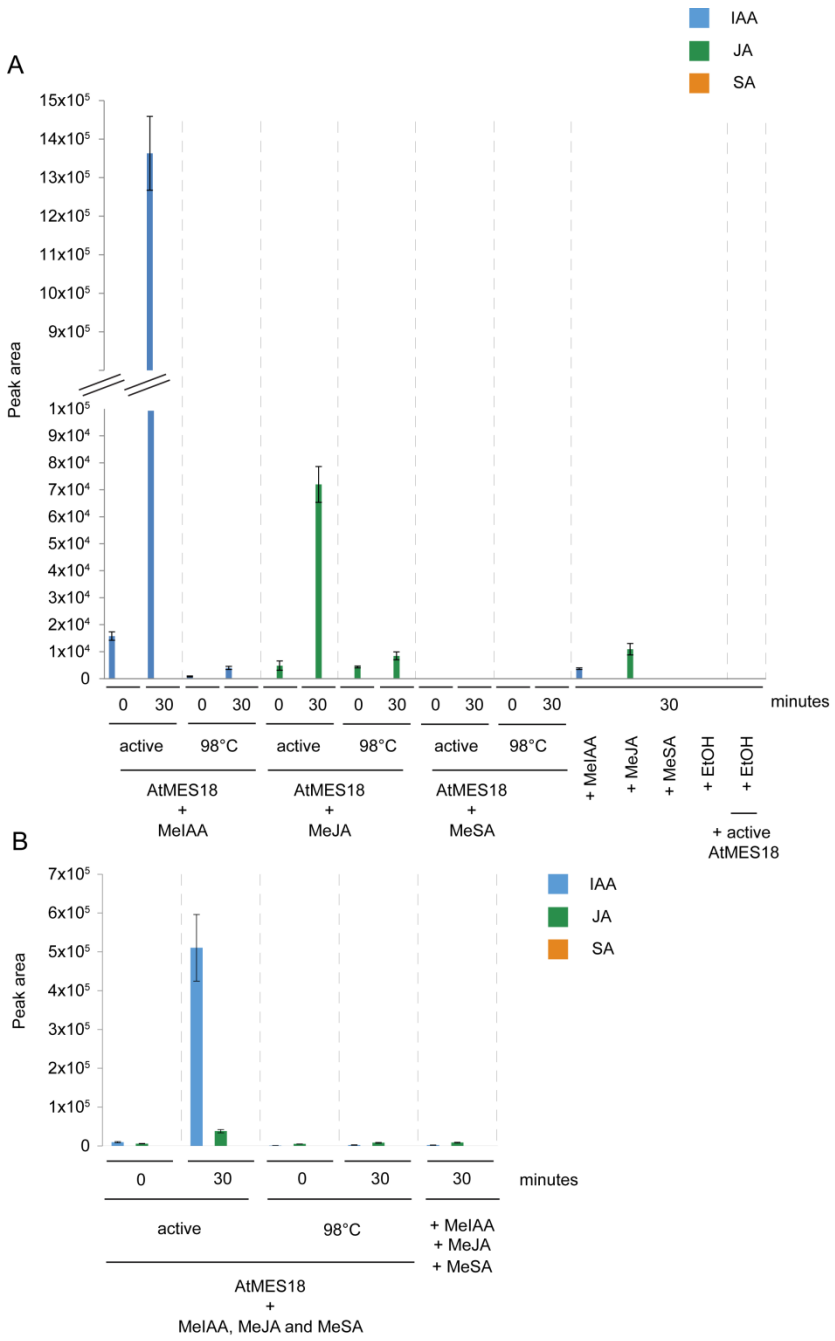

Figure 24: MES18 catalises the formation of IAA and JA in the presence of the substrates MeIAA, MeJA and MeSA. To investigate substrate preferences of MES18, the formation of hydrolysis products was measured using UPLC-nanoESI-MS/MS. Either active or heat-inactivated (98°C) recombinant His_6-MES18 (~0.015 mg) was incubated in 10 mM NaCl and 50 mM TRIS-HCl buffer (pH 8.0) with (**A**) 1 mM of MeIAA, MeJA or MeSA, respectively or (**B**) with a mixture of MeIAA, MeJA and MeSA (1 mM each) at 24°C. Reactions were stopped by addition of 100 µL pure (100 %) acetonitrile either immediately (t0) or after 30 minutes incubation time (t30). Bars represent the mean value of three technical replicates ±SD. As control, TRIS-HCl buffer was incubated only with substrates (MeSA, MeJA and MeIAA). Substrates are dissolved in ethanol. As control, 10 mM NaCl and 50 mM TRIS-HC, buffer (pH 8.0) was incubated with and without active enzyme and with just ethanol without MeIAA, MeJA or MeSA as potential substrates. The experiment was conducted once. SA, salicylic acid (indicated in orange); JA, jasmonic acid (indicated in green); IAA, indole-3-acetic acid (indicated in blue); MeSA, methyl salicylic acid; MeJA, methyl jasmonic acid; MeIAA, methyl indole-3-acetic acid. After reactions were stopped by addition of acetonitrile, the samples were measured by Dr. Cornelia Herrfurth (University of Goettingen, Germany).

In summary, the data obtained by the enzymatic assays and subsequent UPLC-nanoESI-MS/MS analysis indicate that MES18 is a methyl esterase that catalyses the hydrolysis of MeIAA and MeJA to the hydrolysis products IAA and JA, respectively. In contrast, the analysis indicates that MeSA is no substrate of MES18. However, in none of the MeSA-containing samples SA was detected. It cannot be excluded that SA was not formed due to the fact that the volatile MeSA was vaporised either before or during the reaction. Therefore, the question is still open if MeSA is a substrate of MES18. In addition, any conclusions about a preferred substrate of MES18 are not possible from the results shown in Figure 24. All tested substrates and products have distinct volatilities that effect the recovery rate after the enzymatic assay. In addition, the ionization efficiencies of the compounds during the UPLC-nanoESI-MS/MS measurements are also compound-specific. Therefore, it was an aim of this study to independently validate the obtained UPLC-nanoESI-MS/MS data with an additional method. Isothermal Titration Calorimetry (ITC) measurements were chosen to investigate the activity of MES18 towards MeSA, MeJA or MeIAA.

3.3.8 Kinetic parameter of MES18 enzymatic activity

The UPLC-nanoESI-MS/MS analysis revealed MeJA and MeIAA as potential substrates of MES18 (Figure 24). In order to confirm and support these data with an independent method and to further examine kinetic parameters of MES18 enzymatic activity with suitable substrates, kinetic Isothermal Titration Calorimetry (ITC) measurements were conducted. ITC is a reliable method to characterize the kinetics of enzymes (Todd and Gomez, 2001). The method was carried out as described in Kupski (2016) and modified for MES18 as described below.

In general, an ITC device is equipped with two different cells, which are filled with water (reference cell) and substrate (sample cell). A defined concentration of the enzyme is loaded into a syringe, and after establishment of an equilibrated baseline on a defined devise temperature, the enzyme is titrated into the sample cell and mixed rapidly to avoid mixing artefacts. After the injection of the enzyme, the ITC instrument allows the detection of heat generation or consumption as a result of either an exothermic or endothermic reaction caused by enzyme and substrate interaction. Here, heat generation/consumption was detected by measuring the power that was needed to maintain isothermal conditions between the reference cell containing water, and the sample cell containing a buffer-enzyme-substrate mix (Srivastava and Yadav, 2019).

For this assay, recombinant His_6-MES18 in 10 mM NaCl and 50 mM TRIS-HCl buffer (pH 8.0) was concentrated to a 400 µM stock using a Corning® Spin-X® Concentrator (Sigma-Aldrich, Munich, Germany) and the protein concentration was determined using a NanoDrop™ One Microvolume UV-Vis Spectrophotometer. The recombinant His_6-MES18

was mixed with DMSO (2 %) and 10 mM NaCl and 50 mM TRIS-HCl buffer (pH 8.0) buffer to a final concentration of 380 µM. The reason for the addition of DMSO is explained below. Initial ITC measurements that were performed as a trail experiment already indicated that higher amounts of His_6-MES18 are needed to perform this assay (data not shown). The His_6-MES18-buffer-DMSO mix was loaded into the syringe, while 2 mM substrate (MeSA, MeJA or MeIAA) in 10 mM NaCl and 50 mM TRIS-HCl buffer (pH 8.0) with 2 % DMSO was placed into the sample cell. All tested substrates (MeSA, MeJA and MeIAA) were not soluble in water therefore DMSO was used as a solvent. In order to prevent buffer mismatches, which would result in production of non-specific heat for the measured reaction, the enzyme-buffer mix as well as the substrate-buffer mix contained the same amount of DMSO. All reactions were performed at 20°C over a time period of 4000 seconds. The reaction starts with the first injection after an initial equilibration time of 60 seconds. After the spacing time of 4000 seconds a second injection was performed. The results of the second injection can be used to evaluate if the substrate of the reaction was already completely consumed. The interaction of MES18 with a suitable substrate resulted in heat changes, which were measured by the ITC device by decreasing or increasing differential power (dp), given in µcal/s. The dp value describes the power that was needed over time to maintain isothermal conditions between the reference and the sample cell and integration of this power allow to determine the reaction enthalpy (ΔH).

10 µL of the 380 µM His_6-MES18 stock solution in 10 mM NaCl and 50 mM TRIS-HCl buffer (pH 8.0) and DMSO was injected into the sample cell containing 2 mM MeSA in the same buffer and DMSO. This resulted in a final concentration of 18 µM His_6-MES18 in the sample cell. The injection of His_6-MES18 into the sample cell containing MeSA did not result in heat changes between the sample cell and the reference cell, indicated by non-significant change in dp values. The minor peaks that were detectable after the first injection of His_6-MES18 emerged from the heat change that is caused by mixing the buffer-substrate and His_6-MES18-buffer solutions. In addition, a second injection of 18 µM His_6-MES18 resulted also only in minor heat changes (Figure 25 A, green line). Since these minor peaks were also measured in the buffer control it can be concluded that the signals are not caused by an interaction of MES18 and MeSA. Hence, the kinetic ITC measurements indicate that no catalytic reaction of MES18 occurs in the presence of MeSA under the chosen reaction conditions (Figure 25, A, green line).

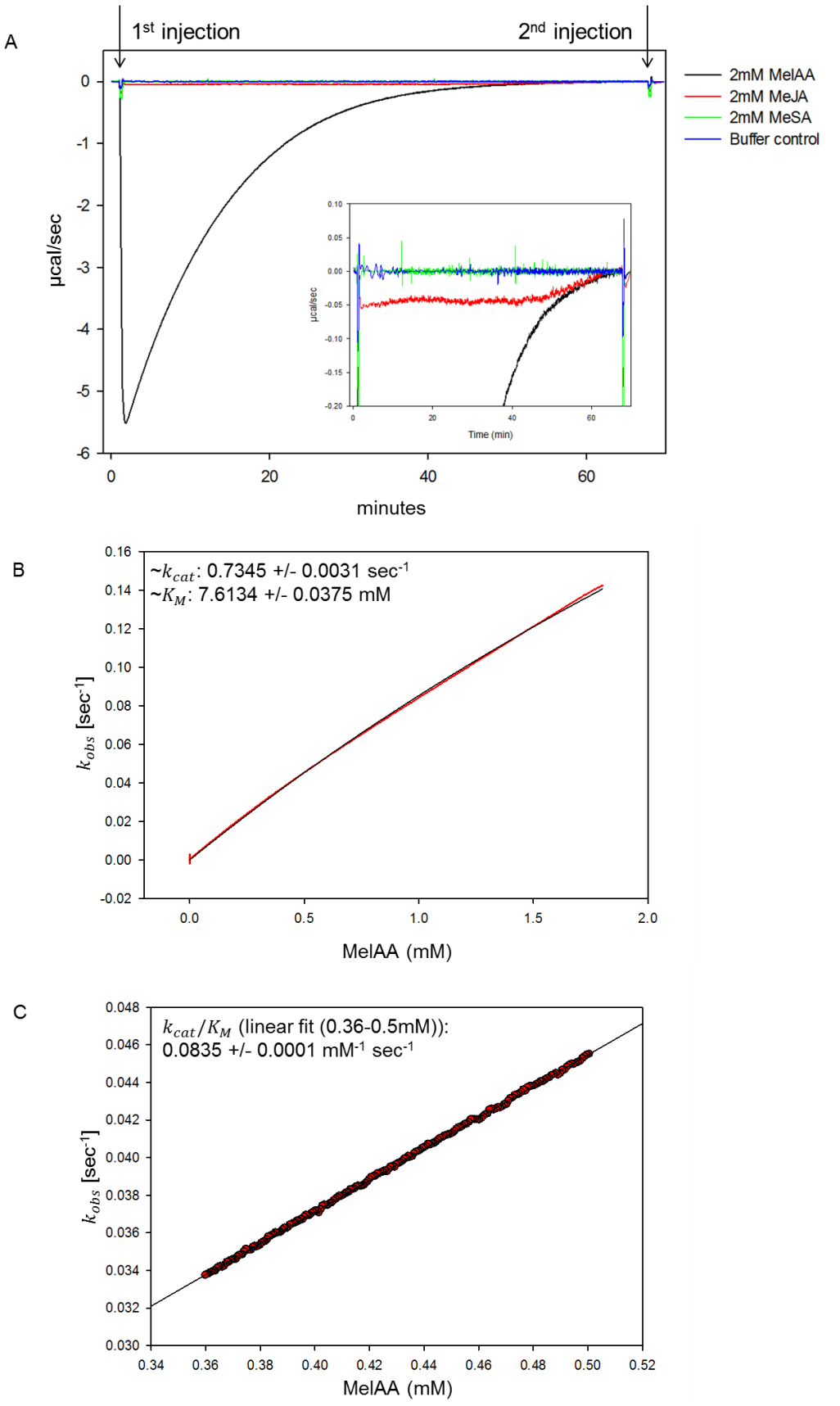

Figure 25: ITC analysis showing the catalytic conversion of MeIAA by MES18. (**A**) Calorimetric progress curve of the reaction of MeSA, MeJA and MeIAA with His_6-MES18. Measurements were performed in 10 mM NaCl and 50 mM TRIS-HCl buffer (pH 8.0) with 2 % DMSO. After initial equilibration (60 seconds), 18 µM

His_6-MES18 (final concentration) was injected to 2 mM substrate (MeSA, MeJA or MeIAA) and the change in instrumental thermal power was monitored until the substrates were completely consumed. Reactions of His_6-MES18 with MeSA (green line), MeJA (red line), MeIAA (black line) or without substrate (buffer control, blue line) are displayed. The inset provides a detailed view of the values obtained for the reaction with MeJA (red line) and MeSA (green line). 1st and 2nd injections are marked with black arrows. (**B**) and (**C**) Michaelis–Menten plot for the reaction of MES18 and MeIAA is displayed. Determined k_{obs} values and the substrate concentration at each time point were plotted and fitted according to the linear range [0.36 – 0.5 mM; see zoom which is displayed in (**C**)] of the Michaelis-Menten equation [7] with SigmaPlot from Systat Software Inc (see 2.2.7.2). The obtained kinetic parameters k_{cat}, K_M and k_{cat}/K_M are displayed in the Michaelis-Menten plot. MeSA, methyl salicylic acid; MeJA, methyl jasmonic acid; MeIAA, methyl indole-3-acetic acid. Samples were measured with the help of Lisa-Marie Funk (University of Goettingen, Germany).

In contrast, injection of 18 µM His_6-MES18-buffer-DMSO solution into the sample cell containing 2 mM MeJA-buffer-DMSO solution resulted in minor heat changes after the first injection (Figure 25 A, red line). The second injection of 18 µM His_6-MES18-buffer-DMSO solution caused only minor dp values, illustrating that the substrate MeJA was consumed during the reaction. However, the changes occurring after the first injection were clearly distinguishable from the peaks that were observed in the buffer control. Thus, these data suggests low interaction of MES18 and MeJA. Unfortunately, the interaction was too weak to analyse catalytic parameters of this reaction. In order to increase the heat signal of the reaction between MES18 and MeJA, a higher protein concentration is needed. However, higher concentrations of His_6-MES18 in the sample cell were technically not possible to measure with the 400 µM stock that was prepared for this assay. The amount of purified His_6-MES18 was a limiting factor. The preparation of a higher concentrated stock could only be achieved by a strong reduction of the stock volume which would lead on the one hand to a loss of purified protein and on the other hand ITC measurements from different stock concentrations are not comparable to each other. Therefore, measurements with higher concentrations of His_6-MES18 were not performed in the course of this study but should be conducted in the future.

In contrast to MeSA and MeJA, the dp values changed drastically when 18 µM His_6-MES18 was injected into a sample cell that was provided with 2 mM MeIAA-buffer solution. Negative dp values indicated that the catalytic reaction of MES18 and MeIAA is an exothermic reaction (Figure 25 A, black line). At the beginning of the measurement, immediately after the first injection of His_6-MES18 to the sample cell, a rapid increase in instrumental thermal power occurred. These changes in differential power correspond to the formation of the Michaelis-Menten complex. Generally, the differential power reaches a maximum stabile plateau after injection of the enzyme into the substrate solution after both are homogenised. This point represents the status where the enzyme is completely

saturated with the substrate and reflects the steady state and the maximum reaction velocity (V_{max}) of the reaction. In the case of MES18, a maximum stabile plateau was never reached, indicating that MES18 was never completely saturated with MeIAA under the tested concentrations of the enzyme and substrate (Figure 25 A, black line, bottom of the peak). In order to reach complete saturation, higher concentrations of MeIAA were necessary. Hence, the substrate concentration was increased from 2 mM to 4 mM MeIAA for a subsequent measurement. Similar to the data obtained for 2 mM substrate concentration, 4 mM MeIAA did also not result in a saturation of MES18 with the substrate (Supplementary Figure 9). Due to the insolubility of MeIAA at higher concentrations, measurements with substrate concentrations above 4 mM could not be conducted. Therefore, V_{max} could not be determined. Over time MeIAA was depleted and MES18 was less saturated with the substrate. Consequently, the formation of the catalytic product IAA increased (Figure 25 A, black line). The conversion from the substrate to the product leads to a decrease in substrate amount, which results in decreasing substrate saturation at each measurement point, causing a diminution of heat release. This was indicated by increasing dp values (Figure 25 A, black line). At the end of the reaction, the substrate MeIAA was completely converted to the enzymatic product IAA, indicated by the values obtained for a second 10 µL injection of His_6-MES18 into the sample cell. No changes in dp values were observed after the second injection, showing that MeIAA was completely depleted (Figure 25 A, black line).

To obtain catalytic parameters for the reaction of MES18 with MeIAA, the released heat over time of the calorimetric progress curve was used to determine the molar reaction enthalpy (Δ*H*; [1] see 2.2.7.2). To obtain this value, the total enthalpy (µCal) determined during the course of an ITC measurement was divided by the total concentration of the substrate MeIAA (mol). A value of -1.01x10^{10} µCal/mol was calculated for Δ*H*. Subsequently, Δ*H* was used to calculate the rate constants k_{obs}. (see 2.2.7.2). K_{obs} values were plotted as function of the substrate concentration (Figure 25 B). The turnover number of the reaction (k_{cat}) and the Michaelis-Menten constant (K_M) were calculated from the hyperbolic fit of k_{obs} values against the substrate concentration (see 2.2.7.2). The K_M value describes the substrate concentration at which half of the enzyme´s maximal activity is reached. k_{cat} and K_M values of 0.7345 ± 0.0031 sec^{-1} and of 7.6134 ± 0.0375 mM were determined, respectively (Figure 25 B). Due to the fact that MES18 was never completely saturated with MeIAA, the calculated k_{cat} and K_M values for MES18 need to be interpreted with caution. Nevertheless, the ratio of k_{cat} to K_M (k_{cat}/K_M) provides a reliable catalytic parameter to measure catalytic efficiency (Eisenthal *et al.*, 2007), which is described by the linear range of a Michaelis-Menten (MM) kinetic. The catalytic efficiency of MES18 towards MeIAA was calculated at a value of 0.0835 ± 0.0001 mM^{-1} sec^{-1}, when fitted to the linear range of the

MM kinetic (0.36 – 0.5 mM; Figure 25 C; [7] see 2.2.7.2). In particular in the case of MES18, the catalytic efficiency provides a more reliable value. Since V_{max} could not be determined for the reaction of MES18 and MeIAA, values from the linear fit are more accurate.

Taken together, the ITC measurements revealed no interaction of MES18 with MeSA, while MES18 showed weak interaction with MeJA and strong interaction with MeIAA (Figure 25 A). The ITC data suggests that MeIAA is a substrate of MES18. However, MeJA can also be considered as a substrate of MES18, albeit it only led to a very weak reaction in the ITC measurements. Since there was no heat change measured that was specific for the reaction of MES18 and MeSA (Figure 25 A, green line), this data indicates that MeSA is no substrate of MES18. However, as described for the UPLC-nanoESI-MS/MS analysis (3.3.7) it also cannot be completely excluded for the ITC analysis that the volatile substrate MeSA has been vaporized during the preparation of the stock solutions or loading the syringe. Nevertheless, the ITC data support the outcome of the UPLC-nanoESI-MS/MS analysis that among the three methylated plant hormones tested in this study, MeIAA appears to be the major substrate for MES18. Furthermore, the catalytic efficiency from the reaction of MES18 with MeIAA was determined at a value of 0.0835 ± 0.0001 mM^{-1} sec^{-1} (Figure 25 C).

3.3.9 IAA does not inhibit the MES18 catalyzed hydrolysis of MeIAA

The catalytic efficiency (k_{cat}/K_M) of MES18 to the substrate MeIAA was calculated from the linear range of the MM kinetic (0.36 – 0.5 mM) at a value of 0.0835 ± 0.0001 mM^{-1} sec^{-1}. Catalytic parameters were obtained from the calorimetric progress curve measured by ITC as explained in 3.3.8 and depicted in Figure 25. From the ITC measurements (Figure 25) it cannot be concluded if the K_M value of the reaction is high which would indicate a low affinity of the substrate to the enzyme or if the product formation decelerates the reaction. Previous studies already described competitive inhibition of the esterase activity of *Nt*SABP2 and *Cs*MES1 enzymes by product analogues (Park *et al.*, 2009; de Lima Silva *et al.*, 2019). Hence, a product inhibition assay was conducted to examine if the hydrolysis product IAA may inhibit the reaction.

The influence of the presence of IAA to the catalytic reaction of MES18 with MeIAA was assessed using ITC measurements. The measurements were conducted as described in 3.3.8. A 380 µM His_6-MES18 stock in 10 mM NaCl and 50 mM TRIS-HCl buffer (pH 8.0) with 4 % DMSO was filled in the syringe, while 2 mM MeIAA substrate in 10 mM NaCl and 50 mM TRIS-HCl buffer (pH 8.0) with 4 % DMSO was placed into the sample cell. For this experiment, the DMSO concentration had to be increased from 2 % (as described in 3.3.8) to 4 %. This allowed a comparison between the measurements of His_6-MES18 and the substrate MeIAA with additional measurements, where the substrate MeIAA and the product IAA are present at the same time. Both, MeIAA and IAA are not soluble in water and

therefore DMSO was used as a solvent. 100 mM stocks were prepared in 100 % DMSO. Subsequently, 2 mM stocks of MeIAA or IAA in 10 mM NaCl and 50 mM TRIS-HCl buffer (pH 8.0) contained a final concentration of 2 % DMSO for each stock. Therefore, the measurement of His_6-MES18 with IAA and MeIAA contained a final concentration of DMSO of 4 %.

First, the measurement to access the catalytic efficiency of MES18 only in the present of the substrate MeIAA and without the product IAA was performed. The reaction started with the injection of 10 µL of the 380µM His_6-MES18 stock with DMSO (4 %) into the sample cell. MeIAA was converted into the reaction product IAA. The generated heat was measured by the ITC device (Figure 26 A, black line). As described in 3.3.8, the rate constant k_{obs} and the catalytic efficiency (k_{cat}/K_M) were determined (Figure 26 B). k_{cat}/K_M was calculated at a value of 0.0778 ± 0.0001 mM^{-1} sec^{-1} when fitted to the linear range of the MM kinetic (0.36 – 0.5 mM; Figure 26 B; [7] see 2.2.7.2). As already described in 3.3.8, values from the linear fit are more accurate and therefore more reliable in the case of MES18.

In order to examine the influences of the reaction product IAA a second measurement was conducted. The ITC measurement was repeated under the same conditions as described prior, but this time a 2 mM MeIAA / 2 mM IAA mix dissolved in 10 mM NaCl and 50 mM TRIS-HCl buffer (pH 8.0) with a final concentration of 4 % DMSO were placed into the sample cell. Similar to the previous measurement, the changes in differential power were detected by the ITC device and recorded (Figure 26 A, red line). Calculation of catalytic parameters revealed that the presence of IAA had almost no effect on the catalytic efficiency (Figure 26 B). The k_{cat}/K_M value was determined at 0.0752 ± 0.0001 mM^{-1} sec^{-1} (linear fit). The calculated k_{cat}/K_M values demonstrate that the reaction of MES18 and MeIAA without and with IAA only differ by 3.3 % from each other, which is within the range of the error that occur by the calculation the catalytic efficiency. These findings indicate that the esterase activity of MES18 is not affected in the presence of IAA and further suggest that IAA does not compete with MeIAA for MES18 binding under the tested reaction conditions.

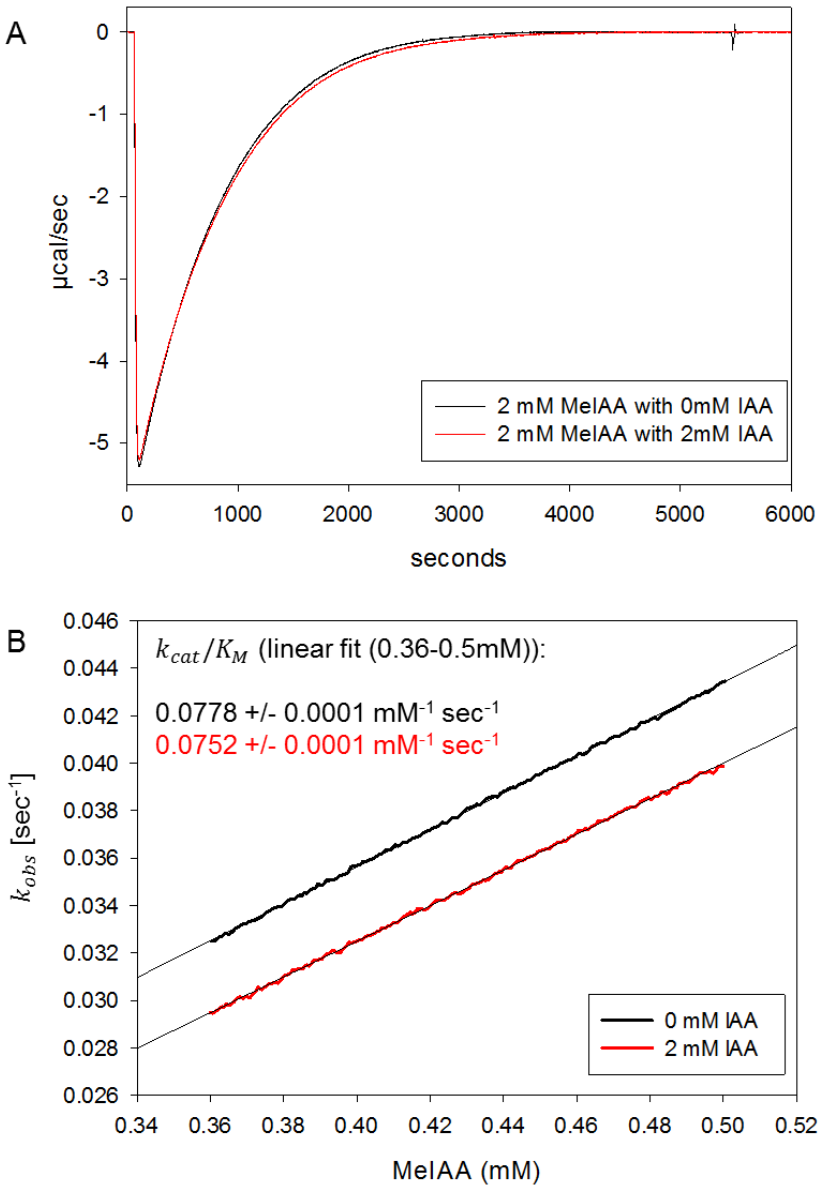

Figure 26: The catalytic efficiency of MES18 towards MeIAA is not affected by the presence auf IAA. (**A**) Calorimetric progress curves of the reaction of MeIAA (with and without IAA) with MES18 are depicted. Measurements were performed in 10 mM NaCl and 50 mM TRIS-HCl, (pH 8.0) buffer with 4 % DMSO. After equilibration (60 seconds), 18 µm His_6-MES18 (final concentration) was injected to 2 mM MeIAA without IAA (black line) and with 2 mM IAA (red line). Changes in instrumental thermal power caused by the reactions were monitored until substrate was completely consumed. **(B**) Determined k_{obs} values and the substrate concentration at each time point were plotted and fitted according to the linear range (0.36 – 0.5 mM) of the MM equation [7] with SigmaPlot from Systat Software Inc (see 2.2.7.2). The obtained kinetic parameters k_{cat}, K_M and k_{cat}/K_M are displayed in the Michaelis-Menten plot. MeIAA, methyl indole-3-acetic acid; IAA, indole-3-acetic acid. Samples were measured with the help of Lisa-Marie Funk (University of Goettingen, Germany).

To summarize the last part of the results section (3.3), the predicted methyl esterase *MES18* and the RNA-binding protein *PUM9* were identified in a genome-wide transcriptome analysis of the two nuceloporin mutants *mos3* and *nup160* that aimed to identify new components of plant immunity (Figure 5 B). Quantitative RT-PCR analyses confirmed

reduced transcript abundance of *MES18* and *PUM9* in *mos3* and *nup160* mutant plants (Figure 17). To further investigate the potential biological function of the two candidate genes *MES18* and *PUM9*, homozygous T-DNA insertion lines were isolated for both genes (Figure 18 A, B). The *mes18*-2 mutant (SAIL_609_A08) still contained functional transcripts and was excluded from further analysis (Figure 18 B). A second mutant allele of *mes18* generated by CRISPR/Cas9, and transgenic *mes18*-1 complementation lines are currently in the process of being selected. However, *Pseudomonas* growth assays with *mes18*-1, *pum9*-1 and *pum9*-2 indicate that *MES18* is involved in basal defence towards the hemi-biotrophic plant pathogen *P. syringae*, but not in RPS4- and RPM1-mediated ETI towards this pathogen expressing the effectors *avrRps4* and *avrRpm1*, respectively (Figure 19 A-C). *Pum9* mutant alleles are neither impaired in basal resistance nor in immunity mediated by RPS4 or RPM1 towards *P. syringae* (Figure 19 A-C). Since *MES18* appears to be required for basal immunity towards *Pseudomonas*, the biological function of the MES18 protein was further investigated. Multiple protein sequence alignment of the 20 predicted methyl esterases (MES1-20) encoded in the *Arabidopsis* genome revealed sequence homology to the methyl esterases *Nt*SABP2 and *Le*MJE (Supplementary Figure 6). Phylogenetic analysis revealed MES16 and MES17 as the closest orthologs of the *Arabidopsis* MES18 protein (Figure 21). Finally, the MES18 protein was heterologously expressed in *E. coli* to investigate the catalytic properties of MES18 in more detail. MES18 has a predicted size of approximately 29.1 kDa (Supplementary Figure 7) and appears as dimer in solution (Figure 22). Photometrical assays revealed esterase activity of MES18 towards the commonly used esterase substrate *p*-nitrophenyl acetate (*p*-NPA) (Figure 23 B). UPLC-nanoESI-MS/MS analysis subsequently showed that the hydrolysis products JA and IAA are formed in the presence of MES18 and MeJA and MeIAA, respectively (Figure 24). These findings indicate that MeJA and MeIAA are potential substrates of MES18. ITC measurements independently validate these findings (Figure 25 A). The catalytic efficiency of MES18 in the presence of MeIAA was calculated at a value of $0.0835 \pm 0.0001\ mM^{-1}\ sec^{-1}$ (Figure 25 C). Additional ITC measurements revealed that the presence of the reaction product IAA has no impact on the catalytic efficiency of MES18 towards the substrate MeIAA under the tested reaction conditions. These findings indicating that the catalytic demethylation of MeIAA to IAA by MES18 is not inhibited by the reaction product itself (Figure 26).

4 Discussion

The NPC facilitates the translocation of macromolecules such as proteins and RNAs between the nucleus and the cytoplasm and is therefore indispensable for cellular signaling processes and gene regulation in eukaryotic cells (Merkle, 2011; Tamura and Hara-Nishimura, 2013; Beck and Hurt, 2017). The activation of defence gene expression during PTI and ETI depends on the transduction of defence signals into the nucleus and the export of defence-related mRNAs into the cytosol (Cui *et al.*, 2015; Li *et al.*, 2016). Accordingly, the selective nucleocytoplasmic trafficking through the NPC is important for the establishment of plant defence responses. MOS3/NUP96 and NUP160 are two constituent members of the evolutionary conserved NUP107-160 complex (called the NUP84 complex in yeast) which is the largest subunit of the NPC (Xu and Meier, 2008; Tamura *et al.*, 2010; Wiermer *et al.*, 2012; Tamura and Hara-Nishimura, 2013; Von Appen *et al.*, 2015; Stuwe *et al.*, 2015; Meier *et al.*, 2017). Both, *mos3/nup96* and *nup160* mutant plants are impaired in basal defence and TIR-type NLR protein mediated resistance and compromise autoimmunity of *snc1* in *Arabidopsis* (Zhang and Li, 2005; Roth and Wiermer, 2012; Wiermer *et al.*, 2012). Both mutants also display defects in nuclear mRNA export and show reduced transcript abundance of the key defence regulator *EDS1* and the pattern recognition receptor *EFR* (Parry et al., 2006; Dong et al., 2006; Wiermer et al., 2012; Stepanets, M.Sc. Thesis, 2013; Lüdke, B.Sc. Thesis, 2014; Figure 6, 9, 10 and 12; Supplementary Figure 2 and 3).

4.1 RNAseq-based transcriptome analysis revealed global transcriptional changes in *mos3* and *nup160* mutant

According to published and preliminary unpublished results, it was hypothesized that *MOS3* and *NUP160* are involved in transcriptional regulation of certain defence genes, including *EFR* and *EDS1* (Wiermer *et al.*, 2012; Stepanets, M.Sc. Thesis, 2013; Lüdke, B.Sc. Thesis, 2014). A major aim of the study presented here was to identify defence-associated genes with altered expression in both nucleoporin mutants. Thus, an RNAseq-based transcriptome analysis was conducted to reveal global transcriptional changes in both mutant plants in comparison to the wild-type and *sec13b* control plants that are not impaired in basal resistance (Wiermer *et al.*, 2012; Figure 5). This approach represents the first gene expression analysis that addressed global transcriptional changes in both, *mos3* and *nup160* mutant plants with a main focus on the functional role of *MOS3* and *NUP160* in plant immunity.

4.1.1 The transriptomes of *mos3* and *nup160* mutants differ from wild-type and *sec13b* control plants

The RNAseq experiment was performed on four week old unchallenged Col-0 wild-type, *mos3*-2, *nup160*-3 and *sec13b*-1 control plants (Figure 5). SEC13 is part of the NUP107-160 complex but is not involved in basal plant immunity to *Pseudomonas syringae* pv. *tomato* (*Pst*) DC3000 (Wiermer *et al.*, 2012). Thus, the *sec13b*-1 mutant was used as a control to specifically identify genes that are differentially regulated in *mos3* and *nup160* and play a potential role in plant immunity. A principle component analysis (PCA) revealed that the wild-type and *sec13b*-1 transcriptome profile were rather similar, while the wild-type transcriptome differs from the *mos3* and *nup160* transcriptomes (Supplementary Figure 1 A-C). Surprisingly, only six genes were identified to be differentially regulated in *sec13b*-1 compared to wild-type (Figure 5 B; Supplementary Table 1) indicating that the loss of *SEC13B* function does not lead to strong transcriptional changes. In *Arabidopsis*, two functional homologs of the *SEC13* gene named *SEC13A* and *SEC13B* exist which are functionally redundant with regard to the formation of COPII transport vesicles that mediate protein trafficking from the ER to the Golgi (Hino *et al.*, 2011). SEC13A and SEC13B might have a dual function in mediating protein trafficking and being a functional member of the NUP107-160 complex. Since only six differentially expressed genes (DEGs) were identified, these data indicate that the functional loss of *SEC13B* might be compensated by the presence of *SEC13A.*

4.1.2 DEGs in *mos3* and *nup160* are involved in various biological functions including plant immunity

471 genes have been identified to be differentially expressed in both *mos3* and *nup160* compared to Col-0 wild-type and *sec13b*-1 ($log_2FC > 0.5$ or < -0.5, FDR < 0.05; Figure 5 B and 6; Supplementary Table 1). Gene ontology (GO) enrichment analysis revealed that these 471 DEGs are associated with various biological processes including plant defence responses (Figure 7). This indicates that, in addition to their roles in plant immunity, *MOS3* and *NUP160* have functions in multiple physiological processes. In agreement with this data, both mutants display mild pleiotropic phenotypes such as an early flowering phenotype (Zhang and Li, 2005; Dong *et al.*, 2006; Parry *et al.*, 2006; Wiermer *et al.*, 2012; Cheng *et al.*, 2020; Li *et al.*, 2020). Several other *nup* mutants share pleiotropic phenotypes with *mos3* and *nup160*. Mutations in *TRP1/NUA, NUP62*, *NUP1/NUP136* as well as *HOS1/ELYS* which are involved in several aspects of nuclear trafficking, also lead to an early flowering phenotype. TRP1/NUCLEAR PORE ANCHOR (NUA) is a nuclear basket localized nucleoporin (Jacob *et al.*, 2007; Xu *et al.*, 2007), while NUP62 belongs to the FG-repeat NUPs (Zhao and Meier, 2011; Parry, 2014). *At*NUP1/NUP136 anchors the TREX-2

mRNA export complex on the NPC (Lu *et al.*, 2010). The E3 ubiquitin ligase HOS1/EMBRYONIC LARGE MOLECULE DERIVED FROM YOLK SAC (ELYS) is involved in various molecular processes such as regulation of flower time or cold resistance and is believed to be associated with the NPC (Ishitani *et al.*, 1998; Li *et al.*, 2001; MacGregor and Penfield, 2015; Meier *et al.*, 2017). However, not all plants with defects in the NPC and nucleocytoplasmic transport display altered flowering time. NUP85 and SEH1 are two members of the *Arabidopsis* NUP107-160 complex (Tamura *et al.*, 2010; Wiermer *et al.*, 2012) and *nup85* and *seh1* mutants display wild-type like growth (Parry, 2014). This shows on one hand that defective nuclear transport does not automatically lead to altered flowering time, and on the other hand that members of the NUP107-160 complex probably have distinct functional roles, although there might be overlapping functions.

It has been shown that reduced *FLC* gene expression correlates with an early flowering phenotype. Mutations in the *Arabidopsis* gene *TRANSLOCATED PROMOTER REGION* (*TPR)* lead to reduced gene expression of *FLC*, as revealed by microarray data of the *tpr* mutant (Jacob *et al.*, 2007). Notably, the *FLC* transcript abundance was also reduced in *nup160* (log_2FC of -1.22; Figure 5; row data of RNAseq experiment) but not in *mos3* mutant plants as compared to wild-type (Figure 5; row data of RNAseq experiment). In agreement with this data, Li *et al.* (2020) also showed decreased *FLC* gene expression in *nup160*. This suggest that the early flowering phenotype of *nup160* may, at least partially, be caused by reduced *FLC* transcript abundance. Interestingly, neither this study nor the study of Cheng *et al.* (2020) could show that *FLC* gene expression was reduced in *mos3* compared to wild-type, suggesting that the flowering time defect of *mos3* is *FLC* independent and that further processes/regulatory mechanisms are involved.

Consistent with this idea, recent studies could show that MOS3 physically interacts with the E3 ubiquitin ligase HOS1 (Cheng *et al.,* 2020). The loss of *MOS3* leads to an over-accumulation of CONSTANS (CO) proteins as it has been previously also described for the *hos1* mutant which displays an early flowering phenotype (Ishitani *et al.*, 1998; Li *et al.*, 2001; Lazaro *et al.*, 2012; Jung *et al.*, 2013; MacGregor *et al.*, 2013; Cheng *et al.*, 2020). It has been suggested that both, MOS3 and HOS1 stabilize CONSTANS (CO) protein level by regulating CO protein turnover (Cheng *et al.*, 2020). The transcriptional regulator CO is involved in the regulatory network that is responsible for the control of flower transition (Kinoshita and Richter, 2020). How MOS3 contributes to CO protein turnover on a molecular level has not been fully understood so far. Since NUP160 also physically interact with HOS1 Li *et al.* (2020), it is tempting to postulate that both the accumulation of CO proteins and/or reduced *FLC* gene expression contribute to the early flowering phenotype of *nup160* mutant plants. Nevertheless, the pleiotropic defects of *mos3* and *nup160* mutant plants are rather mild (Zhang and Li, 2005; Dong *et al.*, 2006; Robles *et al.*, 2012; Wiermer *et al.*, 2012).

Beside the described pleiotropic phenotypes of *mos3* and *nup160,* both mutants display also defects in certain defence pathways (Zhang and Li, 2005; Roth and Wiermer, 2012; Wiermer *et al.*, 2012). Enrichment of the GO terms “defence response” and “innate immune response” (Figure 7) in the 471 DEGs of both *mos3* and *nup160* illustrate that the loss of functional *MOS3* and *NUP160* results in altered expression of defence-related genes in *Arabidopsis*. This data further support that *MOS3* and *NUP160* are involved in plant immunity. Interestingly, ~ 47 % of the DEGs identified in *nup160*-3 and ~76 % of the DEGs of *mos3*-2 are common for both mutants (Figure 5) indicating overlapping functions in the regulation of certain cellular processes by MOS3 and NUP160 including plant defence responses.

4.1.3 Plants appear to have a regulatory mechanism to counteract defects in the nuclear transport machinery

Among the 30 DEGs showing the highest elevated expression in *mos3*-2 and *nup160*-3 in comparison to wild-type, six nuclear transport-related genes were found, namely *NUP98B, RAE1*, *RAN1*, *RAN2*, *XPO1B* and *NTF2B* (Figure 8). This elevated gene expression indicates that the loss of *MOS3* and *NUP160* leads to a compensatory up-regulation of genes involved in nuclear transport-related processes. In agreement with this observation, several other microarray and RNAseq-based gene expression analyses of different *nup* mutants revealed elevated expression of the transport genes mentioned above. Microarray data of *tpr* mutant plants showed increased expression for *NUP98B*, *RAE1*, *RAN1*, *XPO1B* and *NTF2B* in comparison to the respective wild-type control (Jacob *et al.*, 2007). Microarray data from seven-day-old *nup160* and *nup62* seedlings showed an at least 1-fold increase in expression of all six transport-related genes that were also up-regulated in *mos3* and *nup160* in comparison to wild-type (Parry, 2014). In an RNAseq analysis of *hos1* mutant plants *NUP98B, RAE1, RAN1, RAN2, XPO1B* but not *NTF2B* were identified as genes that are at least two- or more fold up-regulated in *hos1* compared to wild-type (MacGregor *et al.*, 2013). A recently conducted RNAseq-based analysis of *mos3*-2 and *hos1* mutants revealed an induced gene expression of all six transport-related genes that were also identified in this study (Figure 8; Cheng *et al.*, 2020). Taken together, these data indicate that the up-regulation of genes involved in nucleocytoplasmic transport is a common feature of plants to compensate for the loss of nucleoporin functions, rather than being a specific defect associated with mutations in *MOS3* or *NUP160.* The gene expression analyses as stated above (Jacob *et al.*, 2007; MacGregor *et al.*, 2013; Parry, 2014; Cheng *et al.*, 2020) and this study (Figure 8) described elevated gene expression of *NUP98B, RAE1, RAN1, RAN2, XPO1B* and *NTF2B*. This elevated gene expression was not only independently of the *nup* mutant background but also of the developmental status of the mutants. Whereas

Jacob *et al.* (2007) compared post-flowering mutant with pre-flowering wild-type plants, Parry (2014) used 7-day old seedlings. In the study of MacGregor *et al.* (2013), 14-day old *hos1* seedlings at the point of floral transition were used. In contrast, 12-day old *mos3* and *hos1* seedlings grown under long-day conditions were used in the study of Cheng *et al.* (2020). These data further indicate that the elevated expression of *NUP98B*, *RAE1*, *RAN1*, *RAN2*, *XPO1B* and *NTF2B* are not directly linked to a specific developmental stage of the investigated *nup* mutant plants, but rather a general regulatory mechanism to counteract defects in the nuclear transport machinery.

4.1.4 Defence-related genes show decreased expression in *mos3* and *nup160* as compared to wild-type

Among the 227 DEGs showing reduced expression in *mos3* and *nup160* defence-related genes have been identified. The two tandem copies of *EDS1* (i.e. *EDS1A* and *EDS1B*), a key defence regulator of TIR-type R protein mediated resistance, and its signaling partner *PAD4* were found in both mutants (Figure 5 and 6; Supplementary Table 1). Decreased transcript abundance of *EDS1A* and reduced EDS1 protein level has been previously reported for the *nup160* mutant (Wiermer *et al.*, 2012). However, it has not been accessed so far, if the reduced *EDS1* transcripts levels in *mos3* also lead to reduced protein level. Furthermore, it has not been investigated if PAD4 protein levels are reduced in *mos3* and *nup160* mutant plants. Due to the lack of an available functional antibody recognizing EDS1 and PAD4, both EDS1 and PAD4 protein level were not investigated in this study. This knowledge would provide further hints if the reduced amount of functional EDS1 and PAD4 protein contribute to the observed immunity defects in both mutants. Interestingly, only the expression of genes encoding for TIR-type NLR proteins, but not CC-type NLRs are affected in the *mos3* and *nup160* mutant plants (Figure 6; Supplementary Table 1). Although the molecular basis for this selectively reduced expression is unknown, these findings further support the results of Wiermer *et al.* (2012) that *MOS3* and *NUP160* play an important role in TIR-type R protein-mediated immunity but a less important role in CC-type mediated resistance. In contrast to *mos3* and *nup160*, *mos7*-1 mutant plants are also impaired in CC-type R protein-mediated immunity (Cheng *et al.*, 2009). These findings suggest a certain degree of functional selectivity among different nucleoporins and that *MOS3*, *NUP160* and *MOS7/NUP88* contribute to different extent to particular plant immune pathways.

On the contrary, *NDR1*, a key component in CNL-mediated resistance is down-regulated in *nup160*-3 (log_2FC of -1.32; Figure 5; row data of RNAseq experiment), while its gene expression is not affected in *mos3*-2 as compared to wild-type (Figure 5; row data of RNAseq experiment). Since both mutants are not affected in resistance mediated by the NDR1-dependent CC-type NLR proteins RPM1 and RPS2 (Wiermer *et al.* 2012), it remains

to be investigated if the reduced transcript abundance of *NDR1* also results in altered protein levels in the *nup160* mutant.

Interestingly, *mos3* and *nup160* show significantly reduced expression of the PRR gene *EFR*, but the expression of two other well-known PRRs, *FLS2* and *CERK1*, is not affected (Figure 6 and 10; Supplementary Figure 2). This result further supports the idea that MOS3 and NUP160 contribute selectively to the expression of certain genes. Furthermore, this result indicates that altered perception of *Pseudomonas syringae* by FLS2 has a minor role for the immunity defects of *mos3* and *nup160* against this pathogen (Wiermer *et al.*, 2012). The finding of altered *EDS1* and *EFR* gene expression in *mos3* and *nup160* as revealed by the RNAseq experiment (Figure 6, 9 and 10) and qRT-PCR analyses (Figure 12; Supplementary Figure 2 and 3) are in agreement with previous data of the Wiermer group (Stepanets, M.Sc. Thesis, 2013; Lüdke, B.Sc. Thesis, 2014). In contrast to the data presented here (Figure 6, 9, 10 and 12; Supplementary Figure 2 and 3), the RNAseq-based gene expression analysis of *mos3* seedlings conducted by Cheng *et al.* (2020) did not identify altered transcript levels of *EDS1*, *PAD4* or *EFR*. The discrepancy of the results might be explained by differences in plant age and growth conditions. The RNAseq experiment presented in this study (Figure 5) used four week old *Arabidopsis* plants grown under short day conditions, whereas 12-day old *Arabidopsis* seedlings grown under long day conditions were used in the study of Cheng *et al.* (2020). Several lines of evidence could already show that the expression of genes, including defence-genes, is influenced by growth conditions, plant age or the circadian rhythm. For example, gene expression is changing in response to nutrient content in *Arabidopsis* and soybean (Brumbarova and Ivanov, 2019; O'Rourke *et al.*, 2020). Sano *et al.* (2014) analysed transcriptome data of two week old *Arabidopsis* seedlings that were either illuminated for four hours with light (80 – 100 µmol m^{-2} s^{-1}) or kept in the dark before treated with 1 µM flg22. The study showed that the expression of certain flg22-induced genes depent on light, while the expression of genes that are repressed by flg22 are down-regulated. This illustrates that the stimulus light has an important role in basal plant defence responses. Furthermore, an age-related resistance (ARR) has been described as development-dependent defence response of *Arabidopsis* against *Pseudomonas*. It has been shown that the expression of defence-related genes changes with the plant age (Kus *et al.*, 2002; Wilson *et al.*, 2017).

Over the past years it has also been shown by several groups that the circadian clock is involved in plant defence responses against *Pseudomonas* (Bhardwaj *et al.*, 2011; Fu and Wang, 2011; Zhang *et al.*, 2013a). Interestingly, de Leone *et al.* (2020) could show that wild-type infected with *Pseudomonas* display decreased expression of *NIGHT LIGHT-INDUCIBLE AND CLOCK-REGULATED* (*LNK*) genes one-hour post infiltration. One hypothesis is that the expression of defence genes is differently regulated in *mos3* mutant

plants depending on the plant age or circadian rhythm, which could explain differences between the outcome of the study of Cheng *et al.* (2020) and this study.

The RNAseq experiment revealed altered expression of *EDS1*, *PAD4* and *EFR* in *mos3*-2 and *nup160*-3 (Figure 6, 9 and 10). These data aggree with previous data of the Wiermer group (Stepanets, M.Sc. Thesis, 2013; Lüdke, B.Sc. Thesis, 2014) and illustrate that the RNAseq experiment presented in this study is a valid approach to identify components of plant immunity. The predicted methyl esterase gene *MES18* and *PUM9* encoding an predicted RNA-binding protein are the two genes showing the most strongly reduced transcript abundance in unchallenged *mos3* and *nup160* mutant plants (Figure 6 and 11; Supplementary Table 1). The contribution of both genes to plant immunity will be discussed in 4.3.

4.1.5 *MOS3* and *NUP160* influence either directly or indirectly the expression of a specific subset of genes

The transcriptome analysis presented in this study revealed that the expression of 614 and 1082 genes are mildly but significantly affected in *mos3*-2 and *nup160*-3 as compared to Col-0 (Figure 5 B). This indicates that both nucleoporins are involved in the regulation of these genes.

For the mouse model, Faria *et al.* (2006) showed that a specific subset of immune-related mRNAs is retained in the nucleus if *NUP96* gene function is impaired, indicating that functional NUP96 is important for the export of certain mRNAs in mice. Recently, a nuclear-cytoplasmic RNAseq experiment of the *Arabidopsis* nucleoporin mutant *nup205* could show that a subset of mRNAs of circadian core-clock genes is retained in the nucleus of this mutant (de Leone *et al.*, 2020). This data supports the idea that plant nucleoporins regulate the nuclear export and expression of certain sets of mRNAs which contributes to the regulation of certain cellular processes. Since *mos3* and *nup160* mutant plants also display mRNA export defects (Parry *et al.*, 2006; Dong *et al.*, 2006; Muthuswamy and Meier, 2011; Roth and Wiermer, 2012), this raises the question if both mutants also accumulate particular subpopulations of mRNAs in the nucleus, which might influences the expression of particular genes or their cytoplasmic translation into the respective proteins. Since a complete block of the export of all poly(A)-mRNAs from the nucleus into the cytoplasm would most likely result in more drastic pleiotropic phenotypes as observed for *mos3* and *nup160* mutant plants (Zhang and Li, 2005; Dong *et al.*, 2006; Robles *et al.*, 2012; Wiermer *et al.*, 2012), it seems rather unlikely that the retained mRNAs in both mutants represent the whole pool of polyadenylated mRNAs. It seems to be more likely that only certain mRNAs are retained in the nucleus as a consequence of the mutations in *MOS3* and *NUP160*, or that the defects in *mos3* and *nup160* do not result in a full block of mRNA export.

Previous studies of Wiermer *et al.* (2012) could show that *EDS1* mRNAs can be detected in both the nuclear and cytoplasmic RNA pool of *nup160* mutant plants. These data indicate that not all differentially expressed genes of the *nup160* mutant are specifically retained in the nucleus (i.e. *EDS1* mRNA), but it does not exclude the possibility that the translocation of certain subsets of mRNAs is affected in *nup160* as well as *mos3*. Wiermer *et al.* (2012) concluded from their findings that the loss of *NUP160* function does not result in specific nuclear retention of *EDS1* mRNA, but rather leads to a more general defect on *EDS1* gene expression. The study presented here investigated total RNA pools of unchallenged *mos3* and *nup160* leave tissue (Figure 5). Therefore, this study provides a general view on altered gene expression in the absence of functional *MOS3* and *NUP160*, but cannot answer the question if specific mRNA species are retained in the nucleus of *mos3* and/or *nup160*. A RNAseq analyses of cytoplasmic and nuclear fractions of *mos3* and *nup160* in comparison to wild-type would be useful to assess if specific subsets of mRNAs are retained in the nucleus or whether the loss of *MOS3* and *NUP160* generally affect gene expression. Furthermore, fluorescent *in situ* hybridization (FISH) experiments could be performed in which specific target mRNAs are labeled and subsequently investigated for their subcellular localization in *mos3* and *nup160*. This would further expand our knowledge on how *MOS3* and *NUP160* contribute to gene expression of particular genes.

Several gene expression analyses of different plant *nup* mutants revealed global transcriptional changes (Jacob *et al.*, 2007; MacGregor *et al.*, 2013; Parry, 2014; Cheng *et al.*, 2020; de Leone *et al.*, 2020). Although transcriptional changes in all studies including the data presented here (Figure 5 and 6) are rather mild it nevertheless indicates the importance of the nuclear trafficking machinery for the regulation of gene expression. Interestingly, Menon *et al.* (2005) revealed that members of the yeast NUP84 complex can activate gene transcription by tethering target genes to the inner side of the nuclear pore which couples transcription with mRNA export. This data illustrate that the NPC might acts as a transcriptional activator itself. In addition, the yeast NUP170 interacts with heterochromatin and contributes to gene silencing (Van de Vosse *et al.*, 2011). Further studies in *Drosophila* demonstrated that NUPs can directly bind to chromatin to activate gene expression (Kalverda *et al.*, 2010; Maya Capelson *et al.*, 2010). In *Arabidopsis HOS1* interacts with *FLC* chromatin and thereby regulates *FLC* expression (Jung *et al.*, 2013). This links MOS3 and NUP160, which can physically interact with HOS1, indirectly to gene regulation via HOS1-mediated chromatin interactions (Cheng *et al.*, 2020; Li *et al.*, 2020). So far, it remains unclear whether *MOS3* and *NUP160* also regulate gene expression by recruiting target genes to the NPC. In future, this could be elucidated by ChIPseq analysis of stable transgenic plants expressing epitope-tagged MOS3 and NUP160.

Regulation of gene expression by MOS3 and NUP160 might alternatively be facilitated by modulating the nuclear translocation and accumulation of transcriptional regulators. In agreement with this hypothesis, it has been reported that the auxin-regulated transcriptional repressor IAA17 exhibits reduced accumulation in *mos3* and *nup160* nuclei (Parry *et al.*, 2006).

This study supports the notion that the plant NPC is an essential platform in the regulation of gene expression. The RNAseq experiment (Figure 5) and GO term analysis (Figure 7) indicate that *Arabidopsis MOS3* and *NUP160* are involved in the regulation of expression of genes that are involved in several molecular processes including defence responses. However, the exact molecular mechanism how the abundance of certain transcripts including those of defence-related genes is regulated by MOS3 and NUP160 remains to be elucidated. It seems possible that MOS3/NUP96 and NUP160 are involved in regulating efficient mRNA export, gene tethering to the NPC, the direct or indirect interaction with chromatin of specific target genes or a combination of these mechanisms. Furthermore, more indirect effects such as the proper expression and nuclear localization/accumulation of transcriptional modulators might influence the gene expression mediated by MOS3/NUP96 and NUP160. Although the molecular bases of this gene regulation is far from being comprehensive, it seems likely that only certain target genes are affected. The overlap of DEGs identified in *mos3* and *nup160* additionally indicates overlapping functions between both NUPs and it will be interesting to further investigate the transcriptional changes of *mos3* and *nup160* as compared to wild-type plants in response to different pathogen stimuli and in nuclear/cytoplasmic fractions.

4.2 Phenotypic consequences of reduced *EFR* transcript levels in *mos3* and *nup160* mutant plants

4.2.1 The nucleoporin mutants *mos3* and *nup160* are more susceptible to *Agrobacterium*-mediated transient plant transformation

The soil-born bacterium *Agrobacterium tumefaciens* causes crown gall disease in various plant species including *Arabidopsis* and relies for its infection process on an efficient transfer and integration of its T-DNA into the plant host genome (Gohlke and Deeken, 2014). The GUS reporter assay used in this study (Figure 13) is a standard assay to evaluate the efficiency of the *Agrobacterium*-mediated transient transformation event and was previously used by several other research groups (Nam *et al.*, 1997; Zipfel *et al.*, 2006; Marion *et al.*, 2008; Li *et al.*, 2009; Wu *et al.*, 2014). The *GUS* + *intron* reporter gene construct that was used in the GUS reporter assay allows for plant-specific expression of the GUS reporter, but not for bacterial GUS expression. The assay revealed that *Agrobacterium*-infiltrated leaves

of *mos3* and *nup160* mutant plants exhibit a higher amount of GUS activity in comparison to Col-0, but that the GUS activity was less strong compared to hyper-susceptible *efr*-1 mutant (Figure 13; Zipfel *et al.*, 2006). This indicates that the loss of wild-type *EFR* function has a more pronounced effect on *Agrobacterium* transformation as compared to the loss of *MOS3* and *NUP160*.

Notably, several independent experiments revealed that the *mos3*-1 mutant allele showed a tendency towards less efficient GUS activity as compared to the *mos3*-2 and both *nup160* mutant alleles (Figure 13). One possible explanation for the discrepancy observed between both *mos3* mutant alleles might be the fact that the *mos3*-1 mutant line was isolated in a forward genetic screen (Zhang and Li, 2005), while *mos3*-2 is a T-DNA line (SALK_109959). The *mos3*-1 mutant was backcrossed into the Col-0 wild-type background. However, genetic side effects that are caused by the mutagenesis beside the mutation in the *MOS3* gene cannot be completely excluded. These side mutations might have an effect on the transformation efficiency. In contrast to the *mos3*-2 mutant line which contains a T-DNA insertion in the fifth exon, the *mos3*-1 mutation is a A to C mutation located in the junction between the fifth intron and the sixth exon (Zhang and Li, 2005). Since the *mos3*-1 mutation is located in the last exon oft he *MOS3* gene and although the *mos3*-1 allele is as susceptible to *Pseudomonas* infection as the *mos3*-2 T-DNA allele, a second possible explanation might be that a partially functional MOS3 protein is produced in *mos3*-1 which is capable of attenuating transient transformation. Nevertheless, in contrast to *mos3*-1, the independent T-DNA insertion line *mos3*-2 showed reproducible higher GUS activity in comparison to the wild-type control and was similar to both *nup160* mutant lines. This data indicates that both *MOS3* and *NUP160* are involved in restricting *Agrobacterium*-mediated transient plant transformation. Elevated levels of GUS activity in *mos3* and *nup160* as compared to wild-type are in line with previous observations in the Wiermer Group (Stepanets, M.Sc. Thesis, 2013; Lüdke, B.Sc. Thesis, 2014) and are independent of the inoculation method that was used (dip or pressure infiltration). Interestingly, the higher GUS expression in *mos3* and *nup160* could not be observed for *sec13b*-1 mutant plants, which showed GUS activity that was similar to the wild-type control (Figure 13). Since SEC13B is also a predicted member of the plant NUP107-160 complex, this data suggest a selective role for *MOS3* and *NUP160* in restricting *Agrobacterium*-mediated plant transformation. However, it cannot be fully excluded that a possible function of SEC13B in restricting plant transformation by *Agrobacterium* is hidden in this assay by potential functional redundancy with SEC13A or other members of the NUP107-160 complex.

Significantly, bacterial growth assays could show that the proliferation rate of *Agrobacterium* is not altered in *mos3* and *nup160* in comparison to Col-0 wild-type and *efr*-1 (Figure 14). These findings suggest that the enhanced GUS activity in the *nup* mutants as

well as in the *efr* control is likely due to enhanced transformation rates rather than increased bacterial proliferation. Studies of Zipfel *et al.* (2006) and Wang *et al.* (2018b) could also show similar bacterial growth in *Agrobacterium*-inoculated wild-type and *efr*-1 mutant plants, confirming the data of this study (Figure 14). These results and the data presented here indicate that plant defence responses against *Agrobacterium* in *efr*-1 as well as in *mos3* and *nup160* are still capable to restrict bacterial growth as in wild-type, whereas the transfer of the T-complex appears to be increased.

4.2.2 Elevated transformation rates in the *mos3* and *nup160* mutant plants are most likely caused by compromised plant defence mechanism against *Agrobacterium*

Zipfel *et al.* (2006) showed that *Agrobacterium*-infiltrated *efr*-1 leaves develop chlorotic disease symptoms in contrast to infiltrated wild-type plants that do not show obvious symptoms. Preliminary data of the Wiermer group confirmed this observation and revealed that leaves of *mos3* and *nup160* also show yellowish chlorotic spots after *Agrobacterium* treatment (Stepanets, M.Sc. Thesis, 2013; Lüdke, B.Sc. Thesis, 2014). In line with the development of chloroses on *mos3* and *nup160* leaves upon *Agrobacterium*-inoculation, the production of reactive oxygen species (ROS) upon elf18 treatment is compromised in *mos3* and *nup160* mutant plants (Figure 15). Both, chlorotic symptoms on *Agrobacterium*-infected leaves and impaired elf18-induced ROS production of *mos3* and *nup160* indicate that plant defence mechanisms against *Agrobacterium* are impaired in both mutants. However, both *mos3* and *nup160* mutant plants display similar propagation of agrobacteria as wild-type plants (Figure 14), indicating that defence responses to restrict *Agrobacterium* growth are still functional in both mutants. It is tempting to speculate that inappropriate ROS production in *mos3* and *nup160* mutants influences the success of the transformation event. Interestingly, Franklin *et al.* (2008) reported that ROS affects agrobacterial viability. The co-cultivation of agrobacteria and cell cultures of *Hypericum perforatum* lead to an oxidative burst which resulted in a mortality rate of 99 % of the co-cultivated agrobacteria within the first 12 hours after inoculation (Franklin *et al.*, 2008). This data illustrate that agrobacteria have a poor viability in a ROS-rich environment. The ROS production is described as an early plant defence response (Boller and Felix, 2009). It might be possible that the impaired ROS production in *mos3* and *nup160* has a positive effect on agrobacteria viability at the early stages of the agrobacteria infection. This might lead to an efficient translocation of the T-DNA into the plant cell via the agrobacterial T4SS at early stages of the infection and contribute to the elevated transformation efficiency of both mutants.

Consistent with the observation that *mos3* and *nup160* mutants are impaired in elf18-induced ROS production (Figure 15), both mutants display reduced transcript level of *EFR,* encoding the PRR that perceives elf18 and triggers basal defence response (Figure 6, 10

and 12; Zipfel *et al.*, 2006). The reduced transcript abundance of *EFR* in both mutants is also reflected in reduced EFR protein level in the *mos3*-2 background (Figure 16). Since *EFR* transcript levels are more severely affected in *nup160* as compared to *mos3* (Figure 6, 10 and 12; Supplementary Table 1) *nup160* mutants probably also display reduced EFR protein level. The reduced *EFR* gene expression, and consequently reduced EFR protein level, together with the impaired elf18-induced ROS production indicate that the EFR-mediated perception of the agrobacterial PAMP elf18 is impaired in *mos3* and *nup160*, which might lead to elevated transformation rates in both mutants.

Notably, similar to the elf18-induced ROS production, the ROS production upon treatment with the PAMPs flg22 and chitin is also impaired in *mos3* and *nup160* (Stepanets, M.Sc. Thesis, 2013; Lüdke, B.Sc. Thesis, 2014), albeit transcript levels of the PRRs *FLS2* and *CERK1* that recognize flg22 and chitin, respectively, are not reduced in both *nup* mutants (Figure 10; Supplementary Figure 2). These findings may indicate that the altered production of ROS in the apoplast upon elicitor treatment is generally compromised in both mutants. A potential explanation for these results is that *mos3* and *nup160* mutants display an reduced expression of genes encoding for the RBOH family of NADPH oxidases, including RbohD, which are involved in generating the oxidative burst upon PAMP/MAMP perception by PRRs (Torres *et al.*, 2006; Kadota *et al.*, 2015; Kimura *et al.*, 2017). However, the RNAseq experiment performed in this study did not identify altered expression of *RBOH* genes in unchallenged *mos3* or *nup160* (Supplementary Table 1; row data of the RNAseq experiment), indicating that the explanation for the altered ROS production in both mutants is more complex. In addition to the RBOH-mediated ROS production, several other enzymes including cell wall peroxidases, amine oxidases, lipoxygenases, oxalate oxidases and quinone reductases are involved in the production of apoplastic ROS (Kärkönen and Kuchitsu, 2015; Survila *et al.*, 2016). Functional expression of these genes might be either directly or indirectly affected by MOS3 and NUP160, which could lead to altered ROS production in *mos3* and *nup160* plants upon elf18, flg22 and chitin treatment.

Contrary to the impaired ROS production of both *nup* mutants upon MAMP/PAMP treatment, further PTI responses (e.g. activation of the MAPK cascade) appears to be wild-type like. Notably, both the transcript abundance of the pathogen- and PAMP-responsive MAP kinases *MPK3*, *MPK4* and *MPK6* as well as their activation upon elf18, flg22 and chitin treatment is not obviously altered in *mos3* and *nup160* mutant plants as compared to the wild-type control (Supplementary Table 1; Stepanets, M.Sc. Thesis, 2013; Appel, B.Sc. Thesis, 2018) indicating that this PTI response is functional in both mutants. Recent findings suggesting that the ROS burst and MAPK activation are two signalling mechanism that work independently in plant immunity (Ranf *et al.*, 2011; Segonzac *et al.*, 2011; Xu *et al.*, 2014). This might explain why ROS signalling is impaired, whereas the

activation of the MAPK cascade is functional in both mutants. While an impaired EFR-mediated perception of agrobacteria and an impaired ROS production may contribute to a more efficient translocation of the T-DNA via the T4SS at early stages of the infection, functional activation of the MAPK cascade and further downstream defence signalling (e.g. the activation of defence genes) may restrict *Agrobacterium* growth at later stages of the infection. This would be consistent with the results of the bacterial growth assay (Figure 14).

The EFR-dependent perception of elf18 is impaired both mutants. It might be possible that the activation of plant defence signaling (e.g. activation of MAPK cascade) to restrict bacterial growth is elicited by other MAMPs/PAMPs than elf18 that are present in agrobacteria. While flagellin derived from agrobacteria does not trigger plant defence responses in *Arabidopsis*, *Agrobacterium*-derived peptidoglycan does (Kunze *et al.*, 2004; Zipfel *et al.*, 2006; Erbs *et al.*, 2008). In *Arabidopsis*, CERK1 is involved in binding bacterial peptidoglycan (Willmann *et al.*, 2011). The transcript abundance of *FLS2* and *CERK1* are not altered in both mutants in comparison to wild-type (Figure 10; Supplementary Figure 2). Therefore, bacterial peptidoglycan is likely perceived by CERK1 in *mos3* and *nup160* mutant plants, leading to an immune response. More recently it has also been shown that *N. benthamiana* has an RLP that recognizes bacterial cold-shock proteins (Saur *et al.*, 2016). In *Arabidopsis* such a receptor has not been identified so far. However, it could be possible that *Arabidopsis* also has a receptor that can perceive *Agrobacterium*-derived cold-shock proteins. Alternatively, other receptors that recognize unknown bacterial MAMPs/PAMPs may exist in *Arabidopsis*. Taken together, it seems likely that agrobacteria are still recognized in *mos3* and *nup160* mutant plants, which leads to downstream defence signaling (e.g. via MAPK cascades) to restrict bacterial growth.

4.2.3 The molecular mechanism underlying enhanced transformation rates in *mos3* and *nup160* remains elusive

Mos3 and *nup160* mutants show elevated transient transformation rates by *Agrobacterium* (Figure 13). Since compromised plant defence responses against *Agrobacterium* in *mos3* and *nup160* might be not the only reason for this observation, further possibilities will be discussed. Several aspects of the transformation process can be affected and may lead to an altered transformation efficiency, including *Agrobacterium* attachment, regulation of *vir* gene expression as well as the transport, integration and expression of the T-DNA (Gelvin, 2010; Hwang *et al.*, 2017).

Arabidopsis importin-α proteins can interact with the agrobacterial Vir proteins, VirD2 and VirE2, which protect the T-complex and facilitate its import into the plant nucleus (Bhattacharjee *et al.*, 2008; Lee *et al.*, 2008). Notably, a mutation in *Arabidopsis IMP-α4,* but not in other tested *Arabidopsis* importin-α proteins lead to enhanced resistance against

Agrobacterium-mediated root transformation. This indicates that specifically IMPα-4 is required for plant transformation by *Agrobacterium* and suggests that IMPα-4 is involved in mediating nuclear import of the T-complex (Bhattacharjee *et al.*, 2008). However, the details on how IMPα-4 is responsible for nuclear targeting of the T-complex is not fully understood. Additional research should assess the subcellular localization of the VirD2- and VirE2-containing T-complex in the *mos3* and *nup160* mutants. Altered VirD2/E2 localization (e.g. enhanced nuclear accumulation) might contribute to elevated transformation rates in both mutants. The loss of *MOS3* and *NUP160* functions lead to a compensatory transcriptional up-regulation of genes encoding components of the nuclear transport machinery (Figure 8; see 4.1.4). The importin-α-mediated nuclear transport relies on a tightly regulated concentration gradient of the small GTPase RAN in its GTP-bound nuclear and GDP-bound cytoplasmic form. Interestingly, both *mos3* and *nup160* show elevated gene expression of *RAN1/2* (Figure 6 and 8), which might contribute to an elevated importin-α mediated import of the T-complex into the nucleus. Such elevated transport of the T-complex could contribute to the observed enhanced transformation efficiency.

An alternative explanation for the elevated transformation efficiency of *mos3* and *nup160* mutants could be an altered nuclear translocation or retention of transcriptional regulators that are involved in the *Agrobacterium*-mediated plant transformation process. Consistent with this idea, it has been shown that the nuclear accumulation of the auxin responsive transcriptional regulator IAA17 is reduced in root tips of *mos3* and *nup160* (Parry *et al.*, 2006). Interestingly, Sardesai *et al.* (2013) uncovered the myb transcription factor MTF1 as negative regulator of the *A. tumefaciens* transformation process, since m*tf*-1 mutant plants show increased stable and transient transformation efficiencies. Although the basal gene expression of *MTF1* is not affected in unchallenged *mos3* and *nup160* mutant plants (Supplementary Table 1; row data of the RNAseq experiment), preliminary data of the Wiermer group could show that *Agrobacterium*-challenged *mos3* and *nup160* mutants plants display an altered *MTF1* transcript abundance as compared to wild-type. These data revealed that the *MTF1* expression increases in wild-type, *mos3* and *nup160* mutants upon *Agrobacterium* challenge, but with a significantly reduced induction of *MTF1* expression in both *nucleoporin* mutants (Lüdke, B.Sc. Thesis, 2014). So far the molecular basis for this reduced *MTF1* gene activation after *Agrobacterium* challenge of *mos3* and *nup160* is not known. Future research should attempt to clarify where MTF1 localizes in unchallenged mutants plants in comparison to wild-type, and if the subcellular localization of MTF1 changes upon *Agrobacterium* infection in both the mutants and wild-type. Nuclear retention of *MFT1* mRNAs in the mutants might be a possibility that contributes to an altered *MTF1* expression in *mos3* and *nup160* upon *Agrobacterium* challenge. For the *mtf1* mutant,

Sardesai *et al.* (2013) proposed that *ARR3*, a negative regulator of cytokinin signaling (To *et al.*, 2004), decreases *MTF1* gene expression, which leads to the enhanced transformation rates in the *mtf1* mutant. Furthermore, the authors showed that *Agrobacterium*-secreted cytokinins modulate the expression of *MTF1* (Sardesai *et al.*, 2013). This data indicate that the gene expression of *MTF1* is modulated in different ways and seems to be important for *Agrobacterium*-mediated transformation. Since *MTF1* gene expression appears to be altered in *mos3* and *nup160* after *Agrobacterium* challenge (Lüdke, B.Sc. Thesis, 2014), it seems plausible that *MOS3* and *NUP160* are involved in the regulation of *MTF1* expression upon *Agrobacterium* infection.

Another potential explanation for the enhanced transformation efficiency could by altered levels of secondary metabolites such as glucosinolates in *mos3* and *nup160*. Recent data indicate that glucosinolate biosynthesis plays a role in controlling *Agrobacterium* transformation (Shih *et al.*, 2018). It has been shown that in *Agrobacterium*-challenged Col-0 wild-type seedlings genes involved in glucosinolate (GS) biosynthesis are differentially expressed. Interestingly, genes that have a role in the aliphatic glucosinolate (aGS) biosynthesis generally showed a reduced transcript abundance upon *Agrobacterium* infection when compared to the mock control (Shih *et al.*, 2018). In addition, isothiocyanates (ITCs), which are toxic hydrolysis products of aliphatic glucosinolates (Halkier and Gershenzon, 2006; Wittstock and Burow, 2010), influence the transformation efficiency when applied exogenously to wild-type seedlings (Shih *et al.*, 2018). The application of ITCs leads to either elevated or reduced transformation efficiency, dependent on the ITC (Shih *et al.*, 2018). Taken together, these data indicate a connection between aliphatic glucosinolate biosynthesis, the presence of ITCs and the success of *Agrobacterium*-mediated plant transformation. Notably, transcript abundance of *MAM1/2,* two genes which are involved in Met-derived aliphatic glucosinolate biosynthesis (Benderoth *et al.*, 2009; Sønderby *et al.*, 2010) are elevated in *mos3* and *nup160* mutant plants (Supplementary Table 1). Thus, an altered glucosinate biosynthesis and abundance of ITCs in *mos3* and *nup160* compared to wild-type could indirectly influence the transformation efficiency.

The exact molecular mechanism(s) for the elevated transformation efficiency of *mos3* and *nup160* mutants remains to be elucidated. Transcriptome data of *Agrobacterium*-infected mutant leave tissues and subcellular localization studies of promising target proteins such as MTF1 might be helpful to understand why both mutants display higher transformation levels. Although the molecular basis is not understood, the evolutionary conserved *MOS3/NUP96* and *NUP160* are interesting targets that could be mutated/deleted in crop plants which are recalcitrant to transformable in order to enhance their transformation efficiency.

4.3 Functional characterization of the predicted methyl esterase MES18 and the RNA-binding protein PUM9

4.3.1 PUM9 may regulate the expression/mRNA stability of certain DEGs in *mos3* and *nup160*

The RNA binding protein *PUM9* displayed mild but significant decreased expression in unchallenged *mos3* and *nup160* mutant plants. This was revealed by the RNAseq experiment and independently confirmed by qRT-PCR analyses (Figure 6, 11 and 17). Two independent *pum9* T-DNA mutant lines that were isolated in this study (Figure 18), were neither impaired in basal resistance to *Pseudomonas syringae* nor in RPS4 or RPM1 dependent immunity to *P. syringae* expressing the effectors AvrRps4 and AvrRpm1, respectively (Figure 19 A-C). This suggests that *PUM9* is genetically not required for basal resistance or R protein-mediated immune responses against *Pseudomonas*. However, this does not exclude the possibility that *PUM9* plays a role in defence responses against other pathogens. In *Arabidopsis*, PUM9 is one of 26 described pumilio family (PUF) proteins (Wickens *et al.*, 2002; Francischini and Quaggio, 2009; Tam *et al.*, 2010; Wang *et al.*, 2018a). Several *Arabidopsis PUM* genes are a result of a gene duplication event, including the gene pair *PUM9/PUM10* (Tam *et al.*, 2010). Thus, the lack of a defence-related phenotype in the *pum9* single mutants might be hidden by functional redundancy with *PUM10* or other family members.

PUMs are described as posttranscriptional regulators that are able to repress the expression of specific mRNAs targets (Quenault *et al.*, 2011). PUMs interact with their mRNA targets by recognizing specific regulatory *cis*-elements (PREs) in the 3'UTR of their mRNA targets, which governs decay and translational repression of their mRNA targets (Wickens *et al.*, 2002; Tam *et al.*, 2010; Friend *et al.*, 2012; Miles *et al.*, 2012; Lee *et al.*, 2016). The yeast Puf5 is one example for a PUM protein that acts as transcriptional repressor. Puf5 binds directly to a subunit of the deadenylase complex in yeast and thereby facilitates the recruitment of the cytoplasmic exonuclease to the specific mRNA target that are bound to Puf5 (Goldstrohm *et al.*, 2006). The recruitment of the exonuclease leads to the shortening of the mRNA poly(A) tail which influences the stability and the translation of the target mRNA (Goldstrohm and Wickens, 2008). mRNAs can be also degraded from their 5' end by 5' cap removal which is facilitated by decapping enzymes (Li and Kiledjian, 2010). Data from *Arabidopsis* revealed that PUM9 directly interacts with the catalytic subunit of the mRNA decapping complex in plants named DCP2 (Goldstrohm *et al.*, 2006). Nyikó *et al.* (2019) further revealed that PUM9 binds its mRNA targets via a conserved C-terminal RNA-binding domain, which facilitates the decay of the respective targets. The authors suggested that the binding between PUM9 and its mRNA targets influences the translation efficiency of

these targets. Some of the mRNA targets have an important role in seed dormancy (Nyikó *et al.*, 2019). Thus, it was proposed that PUM9 is implicated in the regulation of seed dormancy.

pum9 mutants restricted bacterial growth of virulent and avirulent *Pseudomonas* strains similar to wild-type (Figure 19), indicating that the loss of *PUM9* function in these mutant plants may not influence the mRNA stability or translation efficiency of genes that are involved in the tested disease resistance against *Pseudomonas*. So far, very little is known about the mRNA targets of the different PUM proteins in *Arabidopsis*. Notably, several studies proposed that PUM proteins preferentially interact with a certain subset of mRNA targets (Gerber *et al.*, 2004; Bernstein *et al.*, 2005; Gerber *et al.*, 2006; Uyhazi *et al.*, 2019). This suggests that individual PUM proteins are involved in distinct cellular processes, although there might be overlapping function. This might further indicate that PUM9 does not only play a role in seed dormancy but also in other molecular processes of the plant cell. Additional research is needed to identify further mRNA targets of *PUM9* in order to test this hypothesis.

Although PUM9 might not be genetically required for plant defence responses against *Pseudomonas*, it is tempting to speculate that reduced *PUM9* expression in *mos3* and *nup160* influences the mRNA stability and translation of certain PUM9 targets. However, if mRNAs of defence-related genes are targets of PUM9 remains unknown. Notably, the expression of *PUM9* can be transcriptionally repressed by a transposable element (TE). It has been suggested that TE-mediated regulation of *PUM9* expression is important for several developmental processes including plant growth (Pietzenuk *et al.*, 2016; Nyikó *et al.*, 2019). It might further be possible that the TE-mediated transcriptional regulation of *PUM9* is influenced in *mos3* and *nup160* which could contribute to the reduced *PUM9* transcript amount that was observed in both mutants (Figure 11 and 17). Xiang *et al.* (2014) revealed that transiently overexpressed GFP-PUM9 in *N. benthamiana* localizes to the nucleus and cytoplasm. This subcellular localization is consistent with the predicted function of PUM9 to promote degradation of its mRNA targets which takes place in the cytoplasm. Altered subcellular localization of PUM9 might influence the binding of its target mRNAs. Further knowledge about the subcellular localization of PUM9 in the *mos3* and *nup160* mutant background would be useful since altered subcellular PUM9 localization might lead to a less efficient degradation of PUM9 mRNA targets which may results in altered gene expression of PUM9 targets in both *nup* mutants.

4.3.2 MES18 is a functional methyl esterase

The *Arabidopsis* genome encodes for 20 predicted methyl esterases (MESs) that catalyse de-methylation processes in the plant cell (Yang *et al.*, 2006; Vlot *et al.*, 2008a;

Yang *et al.*, 2008). Phylogenetic analysis revealed that these *Arabidopsis* methyl esterases are related to the methyl esterases MJE of tomato and SABP2 of tobacco based on their full-length amino acid sequence homology (Figure 21; Supplementary Figure 6). *Le*MJE and *Nt*SABP2 are active *in vivo* on methyl jasmonate and methyl salicylate, respectively (Stuhlfelder *et al.*, 2002; Stuhlfelder *et al.*, 2004; Forouhar *et al.*, 2005). In *Arabidopsis*, MES18 is most closely related to MES16, and forms a phylogenic clade with MES16 and MES17 (Figure 21). This phylogenetic analysis is consistent with previous studies by Vlot *et al.* (2008a) and Yang *et al.* (2008). MES18 contains a conserved catalytic triad which is represented by the residues serine (S81), histidine (H238) and aspartic acid (D210) in *Nt*SABP2, while one or more residues of the catalytic triad are missing in the truncated proteins MES19 and MES20 (Supplementary Figure 6). The presence of the predicted catalytic triade (S80, H230, D202) in MES18 indicates that it is an active esterase.

The *p*NPA esterase activity assay is commonly used to address general esterase activity (Anderson *et al.*, 1994; Yang *et al.*, 2008). The predicted esterase activity of MES18 was confirmed by enzymatic activity assays, which were performed with heterologously expressed His_6-MES18 protein and the esterase substrate *p*NPA (Figure 23). Analytic gel filtration experiments revealed that only one species of the heterologously expressed His_6-MES18 is present in the elution which was used for the esterase activity assays (Figure 22). This data indicates that the results of the esterase activity assay are specifically caused by catalytic activity of MES18 and not by other protein contaminations.

4.3.3 MES18 catalyses the formation of IAA and JA in the presence of MeIAA, MeJA and MeSA

UPLC-nanoESI-MS/MS analysis indicates that MES18 is an active methyl esterase that catalyses the hydrolysis of MeIAA and MeJA to IAA and JA, respectively (Figure 24). This analysis provides high sensitivity and selectivity to detect both the substrates (MeIAA, MeJA) as well as the products (IAA, JA). However, the ionization efficiencies of the substrates as well as the products are compound specific. Thus, a direct comparison between the amount of IAA and JA that was produced during the reaction with either MeIAA or MeJA cannot be used to evaluate potential substrate specificity of MES18. To analyse the substrate specificity, kinetic ITC measurements were performed which revealed strong and reliable heat changes for the reaction of MeIAA to IAA, while this effect was less strong in the presence of MeJA (Figure 25). These data indicate that MES18 preferentially catalyses the de-methylation of MeIAA in comparison to MeJA. The observation that MeIAA is a substrate of MES18 agrees with the study of Yang *et al.* (2008). Notably, Yang *et al.* (2008) could not show an activity of MES18 towards MeJA. This discrepancy might be based in a lower sensitivity of the coupled radioactivity esterase assay used by Yang *et al.* (2008) as

compared to the two methods used in this study. The result that MES18 has more than one substrate agrees with data that were obtained for other methyl esterases in *Arabidopsis*. Yang *et al.* (2008) showed that MES1, 2, 3, 9 and 16 possess enzyme activity towards two or more substrates. Likewise, *Nt*SABP2 shows catalytic activity on three substrates (MeSA, MeJA and MeIAA), but possess the strongest catalytic activity on MeSA (Forouhar *et al.*, 2005).

4.3.4 MES18 display a low catalytic efficiency

Heterologously expressed MES18 catalyzes the hydrolysis of MeIAA to IAA (Figure 24 and 25) and catalytic ITC measurements revealed a catalytic efficiency (k_{cat}/K_M) of 0.0835+/-0.001 mM^{-1} sec^{-1} for MES18 towards MeIAA (Figure 25 C). Previous studies addressed the kinetic parameter of the methyl esterases MES17, *Nt*SABP2 and *Cs*MES1 (Forouhar *et al.*, 2005; Yang *et al.*, 2008; de Lima Silva *et al.*, 2019). The kinetic parameters for MES17 which is closely related to MES18 (Figure 21) were determined with a K_M value of 13 µM and a k_{cat} value of 0.18 sec^{-1} for its substrate MeIAA (Yang *et al.*, 2008), resulting in a catalytic efficiency of 13.84 mM^{-1} sec^{-1} for this substrate. *Nt*SABP2, the ortholog of MES18 in tobacco, catalyzes the hydrolysis of MeSA, MeJA and MeIAA, but displays its highest activity for MeSA with a K_M value of 8.6 µM and a k_{cat} value of 0.45 sec^{-1} (Forouhar *et al.*, 2005), which results in a k_{cat}/K_M value of 52.32 mM^{-1} sec^{-1} for MeSA. de Lima Silva *et al.* (2019) reported K_M value of 48.9 µM and a k_{cat}value of 0.38 sec^{-1} (k_{cat}/K_M= 7.91 mM^{-1} sec^{-1}) for *Cs*MES1 and its substrate MeIAA. The catalytic efficiency of MES18 is lower in comparison to efficiencies that have been reported for the other methyl esterases. Methyl esterases belong to the large α/β hydrolase superfamily and show catalytic activity on various substrates and a direct comparison of catalytic parameters from methyl esterases with different substrates is difficult. Nevertheless, the low value for the catalytic efficiency of MES18 indicate a low substrate affinity of MES18 to its substrate MeIAA. As the *in vitro* enzyme activity can be influenced by multiple factors including buffer composition or pH, non-optimal reaction parameters might be one explanation for low catalytic efficiency of MES18. Initial photometric assays showed that MES18 has its highest activity for the artificial esterase substrate *p*NPA at a pH of 8.5 (data not shown). Similarly, Yang *et al.* (2008) showed that MES17 has the highest MeIAA hydrolase activity at a pH of 8.5. Furthermore, Yang *et al.* (2008) addressed the non-enzymatic hydrolysis of MeIAA at different pH values in more detail. This investigation showed that their reaction buffer at a pH of 7.5 resulted in 93 % of the maximal enzymatic activity without non-enzymatic hydrolysis. In the analysis presented here, enzymatic activity of MES18 was tested in a TRIS-HCl buffer at pH 8.0. Although the influence of different pH on MES18 enzymatic activity towards MeIAA was not addressed in detail, based on the data from Yang *et al.*

(2008) it can be hypothesized that a pH of 8.0 should not have a drastic negative impact on the hydrolytic activity of MES18. Another factor that should be consider is that the assays of this study were performed with His_6-MES18 (see 3.3.6). Thus, it cannot be completely excluded that the tag is interfering with the enzymatic activity.

Interestingly, de Lima Silva *et al.* (2019) identified a polymorphic residue on the N-terminus of the methyl salicylate esterase MES1 in citrus, which correspond to an alanine residue at position 13 in the methyl salicylate esterase SAPB2 protein of tobacco. *Cs*MES1 has a valine residue at this polymorphic position (V18). The authors could show that the exchange from the longer and apolar valine residue to a shorter side chain such as alanine or serine increases the binding affinity of *Cs*MES1 to its hydrolysis product SA. This results in overall decreased MeSA esterase activity of *Cs*MES1. These data indicate that the identified polymorphic residue (V18) has a negative effect on the SA binding affinity of the wild-type *Cs*MES1. Consistent with this data, *Nt*SAPB2 which has an alanine residue at the proposed polymorphic site (A13) is strongly inhibit by SA. An exchange of this alanine residue in *Nt*SABP2 decreases the feedback inhibition that SA has on *Nt*SABP2 function (Forouhar *et al.*, 2005; Park *et al.*, 2007). Interestingly, this polymorphism is also found for methyl esterases in *Arabidopsis*. However, the consequences that this polymorphic residue has on esterase activity have so far only been investigated for methyl esterases with methyl salicylat activity (de Lima Silva *et al.*, 2019). MES18 has an alanine residue at the proposed polymorphic position (A12; Supplementary Figure 6), similar to *Nt*SABP2. Whether this alanine residue also influences the binding affinity of MES18 to its substrate MeIAA or the hydrolysis product IAA is not known and should be considered in future investigations.

Competitive product inhibition has been described for the methyl salicylate esterases *Nt*SABP2 and *Cs*MES1 (Forouhar *et al.*, 2005; de Lima Silva *et al.*, 2019). Whether product inhibition also has an impact on the activity of methyl auxin esterases has not been addressed so far. Another possible explanation for low catalytic efficiency of MES18 might be that MES18 esterase activity is inhibited by the presence of the reaction product IAA. However, kinetic measurements with MeIAA and the product IAA suggest that IAA has no major effect on the catalytic efficiency of MES18 within this reaction (Figure 26). This suggest that product inhibition plays a minor role for the low catalytic efficiency of MES18. To investigate the effect of production inhibition on MES18 esterase activity in more detail, the binding affinities of MES18 towards IAA or other product analogue should be determined via ITC measurements.

An alternative reason for low *in vitro* activity of MES18 might be post-translational modifications (PTMs) that are needed for this function. N-glycosylation and phosphorylation are two examples of PTMs that influence protein stability and activity (Müller, 2018). Although MES18 has two potential glycosylation motifs (NetNGyc 1.0 server;

http://www.cbs.dtu.dk/services/NetNGlyc/), it seems rather unlikely that MES18 is exposed to the N-glycosylation machinery of plants that is located in the ER and Golgi apparatus (Strasser, 2016), since the MES18 protein sequence does not contain a predicted signal peptide (SignalP 5.0 http://www.cbs.dtu.dk/services/SignalP/). In contrast, phosphorylation of MES18 seems to be possible. MES18 possess several serines, threonines and tyrosines residues that are potential phosphorylation sites of this protein (NetPhos 3.1 server; http://www.cbs.dtu.dk/services/NetPhos/). MES18 was heterologously expressed in *E. coli* cells. Thus, eukaryotic posttranslational modifications such as N-linked glycosylation and serine/tyrosine phosphorylation are absent in the heterologously expressed MES18 protein. If posttranslational modifications are needed for MES18 function is unknown and should be addressed in further research.

4.3.5 The methyl esterase MES18 is genetically required for basal resistance against *Pseudomonas*

The predicted methyl esterase *MES18* is the gene showing the most strongly decreased expression in unchallenged *mos3* and *nup160* mutant plants. This was revealed by the RNAseq experiment and independently confirmed by qRT-PCR analyses (Figure 6, 11 and 17). Interestingly, bacterial growth assays revealed that a mutation in *MES18* compromises basal resistance towards the hemi-biotrophic pathogen *Pseudomonas syringae*, whereas immunity mediated by the NLR proteins RPS4 and RPM1 remained intact in *mes18*-1 plants (Figure 19 A-C). The bacterial growth of *Pseudomonas*-infected *mes18*-1 leaves was mildly but significantly increased in comparison to wild-type (Figure 19 A). Since 20 predicted methyl esterases have been described in *Arabidopsis* (Yang *et al.*, 2006; Vlot *et al.*, 2008a; Yang *et al.*, 2008), one or more of the other methyl esterases might have partial functional redundancy with *MES18.* This might compensate the loss of *MES18* gene function and lead to the rather mild enhanced susceptibility phenotype of *mes18*-1. Future research should concentrate on the potential functional redundancy of MES18 with other MES family members, especially with the closely related MES16 and MES17. Double or triple mutants could be used in bacterial growth assays to access the question if the loss of all three methyl esterases results in a more drastic susceptibility phenotype.

This study and Yang *et al.* (2008) demonstrated that MeIAA is a substrate of MES18, illustrating that this enzyme catalyzes the hydrolysis from MeIAA to IAA. In plants, the most abundant naturally occurring auxin is indole-3-acetic acid (IAA; Dai *et al.*, 2013; Korasick *et al.*, 2013; Zhao, 2014) that is decribed as classical plant growth hormone (Huot *et al.*, 2014), but has more recently also been shown to play a role in plant resistance (Denancé *et al.*, 2013). The non-polar IAA methyl ester (MeIAA) is reported as biological inactive storage molecule of IAA (Cohen and Bandurski, 1982; Li *et al.*, 2008;

Yang *et al.*, 2008) that can move transporter-independently from cell to cell and through the whole plant (Li *et al.*, 2008; Yang *et al.*, 2008). Since full-length functional transcripts of *MES18* are not detectable in the *mes18*-1 mutant (Figure 18), functional esterase activity of MES18 is probably absent in this mutant. Thus, *mes18*-1 mutants may display elevated MeIAA levels in comparison to wild-type, but this has not been investigated so far.

To date it has not been reported in the literature that elevated levels of MeIAA directly promote disease development. However, it has been shown that levels of IAA, the metabolic active form of auxin plays a role in pathogenesis. Notably, IAA levels raise during plant infection by *Pseudomonas syringae* pv. *tomato* DC3000 and *Xanthomonas campestris* pv. *campestris* in *Arabidopsis* (O'Donnell *et al.*, 2003; Chen *et al.*, 2007). Transgenic *Arabidopsis* plants overexpressing *YUCCA1,* an IAA biosynthesis gene, display an enhanced susceptibility towards *Pst* DC3000 which is most likely caused by increased endogenous IAA levels (Mutka *et al.*, 2013). Enhanced *P. syringae* growth in the presence of elevated IAA levels has also been described by other research groups, who investigated the effect of pathogen-produced or exogenously applied IAA on bacterial growth (Chen *et al.*, 2007; Wang *et al.*, 2007; Aragón *et al.*, 2014; Navarro *et al.*, 2016; McClerklin *et al.*, 2018). How exactly elevated auxin levels promote plant disease is not fully understood. Since previous studies showed that exogenous applied auxin suppresses SA-dependent defence responses including *PR1* gene expression (Park *et al.*, 2007; Wang *et al.*, 2007) one hypothesis is that auxin and SA work antagonistical to each other.

The *Pseudomonas* effector AvrRpt2 is one example for an effector that interferes with the auxin signaling of the host which appears to be an important mechanism of some pathogens to promote pathogenesis. The secretion of AvrRpt2 into the host cell leads to elevated auxin level which promotes disease development (Chen *et al.*, 2007). The underlaying molecular mechanisms are not well understood. Other T3SS transcription factors such as the transcriptional activator-like effectors (TALEs) of the *X. citri Citrus* canker pathogen were shown to induce citrus genes that are involved in auxin synthesis, signaling and transport (Pereira *et al.*, 2014). This data illustrates that pathogens can also actively interfere with auxin host signaling to promote pathogenesis. Since it was shown that MES18 hydrolyses the biological inactive transport form MeIAA to IAA (Figure 24 and 25), high catalytic activity of MES18 may increase endogenous level of free IAA in the plant cell. It is tempting to speculate that increased catalytic activity of MES18 (e.g. activation via phosphorylation) is beneficial for the infection process of pathogens. Consistent with this idea, recent data have shown that a T3SS effector of *Xanthomonas euvesicatoria* possess protein kinase activity and phosphorylate the plant kinase MAPKK/MEK2 (Teper *et al.*, 2018). Since MES18 contains predicted phosphorylation sites (4.3.5) it might be possible

that MES18 is phosphorylated during the infection process by specific effector molecules which than lead to the activation of MES18 to increase IAA level in the host cell.

The loss of MES18 function in the *mes18*-1 mutant presumably leads to elevated MeIAA and reduced IAA levels. If a higher amount of IAA is stored as the transport from MeIAA in the *mes18*-1 mutant the overall pool of IAA might be reduced in *mes18*-1 in comparison to the wild-type. The higher susceptibility phenotype of *mes18*-1 seems counterintuitive to reduced levels of IAA. However, if IAA levels are altered in the *mes18*-1 is unknown and needs to be tested. Similar to MES18, MES17 has also been described to catalyze the hydrolysis of MeIAA to IAA (Yang *et al.*, 2008). Interestingly, *mes17* mutants display a higher expression of a *promoterDR5:GUS* reporter construct in comparison to wild-type. The auxin-inducible *DR5* promoter fused to the GUS reporter is a marker to investigate endogenous distribution and levels of IAA, indicating that *mes17* mutants show higher levels of endogenous auxin in the shoot apex (Yang *et al.*, 2008). The authors suggested that endogenous levels of auxin are not elevated in *mes17 per se*. It might be possible that a more efficient IAA transport via enhanced MeIAA levels lead to elevated IAA levels. Elevated levels of MeIAA might be hydrolysed back into IAA by other methyl esterases than MES17. Such a scenario is also conceivable for the *mes18*-1 mutant and more efficient IAA transport in the *mes18*-1 mutant may lead to elevated IAA level. However, this hypothesis assumes that the volatile MeIAA travels in the *mes17* as well as the *mes18* mutant to distal tissue where other methyl esterases are expressed that catalyze the hydrolysis of MeIAA back into IAA. In agreement with this idea, eight methyl esterases are described that possess *in vitro* activity against MeIAA including MES17 and MES18 (Yang *et al.*, 2008). Moreover, it has been shown that methyl esterases are expressed in different plant tissue. For example, in *Arabidopsis* seedlings *MES17* is expressed predominantly in the shoot apex, but to lower level also in other plant tissues (Yang *et al.*, 2008), whereas *MES18* is highly expressed in the leaves (Arabidopsis eFP Browser 2.0; http://bar.utoronto.ca). The idea that MeIAA travels between different plant tissue would be consistent with data of MeSA that has been described as biological inactive long-distance signalling molecule which is implicated in SAR and travels from the infection site to distal tissue (Park *et al.*, 2007; Vlot *et al.*, 2008b; Attaran *et al.*, 2009; Shah, 2009; Liu *et al.*, 2010; Liu *et al.*, 2011b; Shah and Zeier, 2013). Alternatively, elevated level of MeIAA in *mes18*-1 might be compensated by elevated biosynthesis of IAA in this mutant, potentially leading to elevated IAA level. In *Arabidopsis* four biosynthesis pathways of IAA are described (Tao *et al.*, 2008; Korasick *et al.*, 2013; Ljung, 2013; Zhao, 2014). To test whether *Pseudomonas* growth might be promoted by elevated IAA levels in the *mes18*-1 mutant, additional research is needed to measure IAA levels in unchallended and infected *mes18* mutant and wild-type plants.

Moreover it needs to be considered that *Arabidopsis* plants which accumulate MeIAA, such as the *mes17* mutant or transgenic *Arabidopsis* plants overexpressing the auxin transferase IAMT1, show phenotypes associated with altered auxin responses (Qin *et al.*, 2005; Yang *et al.*, 2008). IAMT1 catalyzes the reaction from IAA to MeIAA and thus overexpression of this transferase lead to elevated MeIAA level. The *mes17* mutant display longer hypocotyl in comparison to wild-type plants and plants carrying the *IAMT1* overexpression construct show a hyponastic leaf phenotype (Qin *et al.*, 2005; Yang *et al.*, 2008). The *mes18*-1 mutant does not display obvious growth defects, although this was not analyzed in detail in this study. Notably, *mes16* mutants display no obvious auxin-related phenotypes either, although *mes16* plants likely also display elevated MeIAA as well as MeJA levels, because MES16 displays esterase activity on MeIAA and MeJA as substrates (Yang *et al.*, 2008; Christ *et al.*, 2012). These data suggest that altered MeIAA level cause auxin-related phenotypes in a dose dependent manner. Therefore, a normal growth morphology of *mes*18-1 mutant plants does not exclude the possibility that auxin levels and responses are altered in this mutant. Whether altered IAA/MeIAA levels in *mes18* lead to the observed susceptibility phenotype are unknown and needs to be tested by hormone measurements of *mes18* mutants in comparison to wild-type plants.

An alternative explanation for the higher susceptibility of *mes18*-1 mutant plants might be elevated levels of MeJA. Two independent assays presented in this study revealed that MES18 also possesses esterase activity towards the substrate MeJA (Figure 24 and 25). Thus, disruption of *MES18* function may also lead to elevated MeJA levels. It has been shown that MeJA induces the expression of *Arabidopsis BSMT1* and tomato *SAMT*, two methyl transferases catalyzing the conversion from SA to MeSA (Chen *et al.*, 2003; Ament *et al.*, 2004; Koo *et al.*, 2007). Thus, elevated MeJA level in *mes18*-1 might also affect SA levels and result in elevated amounts of MeSA. Koo *et al.* (2007) showed that transgenic *Arabidopsis* plants accumulating high levels of MeSA but no SA/SAG are more susceptible to *P. syringae* infection as compared to wild-type plants. Therefore, elevated MeJA may result in an enhanced MeSA level in *mes18*-1 and enhance the susceptibility towards *Pseudomonas*. Genetically MES18 is required for basal resistance against *Pseudomonas syringae* pv. *tomato* DC3000. Although the higher susceptibility of *mes18* mutant plants is not fully understood, it is tempting to speculate that an certain imbalance between the biological inactive transport forms MeIAA/MeJA and their respective active from IAA/JA in the plant cell may support the establishment of *Pseudomonas* infection and/or affect the efficiency of plant defence responses.

4.4 Outlook

This study revealed that MOS3/NUP96 and NUP160 are involved in regulating the expression of genes that are implicated in different biological processes including plant immunity. To access the molecular role of MOS3 and NUP160 in defence-related gene expression in more detail, it would be highly valuable to investigate transcriptional changes of both mutants in response to different pathogen stimuli, such as *Agrobacterium* inoculation. Further research should also concentrate on the question if MOS3 and NUP160 are involved in mediating the selective nuclear export of particular subsets of mRNAs. The specific retention of mRNAs inside nuclei of *mos3* and *nup160* which encode for defence-related proteins might contribute to the immunity defects of both mutants. Defects in transcript-specific mRNA export could be revealed by analyzing transcript levels in nuclear and cytoplasmic fractions of unchallenged and infected *mos3* and *nup160* mutant plants using RNAseq. Gene tethering to the NPC might be another explanation on how MOS3 and NUP160 regulate gene expression and facilitate subsequent mRNA export. So far, it remains unclear whether MOS3 and NUP160 are involved in the transcriptional regulation of target genes by recruiting these to the nuclear side of the NPC. Such regulatory mechanisms are known from other model organisms including *Drosophila* or yeast. ChIPseq analyses of stable transgenic plants expressing epitope-tagged MOS3 and NUP160 are needed to investigate if MOS3 and NUP160 are bound to chromatin to activate the expression of specific target genes in unchallenged and/or pathogen challenged tissues.

The predicted methyl esterase *MES18* is the gene that shows the most strongly reduced expression in unchallenged *mos3* and *nup160* mutant plants. The loss of *MES18* function leads to a higher susceptibility against *Pseudomonas syringae* pv. *tomato* DC3000. Future research should therefore also address the question how MES18 is involved in regulating basal defence responses against *P. syringae* mechanistically. Expanded bacterial growth assays with an independent *mes18* ko line being generated by CRISPR/Cas9-based genome editing or with transgenic *mes18*-1 complementation lines are required in the first place to confirm the enhanced susceptibility phenotype of *mes18*-1 towards this pathogen. Also, potential functional redundancy of MES18 with other MES family members, in particular with the closely related MES16 and MES17, should be addressed. Double and triple mutant combinations should be used in bacterial growth assays to investigate if the loss of all three methyl esterases results in a more drastic susceptibility phenotype. Detailed hormone measurements and/or metabolome analyses of unchallenged and infected *mes18* plants will be vital to test the hypothesis if elevated MeIAA and/or MeJA levels and/or imbalances in the ratios of MeIAA/IAA and/or MeJA/JA lead to the higher susceptibility of *mes18* plants.

5 References

Aarts, N., Metz, M., Holub, E., Staskawicz, B.J., Daniels, M.J. and Parker, J.E. (1998) Different requirements for EDS1 and NDR1 by disease resistance genes define at least two R gene-mediated signaling pathways in Arabidopsis. *Proc. Natl. Acad. Sci. U. S. A.*, **95**, 10306–10311.

Abbas, M., Hernández-García, J., Pollmann, S., et al. (2018) Auxin methylation is required for differential growth in Arabidopsis. *Proc. Natl. Acad. Sci. U. S. A.*, **115**, 6864–6869.

Aguilar, J., Cameron, T.A., Zupan, J. and Zambryski, P. (2011) Membrane and core periplasmic Agrobacterium tumefaciens virulence type IV secretion system components localize to multiple sites around the bacterial perimeter during lateral attachment to plant cells. *MBio*, **2**, 00218-11.

Alber, F., Dokudovskaya, S., Veenhoff, L.M., et al. (2007) The molecular architecture of the nuclear pore complex. *Nature*, **450**, 695–701.

Alonso, J.M., Stepanova, A.N., Leisse, T.J., et al. (2003) Genome-wide insertional mutagenesis of Arabidopsis thaliana. *Science*, **301**, 653–657.

Ament, K., Kant, M.R., Sabelis, M.W., Haring, M.A. and Schuurink, R. (2004) Jasmonic Acid Is a Key Regulator of SpiderMite-Induced Volatile Terpenoid and Methyl Salicylate Emission in Tomato. *Plant Physiol.*, **135**, 2025–2037.

Anderson, J., Byrne, T., Woelfel, K.J., Meany, J.E., Spyridis, G.T. and Pocker, Y. (1994) The Hydrolysis of p-Nitrophenyl Acetate: A Versatile Reaction To Study Enzyme Kinetics. *J. Chem. Educ.*, **71**, 715–718.

Appel, J. (2018) *Functional characterization of the Arabidopsis thaliana nucleoporins NUP96 and NUP160 in plant immune responses*.

Appen, A. Von, Kosinski, J., Sparks, L., et al. (2015) In situ structural analysis of the human nuclear pore complex. *Nature*, **526**, 140–143.

Aragón, I.M., Pérez-Martínez, I., Moreno-Pérez, A., Cerezo, M. and Ramos, C. (2014) New insights into the role of indole-3-acetic acid in the virulence of Pseudomonas savastanoi pv. savastanoi. *FEMS Microbiol. Lett.*, **356**, 184–192.

Aramburu, I.V. and Lemke, E.A. (2017) Floppy but not sloppy: Interaction mechanism of FG-nucleoporins and nuclear transport receptors. *Semin. Cell Dev. Biol.*, **68**, 34–41.

Attaran, E., Zeier, T.E., Griebel, T. and Zeier, J. (2009) Methyl salicylate production and jasmonate signaling are not essential for systemic acquired resistance in Arabidopsis. *Plant Cell*, **21**, 954–971.

Bartsch, M., Gobbato, E., Bednarek, P., Debey, S., Schultze, J.L., Bautor, J. and Parker, J.E. (2006) Salicylic Acid–Independent ENHANCED DISEASE SUSCEPTIBILITY1 Signaling in Arabidopsis Immunity and Cell Death Is Regulated by the Monooxygenase FMO1 and the Nudix Hydrolase NUDT. *Plant Cell*, **18**, 1038–1051.

Beck, M. and Hurt, E. (2017) The nuclear pore complex: Understanding its function through structural insight. *Nat. Rev. Mol. Cell Biol.*, **18**, 73–89.

Bellincampi, D., Cervone, F. and Lionetti, V. (2014) Plant cell wall dynamics and wall-

related susceptibility in plant-pathogen interactions. *Front. Plant Sci.*, **5**, 228.

Benderoth, M., Pfalz, M. and Kroymann, J. (2009) Methylthioalkylmalate synthases: Genetics, ecology and evolution. *Phytochem. Rev.*, **8**, 255–268.

Bentley, D.L. (2014) Coupling mRNA processing with transcription in time and space. *Nat. Rev. Genet.*, **15**, 163–175.

Bernstein, D., Hook, B., Hajarnavis, A., Opperman, L. and Wickens, M. (2005) Binding specificity and mRNA targets of a *C. elegans* PUF protein, FBF-1. *RNA*, **11**, 447–458.

Bhardwaj, V., Meier, S., Petersen, L.N., Ingle, R.A. and Roden, L.C. (2011) Defence responses of arabidopsis thaliana to infection by pseudomonas syringae are regulated by the circadian clock. *PLoS One*, **6**, e26968.

Bhattacharjee, S., Lee, L.Y., Oltmanns, H., Cao, H., Veena, Cuperus, J. and Gelvin, S.B. (2008) IMPa-4, an Arabidopsis importin alpha isoform, is preferentially involved in agrobacterium-mediated plant transformation. *Plant Cell*, **20**, 2661–2680.

Björk, P. and Wieslander, L. (2014) Mechanisms of mRNA export. *Semin. Cell Dev. Biol.*, **32**, 47–54.

Blanvillain, R., Boavida, L.C., Mccormick, S. and Ow, D.W. (2008) EXPORTIN1 Genes Are Essential for Development and Function of the Gametophytes in Arabidopsis thaliana. *Genetics*, **180**, 1493-1500.

Boeglin, M., Fuglsang, A.T., Luu, D., Sentenac, H., Gaillard, I. and Chérel, I. (2016) Reduced expression of AtNUP62 nucleoporin gene affects auxin response in Arabidopsis. *BMC Plant Biol.*, **16**, 2.

Bohn, J.A., Etten, J.L. Van, Schagat, T.L., Bowman, B.M., McEachin, R.C., Freddolino, P.L. and Goldstrohm, A.C. (2018) Identification of diverse target RNAs that are functionally regulated by human pumilio proteins. *Nucleic Acids Res.*, **46**, 362–386.

Boller, T. and Felix, G. (2009) A Renaissance of Elicitors: Perception of Microbe-Associated Molecular Patterns and Danger Signals by Pattern-Recognition Receptors. *Annu. Rev. Plant Biol.*, **60**, 379–406.

Boller, T. and He, S.Y. (2009) Innate Immunity in Plants : An Arms Race Between Pattern Recognition Receptors in Plants and Effectors in Microbial Pathogens. *Science*, **324**, 742–743.

Bonardi, V. and Dangl, J.L. (2012) How complex are intracellular immune receptor signaling complexes? *Front. Plant Sci.*, **3**, 237.

Bourne, D.J., Barrow, K.D. and Milborrow, B. V. (1991) Salicyloylaspartate as an endogenous component in the leaves of Phaseolus vulgaris. *Phytochemistry*, **30**, 4041–4044.

Bradford, M.M. (1976) A Rapid and Sensitive Method for the Quantitation of Microgram Quantities of Protein Utilizing the Principle of Protein-Dye Binding. *Anal. Biochem.*, **72**, 248–254.

Brumbarova, T. and Ivanov, R. (2019) The Nutrient Response Transcriptional Regulome of Arabidopsis. *iScience*, **19**, 358–368.

Bruyne, L. De, Höfte, M. and Vleesschauwer, D. De (2014) Connecting growth and defence: The emerging roles of brassinosteroids and gibberellins in plant innate immunity. *Mol. Plant*, **7**, 943–959.

Campos, M.L., Kang, J.-H. and Howe, G.A. (2014) JASMONATE-TRIGGERED PLANT IMMUNITY. *J Chem Ecol.*, **40**, 657–675.

Cao, J., Li, M., Chen, J., Liu, P. and Li, Z. (2016) Effects of MeJA on Arabidopsis metabolome under endogenous JA deficiency. *Sci. Rep.*, **6**.

Caplan, J., Padmanabhan, M. and Dinesh-Kumar, S.P. (2008) Plant NB-LRR Immune Receptors: From Recognition to Transcriptional Reprogramming. *Cell Host Microbe*, **3**, 126–135.

Century, K.S., Shapiro, A.D., Repetti, P.P., Dahlbeck, D., Holub, E. and Staskawicz, B.J. (1997) NDR1, a pathogen-induced component required for Arabidopsis disease resistance. *Science*, **278**, 1963–1965.

Chatterjee, S., Chaudhury, S., McShan, A.C., Kaur, K. and Guzman, R.N. De (2013) Structure and Biophysics of Type III Secretion in Bacteria. *Biochemistry*, **52**, 2508–2517.

Chaudhari, P., Ahmed, B., Joly, D.L. and Germain, H. (2014) Effector biology during biotrophic invasion of plant cells. *Virulence*, **5**, 703–709.

Chen, Y., Shen, H., Wang, M., Li, Q. and He, Z. (2013) Salicyloyl-aspartate synthesized by the acetyl-amido synthetase GH3.5 is a potential activator of plant immunity in Arabidopsis. *Acta Biochim. Biophys. Sin. (Shanghai).*, **45**, 827–836.

Chen, Z., Agnew, J.L., Cohen, J.D., He, P., Shan, L., Sheen, J. and Kunkel, B.N. (2007) Pseudomonas syringae type III effector AvrRpt2 alters Arabidopsis thaliana auxin physiology. *Proc. Natl. Acad. Sci. U. S. A.*, **104**, 20131–20136.

Cheng, H. Lo, Lin, C.T., Huang, K.W., Wang, S., Lin, Y.T., Toh, S.I. and Hsiao, Y.Y. (2018) Structural insights into the duplex DNA processing of TREX2. *Nucleic Acids Res.*, **46**, 12166–12176.

Cheng, Y.T., Germain, H., Wiermer, M., et al. (2009) Nuclear pore complex component MOS7/Nup88 is required for innate immunity and nuclear accumulation of defence regulators in arabidopsis. *Plant Cell*, **21**, 2503–2516.

Cheng, Y.T., Germain, H., Wiermer, M., et al. (2009) Nuclear Pore Complex Component MOS7/Nup88 Is Required for Innate Immunity and Nuclear Accumulation of Defence Regulators in Arabidopsis. *Plant Cell*, **21**, 2503–2516.

Cheng, Z., Zhang, X., Huang, P., et al. (2020) NUP96 and HOS1 are mutually stabilized and gate constans protein level, conferring long-day photoperiodic flowering regulation in Arabidopsis. *Plant Cell*, **32**, 374–391.

Chisholm, S.T., Coaker, G., Day, B. and Staskawicz, B.J. (2006) Host-microbe interactions: Shaping the evolution of the plant immune response. *Cell*, **124**, 803–814.

Christ, B., Schelbert, S., Aubry, S., Süssenbacher, I., Müller, T., Kräutler, B. and Hörtensteiner, S. (2012) MES16, a member of the methylesterase protein family, specifically demethylates fluorescent chlorophyll catabolites during chlorophyll

breakdown in Arabidopsis. *Plant Physiol.*, **158**, 628–641.

Clough, S.J. and Bent, A.F. (1998) Floral dip: A simplified method for Agrobacterium-mediated transformation of Arabidopsis thaliana. *Plant J.*, **16**, 735–743.

Cohen, J.D. and Bandurski, R.S. (1982) Chemistry and Physiology of the Bound Auxins. *Annu. Rev. Plant Physiol.*, **33**, 403–430.

Copeland, C., Xu, S., Qi, Y. and Li, X. (2013) MOS2 has redundant function with its homolog MOS2H and is required for proper splicing of SNC1. *Plant Signal. Behav.*, **8**, e25372.

Cui, H., Tsuda, K. and Parker, J.E. (2015) Effector-triggered immunity: From pathogen perception to robust defence. *Annu. Rev. Plant Biol.*, **66**, 487–511.

D'Auria, J.C., Chen, F., Tholl, D., Ross, J.R., Gershenzon, J., Noel, J.P. and Pichersky, E. (2003) An Arabidopsis thaliana gene for methylsalicylate biosynthesis, identified by a biochemical genomics approach, has a role in defence. *Plant J.*, **36**, 577–588.

Dai, X., Mashiguchi, K., Chen, Q., Kasahara, H., Kamiya, Y., Ojha, S., DuBois, J., Ballou, D. and Zhao, Y. (2013) The biochemical mechanism of auxin biosynthesis by an arabidopsis YUCCA flavin-containing monooxygenase. *J. Biol. Chem.*, **288**, 1448–1457.

Dangl, J.L., Horvath, D.M. and Staskawicz, B.J. (2013) Pivoting the plant immune system from dissection to deployment. *Science*, **341**, 746–51.

DeGrasse, J.A., Dubois, K.N., Devos, D., Siegel, T.N., Sali, A., Field, M.C., Rout, M.P. and Chait, B.T. (2009) Evidence for a shared nuclear pore complex architecture that is conserved from the last common eukaryotic ancestor. *Mol. Cell. Proteomics*, **8**, 2119–2130.

Dempsey, D.A., Vlot, A.C., Wildermuth, M.C. and Klessig, D.F. (2011) Salicylic Acid Biosynthesis and Metabolism. In *The Arabidopsis Book*. pp. 1–24.

Denancé, N., Sánchez-Vallet, A., Goffner, D. and Molina, A. (2013) Disease resistance or growth: The role of plant hormones in balancing immune responses and fitness costs. *Front. Plant Sci.*, **4**, 155.

Devoto, A., Ellis, C., Magusin, A., Chang, H.S., Chilcott, C., Zhu, T. and Turner, J.G. (2005) Expression profiling reveals COI1 to be a key regulator of genes involved in wound- and methyl jasmonate-induced secondary metabolism, defence, and hormone interactions. *Plant Mol. Biol.*, **58**, 497–513.

Dharmasiri, S. and Estelle, M. (2002) The role of regulated protein degradation in auxin response. *Plant Mol. Biol.*, **49**, 401–409.

Ding, P. and Ding, Y. (2020) Stories of Salicylic Acid: A Plant Defence Hormone. *Trends Plant Sci.*, **25**, 549–565.

Dobin, A., Davis, C.A., Schlesinger, F., Drenkow, J., Zaleski, C., Jha, S., Batut, P., Chaisson, M. and Gingeras, T.R. (2013) STAR: Ultrafast universal RNA-seq aligner. *Bioinformatics*, **29**, 15–21.

Dodson, R.E. and Shapiro, D.J. (2002) Regulation of pathways of mRNA destabilization

and stabilization. *Prog. Nucleic Acid Res. Mol. Biol.*, **72**, 129–164.

Does, D. Van der, Leon-Reyes, A., Koornneef, A., et al. (2013) Salicylic acid suppresses jasmonic acid signaling downstream of SCFCOI1-JAZ by targeting GCC promoter motifs via transcription factor ORA59. *Plant Cell*, **25**, 744–761.

Dolata, J., Taube, M., Bajczyk, M., Jarmolowski, A., Szweykowska-Kulinska, Z. and Bielewicz, D. (2018) Regulation of plant microprocessor function in shaping microrna landscape. *Front. Plant Sci.*, **9**, 753.

Dong, C.-H., Hu, X., Tang, W., Zheng, X., Kim, Y.S., Lee, B. and Zhu, J.-K. (2006) A putative Arabidopsis nucleoporin, AtNUP160, is critical for RNA export and required for plant tolerance to cold stress. *Mol. Cell. Biol.*, **26**, 9533–9543.

Dong, O.X., Johnson, K., Li, X. and Zhang, Y. (2011) The mRNA export pathway in plants. *Front. Biol. (Beijing).*, **6**, 246–250.

Doughari, J. (2015) An Overview of Plant Immunity. *J. Plant Pathol. Microbiol.*, **6**, 322.

Durinck, S., Spellman, P.T., Birney, E. and Huber, W. (2009) Mapping Identifiers for the Integration of Genomic Datasets with the R/Bioconductor package biomaRt Steffen. *Nat. Protoc.*, **4**, 1184–1191.

Ehrnsberger, H.F., Grasser, M. and Grasser, K.D. (2019) Nucleocytosolic mRNA transport in plants: Export factors and their influence on growth and development. *J. Exp. Bot.*, **70**, 3757–3763.

Eisenthal, R., Danson, M.J. and Hough, D.W. (2007) Catalytic efficiency and kcat/KM: a useful comparator? *Trends Biotechnol.*, **25**, 247–249.

Erbs, G., Silipo, A., Aslam, S., et al. (2008) Peptidoglycan and Muropeptides from Pathogens Agrobacterium and Xanthomonas Elicit Plant Innate Immunity: Structure and Activity. *Chem. Biol.*, **15**, 438–448.

Escobar, M.A. and Dandekar, A.M. (2003) Agrobacterium tumefaciens as an agent of disease. *Trends Plant Sci.*, **8**, 380–386.

Evans, D.E., Shvedunova, M. and Graumann, K. (2011) The nuclear envelope in the plant cell cycle: Structure, function and regulation. *Ann. Bot.*, **107**, 1111–1118.

Faria, A.M.C., Levay, A., Wang, Y., et al. (2006) The nucleoporin Nup96 is required for proper expression of interferon-regulated proteins and functions. *Immunity*, **24**, 295–304.

Farmer, E.E. and Ryan, C.A. (1990) Interplant communication: Airborne methyl jasmonate induces synthesis of proteinase inhibitors in plant leaves. *Proc. Natl. Acad. Sci. U. S. A.*, **87**, 7713–7716.

Felix, G., Duran, J.D., Volko, S. and Boller, T. (1999) Plants have a sensitive perception system for the most conserved domain of bacterial flagellin. *Plant J.*, **18**, 265–276.

Felsenstein, J. (1985) CONFIDENCE LIMITS ON PHYLOGENIES: AN APPROACH USING THE BOOTSTRAP. *Evolution (N. Y).*, **39**, 783–791.

Ferrández-Ayela, A., Alonso-Peral, M.M., Sánchez-García, A.B., Micol-Ponce, R., Pérez-

Pérez, J.M., Micol, J.L. and Ponce, M.R. (2013) Arabidopsis TRANSCURVATA1 Encodes NUP58, a Component of the Nucleopore Central Channel. *PLoS One*, **8**, e67661.

Fiserova, J., Kiseleva, E. and Goldberg, M.W. (2009) Nuclear envelope and nuclear pore complex structure and organization in tobacco BY-2 cells. *Plant J.*, **59**, 243–255.

Fonseca, S., Chini, A., Hamberg, M., Adie, B., Porzel, A., Kramell, R., Miersch, O., Wasternack, C. and Solano, R. (2009) (+)-7-iso-Jasmonoyl-L-isoleucine is the endogenous bioactive jasmonate. *Nat. Chem. Biol.*, **5**, 344–350.

Forouhar, F., Yang, Y., Kumar, D., et al. (2005) Structural and biochemical studies identify tobacco SABP2 as a methyl salicylate esterase and implicate it in plant innate immunity. *PNAS*, **102**, 1773–1778.

Francischini, C.W. and Quaggio, R.B. (2009) Molecular characterization of Arabidopsis thaliana PUF proteins - Binding specificity and target candidates. *FEBS J.*, **276**, 5456–5470.

Franklin, G., Conceição, L.F.R., Kombrink, E. and Dias, A.C.P. (2008) Hypericum perforatum plant cells reduce Agrobacterium viability during co-cultivation. *Planta*, **227**, 1401–1408.

Friend, K., Campbell, Z.T., Cooke, A., Kroll-Conner, P., Wickens, M.P. and Kimble, J. (2012) A conserved PUF/Ago/eEF1A complex attenuates translation elongation. *Nat Struct Mol Biol.*, **19**, 176–183.

Fu, J. and Wang, S. (2011) Insights into auxin signaling in plant – pathogen interactions. *Front. Plant Sci.*, **2**, 74.

Fu, Z.Q. and Dong, X. (2013) Systemic acquired resistance: Turning local infection into global defence. *Annu. Rev. Plant Biol.*, **64**, 839–863.

Gao, X., Cox, K.L. and He, P. (2014) Functions of calcium-dependent protein kinases in plant innate immunity. *Plants*, **3**, 160–176.

Garneau, N.L., Wilusz, J. and Wilusz, C.J. (2007) The highways and byways of mRNA decay. *Nat. Rev. Mol. Cell Biol.*, **8**, 113–126.

Gelvin, S.B. (2010) Plant proteins involved in Agrobacterium-mediated genetic transformation. *Annu. Rev. Phytopathol.*, **48**, 45–68.

Genenncher, B., Wirthmueller, L., Roth, C., Klenke, M., Ma, L., Sharon, A. and Wiermer, M. (2016) Nucleoporin-regulated MAP kinase signaling in immunity to a necrotrophic fungal pathogen. *Plant Physiol.*, **172**, 1293–1305.

Gerber, A.P., Herschlag, D. and Brown, P.O. (2004) Extensive association of functionally and cytotopically related mRNAs with Puf family RNA-binding proteins in yeast. *PLoS Biol.*, **2**, 0342–0354.

Gerber, A.P., Luschnig, S., Krasnow, M.A., Brown, P.O. and Herschlag, D. (2006) Genome-wide identification of mRNAs associated with the translational regulator PUMILIO in Drosophila melanogaster. *Proc. Natl. Acad. Sci. U. S. A.*, **103**, 4487–4492.

Germain, H., Na, Q., Cheng, Y.T., et al. (2010) MOS11: A new component in the mRNA

export pathway. *PLoS Genet.*, **6**, e1001250.

Ghosh, P. (2004) Process of Protein Transport by the Type III Secretion System. *Microbiol. Mol. Biol. Rev.*, **68**, 771–795.

Gimenez-Ibanez, S., Boter, M., Fernández-Barbero, G., Chini, A., Rathjen, J.P. and Solano, R. (2014) The Bacterial Effector HopX1 Targets JAZ Transcriptional Repressors to Activate Jasmonate Signaling and Promote Infection in Arabidopsis. *PLoS Biol.*, **12**, 1–15.

Glazebrook, J. (2005) Contrasting Mechanisms of Defence Against Biotrophic and Necrotrophic Pathogens. *Annu. Rev. Phytopathol.*, **43**, 205–227.

Glisovic, T., Bachorik, J.L., Yong, J. and Dreyfuss, G. (2008) RNA-binding proteins and post-transcriptional gene regulation. *FEBS Lett.*, **582**, 1977–1986.

Gohlke, J. and Deeken, R. (2014) Plant responses to Agrobacterium tumefaciens and crown gall development. *Front. Plant Sci.*, **5**, 155.

Goldfarb, D.S., Corbett, A.H., Mason, D.A., Harreman, M.T. and Adam, S.A. (2004) Importin α: a multipurpose nuclear-transport receptor. *Trends Cell Biol.*, **14**, 505–514.

Goldstrohm, A.C., Hook, B.A., Seay, D.J. and Wickens, M. (2006) PUF proteins bind Pop2p to regulate messenger RNAs. *Nat. Struct. Mol. Biol.*, **13**, 533–539.

Goldstrohm, A.C. and Wickens, M. (2008) Multifunctional deadenylase complexes diversify mRNA control. *Nat. Rev. Mol. Cell Biol.*, **9**, 337–344.

Gómez-Gómez, L. and Boller, T. (2002) Flagellin perception: A paradigm for innate immunity. *Trends Plant Sci.*, **7**, 251–256.

Gong, Z., Dong, C.H., Lee, H., Zhu, J., Xiong, L., Gong, D., Stevenson, B. and Zhu, J.K. (2005) A DEAD box RNA helicase is essential for mRNA export and important for development and stress responses in Arabidopsis. *Plant Cell*, **17**, 256–267.

Goritschnig, S., Zhang, Y. and Li, X. (2007) The ubiquitin pathway is required for innate immunity in Arabidopsis. *Plant J.*, **49**, 540–551.

Görlich, D., Prehn, S., Laskey, R.A. and Hartmann, E. (1994) Isolation of a protein that is essential for the first step of nuclear protein import. *Cell*, **79**, 767–778.

Grant, M.R., Laurence, G., Straube, E., Ashfield, T., Lewald, J., Sattler, A., Innes, R.W. and Dangl, J.L. (1995) Structure of the Arabidopsis RPM1 Gene Enabling Dual Specificity Disease Resistance. *Science*, **269**, 843–846.

Gray, W.M. and Estelle, M. (2000) Function of the ubiquitin-proteasome pathway in auxin response. *Trends Biochem. Sci.*, **25**, 133–138.

Grossman, E., Medalia, O. and Zwerger, M. (2012) Functional Architecture of the Nuclear Pore Complex. *Annu. Rev. Biophys.*, **41**, 557–584.

Groth, M., Takeda, N., Perry, J., et al. (2010) NENA, a Lotus japonicus homolog of Sec13, is required for rhizodermal infection by arbuscular mycorrhiza fungi and rhizobia but dispensable for cortical endosymbiotic development. *Plant Cell*, **22**, 2509–2526.

Gu, Y., Zebell, S.G., Liang, Z., Wang, S., Kang, B. and Dong, X. (2016) Nuclear Pore

Permeabilization Is a Convergent Signaling Event in Effector-Triggered Immunity. *Cell*, **166**, 1526–1538.

Guzik, B.W., Levesque, L., Prasad, S., Bor, Y.-C., Black, B.E., Paschal, B.M., Rekosh, D. and Hammarskjöld, M.-L. (2001) NXT1 (p15) Is a Crucial Cellular Cofactor in TAP-Dependent Export of Intron-Containing RNA in Mammalian Cells. *Mol. Cell. Biol.*, **21**, 2545–2554.

Haasen, D., Köhler, C., Neuhaus, G. and Merkle, T. (1999) Nuclear export of proteins in plants: AtXPO1 is the export receptor for leucine-rich nuclear export signals in Arabidopsis thaliana. *Plant J.*, **20**, 695–705.

Halkier, B.A. and Gershenzon, J. (2006) Biology and biochemistry of glucosinolates. *Annu. Rev. Plant Biol.*, **57**, 303–333.

Harel, A., Orjalo, A. V., Vincent, T., Lachish-Zalait, A., Vasu, S., Shah, S., Zimmerman, E., Elbaum, M. and Forbes, D.J. (2003) Removal of a single pore subcomplex results in vertebrate nuclei devoid of nuclear pores. *Mol. Cell*, **11**, 853–864.

Heath, C.G., Viphakone, N. and Wilson, S.A. (2016) The role of TREX in gene expression and disease. *Biochem. J.*, **473**, 2911–2935.

Heil, M. and Ton, J. (2008) Long-distance signalling in plant defence. *Trends Plant Sci.*, **13**, 264–272.

Hellens, R.P., Edwards, E.A., Leyland, N.R., Bean, S. and Mullineaux, P.M. (2000) Biotechnology resources for arable crop transformation (bract)\npGreen: a versatile and flexible binary Ti vector for Agrobacterium-mediated plant transformation. *Plant Mol Biol*, **42**, 819–832.

Herrfurth, C. and Feussner, I. (2020) Quantitative Jasmonate Profiling Using a High-Throughput UPLC-NanoESI-MS/MS Method. *Methods Mol. Biol.*, **2085**, 169—187.

Hino, T., Tanaka, Y., Kawamukai, M., Nishimura, K., Mano, S. and Nakagawa, T. (2011) Two Sec13p homologs, AtSec13A and AtSec13B, redundantly contribute to the formation of COPII transport vesicles in arabidopsis thaliana. *Biosci. Biotechnol. Biochem.*, **75**, 1848–1852.

Hinsch, M. and Staskawicz, B. (1996) Identification of a new Arabidopsis disease resistance locus, RPS4, and cloning of the corresponding avirulence gene, avrRps4, from Pseudomonas syringae pv. pisi. *Mol. Plant-Microbe Interact.*, **9**, 55–61.

Hocine, S., Singer, R.H. and Grünwald, D. (2010) RNA processing and export. *Cold Spring Harb. Perspect. Biol.*, **2**, a000752.

Houston, K., Tucker, M.R., Chowdhury, J., Shirley, N. and Little, A. (2016) The plant cell wall: A complex and dynamic structure as revealed by the responses of genes under stress conditions. *Front. Plant Sci.*, **7**, 984.

Hulsen, T., Vlieg, J. De and Alkema, W. (2008) BioVenn – a web application for the comparison and visualization of biological lists using area-proportional Venn diagrams. *BMC Genomics*, **9**, 488.

Huot, B., Yao, J., Montgomery, B.L. and He, S.Y. (2014) Growth-defence tradeoffs in plants: A balancing act to optimize fitness. *Mol. Plant*, **7**, 1267–1287.

Hwang, H.-H., Yu, M. and Lai, E.-M. (2017) Agrobacterium -Mediated Plant Transformation: Biology and Applications. In *The Arabidopsis Book*. pp. 1–31.

Inoue, H., Nojima, H. and Okayama, H. (1990) High efficiency transformation of Escherichia coli with plasmids. *Gene*, **96**, 23–28.

Ishitani, M., Xiong, L., Lee, H., Stevenson, B. and Zhu, J.K. (1998) HOS1, a genetic locus involved in cold-responsive gene expression in arabidopsis. *Plant Cell*, **10**, 1151–1161.

Izaurralde, E., Kutay, U., Kobbe, C. Von, Mattaj, L.W. and Görlich, D. (1997) The asymmetric distribution of the constituents of the Ran system is essential for transport into and out of the nucleus. *EMBO J.*, **16**, 6535–6547.

Jacob, F., Vernaldi, S. and Maekawa, T. (2013) Evolution and conservation of plant NLR functions. *Front. Immunol.*, **4**, 297-312.

Jacob, Y., Mongkolsiriwatana, C., Veley, K.M., Sang, Y.K. and Michaels, S.D. (2007) The nuclear pore protein AtTPR is required for rna homeostasis, flowering time, and auxin signaling. *Plant Physiol.*, **144**, 1383–1390.

Jinek, M., Scott, C.M. and Doudna, J.A. (2011) Coupled 5′ nucleotide recognition and processivity in Xrn1- mediated mRNA decay. *Mol Cell.*, **41**, 600–608.

Jones, C.I., Zabolotskaya, M.V. and Newbury, S.F. (2012) The 5′ → 3′ exoribonuclease XRN1/Pacman and its functions in cellular processes and development. *Wiley Interdiscip. Rev. RNA*, **3**, 455–468.

Jones, J. and Dangl, J. (2006) The plant immune system. *Nature*, **444**, 323–329.

Jung, J.H., Park, J.H., Lee, S., To, T.K., Kim, J.M., Seki, M. and Park, C.M. (2013) The cold signaling attenuator HIGH EXPRESSION OF OSMOTICALLY RESPONSIVE GENE1 activates FLOWERING LOCUS C transcription via chromatin remodeling under short-term cold stress in Arabidopsis. *Plant Cell*, **25**, 4378–4390.

Kadota, Y., Shirasu, K. and Zipfel, C. (2015) Regulation of the NADPH Oxidase RBOHD During Plant Immunity. *Plant Cell Physiol.*, **56**, 1472–1480.

Kalverda, B., Pickersgill, H., Shloma, V. V. and Fornerod, M. (2010) Nucleoporins Directly Stimulate Expression of Developmental and Cell-Cycle Genes Inside the Nucleoplasm. *Cell*, **140**, 360–371.

Kammel, C., Thomaier, M., Sørensen, B.B., Schubert, T., Längst, G., Grasser, M. and Grasser, K.D. (2013) Arabidopsis DEAD-Box RNA Helicase UAP56 Interacts with Both RNA and DNA as well as with mRNA Export Factors. *PLoS One*, **8**, 1–12.

Kärkönen, A. and Kuchitsu, K. (2015) Reactive oxygen species in cell wall metabolism and development in plants. *Phytochemistry*, **112**, 22–32.

Katahira, J. (2012) MRNA export and the TREX complex. *Biochim. Biophys. Acta - Gene Regul. Mech.*, **1819**, 507–513.

Katahira, J. (2015) Nuclear export of messenger RNA. *Genes (Basel)*, **6**, 163–184.

Katahira, J., Sträßer, K., Podtelejnikov, A., Mann, M., Jung, J.U. and Hurt, E. (1999) The Mex67p-mediated nuclear mRNA export pathway is conserved from yeast to human.

EMBO J., **18**, 2593–2609.

Kearse, M., Moir, R., Wilson, A., et al. (2012) Geneious Basic: An integrated and extendable desktop software platform for the organization and analysis of sequence data. *Bioinformatics*, **28**, 1647–1649.

Keene, J.D. (2007) RNA regulons: Coordination of post-transcriptional events. *Nat. Rev. Genet.*, **8**, 533–543.

Kentaro Tamura and Ikuko Hara-Nishimura (2013) The molecular architecture of the plant nuclear pore complex. *J. Exp. Bot.*, **64**, 823–832.

Kim, J.-G., Stork, W. and Mudgett, M.B. (2013) Xanthomonas Type III Effector XopD Desumoylates Tomato Transcription Factor SlERF4 to Suppress Ethylene Responses and Promote Pathogen Growth. *Cell Host Microbe*, **13**, 143–154.

Kimura, M. and Imamoto, N. (2014) Biological Significance of the Importin-β Family-Dependent Nucleocytoplasmic Transport Pathways. *Traffic*, **15**, 727–748.

Kimura, S., Waszczak, C., Hunter, K. and Wrzaczek, M. (2017) Bound by fate: The role of reactive oxygen species in receptor-like kinase signaling. *Plant Cell*, **29**, 638–654.

Kinoshita, A. and Richter, R. (2020) Genetic and molecular basis of floral induction in Arabidopsis thaliana. *J. Exp. Bot.*, **71**, 2490–2504.

Kleinboelting, N., Huep, G., Kloetgen, A., Viehoever, P. and Weisshaar, B. (2012) GABI-Kat SimpleSearch: New features of the Arabidopsis thaliana T-DNA mutant database. *Nucleic Acids Res.*, **40**, 1211–1215.

Knepper, C., Savory, E.A. and Day, B. (2011) Arabidopsis NDR1 is an integrin-like protein with a role in fluid loss and plasma membrane-cell wall adhesion. *Plant Physiol.*, **156**, 286–300.

Knockenhauer, K.E. and Schwartz, T.U. (2016) The Nuclear Pore Complex as a Flexible and Dynamic Gate. *Cell*, **164**, 1162–1171.

Köhler, A. and Hurt, E. (2007) Exporting RNA from the nucleus to the cytoplasm. *Nat. Rev. Mol. Cell Biol.*, **8**, 761–773.

Koncz, C. and Schell, J. (1986) The promoter of TL-DNA gene 5 controls the tissue-specific expression of chimaeric genes carried by a novel type of Agrobacterium binary vector. *MGG Mol. Gen. Genet.*, **204**, 383–396.

Koo, Y.J., Kim, M.A., Kim, E.H., et al. (2007) Overexpression of salicylic acid carboxyl methyltransferase reduces salicylic acid-mediated pathogen resistance in Arabidopsis thaliana. *Plant Mol. Biol.*, **64**, 1–15.

Korasick, D.A., Enders, T.A. and Strader, L.C. (2013) Auxin biosynthesis and storage forms. *J. Exp. Bot.*, **64**, 2541–2555.

Kumar, D. and Klessig, D.F. (2003) High-affinity salicylic acid-binding protein 2 is required for plant innate immunity and has salicylic acid-stimulated lipase activity. *Proc. Natl. Acad. Sci. U. S. A.*, **100**, 16101–16106.

Kumar, S., Stecher, G., Li, M., Knyaz, C. and Tamura, K. (2018) MEGA X: Molecular

evolutionary genetics analysis across computing platforms. *Mol. Biol. Evol.*, **35**, 1547–1549.

Kunkel, B.N. and Harper, C.P. (2018) The roles of auxin during interactions between bacterial plant pathogens and their hosts. *J. Exp. Bot.*, **69**, 245–254.

Kunze, G., Zipfel, C., Robatzek, S., Niehaus, K., Boller, T. and Felix, G. (2004) The N Terminus of Bacterial Elongation Factor Tu Elicits Innate Immunity in Arabidopsis Plants. *Plant Cell*, **16**, 3496–3507.

Kupski, O. (2016) *Structure, Mechanism and Inhibition of the human Glutaminyl Cyclase*.

Kus, J. V., Zaton, K., Sarkar, R. and Cameron, R.K. (2002) Age-related resistance in Arabidopsis is a developmentally regulated defence response to Pseudomonas syringae. *Plant Cell*, **14**, 479–490.

Łabno, A., Tomecki, R. and Dziembowski, A. (2016) Cytoplasmic RNA decay pathways - Enzymes and mechanisms. *Biochim. Biophys. Acta - Mol. Cell Res.*, **1863**, 3125–3147.

Laflamme, B., Dillon, M.M., Martel, A., Almeida, R.N.D., Desveaux, D. and Guttman, D.S. (2020) The pan-genome effector-triggered immunity landscape of a host-pathogen interaction. *Science*, **367**, 763–768.

Lazaro, A., Valverde, F., Piñeiro, M. and Jarillo, J.A. (2012) The Arabidopsis E3 ubiquitin ligase HOS1 negatively regulates CONSTANS abundance in the photoperiodic control of flowering. *Plant Cell*, **24**, 982–999.

Lee, H.S., Lee, D.H., Cho, H.K., Kim, S.H., Auh, J.H. and Pai, H.S. (2015) InsP6-sensitive variants of the Gle1 mRNA export factor rescue growth and fertility defects of the ipk1 low-phytic-acid mutation in Arabidopsis. *Plant Cell*, **27**, 417–431.

Lee, L.Y., Fang, M.J., Kuang, L.Y. and Gelvin, S.B. (2008) Vectors for multi-color bimolecular fluorescence complementation to investigate protein-protein interactions in living plant cells. *Plant Methods*, **4**, 24.

Lee, S., Kopp, F., Chang, T.-C., Sataluri, A., Beibei, C., Sivakumar, S., Yu, H., Xie, Y. and Mendell, J.T. (2016) Noncoding RNA NORAD regulates genomic stability by sequestering PUMILIO proteins. *Cell*, **164**, 69–80.

Leksa, N.C. and Schwartz, T.U. (2010) Membrane-coating lattice scaffolds in the nuclear pore and vesicle coats. *Nucleus*, **1**, 314–318.

Leone, M.J. de, Hernando, C.E., Romanowski, A., et al. (2020) Bacterial Infection Disrupts Clock Gene Expression to Attenuate Immune Responses. *Curr. Biol.*, **30**, 1740–1747.

Li, C., Liu, L., Teo, Z.W.N., Shen, L. and Yu, H. (2020) Nucleoporin 160 Regulates Flowering through Anchoring HOS1 for Destabilizing CO in Arabidopsis. *Plant Commun.*, **1**, 100033,.

Li, J.F., Park, E., Arnim, A.G. Von and Nebenführ, A. (2009) The FAST technique: A simplified Agrobacterium-based transformation method for transient gene expression analysis in seedlings of Arabidopsis and other plant species. *Plant Methods*, **5**, 6.

Li, L., Hou, X., Tsuge, T., Ding, M., Aoyama, T., Oka, A., Gu, H., Zhao, Y. and Qu, L.J.

(2008) The possible action mechanisms of indole-3-acetic acid methyl ester in Arabidopsis. *Plant Cell Rep.*, **27**, 575–584.

Li, L., Yu, Y., Zhou, Z. and Zhou, J. (2016) Plant pattern-recognition receptors controlling innate immunity. *Sci. China Life Sci.*, **59**, 878–888.

Li, X., Clarke, J.D., Zhang, Y. and Dong, X. (2001) Activation of an EDS1-mediated R-gene pathway in the snc1 mutant leads to constitutive, NPR1-independent pathogen resistance. *Mol. Plant-Microbe Interact.*, **14**, 1131–1139.

Li, Y., Dong, O.X., Johnson, K., Li-Sup, X. and Zhang, Y. (2011) MOS1 epigenetically regulates the expression of plant Resistance gene SNC1. *Plant Signal. Behav.*, **6**, 434–436.

Li, Y. and Kiledjian, M. (2010) Regulation of mRNA decapping. *Wiley Interdiscip. Rev. RNA*, **1**, 253–265.

Liao, Y., Smyth, G.K. and Shi, W. (2013) The Subread aligner: Fast, accurate and scalable read mapping by seed-and-vote. *Nucleic Acids Res.*, **41**, e108.

Lima Silva, C.C. de, Shimo, H.M., Felício, R. De, Mercaldi, G.F., Rocco, S.A. and Benedetti, C.E. (2019) Structure-function relationship of a citrus salicylate methylesterase and role of salicylic acid in citrus canker resistance. *Sci. Rep.*, **9**, 3901.

Litman, G.W., Rast, J.P. and Fugmann, S.D. (2010) The origins of vertebrate adaptive immunity. *Nat Rev Immunol.*, **10**, 543–553.

Liu, P.-P., Dahl, C.C. von and Klessig, D.F. (2011a) The extent to which methyl salicylate is required for signaling systemic acquired resistance is dependent on exposure to light after infection. *Plant Physiol.*, **157**, 2216–2226.

Liu, P.-P., Dahl, C.C. von, Park, S.W. and Klessig, D.F. (2011b) Interconnection between methyl salicylate and lipid-based long-distance signaling during the development of systemic acquired resistance in Arabidopsis and Tobacco. *Plant Physiol.*, **155**, 1762–1768.

Liu, P.P., Yang, Y., Pichersky, E. and Klessig, D.F. (2010) Altering expression of benzoic acid/salicylic acid carboxyl methyltransferase 1 compromises systemic acquired resistance and PAMP-triggered immunity in Arabidopsis. *Mol. Plant-Microbe Interact.*, **23**, 82–90.

Ljung, K. (2013) Auxin metabolism and homeostasis during plant development.

Development, **140**, 943–950.

Ljung, K., Hull, A.K., Kowalczyk, M., Marchant, A., Celenza, J., Cohen, J.D. and Sandberg, G. (2002) Biosynthesis, conjugation, catabolism and homeostasis of indole-3-acetic acid in Arabidopsis thaliana. *Plant Mol. Biol.*, **49**, 249–272.

Loïodice, I., Alves, A., Rabut, G., Overbeek, M. van, Ellenberg, J., Sibarita, J.-B. and Doye, V. (2004) The Entire Nup107-160 Complex, Including Three New Members, Is Targeted as One Entity to Kinetochores in Mitosis. *Mol. Biol. Cell*, **15**, 3333–3344.

Lorković, Z.J. (2009) Role of plant RNA-binding proteins in development, stress response and genome organization. *Trends Plant Sci.*, **14**, 229–236.

Lott, K. and Cingolani, G. (2011) The importin β binding domain as a master regulator of nucleocytoplasmic transport. *Biochim. Biophys. Acta - Mol. Cell Res.*, **1813**, 1578–1592.

Love, M.I., Huber, W. and Anders, S. (2014) Moderated estimation of fold change and dispersion for RNA-seq data with DESeq2. *Genome Biol.*, **15**, 550.

Lozano-Durán, R. and Zipfel, C. (2015) Trade-off between growth and immunity: Role of brassinosteroids. *Trends Plant Sci.*, **20**, 12–19.

Lu, Q., Tang, X., Tian, G., et al. (2010) Arabidopsis homolog of the yeast TREX-2 mRNA export complex: Components and anchoring nucleoporin. *Plant J.*, **61**, 259–270.

Lüdke, D. (2014) *Investigating the role of Arabidopsis Nup96 and Nup160 in defence gene expression against Agrobacterium-mediated transformation*.

Lüdke, D., Roth, C., Hartken, D. and Wiermer, M. (2018) MOS6 and TN13 in plant immunity. *Plant Signal. Behav.*, **13**, 72–75.

Lüdke, D., Roth, C., Kamrad, S.A., et al. (2020) Functional requirement of the Arabidopsis importin-α nuclear transport receptor family in autoimmunity mediated by the NLR protein SNC1. *bioRxiv*.

Ludwig-Müller, J. (2011) Auxin conjugates: Their role for plant development and in the evolution of land plants. *J. Exp. Bot.*, **62**, 1757–1773.

Lund, M.K. and Guthrie, C. (2005) The DEAD-box protein Dbp5p is required to dissociate Mex67p from exported mRNPs at the nuclear rim. *Mol. Cell*, **20**, 645–651.

Luo, Y., Wang, Z., Ji, H., Fang, H., Wang, S., Tian, L. and Li, X. (2013) An Arabidopsis homolog of importin β1 is required for ABA response and drought tolerance. *Plant J.*, **75**, 377–389.

Ma, L., Hong, Æ.Z. and Zhang, Æ.Z. (2007) Perinuclear and nuclear envelope localizations of Arabidopsis Ran proteins. *Plant Cell Rep*., **26**, 1373–1382.

Ma, W., Wang, Y. and McDowell, J. (2018) Focus on effector-triggered susceptibility. *Mol. Plant-Microbe Interact.*, **31**, 5.

MacGregor, D.R., Gould, P., Foreman, J., et al. (2013) HIGH EXPRESSION OF OSMOTICALLY RESPONSIVE GENES1 is required for circadian periodicity through the promotion of nucleo-cytoplasmic mRNA export in Arabidopsis. *Plant Cell*, **25**, 4391–4404.

MacGregor, D.R. and Penfield, S. (2015) Exploring the pleiotropy of hos1. *J. Exp. Bot.*, **66**, 1661–1671.

Mackey, D., Holt, B.F., Wiig, A. and Dangl, J.L. (2002) RIN4 interacts with Pseudomonas syringae type III effector molecules and is required for RPM1-mediated resistance in Arabidopsis. *Cell*, **108**, 743–754.

Marion, J., Bach, L., Bellec, Y., Meyer, C., Gissot, L. and Faure, J.D. (2008) Systematic analysis of protein subcellular localization and interaction using high-throughput transient transformation of Arabidopsis seedlings. *Plant J.*, **56**, 169–179.

Maya Capelson, Liang, Y., Schulte, R., Mair, W., Wagner, U. and Hetzer, M.W. (2010) Chromatin-bound nuclear pore components regulate gene expression in higher eukaryotes. *Cell*, **140**, 372.

McClerklin, S.A., Lee, S.G., Harper, C.P., Nwumeh, R., Jez, J.M. and Kunkel, B.N. (2018) Indole-3-acetaldehyde dehydrogenase-dependent auxin synthesis contributes to virulence of Pseudomonas syringae strain DC3000. *PLoS Pathog.*, **14**, e1006811.

McDowell, J.M. (2013) Genomic and transcriptomic insights into lifestyle transitions of a hemi-biotrophic fungal pathogen. *New Phytol.*, **197**, 1032–1034.

Meier, I. (2007) Composition of the plant nuclear envelope: Theme and variations. *J. Exp. Bot.*, **58**, 27–34.

Meier, I., Richards, E.J. and Evans, D.E. (2017) Cell Biology of the Plant Nucleus. *Annu. Rev. Plant Biol.*, **68**, 139–172.

Melotto, M., Underwood, W., He, S.Y. and Staub, T. (2008) Role of Stomata in Plant Innate Immunity and Foliar Bacterial Diseases. *Annu Rev Phytopathol.*, **46**, 101–122.

Meng, X. and Zhang, S. (2013) MAPK Cascades in Plant Disease Resistance Signaling. *Annu. Rev. Phytopathol.*, **51**, 245–266.

Menon, B.B., Sarma, N.J., Pasula, S., Deminoff, S.J., Willis, K.A., Barbara, K.E., Andrews, B. and Santangelo, G.M. (2005) Reverse recruitment: the Nup84 nuclear pore subcomplex mediates Rap1/Gcr1/Gcr2 transcriptional activation. *Proc. Natl. Acad. Sci. U. S. A.*, **102**, 5749–54.

Merkle, T. (2011) Nucleo-cytoplasmic transport of proteins and RNA in plants. *Plant Cell Rep*., **30**, 153–176.

Miles, W.O., Tschöp, K., Herr, A., Ji, J.Y. and Dyson, N.J. (2012) Pumilio facilitates miRNA regulation of the E2F3 oncogene. *Genes Dev.*, **26**, 356–368.

Mitchell, S.F. and Parker, R. (2014) Principles and Properties of Eukaryotic mRNPs. *Mol. Cell*, **54**, 547–558.

Miya, A., Albert, P., Shinya, T., et al. (2007) CERK1, a LysM receptor kinase, is essential for chitin elicitor signaling in Arabidopsis. *Proc. Natl. Acad. Sci. U. S. A.*, **104**, 19613–19618.

Monaghan, J. and Zipfel, C. (2012) Plant pattern recognition receptor complexes at the plasma membrane. *Curr. Opin. Plant Biol.*, **15**, 349–357.

Moon, J., Parry, G. and Estelle, M. (2004) The ubiquitin-proteasome pathway and plant development. *Plant Cell*, **16**, 3181–3195.

Mortazavi, A., Williams, B.A., McCue, K., Schaeffer, L. and Wold, B. (2008) Mapping and quantifying mammalian transcriptomes by RNA-Seq. *Nat. Methods*, **5**, 621–628.

Müller-Mcnicoll, M. and Neugebauer, K.M. (2013) How cells get the message: Dynamic assembly and function of mRNA-protein complexes. *Nat. Rev. Genet.*, **14**, 275–287.

Müller, M.M. (2018) Post-Translational Modifications of Protein Backbones: Unique Functions, Mechanisms, and Challenges. *Biochemistry*, **57**, 177–185.

Muthuswamy, S. and Meier, I. (2011) Genetic and environmental changes in SUMO homeostasis lead to nuclear mRNA retention in plants. *Planta*, **233**, 201–208.

Mutka, A.M., Fawley, S., Tsao, T., Kunkel, B.N. and Louis, S. (2013) Auxin promotes susceptibility to Pseudomonas syringae via a mechanism independent of suppression of salicylic acid-mediated defences. *Plant J.*, **74**, 746–754.

Nagai, S., Dubrana, K., Tsai-Pflugfelder, M., et al. (2008) Functional Targeting of DNA Damage to a Nuclear Pore–Associated SUMO-Dependent Ubiquitin Ligase. *Science*, **322**, 597–602.

Nagarajan, V.K., Jones, C.I., Newbury, S.F. and Green, P.J. (2013) XRN 5'→3' exoribonucleases: Structure, mechanisms and functions. *Biochim. Biophys. Acta*, **1829**, 590–603.

Nam, J., Matthysse, A.G. and Gelvin, S.B. (1997) Differences in susceptibility of arabidopsis ecotypes to crown gall disease may result from a deficiency in T-DNA integration. *Plant Cell*, **9**, 317–333.

Naseem, M., Kaltdorf, M. and Dandekar, T. (2015) The nexus between growth and defence signalling : auxin and cytokinin modulate plant immune response pathways. *J. Exp. Bot.*, **66**, 4885–4896.

Navarro, L., Patrice Dunoyer, Jay, F., Arnold, B., Dharmasiri, N., Estelle, M., Voinnet, O. and Jones, J.D.G. (2016) A Plant miRNA Contributes to Antibacteril Resistance by Repressing Auxin Signaling. *Science*, **312**, 436–439.

Nawrath, C. (2002) The Biopolymers Cutin and Suberin. In *The Arabidopsis Book*. pp. 1–14.

Ndunguru, J., Taylor, N.J., Yadav, J., Aly, H., Legg, J.P., Aveling, T., Thompson, G. and Fauquet, C.M. (2005) Application of FTA technology for sampling, recovery and molecular characterization of viral pathogens and virus-derived transgenes from plant tissues. *Virol. J.*, **2**, 45.

Nekrasov, V., Li, J., Batoux, M., et al. (2009) Control of the pattern-recognition receptor EFR by an ER protein complex in plant immunity. *EMBO J.*, **28**, 3428–3438.

Neumann, N., Lundin, D. and Poole, A.M. (2010) Comparative genomic evidence for a complete nuclear pore complex in the last eukaryotic common ancestor. *PLoS One*, **5**, e13241.

Nürnberger, T., Brunner, F., Kemmerling, B. and Piater, L. (2004) Innate immunity in plants and animals: Striking similarities and obvious differences. *Immunol. Rev.*, **198**, 249–266.

Nyikó, T., Auber, A. and Bucher, E. (2019) Functional and molecular characterization of the conserved Arabidopsis PUMILIO protein, APUM9. *Plant Mol. Biol.*, **100**, 199–214.

O'Donnell, P.J., Schmelz, E.A., Moussatche, P., Lund, S.T., Jones, J.B. and Klee, H.J. (2003) Susceptible to intolerance - A range of hormonal actions in a susceptible Arabidopsis pathogen response. *Plant J.*, **33**, 245–257.

O'Rourke, J.A., McCabe, C.E. and Graham, M.A. (2020) Dynamic gene expression changes in response to micronutrient, macronutrient, and multiple stress exposures in soybean. *Funct. Integr. Genomics*, **20**, 321–341.

Ohtsu, M., Shibata, Y., Ojika, M., Tamura, K., Hara-Nishimura, I., Mori, H., Kawakita, K. and Takemoto, D. (2014) Nucleoporin 75 is involved in the ethylene-mediated production of phytoalexin for the resistance of Nicotiana benthamiana to Phytophthora infestans. *Mol. Plant-Microbe Interact.*, **27**, 1318–1330.

Östin, A., Kowalyczk, M., Bhalerao, R.P. and Sandberg, G. (1998) Metabolism of indole-3-acetic acid in arabidopsis. *Plant Physiol.*, **118**, 285–296.

Palma, K., Zhang, Y. and Li, X. (2005) An importin α homolog, MOS6, plays an important role in plant innate immunity. *Curr. Biol.*, **15**, 1129–1135.

Palma, K., Zhao, Q., Yu, T.C., Bi, D., Monaghan, J., Cheng, W., Zhang, Y. and Li, X. (2007) Regulation of plant innate immunity by three proteins in a complex conserved across the plant and animal kingdoms. *Genes Dev.*, **21**, 1484–1493.

Pandey, D., Rajendran, S.R.C.K., Gaur, M., Sajeesh, P.K. and Kumar, A. (2016) Plant Defence Signaling and Responses Against Necrotrophic Fungal Pathogens. *J. Plant Growth Regul.*, **35**, 1159–1174.

Park, S., Liu, P., Forouhar, F., Vlot, A.C., Tong, L., Tietjen, K. and Klessig, D.F. (2009) Use of a Synthetic Salicylic Acid Analog to Investigate the Roles of Methyl Salicylate and Its Esterases in Plant Disease Resistance. *Journal of Biological Chemistry*, **284**, 7307–7317.

Park, S.W., Kaimoyo, E., Kumar, D., Mosher, S. and Klessig, D.F. (2007) Methyl salicylate is a critical mobile signal for plant systemic acquired resistance. *Science*, **318**, 113–116.

Parker, R. and Song, H. (2004) The enzymes and control of eukaryotic mRNA turnover. *Nat. Struct. Mol. Biol.*, **11**, 121–127.

Parry, G. (2014) Components of the Arabidopsis nuclear pore complex play multiple diverse roles in control of plant growth. *J. Exp. Bot.*, **65**, 6057–6067.

Parry, G. (2015) The plant nuclear envelope and regulation of gene expression. *J. Exp. Bot.*, **66**, 1673–1685.

Parry, G., Ward, S., Cernac, A., Dharmasiri, S. and Estelle, M. (2006) The Arabidopsis suppressor of auxin resistance proteins are nucleoporins with an important role in hormone signaling and development. *Plant Cell*, **18**, 1590–1603.

Pereira, A.L.A., Carazzolle, M.F., Abe, V.Y., Oliveira, M.L.P. de, Domingues, M.N., Silva, J.C., Cernadas, R.A. and Benedetti, C.E. (2014) Identification of putative TAL effector targets of the citrus canker pathogens shows functional convergence underlying disease development and defence response. *BMC Genomics*, **15**, 157– 172.

Petutschnig, E.K., Jones, A.M.E., Serazetdinova, L., Lipka, U. and Lipka, V. (2010) The Lysin Motif Receptor-like Kinase (LysM-RLK) CERK1 Is a Major Chitin-binding Protein in Arabidopsis thaliana and Subject to Chitin-induced Phosphorylation. *J. Biol. Chem.*, **285**, 28902–28911.

Pfab, A., Bruckmann, A., Nazet, J., Merkl, R. and Grasser, K.D. (2018) The Adaptor Protein ENY2 Is a Component of the Deubiquitination Module of the Arabidopsis SAGA Transcriptional Co-activator Complex but not of the TREX-2 Complex. *J. Mol. Biol.*, **430**, 1479–1494.

Pieterse, C.M.J., Does, D. Van Der, Zamioudis, C., Leon-Reyes, A. and Wees, S.C.M. Van (2012) Hormonal modulation of plant immunity. *Annu. Rev. Cell Dev. Biol.*, **28**, 489–521.

Pietzenuk, B., Markus, C., Gaubert, H., Bagwan, N., Merotto, A., Bucher, E. and Pecinka, A. (2016) Recurrent evolution of heat-responsiveness in Brassicaceae COPIA elements. *Genome Biol.*, **17**, 209.

Platani, M., Santarella-Mellwig, R., Posch, M., Walczak, R., Swedlow, J.R. and Mattaj, I.W. (2009) The Nup107-160 Nucleoporin Complex Promotes Mitotic Events via Control of the Localization State of the Chromosome Passenger Complex. *Mol. Biol. Cell*, **20**, 5260–5275.

Pozo, J.C. Del, Dharmasiri, S., Hellmann, H., Walker, L., Gray, W.M. and Estelle, M. (2002) AXR1-ECR1-dependent conjugation of RUB1 to the Arabidopsis cullin AtCUL1 is required for auxin response. *Plant Cell*, **14**, 421–433.

Pozo, J.C. Del, Timpte, C., Tan, S., Callis, J. and Estelle, M. (1998) The ubiquitin-related protein RUB1 and auxin response in Arabidopsis. *Science*, **280**, 1760–1763.

Qin, G., Gu, H., Zhao, Y., et al. (2005) An indole-3-acetic acid carboxyl methyltransferase regulates Arabidopsis leaf development. *Plant Cell*, **17**, 2693–2704.

Quenault, T., Lithgow, T. and Traven, A. (2011) PUF proteins: Repression, activation and mRNA localization. *Trends Cell Biol.*, **21**, 104–112.

Raices, M. and D'Angelo, M.A. (2012) Nuclear pore complex composition: A new regulator of tissue-specific and developmental functions. *Nat. Rev. Mol. Cell Biol.*, **13**, 687–699.

Ranf, S., Eschen-Lippold, L., Pecher, P., Lee, J. and Scheel, D. (2011) Interplay between calcium signalling and early signalling elements during defence responses to microbe- or damage-associated molecular patterns. *Plant J.*, **68**, 100–113.

Ray, D., Kazan, H., Cook, K.B., et al. (2013) A compendium of RNA-binding motifs for decoding gene regulation. *Nature*, **499**, 172–177.

Robles, L.M., Deslauriers, S.D., Alvarez, A.A. and Larsen, P.B. (2012) A loss-of-function mutation in the nucleoporin AtNUP160 indicates that normal auxin signalling is required for a proper ethylene response in Arabidopsis. *J. Exp. Bot.*, **63**, 2231–2241.

Ross, J.R., Nam, K.H., D'Auria, J.C. and Pichersky, E. (1999) S-adenosyl-L-methionine:salicylic acid carboxyl methyltransferase, an enzyme involved in floral scent production and plant defence, represents a new class of plant methyltransferases. *Arch. Biochem. Biophys.*, **367**, 9–16.

Roth, C., Lüdke, D., Klenke, M., Quathamer, A., Valerius, O., Braus, G.H. and Wiermer, M. (2017) The truncated NLR protein TIR-NBS13 is a MOS6/IMPORTIN-α3 interaction partner required for plant immunity. *Plant J.*, **92**, 808–821.

Roth, C. and Wiermer, M. (2012) Nucleoporins Nup160 and Seh1 are required for disease resistance in Arabidopsis. *Plant Signal. Behav.*, **7**, 1212–1214.

Rymarquis, L.A., Souret, F.F. and Green, P.J. (2011) Evidence that XRN4, an Arabidopsis homolog of exoribonuclease XRN1, preferentially impacts transcripts with certain sequences or in particular functional categories. *Rna*, **17**, 501–511.

Saito, K., Yoshikawa, M., Yano, K., et al. (2007) Nucleoporin85 is required for calcium spiking, fungal and bacterial symbioses, and seed production in Lotus japonicus. *Plant Cell*, **19**, 610–624.

Saitou, N. and Nei, M. (1987) The neighbor-joining method: a new method for reconstructing phylogenetic trees. *Mol. Biol. Evol.*, **4**, 406–425.

Sano, S., Aoyama, M., Nakai, K., et al. (2014) Light-dependent expression of flg22-induced defence genes in Arabidopsis. *Front. Plant Sci.*, **5**, 531.

Sardesai, N., Lee, L.Y., Chen, H., et al. (2013) Cytokinins secreted by agrobacterium promote transformation by repressing a plant myb transcription factor. *Sci. Signal.*, **6**, 1–11.

Saur, I.M.L., Kadota, Y., Sklenar, J., Holton, N.J., Smakowska, E., Belkhadir, Y., Zipfel, C. and Rathjen, J.P. (2016) NbCSPR underlies age-dependent immune responses to bacterial cold shock protein in Nicotiana benthamiana. *Proc. Natl. Acad. Sci. U. S. A.*, **113**, 3389–3394.

Schmidt, H.B. and Görlich, D. (2016) Transport Selectivity of Nuclear Pores, Phase Separation, and Membraneless Organelles. *Trends Biochem. Sci.*, **41**, 46–61.

Schoenberg, D.R. (2011) Mechanisms of endonuclease-mediated mRNA decay. *Wiley Interdiscip. Rev. RNA*, **2**, 582–600.

Schoenberg, D.R. and Maquat, L.E. (2012) Regulation of cytoplasmic mRNA decay. *Nat. Rev. Genet.*, **13**, 246–259.

Scholl, R.L., May, S.T. and Ware, D.H. (2000) Resources and Opportunities Seed and Molecular Resources for Arabidopsis. *Society*, **124**, 1477–1480.

Segonzac, C., Feike, D., Gimenez-Ibanez, S., Hann, D.R., Zipfel, C. and Rathjen, J.P. (2011) Hierarchy and roles of pathogen-associated molecular pattern-induced responses in nicotiana benthamiana. *Plant Physiol.*, **156**, 687–699.

Segref, A., Sharma, K., Doye, V., Hellwig, A., Huber, J., Lührmann, R. and Hurt, E. (1997) Mex67p, a novel factor for nuclear mRNA export. Binds to both poly(A)+ RNA and nuclear pores. *EMBO J.*, **16**, 3256–3271.

Selin, C., Kievit, T.R. de, Belmonte, M.F. and Fernando, W.G.D. (2016) Elucidating the role of effectors in plant-fungal interactions: Progress and challenges. *Front. Microbiol.*, **7**.

Seo, H.S., Song, J.T., Cheong, J.J., Lee, Y.H., Lee, Y.W., Hwang, I., Lee, J.S. and Choi, Y. Do (2001) Jasmonic acid carboxyl methyltransferase: A key enzyme for jasmonate-regulated plant responses. *Proc. Natl. Acad. Sci. U. S. A.*, **98**, 4788–4793.

Sessions, A., Burke, E., Presting, G., et al. (2002) A High-Throughput Arabidopsis Reverse Genetics System. *Plant Cell*, **14**, 2985–2994.

Shah, J. (2009) Plants under attack: systemic signals in defence. *Curr. Opin. Plant Biol.*, **12**, 459–464.

Shah, J. and Zeier, J. (2013) Long-distance communication and signal amplification in systemic acquired resistance. *Front. Plant Sci.*, **4**, 1–16.

Sheard, L.B., Tan, X., Mao, H., et al. (2010) Jasmonate perception by inositol-phosphate-potentiated COI1-JAZ co-receptor. *Nature*, **468**, 400–407.

Shigenaga, A.M. and Argueso, C.T. (2016) No hormone to rule them all: Interactions of plant hormones during the responses of plants to pathogens. *Semin. Cell Dev. Biol.*, **56**, 174–189.

Shih, P.Y., Chou, S.J., Müller, C., Halkier, B.A., Deeken, R. and Lai, E.M. (2018) Differential roles of glucosinolates and camalexin at different stages of Agrobacterium-mediated transformation. *Mol. Plant Pathol.*, **19**, 1956–1970.

Shulaev, V., Silverman, P. and Raskin, Ii. (1997) Airborne signalling by methyl salicylate in plant pathogen resistance. *Nature*, **385**, 718–721.

Snoeren, T.A.L., Mumm, R., Poelman, E.H., Yang, Y., Pichersky, E. and Dicke, M. (2010) The herbivore-induced plant volatile methyl salicylate negatively affects attraction of the parasitoid Diadegma semiclausum. *J. Chem. Ecol.*, **36**, 479–489.

Sønderby, I.E., Geu-Flores, F. and Halkier, B.A. (2010) Biosynthesis of glucosinolates - gene discovery and beyond. *Trends Plant Sci.*, **15**, 283–290.

Sørensen, B.B., Ehrnsberger, H.F., Esposito, S., et al. (2017) The Arabidopsis THO/TREX component TEX1 functionally interacts with MOS11 and modulates mRNA export and alternative splicing events. *Plant Mol. Biol.*, **93**, 283–298.

Spanu, P.D. and Panstruga, R. (2017) Editorial: Biotrophic plant-microbe interactions. *Front. Plant Sci.*, **8**, 192.

Spassov, D.S. and Jurecic, R. (2003) The PUF family of RNA-binding proteins: does evolutionarily conserved structure equal conserved function? *IUBMB Life*, **55**, 359–366.

Spoel, S.H. and Dong, X. (2008) Making Sense of Hormone Crosstalk during Plant Immune Responses. *Cell Host Microbe*, **3**, 348–351.

Srivastava, V.K. and Yadav, R. (2019) Chapter 9 - Isothermal titration calorimetry. In G. B. T.-D. P. H. for C. B. D. S. Misra, ed. *Data Processing Handbook for Complex Biological Data Sources*. Academic Press, pp. 125–137.

Staswick, P.E., Staswick, P.E., Tiryaki, I., Tiryaki, I., Rowe, M.L. and Rowe, M.L. (2002) Jasmonate Response Locus JAR1 and Several Related Arabidopsis Genes Encode Enzymes of the Firefly Luciferase Superfamily That Show Activity on Jasmonic, Salicylic, and Indole-3-Acetic Acids in an Assay for Adenylation. *Plant Cell*, **14**, 1405–1415.

Staswick, P.E. and Tiryaki, I. (2004) The Oxylipin Signal Jasmonic Acid Is Activated by an Enzyme That Conjugates It to Isoleucine in Arabidopsis. *Plant Cell*, **16**, 2117–2127.

Steffan, H., Ziegler, A. and Rapp, A. (1988) N-Salicylol-Asparaginsäure: Eine neue phenolische Verbindung aus Reben. *Vitis*, **27**, 79–86.

Stepanets, D. (2013) *Analysis of the role of Arabidopsis Nup107-160 complex members Nup160, MOS3/Nup96 and Seh1 in resistance to Botrytis cinerea and in Agrobacterium-mediated plant transformation*.

Stewart, M. (2007) Molecular mechanism of the nuclear protein import cycle. *Nat. Rev. Mol. Cell Biol.*, **8**, 195–208.

Stewart, M. (2019) Structure and Function of the TREX-2 Complex. *Subcell. Biochem.*, **93**, 461–470.

Stitz, M., Gase, K., Baldwin, I.T. and Gaquerel, E. (2011) Ectopic expression of at JMT in Nicotiana attenuata: Creating a metabolic sink has tissue-specific consequences for the jasmonate metabolic network and silences downstream gene expression. *Plant Physiol.*, **157**, 341–354.

Stöver, B. and Müller, K.F. (2010) TreeGraph 2: Combining and visualizing evidence from different phylogenetic analyses. *BMC Bioinformatics*, **11**, 7.

Strambio-de-castillia, C., Niepel, M. and Rout, M.P. (2010) The nuclear pore complex : bridging nuclear transport and gene regulation. *Nat. Rev. Mol. Cell Biol.*, **11**, 490–501.

Strasser, R. (2016) Plant protein glycosylation. *Glycobiology*, **26**, 926–939.

Stuhlfelder, C., Lottspeich, F. and Mueller, M.J. (2002) Purification and partial amino acid sequences of an esterase from tomato. *Phytochemistry*, **60**, 233–240.

Stuhlfelder, C., Mueller, M.J. and Warzecha, H. (2004) Cloning and expression of a tomato cDNA encoding a methyl jasmonate cleaving esterase. *Eur. J. Biochem.*, **271**, 2976–2983.

Stuwe, T., Correia, A.R., Lin, D.H., Paduch, M., Lu, V.T., Kossiakoff, A.A. and Hoelz, A. (2015) Architecture of the nuclear pore complex coat. *Science*, **347**, 1148–1152.

Survila, M., Davidsson, P.R., Pennanen, V., Kariola, T., Broberg, M., Sipari, N., Heino, P. and Palva, E.T. (2016) Peroxidase-generated apoplastic ROS impair cuticle integrity and contribute to DAMP-elicited defences. *Front. Plant Sci.*, **7**, 1945.

Tam, P.P., Barrette-Ng, I.H., Simon, D.M., Tam, M.W.C., Ang, A.L. and Muench, D.G. (2010) The Puf family of RNA-binding proteins in plants: phylogeny, structural modeling, activity and subcellular localization. *BMC Plant Biol.*, **10**, 44.

Tamura, K., Fukao, Y., Iwamoto, M., Haraguchi, T. and Hara-Nishimura, I. (2010) Identification and characterization of nuclear pore complex components in Arabidopsis thaliana. *Plant Cell*, **22**, 4084–4097.

Tamura, K. and Hara-Nishimura, I. (2014) Functional insights of nucleocytoplasmic transport in plants. *Front. Plant Sci.*, **5**, 118.

Tamura, K. and Hara-Nishimura, I. (2011) Involvement of the nuclear pore complex in morphology of the plant nucleus. *Nucleus*, **2**, 168–172.

Tamura, K. and Hara-Nishimura, I. (2013) The molecular architecture of the plant nuclear pore complex. *J. Exp. Bot.*, **64**, 823–832.

Tao, Y., Ferrer, J., Ljung, K., et al. (2008) Rapid synthesis of auxin via a new tryptophan-dependent pathway is required for shade avoidance in plants. *Cell*, **133**, 164–176.

Teper, D., Girija, A.M., Bosis, E., Popov, G., Savidor, A. and Sessa, G. (2018) The Xanthomonas euvesicatoria type III effector XopAU is an active protein kinase that

manipulates plant MAP kinase signaling. *PLoS Pathog.*, **14**, e1006880.

Terry, L.J. and Wente, S.R. (2009) Flexible gates: Dynamic topologies and functions for FG nucleoporins in nucleocytoplasmic transport. *Eukaryot. Cell*, **8**, 1814–1827.

Tetenbaum-Novatt, J. and Rout, M.P. (2010) The mechanism of nucleocytoplasmic transport through the nuclear pore complex. *Cold Spring Harb. Symp. Quant. Biol.*, **75**, 567–584.

Thompson, J.D., Gibson, T.J. and Higgins, D.G. (2002) Multiple Sequence Alignment Using ClustalW and ClustalX. *Curr.* Protoc. *Bioinformatics*, **Chapter 2**, Unit 2.3.

Thorpe, M.R., Ferrieri, A.P., Herth, M.M. and Ferrieri, R.A. (2007) 11C-imaging: Methyl jasmonate moves in both phloem and xylem, promotes transport of jasmonate, and of photoassimilate even after proton transport is decoupled. *Planta*, **226**, 541–551.

Tian, T., Liu, Y., Yan, H., You, Q., Yi, X., Du, Z., Xu, W. and Su, Z. (2017) agriGO v2 . 0 : a GO analysis toolkit for the agricultural community , 2017 update. *Nucleic Acids Res.* **45**, W122–W129.

To, J.P.C., Haberer, G., Ferreira, F.J., Deruère, J., Mason, M.G., Schaller, G.E., Alonso, J.M., Ecker, J.R. and Kieber, J.J. (2004) Type-A Arabidopsis response regulators are partially redundant negative regulators of cytokinin signaling. *Plant Cell*, **16**, 658–671.

Todd, M.J. and Gomez, J. (2001) Enzyme kinetics determined using calorimetry: A general assay for enzyme activity? *Anal. Biochem.*, **296**, 179–187.

Torres-Zabala, M. De, Truman, W., Bennett, M.H., Lafforgue, G., Mansfield, J.W., Rodriguez Egea, P., Bögre, L. and Grant, M. (2007) Pseudomonas syringae pv. tomato hijacks the Arabidopsis abscisic acid signalling pathway to cause disease. *EMBO J.*, **26**, 1434–1443.

Torres, M.A., Jones, J.D.G. and Dangl, J.L. (2006) Reactive oxygen species signaling in response to pathogens. *Plant Physiol.*, **141**, 373–378.

Tran, E.J. and Wente, S.R. (2006) Dynamic Nuclear Pore Complexes: Life on the Edge. *Cell*, **125**, 1041–1053.

Tsuda, K. and Katagiri, F. (2010) Comparing signaling mechanisms engaged in pattern-triggered and effector-triggered immunity. *Curr. Opin. Plant Biol.*, **13**, 459–465.

Tsuda, K., Sato, M., Stoddard, T., Glazebrook, J. and Katagiri, F. (2009) Network properties of robust immunity in plants. *PLoS Genet.*, **5**, e1000772.

Tsukaya, H., Iokawa, Y., Kondo, M. and Ohba, H. (2005) Large-scale general collection of wild-plant DNA in Mustang, Nepal. *J. Plant Res.*, **118**, 57–60.

Tutucci, E. and Stutz, F. (2011) Keeping mRNPs in check during assembly and nuclear export. *Nat. Rev. Mol. Cell Biol.*, **12**, 377–384.

Ueda, H., Kikuta, Y. and Matsuda, K. (2012) Plant communication mediated by individual or blended VOCs? *Plant Signal. Behav.*, **7**, 222–226.

Uyhazi, K.E., Yang, Y., Liu, N., Qi, H., Huang, X.A., Weatherbee, S.D., Song, X. and Lin, H. (2019) Pumilio Proteins Exert Distinct Biological Functions and Multiple Modes of

Post - Transcriptional Regulation in Embryonic Stem Cell Pluripotency and Early Embryogenesis. *bioRxiv*.

Verslues, P.E., Guo, Y., Dong, C.H., Ma, W. and Zhu, J.K. (2006) Mutation of SAD2, an importin β-domain protein in Arabidopsis, alters abscisic acid sensitivity. *Plant J.*, **47**, 776–787.

Vlot, A.C., Dempsey, D.A. and Klessig, D.F. (2009) Salicylic Acid, a Multifaceted Hormone to Combat Disease. *Annu. Rev. Phytopathol.*, **47**, 177–206.

Vlot, A.C., Liu, P., Cameron, R.K., et al. (2008a) Identification of likely orthologs of tobacco salicylic acid-binding protein 2 and their role in systemic acquired resistance in Arabidopsis thaliana. *plant J.*, **56**, 445–456.

Vlot, C.A., Klessig, D.F. and Park, S.W. (2008b) Systemic acquired resistance: the elusive signal(s). *Curr. Opin. Plant Biol.*, **11**, 436–442.

Vosse, D.W. Van de, Wan, Y., Wozniak, R.W. and Aitchison, J.D. (2011) Role of the nuclear envelope in genome organization and gene expression. *Wiley Interdiscip. Rev. Syst. Biol. Med.*, **3**, 147–166.

Walther, T.C., Alves, A., Pickersgill, H., et al. (2003) The Conserved Nup107-160 Complex Is Critical for Nuclear Pore Complex Assembly. , **113**, 195–206.

Wang, D., Pajerowska-Mukhtar, K., Culler, A.H. and Dong, X. (2007) Salicylic Acid Inhibits Pathogen Growth in Plants through Repression of the Auxin Signaling Pathway. *Curr. Biol.*, **17**, 1784–1790.

Wang, M., Ogé, L., Perez-Garcia, M.D., Hamama, L. and Sakr, S. (2018a) The PUF protein family: Overview on PUF RNA targets, biological functions, and post transcriptional regulation. *Int. J. Mol. Sci.*, **19**, 19.

Wang, X., Jiang, N., Liu, J., Liu, W. and Wang, G.L. (2014) The role of effectors and host immunity in plant–necrotrophic fungal interactions. *Virulence*, **5**, 722–732.

Wang, Y., Yu, M., Shih, P., Wu, H. and Lai, E. (2018b) Stable pH Suppresses Defence Signaling and is the Key to Enhance Agrobacterium -Mediated Transient Expression in Arabidopsis Seedlings. *Sci. Rep.*, **8**, 1–9.

Wasternack, C. and Song, S. (2017) Jasmonates: Biosynthesis, metabolism, and signaling by proteins activating and repressing transcription. *J. Exp. Bot.*, **68**, 1303–1321.

Wente, S.R. and Rout, M.P. (2010) Transport. *Cold Spring Harb. Perspect. Biol.*, **2**, a000562.

Wickens, M., Bernstein, D.S., Kimble, J. and Parker, R. (2002) A PUF family portrait: 3′UTR regulation as a way of life. *A PUF Fam. portrait 3'UTR Regul. as a W. life*, **18**, 150–157.

Wiermer, M., Cheng, Y.T., Imkampe, J., Li, M., Wang, D., Lipka, V. and Li, X. (2012) Putative members of the Arabidopsis Nup107-160 nuclear pore sub-complex contribute to pathogen defence. *Plant J.*, **70**, 796–808.

Wiermer, M., Palma, K., Zhang, Y. and Li, X. (2007) Should I stay or should I go? Nucleocytoplasmic trafficking in plant innate immunity. *Cell. Microbiol.*, **9**, 1880–1890.

Williams, T., Ngo, L.H. and Wickramasinghe, V.O. (2018) Nuclear export of RNA: Different sizes, shapes and functions. *Semin. Cell Dev. Biol.*, **75**, 70–77.

Willmann, R., Lajunen, H.M., Erbs, G., Newman, M., Kolb, D. and Tsuda, K. (2011) mediate bacterial peptidoglycan sensing and immunity to bacterial infection. *Proc. Natl Acad. Sci. USA*, **108**, 19824–19829.

Wilson, D.C., Kempthorne, C.J., Carella, P., Liscombe, D.K. and Cameron, R.K. (2017) Age-related resistance in arabidopsis thaliana involves the MADS-domain transcription factor SHORT VEGETATIVE PHASE and direct action of salicylic acid on pseudomonas syringae. *Mol. Plant-Microbe Interact.*, **30**, 919–929.

Wirthmueller, L., Roth, C., Fabro, G., et al. (2015) Probing formation of cargo/importin-α transport complexes in plant cells using a pathogen effector. *Plant J.*, **81**, 40–52.

Wittstock, U. and Burow, M. (2010) Glucosinolate Breakdown in Arabidopsis: Mechanism, Regulation and Biological Significance. In *The Arabidopsis Book*. pp. 1–14.

Wu, H.Y., Liu, K.H., Wang, Y.C., Wu, J.F., Chiu, W.L., Chen, C.Y., Wu, S.H., Sheen, J. and Lai, E.M. (2014) AGROBEST: An efficient Agrobacterium-mediated transient expression method for versatile gene function analyses in Arabidopsis seedlings. *Plant Methods*, **10**, 19.

Wu, J., Wang, L. and Baldwin, I.T. (2008) Methyl jasmonate-elicited herbivore resistance: Does MeJA function as a signal without being hydrolyzed to JA? *Planta*, **227**, 1161–1168.

Wu, X., Shi, Y., Li, J., Xu, L., Fang, Y., Li, X. and Qi, Y. (2013) A role for the RNA-binding protein MOS2 in microRNA maturation in Arabidopsis. *Cell Res.*, **23**, 645–657.

Xia, S., Cheng, Y.T., Huang, S., et al. (2013) Regulation of transcription of nucleotide-binding leucine-rich repeat-encoding genes SNC1 and RPP4 via H3K4 trimethylation. *Plant Physiol.*, **162**, 1694–1705.

Xiang, Y., Nakabayashi, K., Ding, J., He, F. and Soppe, W.J.J. (2014) REDUCED DORMANCY5 Encodes a Protein Phosphatase 2C That Is Required for Seed Dormancy in Arabidopsis. *Plant Cell*, **26**, 4362–4375.

Xu, C., Zhou, X. and Wen, C.K. (2015) HYPER RECOMBINATION1 of the THO/TREX Complex Plays a Role in Controlling Transcription of the REVERSION-TO-ETHYLENE SENSITIVITY1 Gene in Arabidopsis. *PLoS Genet.*, **11**, e1004956.

Xu, D., Farmer, A. and Chook, Y.M. (2010) Recognition of nuclear targeting signals by Karyopherin-β proteins. *Curr. Opin. Struct. Biol.*, **20**, 782–790.

Xu, F., Xu, S., Wiermer, M., Zhang, Y. and Li, X. (2012) The cyclin L homolog MOS12 and the MOS4-associated complex are required for the proper splicing of plant resistance genes. *Plant J.*, **70**, 916–928.

Xu, J., Xie, J., Yan, C., Zou, X., Ren, D. and Zhang, S. (2014) A chemical genetic approach demonstrates that MPK3/MPK6 activation and NADPH oxidase-mediated oxidative burst are two independent signaling events in plant immunity. *Plant J.*, **77**, 222–234.

Xu, S., Zhang, Z., Jing, B., Gannon, P., Ding, J., Xu, F., Li, X. and Zhang, Y. (2011)

Transportin-SR is required for proper splicing of resistance genes and plant immunity. *PLoS Genet.*, **7**, e1002159.

Xu, X.M. and Meier, I. (2008) The nuclear pore comes to the fore. *Trends Plant Sci.*, **13**, 20–27.

Xu, X.M., Rose, A., Muthuswamy, S., Sun, Y.J., Venkatakrishnan, S., Zhao, Q. and Meier, I. (2007) NUCLEAR PORE ANCHOR, the Arabidopsis homolog of Tpr/Mlp1/Mlp2/megator, is involved in mRNA export and SUMO homeostasis and affects diverse aspects of plant development. *Plant Cell*, **19**, 1537–1548.

Yang, Y., Varbanova, M., Ross, J., Wang, G., Fridman, E., Shulaev, V. and Noel, J.P. (2006) METHYLATION AND DEMETHYLATION OF PLANT SIGNALING MOLECULES 1Department of Molecular , Cellular and Developmental Biology , University. *Recent Adv. Phytochem.*, **40**, 253–270.

Yang, Y., Xu, R., Ma, C., Vlot, A.C., Klessig, D.F. and Pichersky, E. (2008) Inactive Methyl Indole-3-Acetic Acid Ester Can Be Hydrolyzed and Activated by Several Esterases Belonging to the At MES Esterase Family of Arabidopsis 1. *Plant Physiol.*, **147**, 1034–1045.

Yelina, N.E., Smith, L.M., Jones, A.M.E., Patel, K., Kelly, K.A. and Baulcombe, D.C. (2010) Putative Arabidopsis THO/TREX mRNA export complex is involved in transgene and endogenous siRNA biosynthesis. *Proc. Natl. Acad. Sci. U. S. A.*, **107**, 13948–13953.

Yuan, S., Tao, X., Huang, S., Chen, S. and Xu, A. (2014) Comparative Immune Systems in Animals. *Annu. Rev. Anim. Biosci.*, **2**, 235–258.

Zeier, J. (2013) New insights into the regulation of plant immunity by amino acid metabolic pathways. *Plant, Cell Environ.*, **36**, 2085–2103.

Zhang, C., Xie, Q., Anderson, R.G., et al. (2013a) Crosstalk between the Circadian Clock and Innate Immunity in Arabidopsis. *PLoS Pathog.*, **9**, e1003370.

Zhang, C.J., Zhou, J.X., Liu, J., et al. (2013b) The splicing machinery promotes RNA-directed DNA methylation and transcriptional silencing in Arabidopsis. *EMBO J.*, **32**, 1128–1140.

Zhang, N., Wang, Z., Bao, Z., Yang, L., Wu, D., Shu, X. and Hua, J. (2018) MOS1 functions closely with TCP transcription factors to modulate immunity and cell cycle in Arabidopsis. *Plant J.*, **93**, 66–78.

Zhang, Y. and Li, X. (2005) A putative nucleoporin 96 is required for both basal defence and constitutive resistance responses mediated by suppressor of npr1-1, constitutive 1. *Plant Cell*, **17**, 1306–1316.

Zhang, Y., Wang, Y., Liu, J., Ding, Y., Wang, S., Zhang, X., Liu, Y. and Yang, S. (2017) Temperature-dependent autoimmunity mediated by chs1 requires its neighboring TNL gene SOC3. *New Phytol.*, **213**, 1330–1345.

Zhang, Y., Zhang, Y., Goritschnig, S., Goritschnig, S., Dong, X., Dong, X., Li, X. and Li, X. (2003) A Gain-of-Function Mutation in a Plant Disease Resistance Gene Leads to Constitutive Activation of Downstream Signal Transduction Pathways in. *Society*, **15**, 2636–46.

Zhao, N., Ferrer, J.L., Ross, J., Guan, J., Yang, Y., Pichersky, E., Noel, J.P. and Chen, F. (2008) Structural, biochemical, and phylogenetic analyses suggest that indole-3-acetic acid methyltransferase is an evolutionarily ancient member of the SABATH family. *Plant Physiol.*, **146**, 455–467.

Zhao, Q., Leung, S., Corbett, A.H. and Meier, I. (2006) Identification and Characterization of the Arabidopsis Orthologs of Nuclear Transport Factor 2, the Nuclear Import Factor of Ran 1. *Plant Physiology*, **140**, 869–878.

Zhao, Q. and Meier, I. (2011) Identification and characterization of the arabidopsis FG-repeat nucleoporin Nup62. *Plant Signal. Behav.*, **6**, 330–334.

Zhao, Y. (2014) Auxin Biosynthesis. In *The Arabidopsis Book*. pp. 1–14.

Zhu, Y., Wang, B., Tang, K., Hsu, C.C., Xie, S., Du, H., Yang, Y., Tao, W.A. and Zhu, J.K. (2017) An Arabidopsis Nucleoporin NUP85 modulates plant responses to ABA and salt stress. *PLoS Genet.*, **13**, e1007124.

Zipfel, C. (2009) Early molecular events in PAMP-triggered immunity. *Curr. Opin. Plant Biol.*, **12**, 414–420.

Zipfel, C. (2008) Pattern-recognition receptors in plant innate immunity. *Curr. Opin. Immunol.*, **20**, 10–16.

Zipfel, C., Kunze, G., Chinchilla, D., Caniard, A., Jones, J.D.G., Boller, T. and Felix, G. (2006) Perception of the Bacterial PAMP EF-Tu by the Receptor EFR Restricts Agrobacterium-Mediated Transformation. *Cell*, **125**, 749–760.

Zipfel, C., Robatzek, S., Navarro, L., Oakeley, E.J., Jones, J.D.G., Felix, G. and Boller, T. (2004) Bacterial disease resistance in Arabidopsis through flagellin perception. *Nature*, **428**, 764–767.

Zubieta, C., Ross, J.R., Koscheski, P., Yang, Y., Pichersky, E. and Noel, J.P. (2003) Structural basis for substrate recognition in the salicylic acid carboxyl methyltransferase family. *Plant Cell*, **15**, 1704–1716.

Zuccolo, M., Alves, A., Galy, V., et al. (2007) The human Nup107-160 nuclear pore subcomplex contributes to proper kinetochore functions. *EMBO J.*, **26**, 1853–1864.

Zuckerkandl, E. and Pauling, L. (1965) Evolutionary Divergence and Convergence in Proteins. New York: Academic Press, pp. 97–166.

6 Supplemental Material

Supplementary Table 1: 471 genes are differentially expressed in *mos3*-2, *nup160*-3 and *sec13b*-1 as compared to Col-0 wild-type ($log_2FC > 0.5$ or < -0.5, FDR < 0.05).

		wild-type vs. *sec13b*-1	wild-type vs. *mos3*-2	wild-type vs *nup160*-3
AGI code	**gene name / description**	**log_2FC**		
AT1G63530	Hypothetical protein		3.05	4.07
AT5G60250	Zinc finger (C3HC4-type RING finger) family protein		2.11	3.12
AT1G59660	NUP98B		1.85	2.82
AT1G80660	AHA9		1.83	2.79
AT1G72800	RNA-binding (RRM/RBD/RNP motifs) family protein		2.12	2.27
AT1G02190	Fatty acid hydroxylase superfamily		1.50	2.08
AT1G69680	Ran guanine nucleotide release factor, putative		1.33	2.07
AT5G20010	RAN1		1.45	2.03
AT1G24260	SEP3		1.43	1.99
AT5G24780	VSP1		1.59	1.93
AT4G17470	Alpha/beta-Hydrolases superfamily protein		1.93	1.93
AT3G29639	hypothetical protein		1.76	1.93
AT3G11260	WOX5		1.02	1.87
AT5G24770	VSP2		1.99	1.86
AT2G39330	JAL23		2.01	1.85
AT5G24160	SQE6		1.98	1.72
AT1G78080	RAP2-4		1.67	1.60
AT3G53980	Bifunctional inhibitor/lipid-transfer protein/seed storage 2S albumin superfamily protein		1.09	1.56
AT1G80670	RAE1		1.07	1.54
AT5G57810	TET15		1.15	1.53
AT5G20020	RAN2		0.98	1.49
AT5G57785	Hypothetical protein		1.17	1.49
AT3G55920	CYP21-2	0.87	1.44	1.48
AT3G03110	XPO1B		1.31	1.45
AT1G65890	AAE12		1.59	1.45
AT5G47590	Heat shock protein HSP20/alpha crystallin family		1.56	1.40
AT1G27970	NTF2B		0.94	1.36
AT4G13290	CYP71A19		0.97	1.35
AT5G21150	AGO9		0.76	1.34
AT2G41480	PER25		1.20	1.33
AT5G50335	Hypothetical protein		0.92	1.33
AT5G23020	MAM3		1.49	1.32
AT5G51810	GA20OX2		1.05	1.32
AT2G45930	hypothetical protein		0.83	1.31
AT3G18773	ATL77		0.73	1.30
AT2G31250	HEMA3		1.11	1.30

AT2G25820	ERF042		1.06	1.29
AT2G46610	RS31A		1.07	1.27
AT4G11210	DIR14		0.70	1.27
AT1G62540	FMO GS-OX2		1.29	1.27
AT5G64910	Serine/Threonine-kinase		1.20	1.27
AT3G26460	Polyketide cyclase/dehydrase and lipid transport superfamily protein		1.38	1.26
AT2G34810	FAD-binding Berberine family protein		1.26	1.25
AT1G13245	RTFL17		0.83	1.25
AT2G22510	Hydroxyproline-rich glycoprotein family protein		0.92	1.25
AT1G69410	ELF5A-3		0.92	1.25
AT2G24300	Calmodulin-binding protein		0.60	1.24
AT4G27480	Core-2/I-branching beta-1,6-N-acetylglucosaminyltransferase family protein		1.00	1.23
AT1G10657	DEG17		1.12	1.23
AT4G07815	Long_noncoding_rna		1.36	1.22
AT4G23680	Polyketide cyclase/dehydrase and lipid transport superfamily protein		1.19	1.22
AT4G30290	XTH19		0.84	1.22
AT3G03840	SAUR-like auxin-responsive protein family		0.89	1.21
AT1G28010	ABCB14		1.02	1.21
AT1G53260	Hypothetical protein		1.06	1.21
AT3G19240	Vacuolar import/degradation, Vid27-related protein		0.83	1.21
AT1G10070	BCAT2		1.03	1.19
AT4G12470	AZI1		1.08	1.19
AT3G58270	Phospholipase-like protein (PEARLI 4) with TRAF-like domain protein		1.06	1.18
AT1G14250	APY5		1.62	1.18
AT5G54190	PORA		0.90	1.17
AT3G55290	NAD(P)-binding Rossmann-fold superfamily protein		0.82	1.17
AT3G45650	NAXT1		0.57	1.16
AT5G63580	FLS2		1.28	1.15
AT2G30230	6,7-dimethyl-8-ribityllumazine synthase		0.71	1.15
AT4G22880	LDOX		1.35	1.15
AT5G17700	DTX25		1.04	1.14
AT4G37410	CYP81F4		0.75	1.13
AT3G58000	VQ25		1.11	1.13
AT5G47330	Alpha/beta-Hydrolases superfamily protein		0.95	1.13
AT2G42005	AVT3B		1.06	1.13
AT2G38530	LTP2		0.89	1.13
AT4G31330	transmembrane protein, putative		0.79	1.12
AT2G46410	CPC		0.87	1.11
AT2G47780	LD-ASSOCIATED PROTEIN 2		0.94	1.11
AT5G42800	DFRA		1.30	1.11
AT4G22950	AGL19		1.12	1.11
AT3G61920	UvrABC system protein C		0.95	1.10
AT1G22340	UGT85A7		0.92	1.09

AT5G17830	Plasma-membrane choline transporter family protein		0.90	1.08
AT3G22910	ACA13		1.10	1.07
AT3G48450	RPM1-interacting protein 4 (RIN4) family protein		0.80	1.06
AT5G58980	NCER3		1.30	1.06
AT2G22930	UGT79B8		0.93	1.06
AT4G39950	CYP79B2		0.81	1.05
AT2G18193	P-loop containing nucleoside triphosphate hydrolases superfamily protein		1.09	1.05
AT5G44620	CYP706A3		0.79	1.05
AT5G58610	PHD finger transcription factor		1.18	1.04
AT4G33790	FAR3		0.95	1.04
AT1G10790	Hydroxyproline-rich glycoprotein family protein		0.86	1.04
AT5G43180	Transmembrane protein, putative		0.81	1.03
AT3G04000	ChlADR2		0.89	1.03
AT1G31820	POLYAMINE UPTAKE TRANSPORTER 1, PUT1		0.89	1.02
AT4G11320	RDL5		0.79	1.01
AT3G52550	Transcription repressor OFP15-like protein		0.80	1.01
AT1G19670	CLH1		1.00	1.01
AT4G08870	ARGAH2		0.96	1.01
AT2G23010	SCPL9		1.14	1.00
AT5G45990	Crooked neck protein, putative / cell cycle protein		1.66	1.00
AT1G52030	F-ATMBP		1.02	1.00
AT2G32100	OFP16		0.72	1.00
AT1G77380	AAP3		0.89	1.00
AT5G22460	Alpha/beta-Hydrolases superfamily protein		0.61	1.00
AT1G20823	ATL80		0.70	1.00
AT3G03820	SAUR29, SMALL AUXIN UP RNA 29		0.74	0.99
AT5G23820	ML3		0.92	0.97
AT4G09820	TT8		1.12	0.97
AT4G08290	UMAMIT20		1.47	0.97
AT5G46130	ATDOA12, DUF295 ORGANELLAR A 12		0.80	0.97
AT3G50450	HR1		0.74	0.96
AT1G33770	Protein kinase superfamily protein		0.76	0.96
AT3G27970	Exonuclease family protein		0.79	0.96
AT1G11450	UMAMIT27		0.80	0.96
AT3G29590	5MAT		1.17	0.95
AT1G34060	TAR4		1.03	0.95
AT2G42680	MBF1A		0.66	0.95
AT2G32487	Hypothetical protein		1.23	0.94
AT5G62730	NPF4.7		0.96	0.93
AT4G37445	Calcium ion-binding protein		0.78	0.93
AT1G64200	VHA-E3		0.78	0.93
AT5G17220	GSTF12		1.19	0.92
AT1G44800	SIAR1		0.72	0.92
AT4G29700	Alkaline-phosphatase-like family protein		0.92	0.91
AT1G28760	INNER NUCLEAR MEMBRANE PROTEIN A		0.75	0.90

AT4G17480	Alpha/beta-Hydrolases superfamily protein		0.90	0.90
AT5G56320	ATEXPA14		0.68	0.89
AT3G53230	CDC48D		0.79	0.89
AT3G06630	Protein kinase family protein		0.80	0.89
AT1G60270	BGLU6		0.94	0.89
AT3G16470	JAL35		0.90	0.89
AT5G13740	ZIF1		0.80	0.89
AT4G01600	GRAM domain family protein		1.23	0.89
AT1G29500	SAUR66		0.75	0.89
AT2G36080	ARF31		0.70	0.88
AT4G39480	CYP96A9		0.97	0.88
AT5G23370	GRAM domain-containing protein / ABA-responsive protein-like protein		0.77	0.87
AT3G47180	RING/U-box superfamily protein		0.77	0.87
AT1G77885	Hypothetical protein		0.93	0.87
AT1G35290	ALT1		0.96	0.87
AT2G31200	ADF6		0.72	0.86
AT3G22740	HMT3		0.70	0.86
AT2G24210	TPS10		0.97	0.86
AT2G33380	PXG3		0.83	0.85
AT2G23000	SCPL10		0.83	0.85
AT2G37260	WRKY44		0.95	0.85
AT1G51460	ABCG13		0.67	0.85
AT1G02850	BGLU11		1.01	0.84
AT4G39940	APK2		0.67	0.84
AT1G02940	ATGSTF5		0.77	0.84
AT3G58990	IPMI1		0.75	0.83
AT1G79840	GL2		0.70	0.83
AT5G55720	Pectin lyase-like superfamily protein		0.59	0.82
AT1G72140	NPF5.12		1.04	0.81
AT4G14550	IAA14		0.76	0.81
AT4G11920	FZR1		0.59	0.80
AT5G14700	NAD(P)-binding Rossmann-fold superfamily protein		0.71	0.80
AT1G16060	ADAP		0.75	0.80
AT2G23170	GH3.3		0.71	0.80
AT3G21420	LBO1		0.75	0.80
AT4G34860	INVB		0.63	0.79
AT1G22900	DIR11		0.82	0.79
AT1G62660	BFRUCT3		0.68	0.79
AT5G43620	PCFS5		0.66	0.78
AT3G19710	BCAT4		0.65	0.78
AT4G14020	Rapid alkalinization factor (RALF) family protein		0.86	0.78
AT4G14090	UGT75C1		1.22	0.78
AT5G03380	HIPP06		0.52	0.77
AT2G29320	NAD(P)-binding Rossmann-fold superfamily protein		0.65	0.77
AT5G42880	WEL3		0.81	0.77
AT1G77690	LAX3		0.54	0.77
AT3G53370	S1FA1		0.65	0.76

AT1G24265	bZIP transcription factor, putative (DUF1664)		0.60	0.76
AT2G38870	Predicted to encode a PR (pathogenesis-related) peptide that belongs to the PR-6 proteinase inhibitor family		0.61	0.76
AT2G43590	Chitinase family protein		0.67	0.76
AT5G07990	CYP75B1		0.91	0.75
AT2G43100	IPMI2		0.63	0.75
AT1G06640	encodes a protein whose sequence is similar to a 2-oxoglutarate-dependent dioxygenase		0.79	0.75
AT3G50570	Hydroxyproline-rich glycoprotein family protein		0.82	0.74
AT2G37060	NFYB8		0.60	0.74
AT1G01600	CYP86A4		0.58	0.74
AT1G15150	DTX10		0.72	0.74
AT3G03850	SAUR26		0.74	0.73
AT1G60360	RING/U-box superfamily protein		0.67	0.73
AT4G15765	FAD/NAD(P)-binding oxidoreductase family protein		0.75	0.73
AT5G65530	ATRLCK VI_A3		0.81	0.72
AT3G61460	BRH1		0.64	0.71
AT5G09530	PELPK1		0.73	0.71
AT4G26990	Polyadenylate-binding protein interacting protein		0.56	0.71
AT3G57600	DREB2F		0.95	0.71
AT2G29440	GSTU6		0.77	0.71
AT3G56620	UMAMIT10		0.90	0.71
AT2G32510	MAPKKK17		0.82	0.70
AT5G25980	TGG2		0.80	0.70
AT3G11210	CPRD49		0.50	0.70
AT5G13490	AAC2		0.59	0.70
AT1G29510	SAUR67		0.57	0.70
AT1G71140	DTX14		0.68	0.69
AT3G53650	Histone superfamily protein		0.55	0.69
AT1G16400	CYP79F2		0.62	0.69
AT5G13820	TRP4		0.81	0.69
AT3G16410	NSP4		0.65	0.69
AT2G38995	O-acyltransferase (WSD1-like) family protein		0.76	0.68
AT1G02065	SPL8		0.61	0.68
AT4G33150	LYSINE-KETOGLUTARATE REDUCTASE		0.63	0.68
AT1G19940	AtGH9B5		0.77	0.68
AT1G06100	Fatty acid desaturase family protein		0.67	0.68
AT2G34070	TBL37		0.56	0.68
AT4G27070	TSB2		0.63	0.67
AT2G39350	ABCG1		0.54	0.67
AT5G59740	UTR5B		0.66	0.67
AT4G30530	GGP1		0.62	0.67
AT5G42680	MIZU-KUSSEI-like protein		0.67	0.67
AT5G23010	MAM1		0.50	0.66
AT5G56490	GULLO4		0.81	0.64
AT1G27940	ABCB13		0.78	0.64

AT5G61290	Flavin-binding monooxygenase family protein		0.94	0.64
AT2G44930	Transmembrane protein, putative (DUF247)		0.55	0.64
AT4G01440	UMAMIT31		0.76	0.63
AT4G27730	OPT6		0.50	0.63
AT5G64667	IDL2		0.92	0.63
AT4G18440	L-Aspartase-like family protein		1.10	0.63
AT5G42280	Cysteine/Histidine-rich C1 domain family protein		0.73	0.63
AT1G65450	GLC		0.69	0.62
AT1G02930	GSTF6		0.77	0.62
AT5G17000	Zinc-binding dehydrogenase family protein		0.84	0.62
AT1G04700	PB1 domain-containing protein tyrosine kinase		0.52	0.61
AT1G15110	ATPSS1		0.56	0.61
AT5G54060	A3G2XYLT		1.10	0.60
AT3G27030	Transmembrane protein		0.54	0.60
AT1G47960	C/VIF1		0.75	0.60
AT1G72230	Cupredoxin superfamily protein		0.51	0.60
AT3G08770	LTP6		0.52	0.60
AT4G10390	Protein kinase superfamily protein		0.74	0.60
AT1G65150	TRAF-like family protein		0.68	0.59
AT4G04610	APR1		0.75	0.58
AT4G32690	GLB3		0.63	0.58
AT1G52410	TSA1		0.86	0.58
AT4G27300	SD11		0.59	0.57
AT4G14040	SBP2		0.50	0.57
AT4G14560	IAA1		0.59	0.57
AT3G18260	RTNLB9		0.59	0.57
AT1G52400	BGLU18		0.86	0.57
AT2G33850	E6-LIKE 1		0.62	0.55
AT1G09470	NEAP3		0.67	0.52
AT5G47140	GATA27		-0.55	-0.50
AT4G04360	Transmembrane protein, putative (DUF1068)		-0.62	-0.51
AT5G51010	Rubredoxin-like superfamily protein		-0.65	-0.53
AT3G25670	Leucine-rich repeat (LRR) family protein		-0.66	-0.53
AT5G41700	UBC8		-0.61	-0.55
AT3G43790	ZIFL2		-0.76	-0.55
AT5G45490	P-loop containing nucleoside triphosphate hydrolases superfamily protein		-0.63	-0.55
AT2G21650	RL2		-1.05	-0.57
AT2G29180	Transmembrane protein		-0.60	-0.57
AT3G16770	RAP2-3		-0.64	-0.57
AT4G29260	VSP3		-0.67	-0.58
AT1G72840	Disease resistance protein (TIR-NBS-LRR class)		-0.54	-0.58
AT5G24735	SORF31		-0.60	-0.59
AT4G30140	CDEF1		-1.69	-0.60
AT3G28950	AIG2C		-0.61	-0.61

AT5G09300	Thiamin diphosphate-binding fold (THDP-binding) superfamily protein		-0.62	-0.61
AT3G18970	PCMP-E93		-0.64	-0.61
AT1G30860	RING/U-box superfamily protein		-0.73	-0.61
AT4G04955	ALN		-0.58	-0.62
AT5G37480	Maltase-glucoamylase, intestinal protein		-0.59	-0.63
AT3G50380	Vacuolar protein sorting-associated protein, putative (DUF1162)		-0.57	-0.64
AT2G43970	LARP6B		-0.58	-0.64
AT1G56280	ATDI19		-0.80	-0.64
AT5G62630	HIPL2		-0.62	-0.65
AT5G34940	AtGUS3		-0.51	-0.65
AT4G29890	Choline monooxygenase, putative (CMO-like)		-0.57	-0.65
AT4G07950	DNA-directed RNA polymerase, subunit M, archaeal		-0.63	-0.65
AT4G30570	Glucose-1-phosphate adenylyltransferase family protein		-0.70	-0.65
AT4G22830	YCF49-like protein		-0.57	-0.65
AT2G40100	LHCB4.3		-0.63	-0.66
AT4G33360	FLDH		-0.55	-0.67
AT4G11410	NAD(P)-binding Rossmann-fold superfamily protein		-0.53	-0.67
AT3G22210	Transmembrane protein		-0.59	-0.68
AT2G05380	GRP3S		-1.19	-0.68
AT1G57790	ATFDR1		-0.54	-0.68
AT4G16745	Exostosin family protein		-0.58	-0.69
AT1G07440	NAD(P)-binding Rossmann-fold superfamily protein		-0.70	-0.69
AT5G40240	UMAMIT40		-0.53	-0.69
AT5G39730	AIG2LB		-0.56	-0.70
AT5G05890	UGT76C5		-0.87	-0.70
AT3G54366	Unknown gene		-0.64	-0.70
AT5G45840	MDIS1		-0.88	-0.70
AT3G55260	HEXO1		-0.54	-0.71
AT2G16060	AHB1		-0.90	-0.71
AT3G08920	STR10		-0.66	-0.72
AT2G14878	Unknown gene		-0.80	-0.73
AT2G20630	PPC3-1.2		-0.59	-0.74
AT4G02050	STP7		-0.56	-0.74
AT5G07360	Amidase family protein		-0.69	-0.75
AT5G25990	Core-2/I-branching beta-1,6-N-acetylglucosaminyltransferase family protein		-0.84	-0.76
AT5G44930	ARAD2		-0.52	-0.76
AT2G01870	Transmembrane protein		-0.60	-0.77
AT1G01390	UDP-Glycosyltransferase superfamily protein		-0.82	-0.78
AT1G51370	F-box/RNI-like/FBD-like domains-containing protein		-0.73	-0.78
AT1G48430	Dihydroxyacetone kinase		-0.60	-0.78
AT1G76955	Unknown gene		-0.82	-0.79

AT1G03290	ELKS/Rab6-interacting/CAST family protein		-0.78	-0.79
AT5G08600	U3 ribonucleoprotein (Utp) family protein		-0.70	-0.79
AT2G03530	UPS2		-0.84	-0.79
AT3G51750	Hypothetical protein		-0.67	-0.79
AT3G48090	**EDS1**		-0.63	-0.79
AT5G25970	Core-2/I-branching beta-1,6-N-acetylglucosaminyltransferase family protein		-1.00	-0.79
AT3G51000	Alpha/beta-Hydrolases superfamily protein		-0.52	-0.79
AT5G25995	Hypothetical protein		-0.69	-0.80
AT4G20140	GSO1		-0.85	-0.82
AT3G23510	Cyclopropane-fatty-acyl-phospholipid synthase		-1.29	-0.82
AT1G56120	Leucine-rich repeat transmembrane protein kinase		-0.67	-0.83
AT5G24210	Alpha/beta-Hydrolases superfamily protein		-0.76	-0.83
AT3G05625	Tetratricopeptide repeat (TPR)-like superfamily protein		-0.60	-0.83
AT5G05060	Cystatin/monellin superfamily protein		-0.73	-0.83
AT3G62780	Calcium-dependent lipid-binding (CaLB domain) family protein		-0.72	-0.83
AT1G18265	Zein-binding protein (Protein of unknown function, DUF593)		-0.62	-0.85
AT5G23980	FRO4		-0.86	-0.85
AT5G48440	FAD-dependent oxidoreductase family protein		-0.54	-0.86
AT3G22750	Protein kinase superfamily protein		-0.71	-0.86
AT5G44590	S-adenosyl-L-methionine-dependent methyltransferases superfamily protein		-0.88	-0.86
AT5G60780	NRT2.3		-1.17	-0.87
AT1G68540	TKPR2		-0.92	-0.87
AT1G65520	ECI1		-0.90	-0.87
AT5G49900	Beta-glucosidase, GBA2 type family protein		-0.91	-0.87
AT5G27410	D-aminoacid aminotransferase-like PLP-dependent enzymes superfamily protein		-1.09	-0.87
AT5G06811	Transcription termination factor family protein		-0.62	-0.87
AT1G52570	PLDALPHA2		-0.86	-0.88
AT4G18960	AG		-1.17	-0.88
AT3G59210	F-box/RNI-like superfamily protein		-0.91	-0.88
AT3G60180	UMK1		-0.59	-0.89
AT2G03965	Hypothetical protein		-0.67	-0.89
AT4G12917	Unknown gene		-0.68	-0.89
AT4G25780	CAP (Cysteine-rich secretory proteins, Antigen 5, and Pathogenesis-related 1 protein) superfamily protein		-0.84	-0.89
AT2G03710	AGL3		-0.62	-0.90
AT3G14470	RPPL1		-0.59	-0.90
AT3G55890	Yippee family putative zinc-binding protein		-1.03	-0.90
AT2G14580	PRB1		-1.07	-0.90

AT2G17120	LYM2		-0.72	-0.91
AT4G02405	S-adenosyl-L-methionine-dependent methyltransferases superfamily protein		-0.64	-0.91
AT3G56090	FER3		-0.92	-0.91
AT1G28560	SRD2		-0.76	-0.91
AT5G59470	Mannose-P-dolichol utilization defect 1 protein		-0.62	-0.92
AT5G13320	PBS3		-0.79	-0.92
AT2G04170	TRAF-like family protein		-0.86	-0.92
AT1G53920	GLIP5		-0.79	-0.93
AT4G01935	Insulin-induced protein		-0.70	-0.93
AT5G21020	Transmembrane protein		-0.92	-0.94
AT1G03400	Unknown gene		-0.71	-0.94
AT2G13790	SERK4		-0.73	-0.95
AT5G55170	SUMO3		-0.76	-0.95
AT5G18360	Disease resistance protein (TIR-NBS-LRR class) family		-0.79	-0.95
AT5G39030	MDS4		-0.59	-0.95
AT5G27100	GLR2.1		-0.50	-0.95
AT3G15400	ATA20		-1.07	-0.96
AT3G57770	Protein kinase superfamily protein		-0.80	-0.97
AT2G02980	PCMP-H26		-0.58	-0.97
AT3G52430	**PAD4**		-0.82	-0.97
AT3G11080	AtRLP35		-0.85	-0.97
AT3G59250	F-box/RNI-like superfamily protein		-0.93	-0.98
AT5G16170	Core-2/I-branching beta-1,6-N-acetylglucosaminyltransferase family protein		-0.83	-0.98
AT2G45510	CYP704A2		-0.74	-0.98
AT2G26355	antisense long noncoding rna		-0.88	-0.98
AT3G15900	Homoserine O-acetyltransferase		-0.63	-0.99
AT2G34940	VSR5		-0.80	-0.99
AT5G52810	SARD4		-0.65	-0.99
AT3G19230	LLR4		-0.75	-0.99
AT2G30432	TCL1		-0.76	-0.99
AT2G32160	S-adenosyl-L-methionine-dependent methyltransferases superfamily protein		-0.88	-0.99
AT1G13950	ELF5A-1		-0.99	-0.99
AT4G20110	VSR7		-0.76	-0.99
AT5G61250	AtGUS1		-0.76	-1.00
AT4G22050	Eukaryotic aspartyl protease family protein		-1.20	-1.01
AT1G65800	SD16		-0.69	-1.01
AT1G74300	Alpha/beta-Hydrolases superfamily protein		-0.90	-1.02
AT5G35740	Carbohydrate-binding X8 domain superfamily protein		-0.81	-1.02
AT2G24592	long noncoding rna		-0.66	-1.04
AT2G31585	Unknown gene		-0.80	-1.05
AT3G47010	Beta-D-glucan exohydrolase-like protein		-0.91	-1.05
AT1G02220	NAC003		-1.18	-1.05
AT1G49990	F-box family protein		-0.61	-1.06
AT4G08470	MAPKKK10		-0.83	-1.07

AT4G19950	Polyadenylate-binding protein 1-B-binding protein		-0.57	-1.07
AT1G27565	Hypothetical protein		-0.89	-1.07
AT3G27940	LBD26		-0.83	-1.07
AT1G29418	Transmembrane protein		-0.80	-1.08
AT3G47350	ATHSD2		-0.62	-1.08
AT1G55120	CWINV3		-1.14	-1.08
AT1G31580	ECS1		-0.90	-1.09
AT1G55675	Transmembrane protein		-0.92	-1.09
AT2G27920	SCPL51		-1.06	-1.11
AT4G34930	PLC-like phosphodiesterases superfamily protein		-0.74	-1.11
AT5G64110	PER70		-1.46	-1.11
AT1G02360	Chitinase family protein		-0.77	-1.11
AT1G49750	Leucine-rich repeat (LRR) family protein		-0.74	-1.12
AT4G11530	CRK34		-1.14	-1.13
AT1G51790	Leucine-rich repeat protein kinase family protein		-0.81	-1.14
AT1G16260	WAKL8		-0.76	-1.14
AT1G64110	P-loop containing nucleoside triphosphate hydrolases superfamily protein		-1.40	-1.15
AT1G33470	RNA-binding (RRM/RBD/RNP motifs) family protein		-0.69	-1.15
AT1G20490	AMP-dependent synthetase and ligase family protein		-0.79	-1.15
AT2G05160	CCCH-type zinc fingerfamily protein with RNA-binding domain-containing protein		-0.90	-1.16
AT4G01700	Chitinase family protein		-0.97	-1.16
AT1G17600	SOC3		-0.85	-1.17
AT3G45390	LECRK12		-0.94	-1.18
AT2G43690	LECRK53		-0.65	-1.18
AT5G50240	PIMT2		-1.41	-1.18
AT2G18050	HIS1-3		-1.31	-1.19
AT5G20480	**EFR**		-0.65	-1.20
AT3G43670	COPPER AMINE OXIDASE GAMMA 2		-1.10	-1.20
AT2G25590	Plant Tudor-like protein		-0.95	-1.21
AT1G14100	FUT8		-0.98	-1.21
AT1G78030	Hypothetical protein		-0.97	-1.21
AT5G51720	NEET		-0.84	-1.21
AT2G24040	Low temperature and salt responsive protein family		-0.88	-1.22
AT5G40780	LHT1		-0.81	-1.22
AT4G25110	AMC2		-1.11	-1.24
AT1G74440	ER membrane protein, putative (DUF962)		-0.77	-1.25
AT2G25510	Transmembrane protein		-0.85	-1.26
AT2G05995	Unknown gene		-1.16	-1.26
AT3G48080	EDS1B		-0.95	-1.27
AT1G03210	Phenazine biosynthesis PhzC/PhzF protein		-1.01	-1.27
AT2G43700	LECRK54		-1.02	-1.28

AT5G05460	ENGASE1		-0.96	-1.28
AT4G37690	GT6		-0.99	-1.28
AT3G51340	Eukaryotic aspartyl protease family protein		-0.85	-1.28
AT5G55460	Bifunctional inhibitor/lipid-transfer protein/seed storage 2S albumin superfamily protein		-1.05	-1.28
AT2G17280	PGM		-1.03	-1.29
AT1G50520	CYP705A27		-0.80	-1.30
AT5G35926	Protein with RNI-like/FBD-like domain		-0.86	-1.30
AT1G34750	CIPP1		-0.99	-1.31
AT1G13750	PAP1		-0.94	-1.32
AT4G23260	CRK18		-0.55	-1.33
AT5G25040	Major facilitator superfamily protein		-0.71	-1.33
AT1G65240	Eukaryotic aspartyl protease family protein		-1.24	-1.35
AT2G44290	YLS3		-0.82	-1.40
AT2G12190	Cytochrome P450 superfamily protein		-0.93	-1.41
AT1G29600	Zinc finger C-x8-C-x5-C-x3-H type family protein		-0.99	-1.41
AT3G59480	FRK4		-1.92	-1.41
AT2G24190	Unknown gene		-1.07	-1.42
AT1G02230	NAC004		-0.99	-1.44
AT5G59670	Leucine-rich repeat protein kinase family protein		-0.85	-1.47
AT5G36930	Disease resistance protein (TIR-NBS-LRR class) family		-0.94	-1.47
AT3G25020	AtRLP42		-0.86	-1.47
AT1G65790	SD17		-0.78	-1.48
AT5G38865	Hypothetical protein		-0.87	-1.48
AT5G44820	Nucleotide-diphospho-sugar transferase family protein		-0.85	-1.50
AT5G61010	ATEXO70E2		-0.89	-1.50
AT2G15292	Unknown gene		-0.82	-1.51
AT1G69720	HO3		-0.97	-1.52
AT1G76720	Eukaryotic translation initiation factor 2 (eIF-2) family protein		-1.05	-1.53
AT4G04695	CPK31		-1.15	-1.58
AT5G52070	Agenet domain-containing protein		-1.21	-1.59
AT3G55710	UGT76F2		-0.99	-1.61
AT4G10695	CDC68-like protein		-1.71	-1.61
AT5G46260	Disease resistance protein (TIR-NBS-LRR class) family		-0.93	-1.64
AT3G05955	long noncoding rna		-1.29	-1.65
AT1G22590	AGL87		-1.55	-1.66
AT3G11010	AtRLP34		-0.93	-1.67
AT4G21380	SD18		-1.03	-1.71
AT3G61280	O-glucosyltransferase rumi-like protein (DUF821)		-0.87	-1.73
AT5G60900	RLK1		-0.84	-1.74

AT5G59680	Leucine-rich repeat protein kinase family protein		-1.16	-1.77
AT2G17920	Nucleic acid binding / zinc ion binding protein		-1.47	-1.78
AT4G34580	SFH1		-1.30	-1.80
AT4G11900	S-locus lectin protein kinase family protein		-0.77	-1.87
AT3G03480	CHAT		-0.92	-1.87
AT3G23110	AtRLP37		-1.05	-1.92
AT2G23590	MES8		-1.48	-2.13
AT5G44565	Transmembrane protein		-1.56	-2.13
AT1G35730	**PUM9**		-1.50	-2.17
AT5G58310	**MES18**		-2.59	-3.96

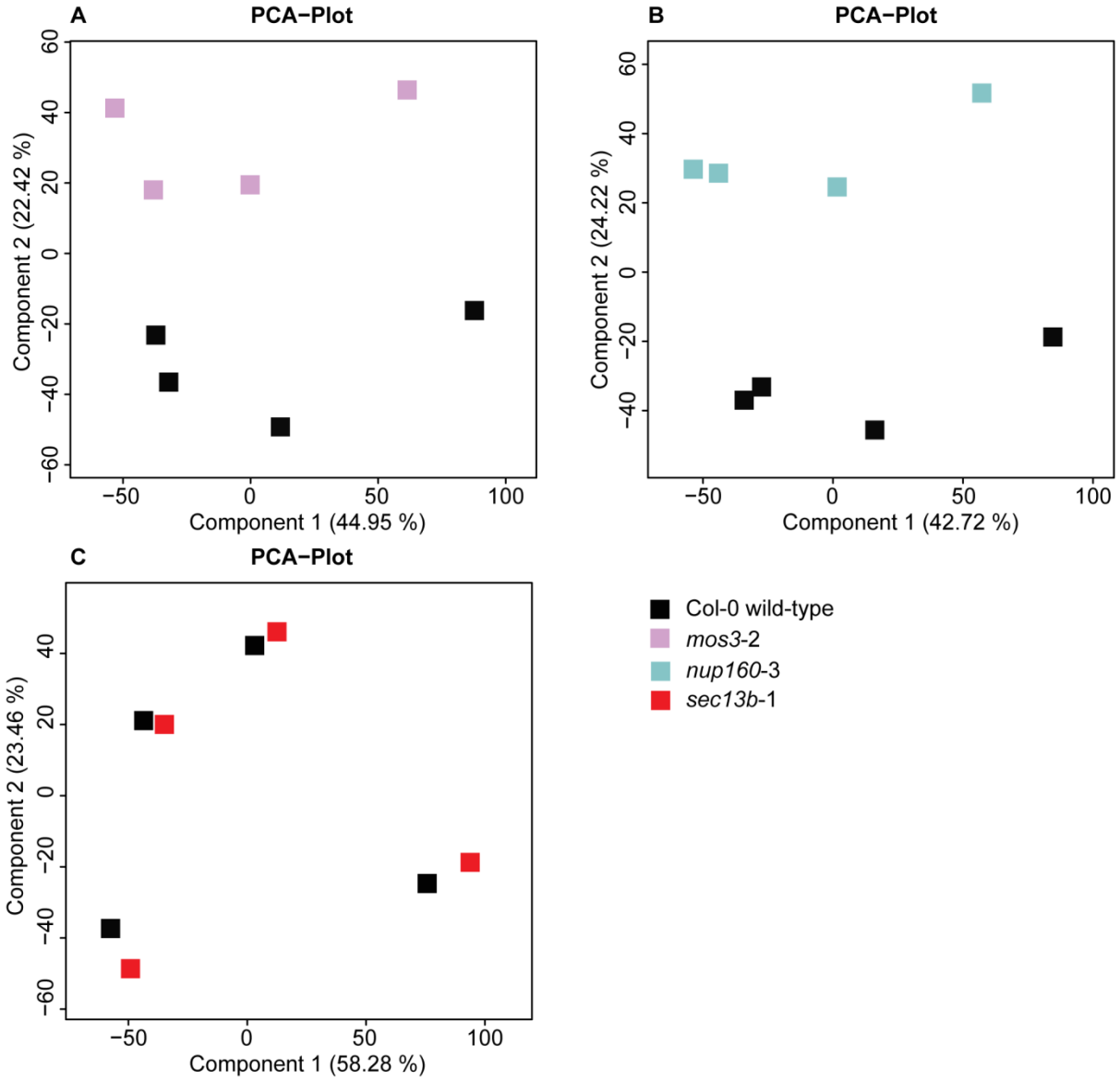

Supplementary Figure 1: Principal Component Analysis (PCA) of the Col-0 wild-type, *mos3*-2, *nup160*-3 and *sec13b*-1 transcriptome data obtained from the RNAseq analysis depicted in Figure 5. Squares represent four independent biological replicates of Col-0 wild-type (black), *mos3*-2 (light purple), *nup160*-3 (light blue), and *sec13b*-1 (red). (**A**) Wild-type versus *mos3*-2. (**B**) Wild-type versus *nup160*-3. (**C**) Wild-type versus *sec13b*-1.

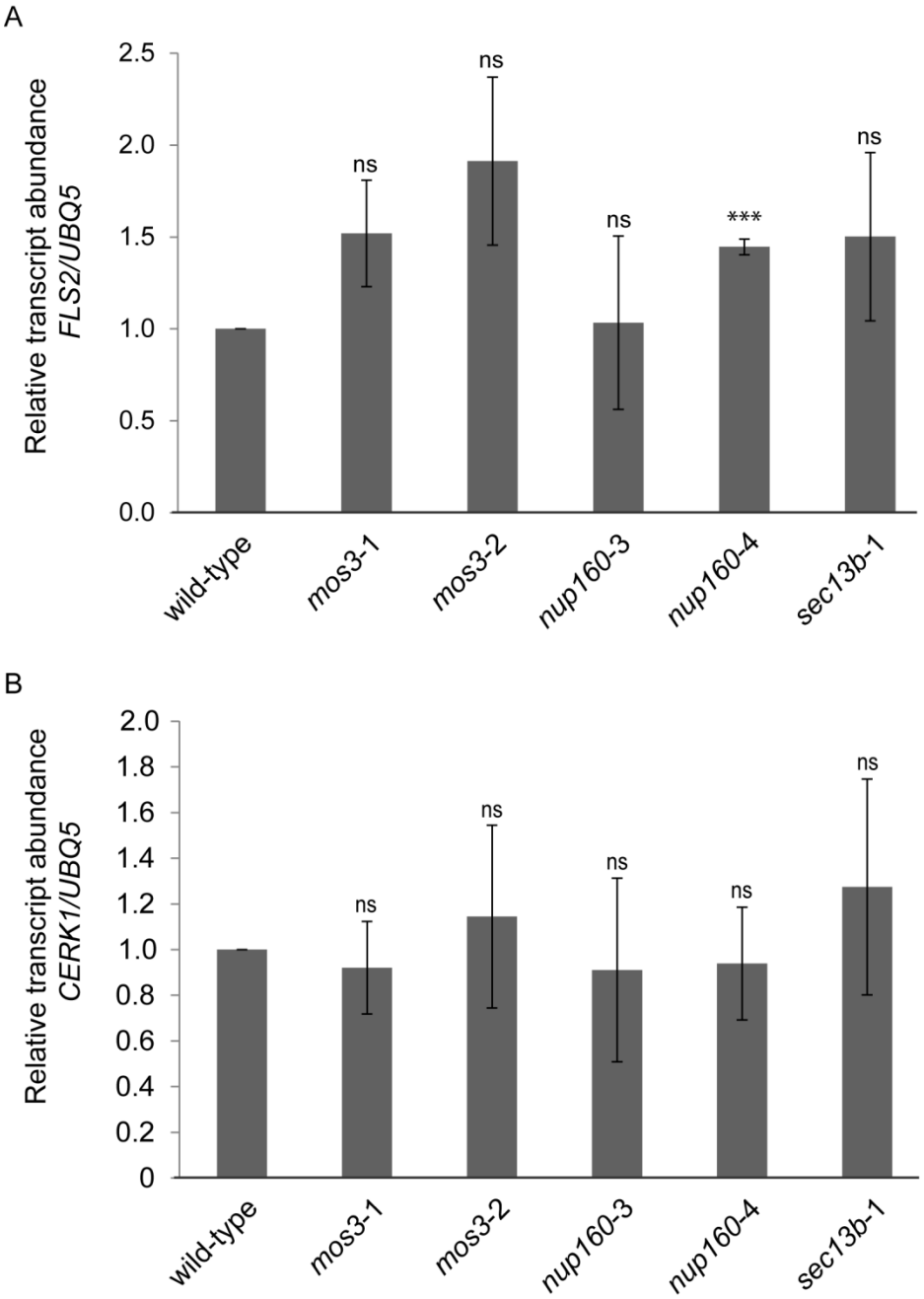

Supplementary Figure 2: *FLS2* and *CERK1* gene expression is not altered in *mos3* and *nup160*-3 mutant plants. Expression of (**A**) *FLS2* and (**B**) *CERK1* was analysed by qRT-PCR of four week old unchallenged *Arabidopsis* plants of the indicated genotypes. All plants were grown under short day conditions on soil. Total RNA for gene expression analysis was extracted from pools of five individual plants per genotype. The experiment was repeated three times with independently grown plants to obtain three biological replicates. *UBIQUITIN5* (*UBQ5*; AT3G62250) served as reference gene for normalizing the expression of *FLS2* and *CERK1.* Bars represent mean values of three biological replicates and error bars represent SEM. Relative transcript abundance of (**A**) *FLS2 and* (**B**) *CERK1* in the mutant plants was normalized to Col-0 wild-type which is set to 1.0. Statistical analysis was performed using Student's t-test for comparison of Col-0 wild-type and mutants; not significant (ns), *P < 0.05, ** P < 0.01, *** P < 0.001.

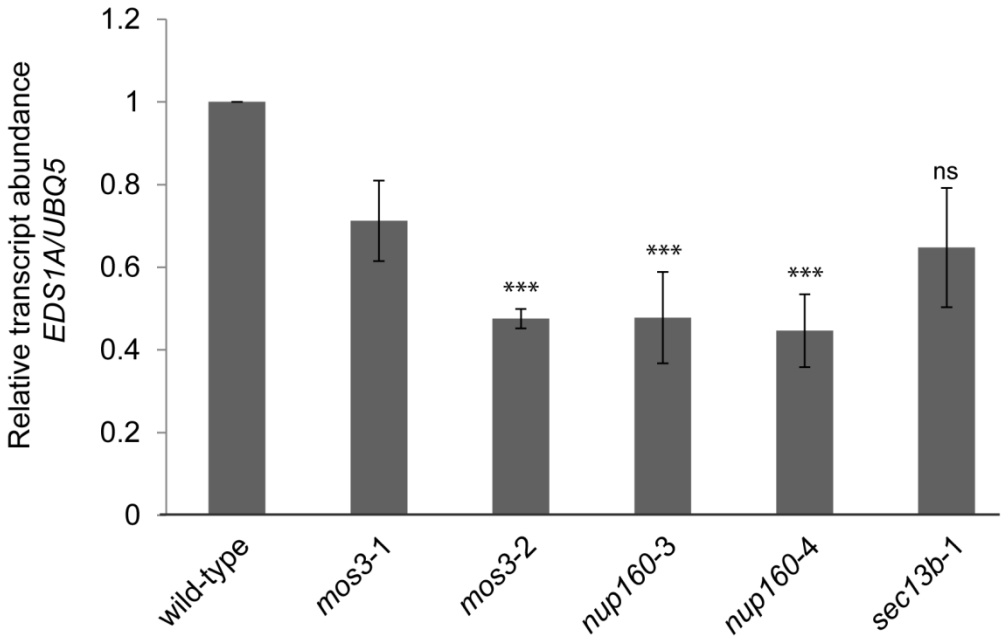

Supplementary Figure 3: *EDS1A* gene expression is reduced in *mos3*-2 and *nup160* mutant plants. Expression of *EDS1A* was analysed by qRT-PCR of four week old unchallenged *Arabidopsis* plants of the indicated genotypes. All plants were grown under short day conditions on soil. Total RNA for gene expression analysis was extracted from pools of five individual plants per genotype. The experiment was repeated three times with independently grown plants to obtain three biological replicates. *UBIQUITIN5* (*UBQ5*; AT3G62250) served as reference gene for normalizing the expression of *EDS1A.* Bars represent mean values of three biological replicates and error bars represent SEM. Relative transcript abundance of *EDS1A* in the mutant plants was normalized to Col-0 wild-type which is set to 1.0. Statistical analysis was performed using Student's t-test for comparison of Col-0 wild-type and mutants; not significant (ns), *P < 0.05, ** P < 0.01, *** P < 0.001.

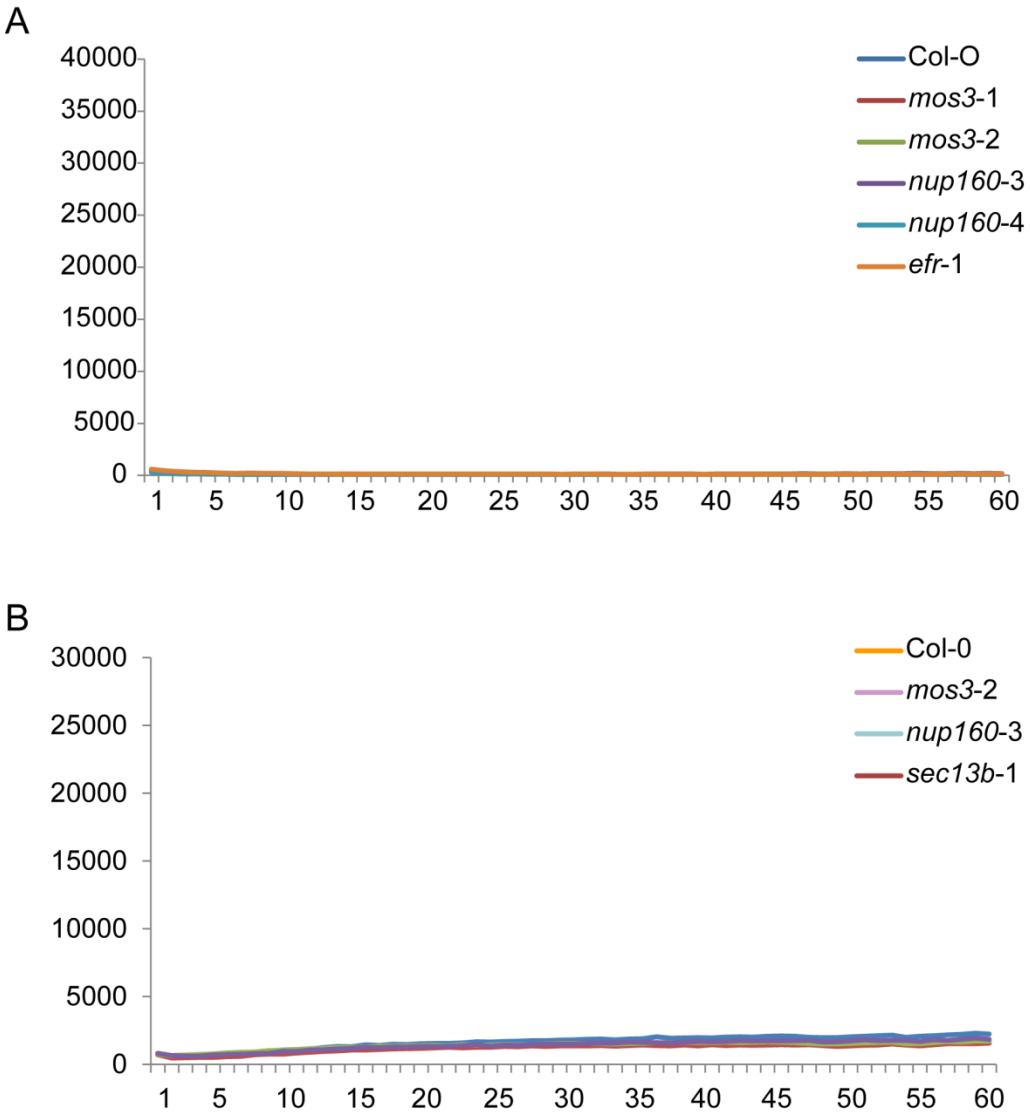

Supplementary Figure 4: Col-0, *mos3, nup160, sec13b*-1 and *efr*-1 mutant plants show no ROS production upon mock treatment. (**A**) and (**B**) Leaf discs of seven week old soil-grown *Arabidopsis* plants were treated with 100 nM elf18/L-012 solution (L-012, luminol-based chemiluminescent probe; shown in Figure 15 and Supplementary Figure 5) or L-012 solution without elf18 peptide (mock control) which is depicted in this figure. Relative luminescence units (RLU) were recorded for the indicated genotypes after elf18 (Figure 15 and Supplementary Figure 5) or mock treatment in 1 minute intervals for a period of 60 minutes. Data show mean values of eight leaf disc per genotype after mock treatment. The experiment was performed (**A**) three times and (**B**) two times with similar results.

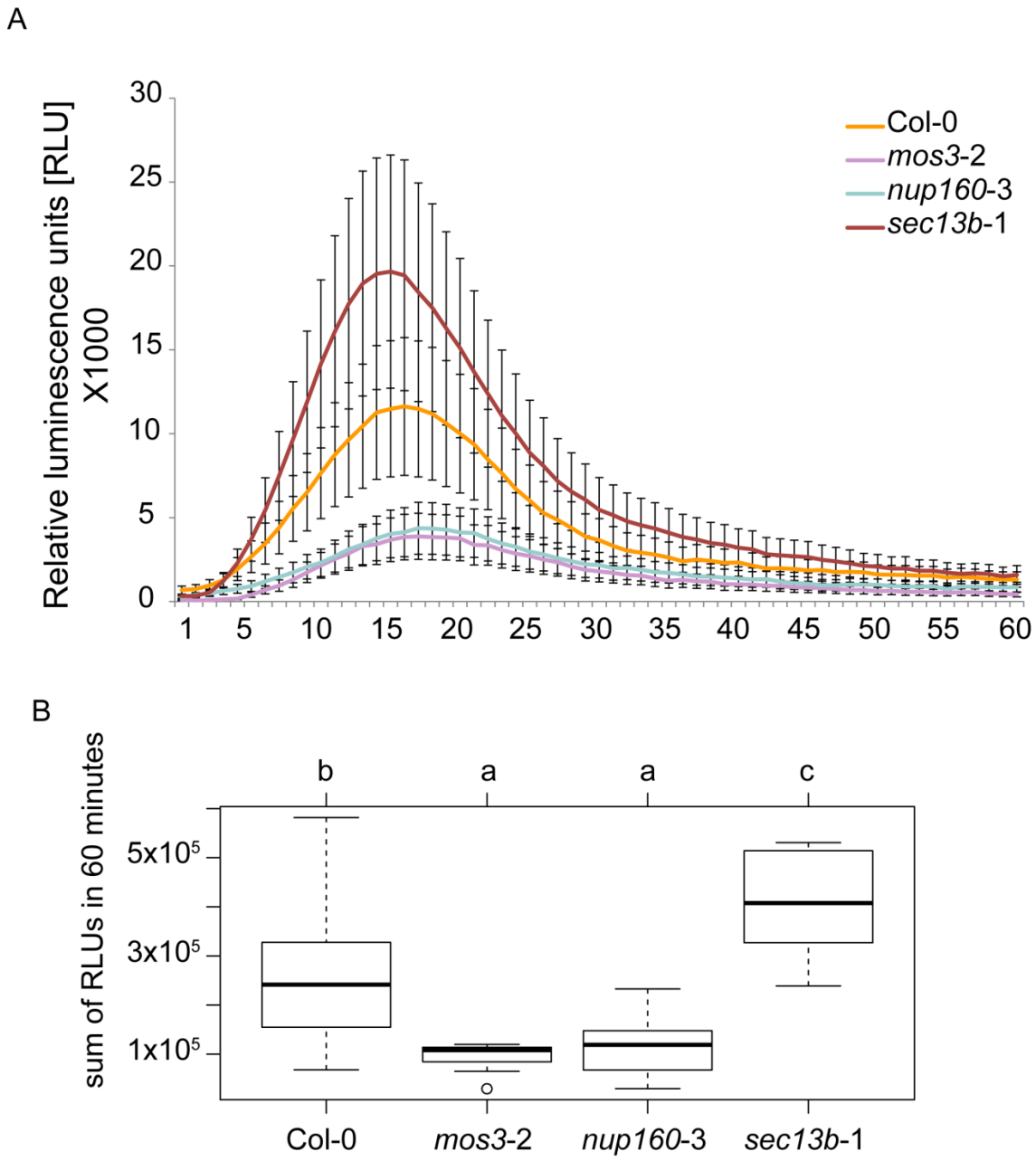

Supplementary Figure 5: ROS production in *sec13b*-1 mutant plants upon elf18 treatment is similar to the response observed in Col-0 wild-type. (**A**) Leaf discs of seven week old soil-grown *Arabidopsis* plants were treated with 100 nM elf18/L-012 solution (L-012, luminol-based chemiluminescent probe) or L-012 solution without elf18 peptide (mock control; see Supplementary Figure 4 B). Relative luminescence units (RLU) were recorded for the indicated genotypes after elf18 or mock treatment in 1 minute intervals for a period of 60 minutes. Data show mean values of eight leaf disc per genotype after subtraction of respective mock control. Error bars denote SEM. The experiment was performed three times with similar results. (**B**) Box plots representing data from (**A**) of eight technical replicates per genotype. Each technical replicate is the sum of all measured RLUs for a time window of 60 minutes. Lower and upper whiskers indicate the 25th and 75th percentile, respectively, and median is depicted by the black line. Open circles represents outliers. Different letters indicate statistical significant differences between the genotypes (one-way Anova and tukey-post hoc test, $P < 0.05$).

```
AtMES1       1 ------------------------------------------------------------
AtMES2       1 ------------------------------------------------------------
AtMES3       1 ------------------------------------------------------------
AtMES4       1 ------------------------------------------------------------
AtMES5       1 ------------------------------------------------------------
AtMES6       1 ------------------------------------------------------------
AtMES7       1 ------------------------------------------------------------
AtMES8       1 ------------------------------------------------------------
AtMES9       1 ------------------------------------------------------------
AtMES10      1 ------------------------------------------------------------
AtMES11      1 MGNLCSLFTPPKPVKKRKP-----------------------------ITKRQSSIGA
AtMES12      1 MGNRVICMKKKD-------------------------------------------VVI
AtMES13      1 MGNSFTCISHEQEQRPKKSSGGGGNNSGKYKYVRRLSLMPSFRRRTLLPSLSCSGSSSTS
AtMES14      1 MGNKIISMMKKD-----------------------------------------SKD
AtMES15      1 MGNSLRCISQEQDPNQKKPSSVVNGNSS-EKHVRRLSLIPSFRRRTLLPSLSCSGSSTSS
AtMES16      1 ------------------------------------------------------------
AtMES17      1 ------------------------------------------------------------
AtMES18      1 ------------------------------------------------------------
LeMJE        1 ------------------------------------------------------------
NtSABP2      1 ------------------------------------------------------------

AtMES1       1 ------------------------------------------------------------
AtMES2       1 ------------------------------------------------------------
AtMES3       1 ------------------------------------------------------------
AtMES4       1 ------------------------------------------------------------
AtMES5       1 ------------------------------------------------------------
AtMES6       1 ------------------------------------------------------------
AtMES7       1 ------------------------------------------------------------
AtMES8       1 ------------------------------------------------------------
AtMES9       1 ------------------------------------------------------------
AtMES10      1 ------------------------------------------------------------
AtMES11     30 SSSGSGLNSNRWNNRVRSSSSRRDNKFEDALIQEHALAAAAVLFRQQNGGGGSLPFDRSA
AtMES12     16 RSGGDGSRSKRVNRSQRKLLADEENLHRRALSMAIHQAQVSQRFDGSMSRR---------
AtMES13     61 SSKKGGIKAKTKKIRERHHHHHQDHEKDSHIIQEQTLAATNLLFNQTPRNSNSVVPPSFR
AtMES14     16 -GGGGGSKSKRMNRSQRKLLADEEMLHRRALSMAIHQAQLSQRFDGSMSRR---------
AtMES15     60 TSKKGGIKTKKKIRERHHQEQHHHDHEKDSLIQDQTLAATNILFSQTPRNSNSAPPFRRS
AtMES16      1 ------------------------------------------------------------
AtMES17      1 ------------------------------------------------------------
AtMES18      1 ------------------------------------------------------------
LeMJE        1 ------------------------------------------------------------
NtSABP2      1 ------------------------------------------------------------

AtMES1       1 ------------------------------------------------------------
AtMES2       1 ------------------------------------------------------------
AtMES3       1 ------------------------------------------------------------
AtMES4       1 ------------------------------------------------------------
AtMES5       1 ------------------------------------------------------------
AtMES6       1 ------------------------------------------------------------
AtMES7       1 ------------------------------------------------------------
AtMES8       1 ----------------------------------------MYENGISFIISLLICGCV
AtMES9       1 ------------------------------------------------------------
AtMES10      1 ---------------------------------------------MTYQKQYQMQTH
```

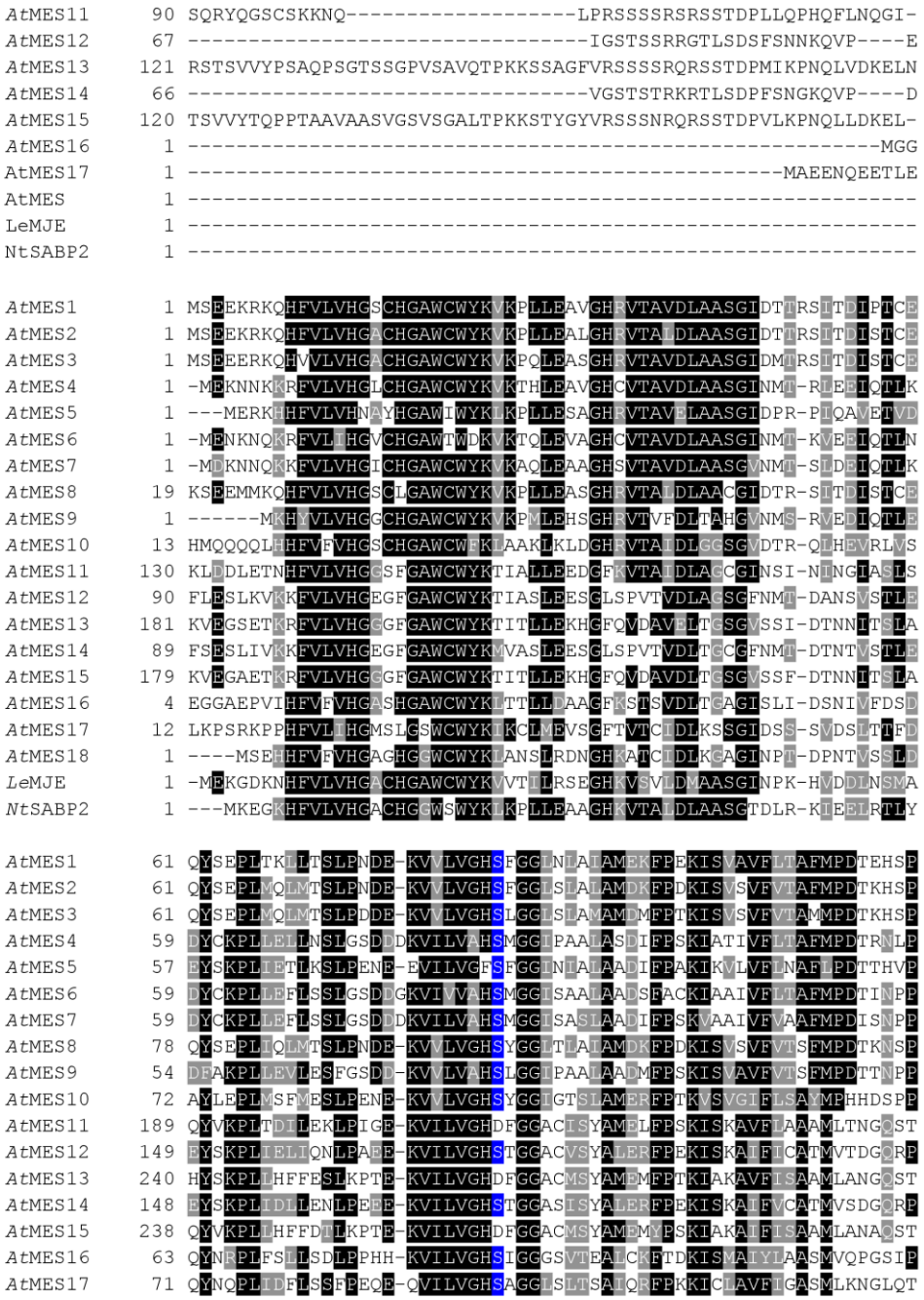

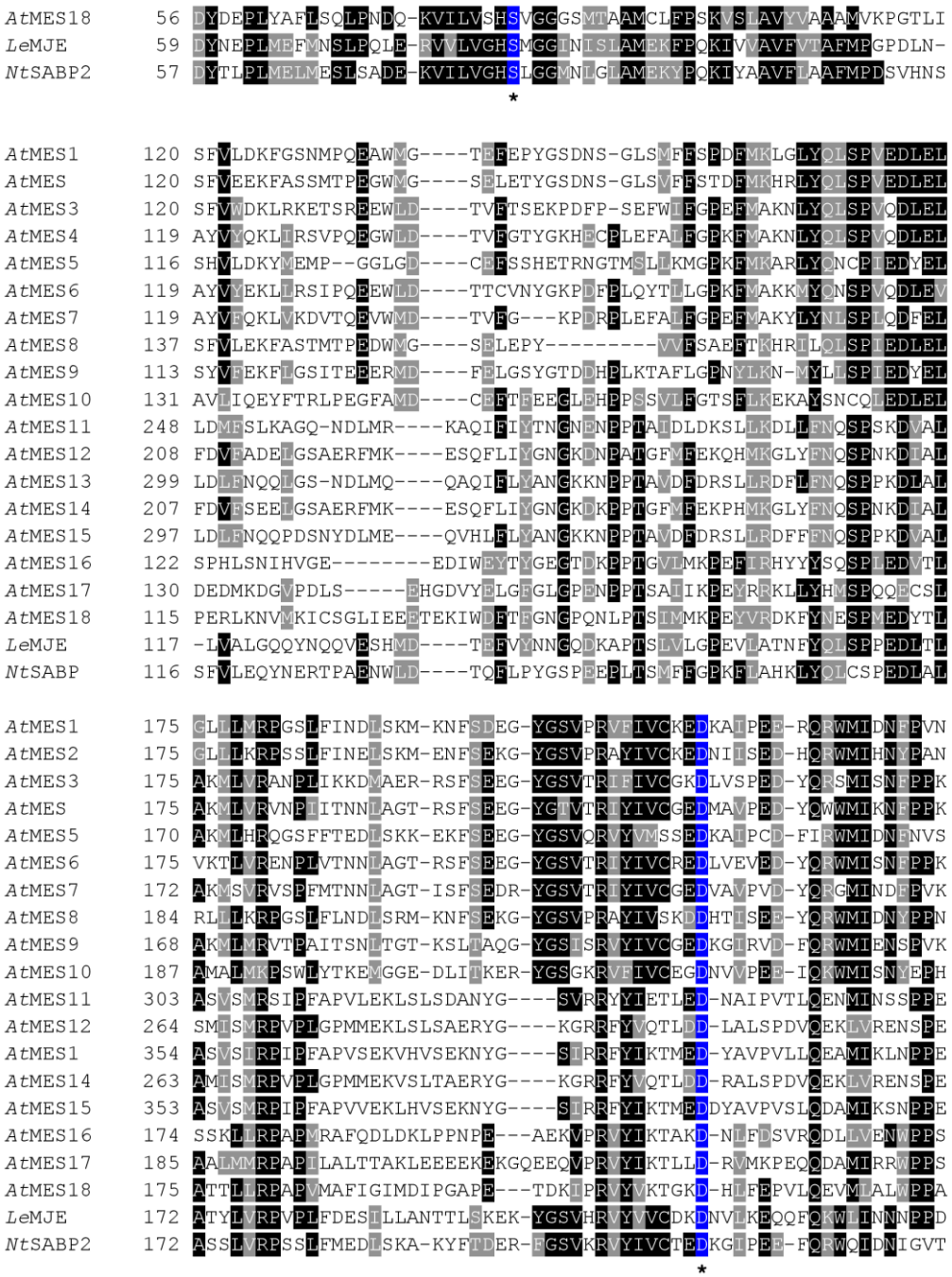

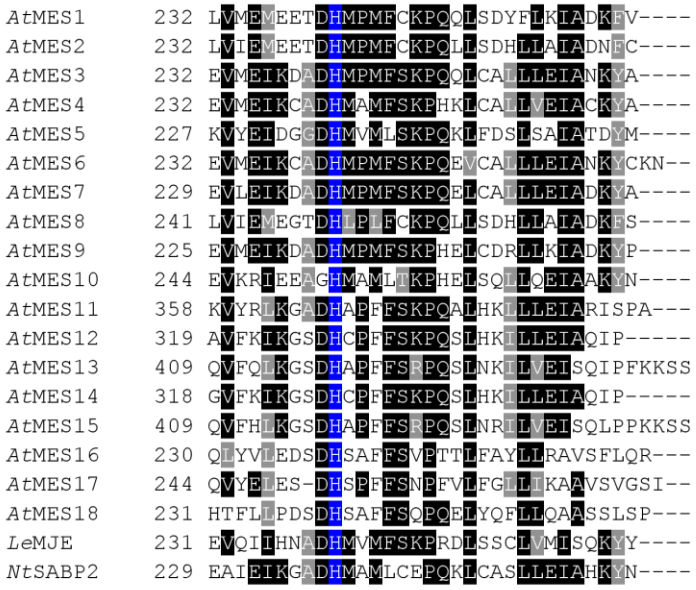

Supplementary Figure 6: Multiple protein sequence alignment of 18 *Arabidopsis* methyl esterases (*At*MES), tobacco SABP2 (*Nt*SABP2) and tomato MJE (*Le*MJE). The sequence alignment was conducted using CLUSTALW (Thompson *et al*., 1997; Kyoto University Bioinformatics Center). The catalytic triad, characteristic for α/β hydrolases and represented by the residues S81, H238 and D210 in *Nt*SABP2, is conserved among most members of the methyl esterase family in *Arabidopsis* (indicated by asterisks and in blue). BoxShade (v3.21) (written by K. Hofmann and M. Baron; https://embnet.vital-it.ch/software/BOX_form.html) was used for shading of multiple alignment file.

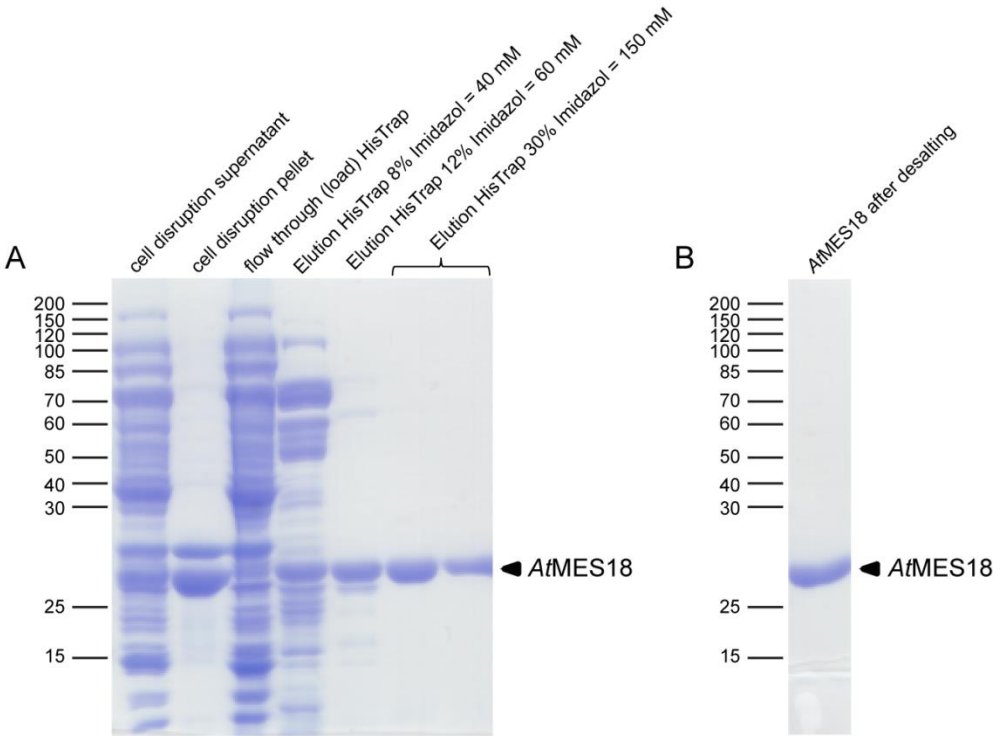

Supplementary Figure 7: Purified MES18 migrates at approximately 28 kDa by SDS PAGE analysis. SDS PAGE is showing the recombinant His_6-MES18 purified by (**A**) affinity chromatography (His Trap®) and (**B**) size exclusion chromatography (desalting, HiPrep™). Black triangle indicates purified MES18.

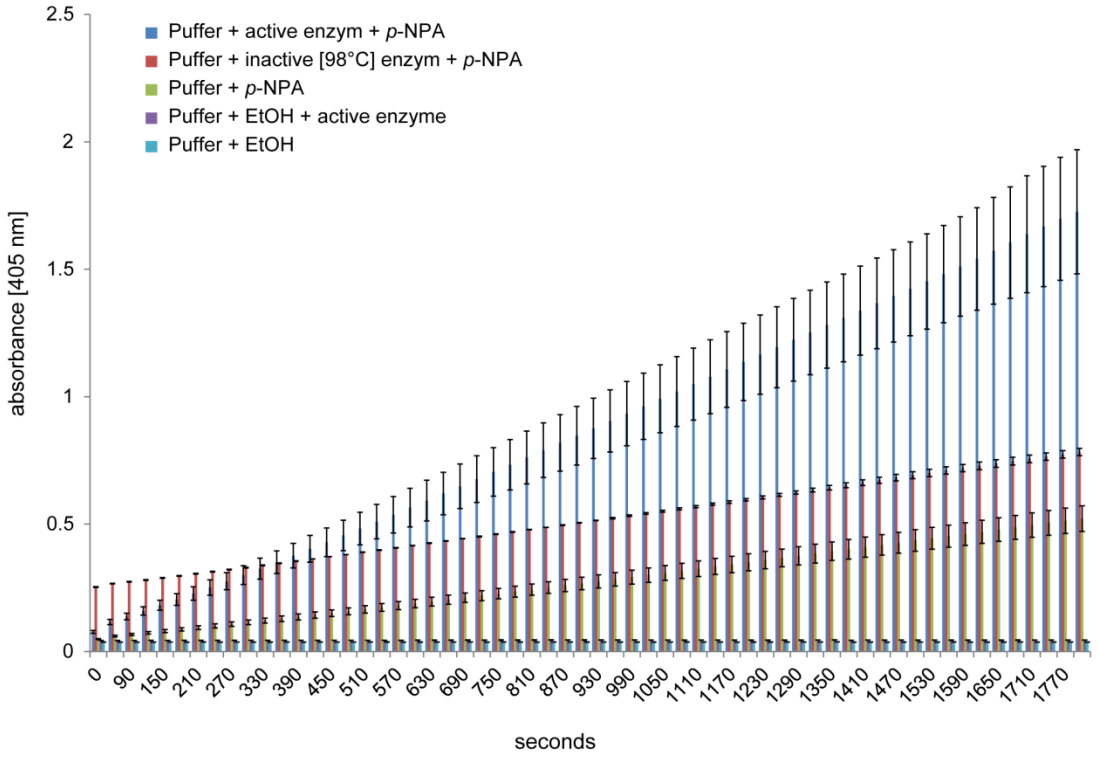

Supplementary Figure 8: MES18 shows esterase activity as identified by a photometric esterase assay. Heat-inactivated and active His_6-MES18 protein which was dissolved in 10 mM NaCl and 50 mM TRIS-HCl buffer (pH 8.0) was incubated with *p*-nitrophenyl acetat (*p*-NPA; depicted in dark blue and red, respectively). The absorbance of the hydrolysis product (*p*-nitrophenol) was measured in a plate reader system at 405 nm every 30 seconds over a time period of 30 minutes. Bars represent mean values of three technical replicates for each reaction. Error bars represent standard deviations of three technical replicates. As control, 10 mM NaCl and 50 mM TRIS-HCl buffer (pH 8.0) was incubated with *p*-NPA (green) or EtOH (light blue). Active MES18 protein which was dissolved in 10 mM NaCl and 50 mM TRIS-HCl buffer (pH 8.0) was incubated with EtOH (dark purple). Experiment was performed five times with independently expressed and purified His_6-MES18 protein, which resulted in similar results. Protein concentrations from 0.015 mg to 0.03 mg were used in this experiment.

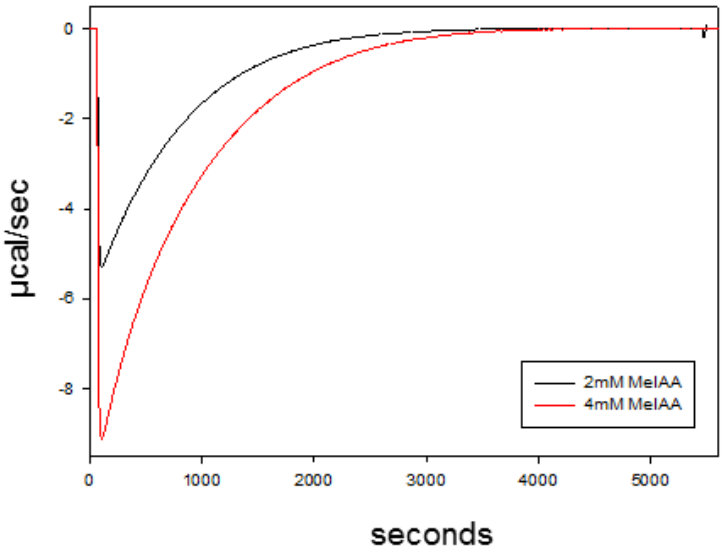

Supplementary Figure 9: ITC analysis showing the catalytic conversion of MeIAA by MES18. Calorimetric progress curve of the reaction of MeIAA with His_6-MES18 is depicted. Measurements were performed in 10 mM NaCl and 50 mM TRIS-HCl (pH 8.0) buffer with 4 % DMSO. After equilibration (60 seconds), 18 µm His_6-MES18 was injected to either 2 mM MeIAA (black line) or 4 mM MeIAA (red line) and the change in instrumental thermal power was monitored until the substrate MeIAA was completely consumed.

7 List of figures

8 List of tables

9 List of supplemental tables and figures

10 Acknowledgements

This work was partly supported by the Goettingen Graduate School for Neurosciences, Biophysics, and Molecular Biosciences (DFG Grant GSC 226/4)

An dieser Stelle möchte ich bei allen bedanken, die mich auf dem Weg meiner Promotion begleitet haben.

Zunächst möchte ich mich bei meinem Doktorvater PD Dr. Marcel Wiermer für die Möglichkeit bedanken, an diesem spannenden Promotionsthema zu arbeiten. Die thematische Vielseitigkeit des Projektes hat mich begeistert und bot mir die Möglichkeit, neue molekularbiologische und biochemische Methoden zu erlernen. Ich möchte mich außerdem für den fachlichen Austausch in unseren regelmäßigen Meetings bedanken. Die zahlreichen wissenschaftlichen Diskussionen und die konstruktive Kritik zu meinem Projekt waren sehr hilfreich. Aber auch außerhalb von festgelegten Meetings stand seine Tür immer offen, sowohl für wissenschaftliche als auch für persönliche Belange. Die Freude an der Forschung und seine stets positive Herangehensweise an wissenschaftliche Probleme sind bewundernswert und waren immer sehr inspirierend und motivierend für mich. Ich bin nicht nur in wissenschaftlicher Sicht, sondern auch aus persönlicher Sicht an diesem Forschungsprojekt gewachsen. Die tolle Arbeitsatmosphäre in Dr. Wiermers Arbeitsgruppe hat die Laborarbeit sehr angenehm gestaltet und half mir dabei, auch an Tagen, die mit Frustration gefüllt waren, nicht die Lust an der wissenschaftlichen Arbeit zu verlieren. Des Weiteren möchte ich mich bei PD Dr. Marcel Wiermer für seine Funktion als Erstprüfer und Gutachter meiner Promotionsarbeit bedanken sowie für das Korrekturlesen dieser Arbeit.

Ich möchte mich ebenfalls bei meinem Zweitgutachter Prof. Dr. Volker Lipka bedanken. Zu einem möchte ich mich für seine Funktion, Teil meines Betreuungsausschusses zu sein bedanken und zum anderen für die Anfertigung des Gutachtes. Außerdem möchte ich mich für die wissenschaftlichen Diskussionen und konstruktive Kritik zu meinem Projekt bedanken, die nicht nur im Rahmen von regelmäßigen TAC Meetings erfolgten, sondern auch in regelmäßigen Seminaren. Die gemeinschaftlichen Seminare der Arbeitsgruppe von Prof. Dr. Volker Lipka und PD Dr. Marcel Wiermer waren eine große wissenschaftliche Bereicherung.

I would also like to thank Prof. Xin Li for being part of my thesis committee and warmly welcoming me in her lab in Vancouver. I am very grateful for the scientific discussions we had during our annual retreats and during my time in Vancouver. Thank you very much for your constructive comments and suggestions regarding my project and the support that I got

from you. I am very happy that you gave me the opportunity to learn how to operate a HPLC machine.

Thank you very much, PD Dr. Marcel Wiermer, Prof. Dr. Volker Lipka and Dr. Xin Li for being my committee members and for being part of my examination board.
Vielen Dank an Prof. Dr. Ivo Feußner, Prof. Dr. Gerhard Braus und Prof. Dr. Kai Heimel, dass Sie zugestimmt haben ebenfalls Teil meiner Prüfungskommission zu sein.

Des Weiteren möchte ich mich bei Dr. Elena Petutschnig, PD Dr. Thomas Teichmann und Dr. Hassan Ghareeb für den wissenschaftlichen Austausch während der gemeinschaftlichen Seminare bedanken und die Unterstützung bei experimentellen Problemen.

Ich möchte mich ebenfalls bei den technischen Assistenten Gaby und Melanie für die Bestellung von Labormaterial bedanken und dafür, dass Sie mir bei experimentellen Fragen mit Rat und Tat zur Seite standen. Ein großes Dankeschön möchte ich auch an Annette aussprechen, für die Bereitstellung von Puffer und Medien, die angenehme Arbeitsatmosphäre im Labor und für die Hilfe bei der Durchführung von Experimenten. Vielen Dank auch für die Unterstützung beim Gießen der Pflanzen in den Klimakammern und der Hilfe beim Sieben von Saatgut. Ein großes Dankeschön möchte ich auch an unsere beiden Gärtnerinnen, Feli und Susanne, aussprechen. Vielen Dank für das Bereitstellen von Erdtöpfen, das Eintüten von Pflanzen, das Sieben von Saatgut und für die Hilfe bei der Pflege der Pflanzen.

Darüber hinaus möchte ich mich bei meinem Bachelorstudenten Jonas Appel bedanken. Er war stets motiviert und mit großem Engagement bei der Arbeit. Die Zeit mit dir im Labor war sehr angenehm und produktiv.

Weiteren Bachelor- und Masterstudenten sowie studentischen Hilfskräften, die mich bei Experimenten unterstützt haben, möchte ich für Ihre Arbeit und Zeit danken.

Ein riesengroßes Dankschön möchte ich ebenfalls an meine Laborpartner und Doktorandenkollegen Daniel und Qiqi aussprechen. I am so grateful for the support that I got from you! Thanks a lot for our scientific discussion about experimental setups and the outcome of certain experiments.

Qiqi, it was so great that you joined our lab one and a half years ago. I am going to miss our cooking experiences and your Chinese food!

Daniel, bei dir möchte ich mich für deine Freundlichkeit und stetige Hilfsbereitschaft und Geduld während der letzten dreieinhalb Jahre bedanken! Du bist immer mein Lieblingsschreibtischnachbar gewesen. Bleib so wie du bist, ein toller Mensch und fabelhafter Wissenschaftler! Es war wunderbar mit dir zusammen zu arbeiten.

Ein riesengroßes Dankeschön geht auch an meine weiteren aktuellen und ehemaligen Doktorandenkollegen Leonie, Dimitri, Julia, Mohammed, Chrissi, Lena, Mo, Mascha und Sina. Die entspannten und schöne Gespräche während gemeinsamer Mittagspausen, die

sich nicht immer nur um die Wissenschaft gedreht haben und so manche Frustration über Experimente, die nicht so verliefen wie geplant, schnell schmälerten. Danke für den Austausch über Experimente und die wertvollen Ratschläge und die kleinen Plaudereien zwischendurch. Vielen Dank Chrissi, dass du während des Schreibprozesses immer ein offenes Ohr für mich hattest. Vielen Dank, Leonie und Sina für eure Freundschaft und die tolle Zeit mit euch im, aber auch außerhalb des Labors. Ich freue mich schon darauf euch in Köln zu besuchen! Liebe Sina, vielen Dank für dein offenes Ohr und die tollen Gespräche, die wir nicht nur über unsere Forschungsprojekte, sondern auch über private Themen geführt haben. Vielen Dank für die Zeit, die du dir für das Lesen der Arbeit genommen hast.

Außerdem möchte ich mich bei der ganzen Abteilung von Prof. Dr. Volker Lipka und PD Dr. Marcel Wiermer für die angenehme Arbeitsatmosphäre bedanken. Ich erinnere mich gerne an die tollen Betriebsausflüge im Sommer zurück und natürlich auch an unser unterhaltsames jährlich stattfindendes Weihnachtskegeln.

I would like to take this opportunity and also thank the whole Li lab for their warm welcome during my stay in Vancouver. Especially Kevin, Karem and Jianhua who helped me to orientate myself in the lab. Furthermore, I would like to thank, Yang, Ana, Kevin, Karem and Hila for being so nice to me that I directly felt welcomed and like home and the great trips that we did together.

Schlussendlich möchte ich mich auch bei meiner Familie und Freuden danken! Ein riesengroßes Dankeschön richte ich an meine ehemalige Göttinger Mädelstruppe. Anna, Anne, Nathalie und Seli, ihr seid meine Herzensmenschen und ich danke euch aus tiefstem Herzen für eure moralische Unterstützung während meiner Doktorarbeit und eurer innigen Freundschaft seit dem Tag, als wir uns vor fast 10 Jahren das erste Mal vor dem alten botanischen Hörsaal kennengelernt haben und zusammen ins Biologiestudium gestartet sind. Ich bin so froh, dass es euch gibt! Liebe Seli, vielen Dank für deine Zeit und das Korrekturlesen meiner Arbeit! Liebe Anne vielen Dank für deine moralische Unterstützung vor Ort und die Zeit, die du dir zum Lesen meiner Arbeit genommen hast! Ich möchte außerdem meiner langjährigen Freundin Eugenia danken! Danke, dass du immer für mich da bist! Ich freue mich auf unsere gemeinsame Zeit in Hamburg!

Liebe Meike, danke für dein offenes Ohr, unsere gemeinsame tolle Zeit und dafür, dass du immer für mich da bist! Danke für die Zeit, die du dir zum Lesen meiner Arbeit genommen hast!

Vielen Dank Matthias für deine Unterstützung, nicht nur während der letzten dreieinhalb Jahre meiner Promotion, sondern auch während unserer ganzen Beziehung. Danke, dass du immer für mich da gewesen bist!